



**HAL**  
open science

# Electrogenerated chemiluminescence: from materials to sensing applications

Haidong Li

► **To cite this version:**

Haidong Li. Electrogenerated chemiluminescence: from materials to sensing applications. Chemical Physics [physics.chem-ph]. Université de Bordeaux, 2017. English. NNT: 2017BORD0560. tel-01529849

**HAL Id: tel-01529849**

**<https://theses.hal.science/tel-01529849>**

Submitted on 31 May 2017

**HAL** is a multi-disciplinary open access archive for the deposit and dissemination of scientific research documents, whether they are published or not. The documents may come from teaching and research institutions in France or abroad, or from public or private research centers.

L'archive ouverte pluridisciplinaire **HAL**, est destinée au dépôt et à la diffusion de documents scientifiques de niveau recherche, publiés ou non, émanant des établissements d'enseignement et de recherche français ou étrangers, des laboratoires publics ou privés.

# THÈSE

PRÉSENTÉE A

**L'UNIVERSITÉ DE BORDEAUX**

ÉCOLE DOCTORALE DES SCIENCES CHIMIQUES

Par Haidong Li

POUR OBTENIR LE GRADE DE DOCTEUR

SPÉCIALITÉ: Chimie-Physique

## **Electrogenerated chemiluminescence: from materials to sensing applications**

Sous la direction du Prof. Neso Sojic

Membres du jury:

Thomas Doneux

Guobao Xu

Francesco Paolucci

Mireille Blanchard-Desce

Valérie Ravaine

Neso Sojic

Professeur, Université Libre de Bruxelles

Professeur, Changchun Institute of Applied Chemistry

Professeur, Université de Bologne

Directeur de recherches CNRS, Université de Bordeaux

Professeur, INP Bordeaux

Professeur, INP Bordeaux

Rapporteur

Rapporteur

Président

Examineur

Examineur

Directeur

Soutenue le 29.03.2017

## Abstract

Electrogenerated chemiluminescence (ECL) involves the energetic electron transfer reactions at the electrode with the generation of excited state of emitter, which then relax to the ground state and emit light. These ECL reactions can be divided into two main pathways: the annihilation and sacrificial co-reactant reactions. The latter has found a lot of applications in analytical chemistry. In this thesis, ECL studies toward three complementary directions are presented, ranging from the molecular scale to macroscopic scale: the research of new ECL luminophores, the study of stimuli-responsive hydrogel films, and the development of new ECL assays.

Firstly, I have studied three types of organic dyes for ECL investigations. These organic dyes exhibit interesting electrochemical and ECL properties. ECL efficiencies of the organic dyes can be tuned by the modification of the structures. Spirofluorene dyes show strong ECL emission, and thus its fluorescence organic nanoparticles (FONs) prepared in water were used as ECL nano-emitters. We also established an energetic ECL “wall” representation and then move forward creating ECL “map” upon electrochemical, photoluminescence and ECL studies on cationic triangulenes and cationic helicenes dyes, respectively.

Secondly, the preparation of thermo-responsive poly(N-isopropylacrylamide) (pNIPAM) hydrogel films covalently incorporating Ru(bpy)<sub>3</sub> redox centers were achieved on glassy carbon electrode (GCE) or carbon fiber by electrochemically induced free radical polymerization. ECL studies on the modified GCEs have provided the main factor (the average distance of Ru(bpy)<sub>3</sub> sites) that governs the ECL process, leading to deciphering the enhanced ECL in the films. The deposition of the films on carbon fiber by bipolar electrochemistry (BPE) has opened new route to for the development of smart hybrid micro objects.

Finally, analytical application is one of the most important features of ECL. We presented two different ECL assays using either the phenylboronic acid modified amine based co-reactants or gold coated optical fiber bundle. The binding of saccharides with boronic acid modified tertiary amines makes the oxidation of amines group inefficient, which decreases ECL signal response. By changing linker length of a bis-boronic acid amine co-reactant, we are able to determine D-glucose and D-fructose selectively. We also studied the ECL generation of Ru(bpy)<sub>3</sub><sup>2+</sup>/TPrA system on the gold coated optical fiber bundle in a wireless manner by BPE, then transmission and remote detection at the opposite end of the same object. This method may extend the applicability of ECL assays in the confined or hazardous environments.

**Key-words:** electrogenerated chemiluminescence, spirofluorene, cationic triangulene,

cationic helicene, poly(N-isopropylacrylamide), stimuli-responsive hydrogels, electrochemical polymerization, bipolar electrochemistry, phenylboronic acid, optical fiber bundle

## Résumé

Le phénomène d'électrochimiluminescence (ECL), également appelé chimiluminescence électrogénérée, consiste en la génération de l'état excité d'un émetteur suite à des réactions de transfert d'électrons se produisant initialement à la surface de l'électrode. L'état excité ainsi produit retourne à l'état fondamental en émettant de la lumière. Les réactions ECL se classent principalement en 2 grandes voies mécanistiques: les réactions d'annihilation et les réactions impliquant un co-réactif sacrificiel. Cette dernière voie a conduit à de très nombreuses applications en chimie analytique. Dans ce manuscrit, j'ai présenté mes travaux de thèse qui ont suivis 3 directions complémentaires depuis l'échelle moléculaire jusqu'à l'échelle macroscopique: la recherche de nouveaux luminophores ECL, l'étude de films d'hydrogels stimulables et le développement de nouvelles applications analytiques de l'ECL.

Dans une première partie, j'ai étudié les propriétés ECL de 3 types de luminophores organiques. Ces composés ont montré des caractéristiques électrochimiques et ECL remarquables. L'efficacité ECL de ces luminophores organiques peut être modulée en jouant sur leurs structures respectives. Des luminophores de type spirofluorène ont produit une émission ECL très intense et les nanoparticules organiques correspondantes ont pu être utilisées comme nano-émetteurs ECL. L'étude des propriétés électrochimiques, photochimiques et ECL de luminophores cationiques de type triangulène et héliène a été réalisée et présentée avec un formalisme montrant un «mur» ECL ou une cartographie ECL complète.

Dans une seconde partie, la préparation de films d'hydrogels thermo-stimulables à base de poly(N-isopropylacrylamide) ou pNIPAM incorporant des centres redox  $\text{Ru}(\text{bpy})_3$  a été réalisée sur des électrodes de carbone vitreux (GCE) et aussi sur des fibres de carbone par polymérisation radicalaire induite électrochimiquement. Les études ECL sur les GCEs modifiées ont montré que le facteur principal gouvernant les propriétés ECL est la distance entre les sites  $\text{Ru}(\text{bpy})_3$ . Le dépôt de tels films de pNIPAM- $\text{Ru}(\text{bpy})_3$  par électrochimie bipolaire ouvre de nouvelles possibilités pour le développement de micro-objets stimulables hybrides.

Dans une dernière partie, comme la chimie analytique constitue un des plus importants attraits de l'ECL, deux applications analytiques sont présentées en utilisant, d'une part, des co-réactifs de type amine modifié par l'acide phénylboronique, et, d'autre part, des faisceaux de fibres optiques recouverts d'or. La réaction de complexation de saccharides par le groupe phénylboronique modifie les propriétés électrochimiques du co-réactif amine en rendant son oxydation à l'électrode inefficace, ce qui provoque la diminution du signal ECL. En changeant la longueur de l'espaceur de ces co-réactifs qui portent deux groupements phénylboroniques, nous avons pu mesurer sélectivement la concentration de D-glucose et de D-fructose. Mon travail a

enfin porté sur le développement d'un objet analytique basé sur un faisceau de fibres optiques doré qui est adressé sans contact par électrochimie bipolaire. L'ECL ainsi générée du système  $\text{Ru}(\text{bpy})_3^{2+}/\text{TPrA}$  a permis de réaliser un outil activable à distance permettant une mesure déportée *via* le faisceau. Ce nouvel objet analytique original devrait permettre d'étendre les mesures ECL à des environnements confinés ou dangereux.

Mots-clés: électrochimiluminescence, luminophores, spirofluorène, triangulène, héliène, poly(N-isopropylacrylamide), hydrogel stimuable électropolymérisation, électrochimie bipolaire, acide phénylboronique, faisceau de fibres optiques

## 中文摘要

电化学发光 (ECL) 的发生是由于在电极表面通过电子转移反应生成了发光体的激发态跃迁到基态,并伴随着发光。这些电子转移反应可划分为两种主要的途径:正负自由基湮灭反应和共反应物反应。而后者被广泛应用于分析化学领域。在本论文中,我们在电化学发光领域中进行了广泛的研究,具体有三个研究方向:新型电化学发光光团的研究、响应水凝胶膜的制备以及电化学发光分析的研究。

首先,我们选择了三种不同类型的有机荧光分子用于电化学发光的研究。这些有机荧光分子展现出许多电化学和电化学发光特性。其中,螺芴荧光分子展现出了非常强的电化学发光。而且用它制备的荧光有机纳米颗粒 (FONs) 在水相中也可以产生电化学发光。基于对阳离子型三角烯和阳离子型螺烯的电化学、光谱学以及电化学发光的研究,我们分别建立了鉴别电化学发光“墙”和“图谱”。

其次,利用自由基电聚合的方法,我们实现了在玻碳电极和碳纤维表面上制备热刺激-响应的聚异丙基丙烯酰胺 (p-NIPAM) 共价嫁接三联吡啶钌  $\text{Ru}(\text{bpy})_3$  荧光分子的水凝胶膜。通过对玻碳电极上水凝胶膜的电化学发光的研究,我们发现了控制水凝胶膜中电化学发光的主要因素,从而揭秘了水凝胶膜中电化学发光增强的成因。而且,利用双电极化学 (BPE) 的方法,我们将此类水凝胶膜的制备应用于碳纤维上,以发展灵敏杂化微米级器件。

最后,鉴于化学分析是电化学发光最重要的特征,我们构建两种不同的电化学发光分析体系:一种是基于硼酸化学修饰的三丙胺共反应物;另一种是利用镀金光导纤维。硼酸对糖类的结合弱化了三丙胺的电化学氧化效率,因此影响电化学发光的强度。通过改变双硼酸修饰共混物之间碳链的长度,我们实现了对葡萄糖和果糖的选择性检测。我们还研究了在镀金光导纤维上三联吡啶钌/三丙胺体系的

电化学发光。此研究是在双电极体系进行的，镀金光导纤维无需外部接线，镀金部位产生的发光透过光纤传输的光纤的远端，再进行检测，因此达到了电化学发光的远程检测。这一方法可应用于狭窄危险环境中的电化学发光分析。

**关键词：**电化学发光，螺芴，阳离子型三角烯，阳离子型螺烯，聚异丙基丙烯酰胺，响应水凝胶，电沉积，双电极化学，苯硼酸，光导纤维

## Acknowledgements

I have had a great time in the three and half years Ph.D study in France, which will be an invaluable experience in my life. I was so lucky to be one of Chinese students in Bordeaux as the first batch selected by the China Scholarship Council (CSC) and University of Bordeaux Ph.D program. I would like to thank firstly my supervisor Prof. Neso Sojic for the continuous support in the application, and then my Ph.D study and research, for his patience, motivation, enthusiasm, and immense knowledge. His guidance help me in all the time of research and writing of this thesis.

I deeply appreciate the fruitful collaborations with several research groups. I want to thank Dr Jonathan Daniel and his supervisor Mireille Blanchard-Desce (Univeristy of Bordeaux) for their helpful discussions and contributions in the work of spirofluorene dyes. Many thanks to the group of Prof Jérôme Lacour (University of Geneva) for their excellent works on the synthesis of triangulene and helicene dyes, together we have published 3 papers, and I believe more papers will come soon. Finally, I would like to thank Prof. Tony D. James and his student Adam C. Sedgwick (University of Bath) for the work on phenylboronic acids.

For the NsysA family, I want to thank all members during my stay in the lab. It is a pleasure time to work with all of you. I would like to thank Dr. Florent Pinaut, who is the first person of the group I met and picked me up in the airport; thanks to Dr. Catherine Adam who led me into organic ECL; thanks to Dr. Milica Sentic for her encouragements and passing me the experimental skills; thanks to Patrick Garrigue for his technical supports on optical fiber and SEM; thanks to Dr. Laurent Bouffier for teaching me spectroelectrochemistry and bipolar electrochemistry; thanks to Prof. Valérie Ravaine and Dr. Dodzi Zigah for the collaboration on the stimuli responsible hydrogels; Special thanks to Aline Simon-Lalande for the administration works in the lab.

For my family, to my parents, I thank you both for raising me and supporting me no matter where I am. To my sister and brothers, I need to thank you for your endless support and taking care of our parents. Finally, I own too much to my wife. You were

always making sure I was fine no matter how far I was. Thank you for your understanding and supporting as always.

I acknowledge all members of the jury committee of my defense for your precious time and advice.

## Contents

Abstract.....	I
Résumé.....	III
中文摘要.....	V
Acknowledgements.....	VII
List of abbreviations.....	XI
General introductions.....	XIV
Chapter 1.....	1
Fundamentals and applications of electrochemiluminescence.....	1
1.1 Introduction.....	2
1.2 Background.....	3
1.2.1 Photoluminescence.....	3
1.2.2 Electroluminescence.....	4
1.2.3 Chemiluminescence.....	6
1.3 Fundamentals of ECL.....	8
1.3.1 Annihilation ECL.....	9
1.3.2 Co-reactant ECL.....	13
1.3.2.1 Oxidative–reduction ECL.....	14
1.3.2.2 Reductive–oxidation ECL.....	20
1.4 Luminophores of ECL.....	22
1.4.1 Inorganic complexes.....	22
1.4.2 Organic molecules.....	27
1.4.3 Nanoparticles.....	31
1.5 ECL applications.....	33
1.5.1 ECL immunoassays.....	34
1.5.2 Commercialized ECL instrumentation.....	37
1.6 Conclusion.....	40
References.....	41
Chapter 2.....	49
Electrochemiluminescence of organic molecules: from spirofluorene, triangulene and helicene luminophores to nanoparticles.....	49
2.1 Introduction.....	50
2.2 Bis-donor quadrupolar spirofluorene dye.....	51
2.2.1 Preparation of the organic dye and its nanoparticles.....	52
2.2.2 Electrochemistry.....	54
2.2.3 Spectroelectrochemistry.....	58
2.2.4 ECL of the dyes.....	61
2.2.5 Electrochemistry and ECL of FONs.....	66
2.3 Cationic triangulene dyes.....	69
2.3.1 Electrochemistry of cationic triangulene dyes.....	70
2.3.2 ECL of cationic triangulene dyes.....	73
2.3.3 ECL efficiency discriminated by ECL “wall”.....	76
2.4 Cationic helicene dyes.....	78

2.4.1	Electrochemistry of cationic helicene dyes.....	79
2.4.2	ECL of cationic helicene dyes.....	82
2.4.2.1	Annihilation pathway.....	82
2.4.2.2	Co-reactant pathway.....	86
2.4.3	ECL efficiency discriminated by ECL “map”.....	88
2.5	Conclusion.....	93
	References.....	96
	Chapter 3.....	103
	Electrochemiluminescence of stimuli-responsive hydrogel films.....	103
3.1	Introduction.....	104
3.2	ECL of hydrogel films on GCE.....	105
3.2.1	Preparation of the hydrogel films.....	108
3.2.2	Electrochemical properties of the hydrogel films.....	111
3.2.3	ECL of the hydrogel films.....	113
3.3	ECL of hydrogel films on BE.....	120
3.3.1	Wireless deposition of the hydrogel films.....	121
3.3.2	Wireless generation of ECL on the hydrogel films.....	124
3.4	Conclusion.....	127
	References.....	129
	Chapter 4.....	135
	New electrochemiluminescence sensing methods.....	135
4.1	Introduction.....	136
4.2	Boronic acid-modified co-reactants.....	137
4.2.1	ECL produced with boronic acid-modified co-reactants.....	140
4.2.2	ECL response induced by binding saccharides.....	143
4.2.3	ECL response induced by selectively binding saccharides.....	146
4.3	Optical fiber bundle.....	150
4.3.1	Gold coated optical fiber bundle tip as BE.....	152
4.3.2	Direct ECL imaging on a optical fiber bundle.....	154
4.3.3	Remote ECL sensing through an optical fiber bundle.....	156
4.4	Conclusion.....	159
	References.....	161
	General conclusions.....	167
	Experimental section.....	171
	List of publications.....	177

## List of abbreviations

---

ADOTA <sup>+</sup>	azadioxotriangulenium
AZAOXA <sup>+</sup>	azaoxa[6]helicene
BE	bipolar electrode
BODIPY	boron dipyrromethene
BPE	bipolar electrochemistry
BPO	benzoyl peroxide
BTA	2,1,3-benzothiaddiazole
CA	chronoamperometry
CCD	charge coupled device
CDs	carbon dots
CE	capillary electrophoresis
CEA	carcinoembryonic antigen
CL	chemiluminescence
CV	cyclic voltammetry
DAOTA <sup>+</sup>	diazaoxotriangulenium
DBAE	2-(dibutylamino)ethanol
DCM	dichloromethane
DIAZA <sup>+</sup>	diaza[6]helicene
DIOXA <sup>+</sup>	dioxa[6]helicene
DLS	dynamic light scattering
DMF	dimethylformamide
DMSO	dimethylsulfoxide
DMQA <sup>+</sup>	dimethoxyquinacridinium
DPA	9,10-diphenylanthracene
DPV	differential pulse voltammetry
ECL	electrochemiluminescence
EDTA	ethylenediaminetetraacetic acid

---

---

EL	electroluminescence
ERET	electrochemiluminescence
	resonance energy transfer
ET	electron transfer
FIA	flow injection analysis
FONs	fluorescence organic nanoparticles
GCE	glassy carbon electrode
GDH	glucose dehydrogenase
HOMO	highest occupied molecular orbital
HPLC	high performance
	liquid chromatography
ICT	intramolecular charge transfer
ITO	Indium tin oxide
LCST	lower critical solution temperature
LEC	light-emitting electrochemical cell
LED	light-emitting diode
LOP	low oxidation potential
LUMO	lowest unoccupied molecular orbital
MWCNT	multi-walled carbon nanotube
NAD <sup>+</sup>	$\beta$ -nicotinamide adenine dinucleotide
NHE	normal hydrogen electrode
NIPAM	N-isopropylacrylamide
NPs	nanoparticles
OFETs	organic field-effect transistors
OLEDs	organic light-emitting diodes
PBS	phosphate buffer saline
PL	photoluminescence
PMT	photomultiplier tube
pNIPAM	poly(N-isopropylacrylamide)

---

---

QDs	quantum dots
RAFT	reversible addition-fragmentation chain transfer
SAR	structure/activity relationship
SCE	saturated calomel electrode
SEM	scanning electron microscopy
TATA <sup>+</sup>	triazatriangulenium
TBAP	tetra- <i>n</i> -butylammonium perchlorate
TBAPF <sub>6</sub>	tetra- <i>n</i> -butylammonium hexafluorophosphate
TEM	transmission electron microscopy
THF	tetrahydrofuran
TMPD	<i>N,N,N',N'</i> -tetramethyl- <i>p</i> -phenylenediamine
TOTA <sup>+</sup>	trioxotriangulenium
TPrA	tri- <i>n</i> -propylamine
VPTT	volume phase transition temperature

---

## General introduction

Electrogenerated chemiluminescence (ECL) is a type of chemiluminescence involving the *in situ* generation of an excited state at the electrode surface by electron transfer (ET) reactions. ECL is known as a highly sensitive analytical method that has been used widely to develop a variety of ECL assays. Since no extra light source and expensive apparatus are involved in ECL, it produces almost zero background signals and thus offers a sensitive and simple tool for analytical applications. Moreover, ECL is flexible to combine with different materials or other analytical methods.

Chapter 1 presents a general review of ECL in the aspects of theoretical studies, annihilation or co-reactant mechanisms, inorganic ECL or organic ECL and analytical applications. For example, this chapter presents brief overviews of ECL history. The most common used luminophore and co-reactant are selected for the demonstration of ECL. Meanwhile, ECL on nano-materials (i.e. carbon dots and graphene dots) and organic dyes are also reviewed. Finally, analytical application and instrumentation of ECL has been described.

In Chapter 2, the goal is to find new ECL luminophores. In this respect, three types of organic dyes will be selected for the ECL investigations. The electrochemical and ECL studies on these organic dyes reveal tunable redox behaviors and ECL efficiencies by the finely modification on the molecular structures. Spirofluorene bearing electron donating triphenylamine end groups exhibits the very good stability of the higher oxidized states and thus produces strong ECL emission. ECL “wall” and ECL “map” are established upon the electrochemical and photoluminescence data of cationic triangulenes and cationic helicenes, respectively. These thermodynamic plots allow the prediction of energy sufficiency needed in the co-reactant ECL systems, which will help to look for new luminophores with a strong ECL proficiency.

Chapter 3 presents the preparation of thermo-responsive pNIPAM hydrogel films with covalently grafted ruthenium luminophores on either a GCE or a carbon fiber. ECL intensity of the hydrogel films shows a remarkable amplification upon the collapse of the films above the volume phase transition temperature (VPTT), whereas the

oxidation current undergoes a reverse decrease in the case of the cationic co-reactant. However, the fact that ECL emission is enhanced whereas less co-reactant radicals are generated is an intriguing observation. Thanks to the study of such films on GCE where antagonistic effects occur, we are able to figure out that ECL enhancement is neither correlated with the oxidation efficiency of the coreactant nor with the hydrophilic–hydrophobic transition, but solely due to film shrinking. Finally, the preparation of such hydrogel films has been successfully employed to a carbon fiber through bipolar electrochemistry (BPE). The combination of bipolar electrochemistry has open a new route for the the preparation of smart hybrid micro-objects in a wireless manner and even in a large scale by a single experiment.

The last chapter presents two original ECL assays. Integrating a boronic acid to the chemical structure of classic tertiary amines co-reactant allows conferring the ability to bind saccharides in water. Then the binding between boronic acid unit and saccharide in solution can modulate the oxidation of amine moiety, which induces corresponding ECL signal decrease. Finally, selective binding toward D-glucose and D-fructose is achieved by tuning the linker length of a bis-boronic acid amine co-reactant. In BPE, gold coated optical fiber bundle serves as a dual platform, on one hand as bipolar electrode (BE) to locally generate ECL of  $\text{Ru}(\text{bpy})_3^{2+}/\text{TPrA}$  system at one tip in a wireless manner, on the other hand as guide line to transmit the resulting ECL signal to the remote opposite end. The linearity of ECL emission depended on TPrA concentration is verified on the system. Thus this approach offers a unique tool for ECL remote sensing.

## **Chapter 1**

# **Fundamentals and applications of electrochemiluminescence**

## 1.1 Introduction

Electrogenerated chemiluminescence (ECL), also called electrochemiluminescence, involves the *in-situ* generation of an excited state near the electrode surface which is initiated by electron transfer reactions.<sup>1,2</sup> Such phenomenon has been described firstly as the emission from the excited state of luminophores that are produced by electrochemical reactions. Related works could date back to as early as 1920s by Harvey.<sup>3,4</sup> However, the first detailed ECL studies were reported on the luminescence of the aromatic hydrocarbons compounds by Chandross *et al.* and Bard *et al.* in the mid-1960s.<sup>5,6</sup> A suggestion of a mechanism and the first theory about electron transfer in ECL were illustrated in their works. Moreover, ECL actually explains the existence of the Marcus inverted region, where ET process preferentially leads to the generation of the excited state rather than the formation of the ground state.<sup>7</sup> The first report of ECL from metal chelate  $\text{Ru}(\text{bpy})_3^{2+}$  was in 1972.<sup>8</sup> The excited state of  $\text{Ru}(\text{bpy})_3^{2+}$  was produced by the annihilation of reduced ( $\text{Ru}(\text{bpy})_3^{1+}$ ) and oxidized ( $\text{Ru}(\text{bpy})_3^{3+}$ ) in the  $\text{CH}_3\text{CN}$  solution. After that,  $\text{Ru}(\text{bpy})_3^{2+}$  has become the most thoroughly studied ECL active molecule due to its strong luminescence and solubility in both aqueous and non-aqueous media and its stable reduced and oxidized forms. In 1981, the first report of ECL in aqueous solution involved  $\text{Ru}(\text{bpy})_3^{2+}$  and the oxalate ion ( $\text{C}_2\text{O}_4^{2-}$ ), which was a great breakthrough in ECL study.<sup>9</sup> Subsequently, one direction scan of the potential in the presence of both luminophores and co-reactant species has been developed in most of ECL studies. The discovery of  $\text{Ru}(\text{bpy})_3^{2+}/\text{TPrA}$  (tri-*n*-propylamine) in 1990<sup>10</sup> allowed efficient ECL not only in aqueous media but also at physiological pH.<sup>11</sup> Many applications have been developed based on such ECL system.<sup>3,12</sup>

Indeed, ECL does not need an extra light source: it simplifies the detection apparatus and most importantly eliminates background signals from scattered light and luminescent impurities, thus providing improved sensitivity. Therefore, ECL has found a wide range of application in the analytical science. Many immunoassays and

DNA probe assays have been developed based on ECL for clinical diagnostic, food and water testing, environmental monitoring, and bio-warfare agent detection.<sup>13-17</sup>

## 1.2 Background

ECL is a type of luminescence produced by the relaxation of an excited state generated by electron transfer reactions near the electrode surface. Thus ECL shares some common points with other kinds of luminescence, such as photoluminescence (PL), electroluminescence (EL) and chemiluminescence (CL). In order to better discriminate ECL and understand its principles, the other three types of luminescence are also presented here, respectively.

### 1.2.1 Photoluminescence

PL results from transitions between excited states and the ground states of molecule after the absorption of photons. Photoluminescence is formally classified into two groups: fluorescence and phosphorescence depending on the processes that occur between the absorption and emission of light.<sup>18</sup> Such processes have been illustrated by the Jablonski diagram (Figure 1).<sup>19</sup> In this diagram,  $S_0$ ,  $S_1$ , and  $S_2$  represent the singlet ground, first, and second electronic states, respectively. At each of these electronic energy levels the molecule can exist in a number of vibrational energy levels, depicted by 0, 1, 2, etc. Following light absorption, several processes usually occur. A molecule is usually excited to some higher vibrational level of either  $S_1$  or  $S_2$ . However, the lifetime of an excited vibration state in the solution is very short (in the range of picoseconds), thus excited vibration states rapidly decay to  $\nu = 0$  (vibrational level of  $S_1$ ). Such process is called as internal conversion and usually occurs within  $10^{-12}$  s or less. Since fluorescence lifetimes are typically near  $10^{-9}$  s, internal conversion has finished prior to emission. Emission occurs from the vibrational level of  $S_1(\nu = 0)$  to the different vibrational levels of  $S_0$ , resulting in fluorescence. Molecule in the  $S_1$  state can also change to the first triplet state  $T_1$  by a spin conversion. Conversion of  $S_1$

to  $T_1$  is called intersystem crossing. Transition from  $T_1$  to the singlet ground state is “forbidden” and results in phosphorescence. As a result, the rate constants for triplet emission are several orders of magnitude smaller than those for fluorescence. Phosphorescence has longer lifetimes (typically milliseconds to seconds) and is shifted to longer wavelengths with fluorescence.

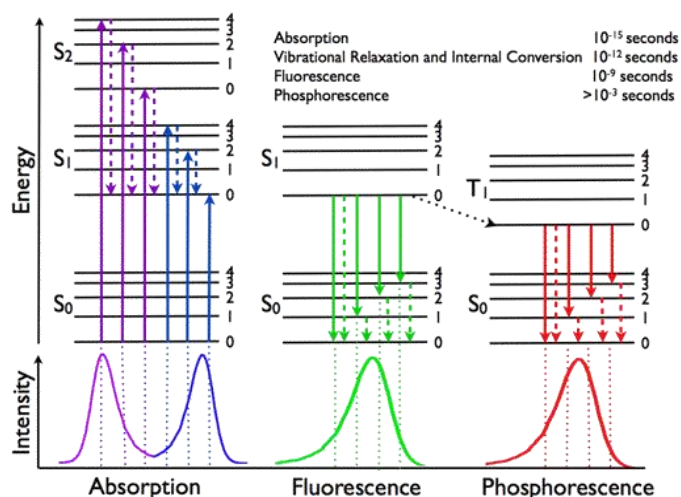


Figure 1. Jablonski diagram of energy level during the absorption and emission of radiation.

Besides, examination of the Jablonski diagram reveals that emission energy is less than that of absorption. This phenomenon explains why emission wavelength is always longer than absorption wavelength. Such wavelength shift is termed as Stokes shift. One major cause of the Stokes shift is the rapid decay to the lowest vibrational level of  $S_1$ . On the other hand, further decay to higher vibrational levels of  $S_0$  could also result in loss of excitation energy by thermalization of the excess vibrational energy. In addition to these effects, solvent, excited-state reactions and complex formation account for the Stokes shifts.<sup>20-22</sup>

## 1.2.2 Electroluminescence

EL actually is a conversion of electric energy into optical energy by the relaxation process of excited electrons when a high electric field is applied to a material. The

material could be inorganic, semiconductor, organic, or liquid crystal etc.<sup>23</sup> There are several basic physical processes that may involve EL emission: (a) injection of charge carriers into the phosphor layer, (b) acceleration of charge carriers to optical energies, (c) excitation of luminescence centers by energetic electrons, (d) irradiative relaxation of luminescent centers.<sup>24</sup> Although with a slight difference, the mechanism of EL in different materials is almost the same.

EL in inorganic materials is divided into two types: high field EL and injection EL. High field EL is generated by raising the luminescence centers to the excited quantum states *via* high-energy electron in the strong electric field. This kind of EL relies on inter- and intra-quantum shell transition at luminescent centers. The first EL produced by this mechanism was observed by Destriau in 1936.<sup>25</sup> In this case, ZnS powder phosphor was mixed in a liquid castor oil. Following by applying a strong electric field, EL emission was produced on a transparent electrode. Injection EL is generated by the direct injection of carriers and subsequent recombination of electron-hole pairs at a *p-n* homo or hetero junction. This is the process responsible for light emission in light-emitting diodes (LED) and semiconductor laser. In injection EL, recombination of minority and majority of carriers across the band gap of the material is a key factor in light emission. There are two methods for the injection of minority carriers (Figure 2):<sup>26</sup> (a) the injection occurs directly by rectifying contact between electrode and crystal. This type of injection EL could be in single crystal of ZnS or its thin films that have contact with electrodes; (b) the electrons are injected from the *n* region into the *p* region while holes are injected in the opposite direction under the electric field. This means that minority carrier injection occurs. For example, if a cathodic current passes through an electrode of ZnS doped with Mn in a solution containing peroxydisulfate ( $S_2O_8^{2-}$ ), intense EL emission is observed with  $\lambda_{max} = 580$  nm. The reduced  $SO_4^{\bullet-}$  can inject into *p-n* junction of ZnS:Mn, resulting in electron-hole recombination and emission.<sup>27</sup> Such EL emission is relatively similar to the case when  $S_2O_8^{2-}$  is used as a coreactant in ECL as described in below section.

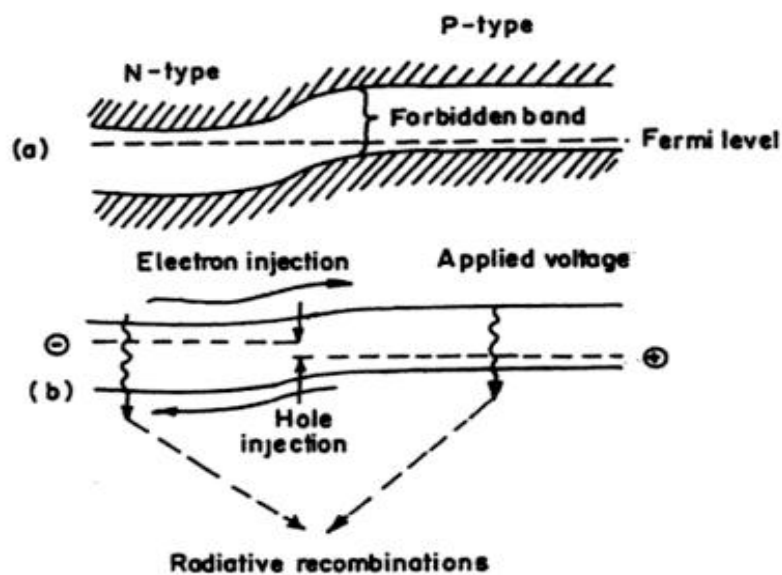


Figure 2. Schematic representation of a  $p-n$  junction: (a) no electric field; (b) electric field applied in forward direction.<sup>26</sup>

### 1.2.3 Chemiluminescence

CL is considered as the emission of electromagnetic radiation resulting from chemical reactions. In CL, the chemical reactions generally yields one of the products in the electronic excited states emitting light by the relaxation to the ground states.<sup>28</sup> The relaxation process and mechanism of light emission is the same as PL although the processes to obtain the excited state are different. Moreover, all reacting species are mixed in a homogenous phase. Once the reactions are triggered, light emission is observed in the entire phase. Because the emission intensity is proportional to the concentration of chemical species involved in the chemical reactions, measurement of CL intensity could be use for analytical purposes.<sup>29-31</sup>

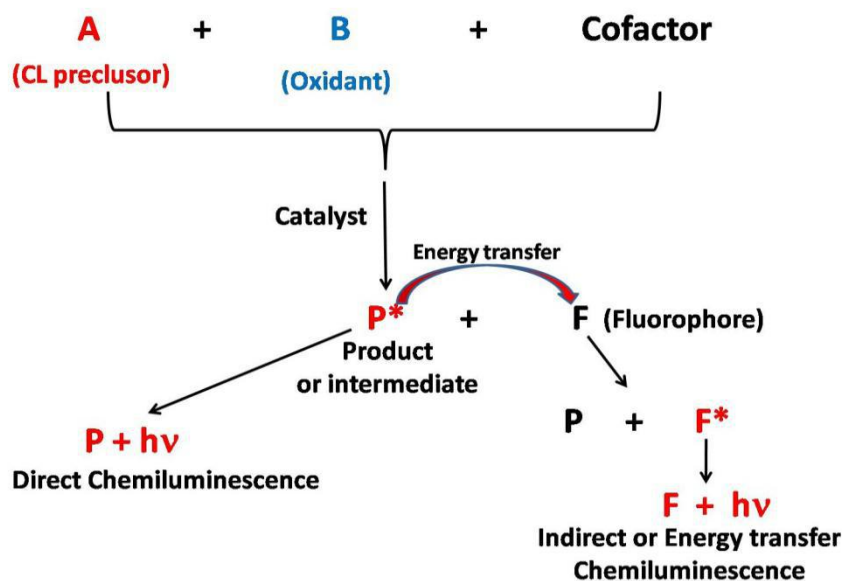


Figure 3. Mechanism of CL reactions

In general, there are two basic mechanisms for CL reactions (Figure 3).<sup>32</sup> In a direct pathway, two reacting species, usually a CL precursor and an oxidant react to generate the product or intermediate. Subsequently, some fractions of the product or intermediate, which is present in an electronically excited state, relax to ground state with emission of a photon. In this process, cofactors sometimes are needed to convert one or more of the precursors into a form capable of reacting and interacting with the catalyst, or to provide an efficient leaving group if bond cleavage is required to produce the excited state. On the other hand, adding catalyst, enzyme or metal ions could reduce the activation energy and create a stable system for producing high CL efficiency. The second pathway is called indirect or energy transfer CL, because this process involves the energy transfer from generated excited state to a different fluorophore that in turn is excited, then releases to its ground state with light emission. This kind of fluorophores can not used for direct CL process. Luminol is one of the most studied and exploited molecule for CL. CL of luminol oxidation could be either performed in aprotic solvents (DMSO, DMF) or protic solvents (water, achohol/water). But the emission lights show different colors, switching from blue light in aqueous solutions to yellow-green in aprotic solvent.<sup>33</sup> Luminol (LH<sub>2</sub>) can be considered as a diprotic acid with  $pK_{A1} = 6$  and  $pK_{A2} = 13$ . In general, CL of luminol

oxidation in protic media occurs in a basic solution (pH 11 – 13) with presence of an oxidant, such as hydrogen peroxide (H<sub>2</sub>O<sub>2</sub>). In the first oxidation step, the prevalent luminol anion (LH<sup>-</sup>) is oxidized to luminol radical anion (LH<sup>•</sup>). This oxidation reaction of luminol also could be achieved by many other one-electron oxidants, such as horseradish peroxidase, cobalt complexes, copper, manganese, iron, and so on. Some free radical species (N<sub>3</sub><sup>•</sup>, CO<sub>3</sub><sup>•-</sup>, ClO<sub>2</sub><sup>•</sup>) are found to be effective for this oxidation. In the second oxidation step, LH<sup>•</sup> is further oxidized to either aminodiazquinone (L) or directly (by superoxide anion) to hydroperoxide adduct (L(O<sub>2</sub>H<sup>-</sup>)). From this adduct, an endoperoxide species can be formed, from which molecular nitrogen is expelled, generating excited state 3-aminophthalate dianion (AP).

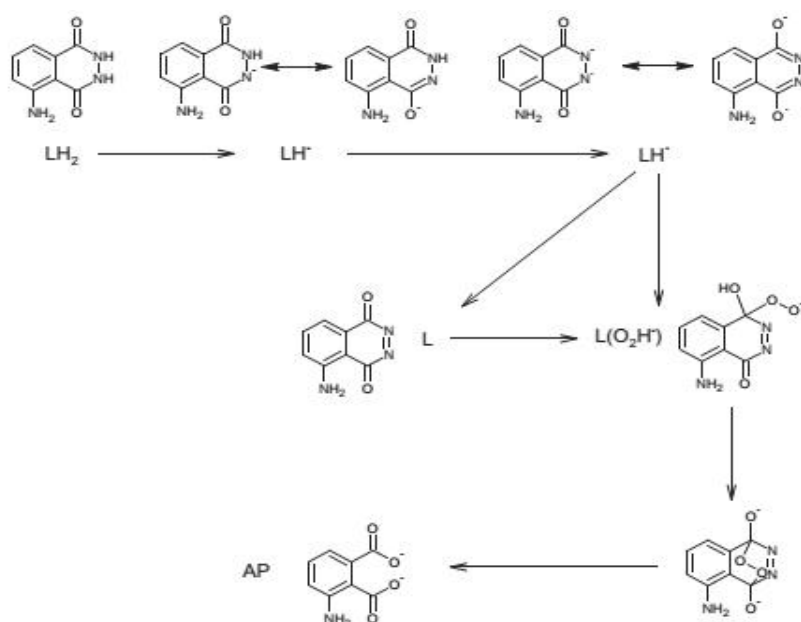


Figure 3. Mechanism of CL luminol oxidation processes.<sup>34</sup>

### 1.3 Fundamentals of ECL

Since ECL is triggered by electron transfer reactions at the electrode surface. Electrochemical behaviors are controlled by the potential applied at the electrode and provide the insights for mechanistic studies. Chronoamperometry(CA) is often used in

ECL. The potential is stepped rather than swept between potentials where the redox processes occur to produce a current  $i$  and ECL signal that vary with time. Cyclic voltammetry (CV) is another powerful tool in ECL. Typically, the potential is applied to the working electrode by sweeping toward a positive direction, or a negative direction. Thus, a current–potential curve ( $i$  vs  $E$ ), which is also called cyclic voltammogram, is obtained for the compound of interest. The corresponding cyclic voltammogram provide an overview of the reduction or oxidation process in the system. For example, the stability of the products can be examined from the CV waves. The reduction of A gives a reduction wave. The reduction formed  $A^{\bullet-}$  can be reoxidized during reverse scan. If  $A^{\bullet-}$  is unstable in the time for traversing the wave at  $v$ , the reverse wave would be absent.<sup>35</sup> During ECL experiment, ECL signal is also plotted as a function of potential forming ECL intensity–potential curve. Illustrations of ECL are done with the comparison of these two curves. ECL mechanisms have been established in two dominant pathways: annihilation and co-reactant pathways. Although ECL produced through co-reactant pathway has been recognized and exploited to great extent in analytical applications, the first ECL study reported in the literature was based on annihilation ECL.

### 1.3.1 Annihilation ECL

An oxidized and a reduced species of the luminophore are electrochemically produced at the electrode surface by applying an alternating pulsed potential. Then, these two species diffuse and undergo an annihilation reaction to generate an electronically excited state. It relaxes to the ground state and emits a photon.

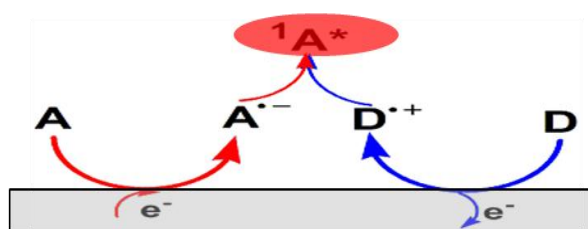
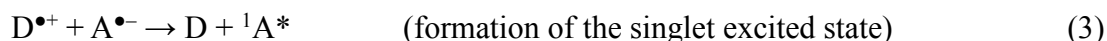
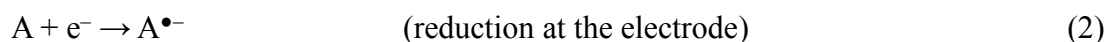
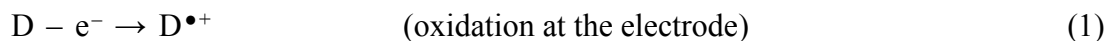
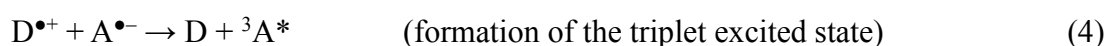


Figure 4. Schematic representation of annihilation ECL.

Therefore, the possible mechanism for the ECL annihilation pathway can be presented as follows:



Or



Where D and A can be the same species,  ${}^1A^*$  is the singlet excited state and  ${}^3A^*$  is the triplet excited state. The enthalpy, which is directly related to the energy available to clarify the involved route for the studied system, can be calculated (Eq. 7) from the redox potentials for the reactions in Eq. 1 and Eq. 2

$$-\Delta H_{ann} \text{ (in eV)} = E^\circ(D^{\bullet+}/D) - E^\circ(A/A^{\bullet-}) - 0.16 \quad (7)$$

$-\Delta H_{ann}$  (in eV) is the enthalpy for annihilation;  $E^\circ$  is the peak potential for the electrochemical oxidation or reduction. The value of 0.16 is the entropy approximation term ( $T\Delta S$ ) estimated to be ~0.1 eV with an addition of 0.057 eV resulting from the difference between two reversible peak potentials of the redox reactions.<sup>36</sup> The values of the energy required to populate the first singlet excited state is given by the equation:

$$E_s \text{ (in eV)} = 1239.8 / \lambda \quad (8)$$

$\lambda$  (in nm) is the wavelength at the maximum fluorescence intensity. If the homogeneous electron-transfer reaction between these electrogenerated species is exergonic enough (*e.g.*,  $-\Delta H_{ann} > E_s$ ), the annihilation process leads directly to the

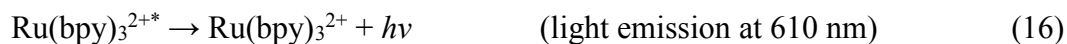
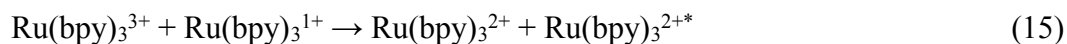
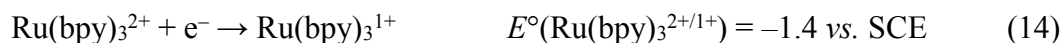
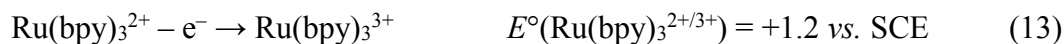
emitting singlet excited state of the luminophore (Eqs. 1–3). In this case with a sufficient available energy, ECL emitted by such a system follows the singlet route, also called “S–route”. This system is called energy sufficient system. If the enthalpy of the annihilation reaction is not sufficient to populate directly the singlet state (*e.g.*,  $E_T < -\Delta H_{ann} < E_S$ ,  $E_T$  is the triplet state energy), the system may follow the “T–route” where the triplet state is first produced (Eq. 4). For such an “energy deficient system”, triplet–triplet annihilation may yield the singlet emitting state in a second step (Eq. 5). If  $-\Delta H_{ann}$  is nearly marginal to  $E_S$ , this system often follows S–T route, where both S–route and T–route can contribute to the formations of the singlet excited state.

A typical example for annihilation ECL of energy sufficient system (following “S–route”) involves 9,10-diphenylanthracene (DPA) in dimethylformamide (DMF). In this experiment, oxidized and reduced radicals of DPA were produced by applying an alternating pulsed potential. The electrochemically generated radicals diffuse and react together, leading to light emission.<sup>5,6</sup>



The oxidation and reduction potentials were determined through cyclic voltammetry before generation of ECL. Thus, the enthalpy for this electron–transfer reaction can be calculated as 3.04 eV according to Eq.7. With its fluorescence peak at 435 nm and 410 nm, the energy required to populate the singlet excited state is calculated to be 2.85 and 3.02 eV, respectively. These electron transfer reactions is exergonic enough, leading directly to the emitting singlet excited state of the luminophore in annihilation process. Another energy sufficient system for annihilation ECL is to use inorganic metal chelate ruthenium (II) tris(2,2'-bipyridine), ( $\text{Ru}(\text{bpy})_3^{2+}$ ) in acetonitrile.<sup>8</sup> The electron transfer reaction has the enthalpy value of ~2.6 eV, whereas the charge-transfer triplet in PL lies at 2.1 eV with emission wavelength 610 nm. The

reaction sequences are detailed as follows:



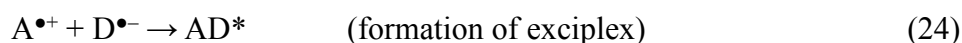
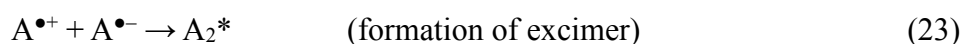
A classic system follows T-route to generate ECL, involving the annihilation reactions in dimethylformamide from two different precursors: DPA/TMPD (TMPD = *N,N,N',N'*-tetramethyl-*p*-phenylenediamine). The triplet excited state of DPA was firstly produced via a “cross-reaction” between the cation radical of TMPD and anion radical of DPA.<sup>37-39</sup>



The enthalpy for the following electron-transfer reaction is calculated to be 1.97 eV which is less than required to reach the emitting single state for DPA (3.02 eV). This system was recognized as energy-sufficient system. The fact lies in that ECL emission was still detected and the emission wavelength is comparable to PL spectra. This indicates that excited singlet state of DPA was the ultimate emitter of ECL electron transfer reactions. Since the system cannot populate directly the singlet excited state, the proposed mechanism involves the formation of additional triplet intermediates, following by triplet-triplet annihilation to generate the excited singlet state.<sup>40</sup>



It is also possible to produce ECL *via* a mixed S and T route mechanism (“S–T route”) in the case of annihilation of rubrene.<sup>41,42</sup> The energy released from the rubrene ion annihilation is close to the energy of the rubrene singlet (2.30 eV). The system is capable to produce both the singlet and triplet excited states, together contributing to ECL emission. In addition to forming singlet and triplet excited states, annihilation reactions in most of the planar polycyclic aromatic hydrocarbons (such as pyrene and perylene) could lead to the generation of excimers and exciplexes. ECL emission from the excimers or exciplexes are said to follow “E–route”.<sup>43-46</sup>



Annihilation ECL has been extensively studied with various systems and applied in light-emitting electrochemical cells (LECs). Given the energy for visible range emission (400 to 700 nm) which range from 3.1 to 1.8 eV, it indicates that the applied potential window should be wide enough from ~3.3 to 2 V. So the major limitation to extend the range of application is that annihilations occur in rigorous conditions, such as highly purified organic solvent, under the inert gas atmosphere. Besides, both anion radicals and cation radicals generated at the electrode should be stable enough to undergo the annihilation reactions.

### 1.3.2 Co-reactant ECL

An alternative method for ECL generation with more complex kinetic mechanisms is based on the use of a sacrificial co-reactant. Upon electrochemical oxidation or reduction at the electrode, intermediates formed from the co-reactant decompose to produce a strong reducing or oxidizing species that are capable to react with the oxidized or reduced luminophores to generate the excited states. Depending on the the applied potential on the electrode, co-reactant ECL is formally divided into two type:

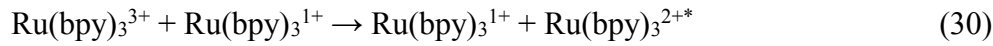
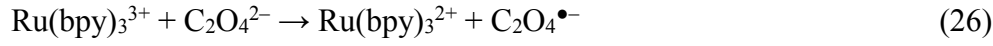
oxidative reduction ECL and reductive oxidation ECL, respectively. In oxidative reduction ECL, oxidation of co-reactant produces strong reducing intermediate, while it would generate strong oxidizing intermediate upon the reduction of co-reactant in reductive oxidation mechanism. The co-reactant ECL exhibits distinct advantages over the annihilation ECL: (a) no need of wide potential window and aqueous solution can be also used; (b) the co-reactant ECL can be generated for some luminophores that have only one reversible reduction or oxidation; (c) presenting more intense ECL emission; (d) negative oxygen quenching effect which frequently encountered in ion annihilation reaction.<sup>3</sup>

Due to its applicability in both organic and aqueous conditions, the discovery of co-reactant ECL has attracted large interests in different fields. Particularly, it has been used in a wide range of analytical applications. Because ECL emission intensity is usually proportional to the concentration of the co-reactant and luminophore, co-reactant ECL can be used in the analysis of various species, including co-reactant, luminophore, or other target species correlated to ECL intensity.<sup>47</sup> Such properties make it an essential part for developing commercial ECL analytical instruments. More and more researches focus on the investigations of the mechanism in co-reactant ECL system, in which they try to design and select new coreactants and luminophore species, then improving the sensitivity and reproducibility of the ECL system. In this section, commonly used co-reactants ECL system and relevant ECL mechanisms are reviewed. For example, ruthenium (II) tris(2,2'-bipyridine)  $\text{Ru}(\text{bpy})_3^{2+}$ , or other related derivatives are used as the emitting species to generate ECL with different co-reactants.

### 1.3.2.1 Oxidative–reduction ECL

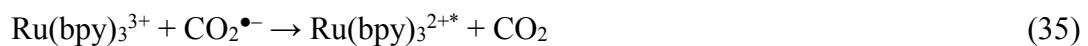
Oxalate was the first co-reactant discovered for ECL by Bard and co-workers, and its related mechanism was demonstrated in acetonitrile,<sup>48</sup> and later primarily upon  $\text{Ru}(\text{bpy})_3^{2+}$  and oxalate in aqueous solutions.<sup>9,49-52</sup> In the latter case, oxidation of oxalate would produce oxalate anion radicals ( $\text{C}_2\text{O}_4^{\bullet-}$ ), which is then followed by a

chemical decomposition to form a highly reducing intermediate ( $\text{CO}_2^{\bullet-}$ ,  $E^\circ=1.9$  V vs. NHE) to react with electrochemically formed  $\text{Ru}(\text{bpy})_3^{3+}$  at the electrode to generation ECL emission. The corresponding mechanism was described in Eqs. (25) – (31).



By applying the anodic potential,  $\text{Ru}(\text{bpy})_3^{2+}$  is firstly oxidized to  $\text{Ru}(\text{bpy})_3^{3+}$  at the electrode surface. This cation is then capable of oxidizing the oxalate ( $\text{C}_2\text{O}_4^{2-}$ ) in the diffusion layer close to the electrode surface to form an oxalate radical anion ( $\text{C}_2\text{O}_4^{\bullet-}$ ) which decomposes to a highly reducing anion radical ( $\text{CO}_2^{\bullet-}$ ) and carbon dioxide. The excited state  $\text{Ru}(\text{bpy})_3^{2+*}$  could be obtained by direct reaction between ( $\text{CO}_2^{\bullet-}$ ) and oxidized  $\text{Ru}(\text{bpy})_3^{3+}$ . On the other hand, ( $\text{CO}_2^{\bullet-}$ ) could also reduce the remained available  $\text{Ru}(\text{bpy})_3^{2+}$  to  $\text{Ru}(\text{bpy})_3^{1+}$  that is then possible to annihilate with  $\text{Ru}(\text{bpy})_3^{3+}$  to generate the excited state.

In the acetonitrile system, oxalate has been found to be easier to oxidize than  $\text{Ru}(\text{bpy})_3^{2+}$  complex.<sup>48</sup> Oxalate is firstly electrochemical oxidized to the oxalate anion radicals that decompose to reducing anion radical ( $\text{CO}_2^{\bullet-}$ ). Same excited state could be produced by the reaction between ( $\text{CO}_2^{\bullet-}$ ) and oxidized  $\text{Ru}(\text{bpy})_3^{3+}$ .

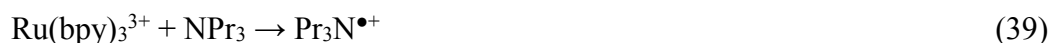


Another typical example of the “oxidative-reductive” ECL is based on the popular model  $\text{Ru}(\text{bpy})_3^{2+}/\text{TPrA}$  system, which is currently the basis of the commercial ECL immunoassays and DNA probes.<sup>53</sup> The mechanism of this system is relative complex and has been elucidated in detail in many reports.<sup>10,11,54-58</sup> According to the reported works on the ECL emission from  $\text{Ru}(\text{bpy})_3^{2+}/\text{TPrA}$  system, the proposed mechanism can be described by the following reactions:

Acid–base equilibrium:



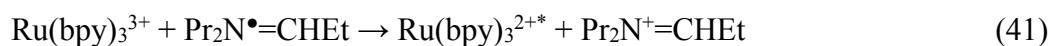
Oxidation step:



Deprotonation:



Excited state formation 1:

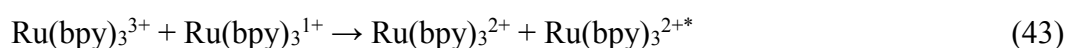
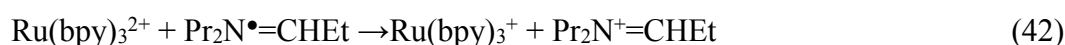


(Where Pr =  $\text{CH}_3\text{CH}_2\text{CH}_2-$  and Et =  $\text{CH}_3\text{CH}_2-$ )

This experiment was performed on a gold electrode in a buffer solution containing TPrA and  $\text{Ru}(\text{bpy})_3^{2+}$ . In aqueous system, the optimum pH value of the buffer solution with TPrA is usually about 7–8 for ECL analysis. In the anodic part of the scanning, both  $\text{Ru}(\text{bpy})_3^{2+}$  and TPrA ( $\text{NPr}_3$ ) are oxidized (Eqs. 37–38). The oxidation of TPrA results in a broad wave due to preceding acid–base equilibrium (Eq. 36) ( $pK_a \sim 10.4$ ). According to the ECL curve and cyclic voltammogram recorded simultaneously, it was found that the ECL emission also tracks the current for the oxidation of TPrA. Upon the oxidation, the short-lived TPrA cation radical  $\text{TPrA}^{\bullet+}$  is losing a proton from an  $\alpha$ -carbon to form the strongly reducing species  $\text{TPrA}^{\bullet}$  (Eq. 40), and then reduces  $\text{Ru}(\text{bpy})_3^{3+}$  to the excited state  $\text{Ru}(\text{bpy})_3^{2+*}$  (Eq. 41). Despite the direct oxidations on the electrode surface, ( $\text{TPrA}^{\bullet+}$ ) can be produced by electrocatalytic

pathway involving the homogeneous oxidation of TPrA and  $\text{Ru}(\text{bpy})_3^{3+}$  (Eq. 39). The contribution of both routes depends on relative concentration of  $\text{Ru}(\text{bpy})_3^{2+}$  and TPrA as well as the factors for the potential and rate of direct oxidation of TPrA at the electrode.<sup>54,59</sup> On the other hand, highly active species  $\text{TPrA}^\bullet$  can also reduce the un-oxidized remained  $\text{Ru}(\text{bpy})_3^{2+}$  to  $\text{Ru}(\text{bpy})_3^+$  which can then react with  $\text{Ru}(\text{bpy})_3^{3+}$  to produce the excited state  $\text{Ru}(\text{bpy})_3^{2+*}$  in annihilation pathway.

Excited state formation 2:



The contribution of this process to the overall ECL intensity depends upon the  $\text{Ru}(\text{bpy})_3^{2+}$  concentration and is not favored when  $\text{Ru}(\text{bpy})_3^{2+}$  concentration is low. It was found that the ECL emission vs potential curves showed two waves when low concentration of  $\text{Ru}(\text{bpy})_3^{2+}$  (nM –  $\mu\text{M}$ ) and high concentration of TPrA (10 – 100 mM) were used in buffer solution.<sup>11</sup> The second peak appears at the potential which can attribute to the oxidation of  $\text{Ru}(\text{bpy})_3^{2+}$ .

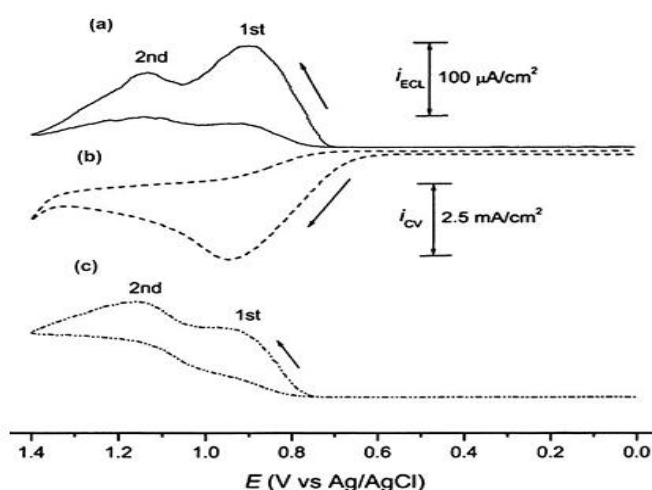
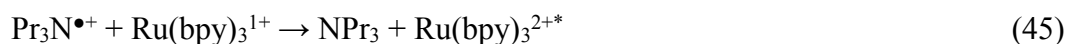
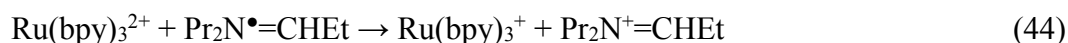


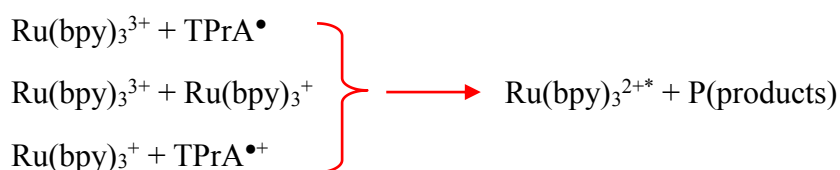
Figure 5. (a) ECL and (b) cyclic voltammogram of 1 nM  $\text{Ru}(\text{bpy})_3^{2+}$  in the presence of 0.1 M TPrA with 0.1 M Tris/0.1 M  $\text{LiClO}_4$  buffer (pH 8) at a 3 mm diameter glassy carbon electrode at a scan rate of 50 mV/s. (c) As in (a) but with 1.0  $\mu\text{M}$   $\text{Ru}(\text{bpy})_3^{2+}$ . The ECL intensity scale is given for (c) and was multiplied by 100 for (a).<sup>11</sup>

But the first one occur at a low oxidation potential (LOP) that is just positive enough to oxidize only TPrA. ECL emission at LOP cannot be explained by the above discussed mechanisms, because LOP is not positive enough to oxidize  $\text{Ru}(\text{bpy})_3^{2+}$ .<sup>54</sup> However, Miao and Bard has proposed a new mechanism to illustrate ECL emission at LOP.<sup>11</sup> The process involves the direct oxidation of TPrA to produce  $\text{TPrA}^{\bullet+}$  and  $\text{TPrA}^\bullet$  at the electrode. The following reaction between  $\text{TPrA}^\bullet$  and  $\text{Ru}(\text{bpy})_3^{2+}$  generates  $\text{Ru}(\text{bpy})_3^+$  which could react with  $\text{TPrA}^{\bullet+}$  to form the excited state  $\text{Ru}(\text{bpy})_3^{2+*}$ . The ECL emission at LOP is more favorable for DNA diagnostic applications because oligonucleotide sequences would be irreversibly damaged at potentials above +1.0 V vs. SCE.<sup>60</sup>

Excited state formation 3:



Therefore, the excited state of  $\text{Ru}(\text{bpy})_3^{2+}$  can be obtained by three different routes: 1)  $\text{Ru}(\text{bpy})_3^{3+}$  reduction by  $\text{TPrA}^\bullet$ ; 2)  $\text{Ru}(\text{bpy})_3^{3+}$  and  $\text{Ru}(\text{bpy})_3^+$  annihilation reaction, and 3)  $\text{Ru}(\text{bpy})_3^+$  oxidation by  $\text{TPrA}^{\bullet+}$  presented as following equations.



There are several factors that could affect the ECL intensity of the  $\text{Ru}(\text{bpy})_3^{2+}$  / TPrA system: (1) pH of the solution. ECL intensity of the system depends on pH value. The ECL intensity increase dramatically when pH is above 5.5, then reaching at maximum value at pH=7.5. But pH value higher than 9 should not be used because of large ECL background signal produced by the reaction between  $\text{Ru}(\text{bpy})_3^{3+}$  and hydroxide ions;<sup>53</sup> (2) material of the working electrode. ECL intensity was found to be much higher at the glassy carbon electrode (GCE) than gold (Au) and platinum (Pt) electrode in

aqueous solution. GC electrode promote the oxidation rate of TPrA, while the formation of anodic oxide layers on Au and Pt electrode surface can block it significantly.<sup>61</sup> The enhancement of the TPrA oxidation could lead to an increase in the ECL intensity; (3) Properties of the electrode surface. It was found that hydrophobic electrode surface could facilitate the oxidation of the TPrA, and then induced the increase in the ECL intensity.<sup>54</sup> For examples, by adding some non-ionic surfactants such as Triton X-100 into the solution, ECL intensity increased significantly at the Au and Pt electrodes.<sup>62,63</sup> Moreover the modification at the Pt and Au electrode surface with thiol mono layers leads to the enhanced ECL intensity.<sup>64,65</sup> Such phenomenon can be explained by the fact that the electrode surface becomes hydrophobic, resulting in the absorption of neutral TPrA at the surface and thus facilitating the direct oxidation of TPrA; (4) dissolved O<sub>2</sub> in the solution. Quenching effect by the dissolved O<sub>2</sub> on the ECL intensity is observed when low concentrations (< 20 mM) of TPrA are used, particularly significant influence on the first ECL wave. At the low TPrA concentration condition, oxidation of TPrA could produce a relatively small amount of reducing species TPrA•. The dissolved O<sub>2</sub> which acts as a quencher destroys the intermediates before they participate in the ECL reaction, which leads to the obvious decrease of the emission intensity;<sup>66</sup> (5) the polarity of the solvents. Considering hydrogen bonding and dipole forces, they can dramatically change the ground and excited state properties of Ru(bpy)<sub>3</sub><sup>2+</sup>. It is possible to enhance the ECL intensity by increasing the polarity of the solvents. For example, ECL enhancement up to 270 folds is found on Ru(bpy)<sub>3</sub><sup>2+</sup> in the solution containing 30% of 2,2,2-trifluoroethanol.<sup>67</sup>

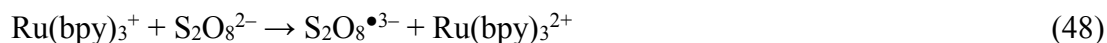
A wide range of amine compounds can also be used as co-reactants in the Ru(bpy)<sub>3</sub><sup>2+</sup> / amine system. Among them, the ECL intensity increases by the following order: primary < secondary < tertiary amines.<sup>10,68</sup> However, the substituent properties of amine compounds have influences on the ECL emission. Generally, electron-donating groups tend to enhance the ECL intensity, while electron-withdrawing ones have the opposite effect.<sup>69</sup> But there is one exceptional case in which ECL intensity enhance significantly by using 2-(dibutylamino)ethanol (DBAE) as co-reactant.<sup>70</sup> The

interesting fact lies in that DBAE contains the electron-withdrawing hydroxyethyl group; on the other hand, the catalytic effect of hydroxyethyl favors the direct oxidation of DBAE at the electrode, which could enhance ECL efficiency of Ru(bpy)<sub>3</sub><sup>2+</sup> / DBAE system. Particularly, it was found that the ECL intensity of the Ru(bpy)<sub>3</sub><sup>2+</sup> / DBAE system at Au and Pt electrode is almost 10 and 100 times greater than that of Ru(bpy)<sub>3</sub><sup>2+</sup> / TPrA system, respectively. Since DBAE is also an aliphatic tertiary amine analogous to TPrA, the ECL of the Ru(bpy)<sub>3</sub><sup>2+</sup> / DBAE system follows similar mechanisms as in the Ru(bpy)<sub>3</sub><sup>2+</sup> / TPrA system. In comparison with TPrA, DBAE is less toxic, more soluble and less volatile.<sup>71</sup> These excellent properties make it promising co-reactant for ECL immunoassays and DNA probes.<sup>72</sup>

### 1.3.2.2 Reductive–oxidation ECL

Persulfate is the first reductive–oxidation co-reactant for ECL studies introduced by Bolletta *et al.*<sup>73</sup> and then Bard *et al.*,<sup>74</sup> respectively. But it was found that ECL of the Ru(bpy)<sub>3</sub><sup>2+</sup> / S<sub>2</sub>O<sub>8</sub><sup>2-</sup> system was not stable in aqueous solutions. In order to produce intense ECL emission, MeCN–H<sub>2</sub>O mixed solutions were chosen to protect the unstable Ru(bpy)<sub>3</sub><sup>1+</sup> on the other hand would not affect the solubility of (NH<sub>4</sub>)<sub>2</sub>S<sub>2</sub>O<sub>8</sub> used for ECL. By applying cathodic potential, S<sub>2</sub>O<sub>8</sub><sup>2-</sup> can be reduced directly or with generated Ru(bpy)<sub>3</sub><sup>+</sup> to form S<sub>2</sub>O<sub>8</sub><sup>•3-</sup> at the electrode. These anion radicals undergo chemical decomposition to produce strong oxidizing specie SO<sub>4</sub><sup>•-</sup>, which then oxidize with Ru(bpy)<sub>3</sub><sup>+</sup> to generate the excited state Ru(bpy)<sub>3</sub><sup>2+\*</sup>. On the other hand, another possible route for producing the excited state involves the oxidation reaction between SO<sub>4</sub><sup>•-</sup> and Ru(bpy)<sub>3</sub><sup>+</sup> to produce Ru(bpy)<sub>3</sub><sup>3+</sup>, then follows by annihilation to give the excited state. Since the ECL of Ru(bpy)<sub>3</sub><sup>2+</sup> / S<sub>2</sub>O<sub>8</sub><sup>2-</sup> system is usually produced by applying a very negative potential, bismuth electrodes are used in the system to avoid serious hydrogen evolution during the experiments.<sup>75</sup>





As for ECL in organic solvent system, acetonitrile is suggested as the best overall non-aqueous solvent on the basis of its wide potential window ( $-2.3$  to  $+2.0$  vs. SCE) and its relative non-toxicity.<sup>36</sup> Benzoyl peroxide (BPO) is a good co-reactant for the generation of ECL due to its high stability and solubility in MeCN. The ECL of  $\text{Ru}(\text{bpy})_3^{2+}$ /BPO system was studied in acetonitrile solution with 0.1M tetra-n-butylammonium perchlorate (TBAP) as supporting electrolyte.<sup>76</sup>

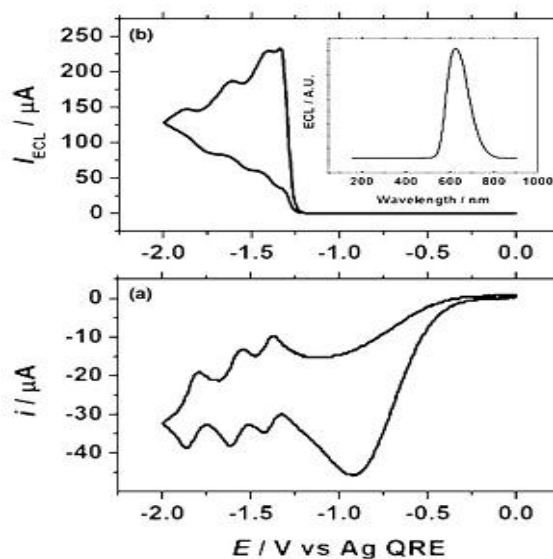
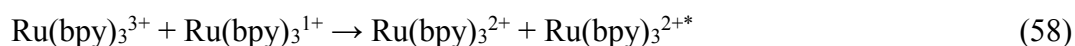
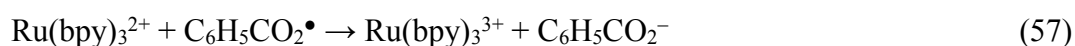
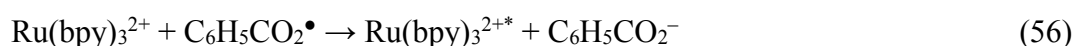


Figure 6. (a) Cyclic voltammogram and (b) ECL curve of 1.0 mM  $\text{Ru}(\text{bpy})_3^{2+}$  and 5 mM BPO in acetonitrile solutions containing 0.1 M TBAP. Inset in (b) is the ECL spectra recorded under the same condition.<sup>76</sup>

When the electrode potential was scanning toward the cathodic direction, BPO was reduced to  $\text{BPO}^{\bullet -}$  at the electrode, and this anion radical  $\text{BPO}^{\bullet -}$  subsequently decomposed to benzoate anion and a strong oxidizing agent benzoate radical ( $\text{C}_6\text{H}_5\text{CO}_2^{\bullet}$ ). The benzoate radical is energetic enough to react with  $\text{Ru}(\text{bpy})_3^{2+}$  to

form the excited states, because the redox potential value for the ( $\text{C}_6\text{H}_5\text{CO}_2^\bullet / \text{C}_6\text{H}_5\text{CO}_2^-$ ) couple is +1.5 V vs. SCE.<sup>77</sup> Three reversible reduction waves were measured at +1.42, +1.61, and +1.88 V vs Ag quasi-reference electrode in CV, corresponding to generation of  $\text{Ru}(\text{bpy})_3^+$ ,  $\text{Ru}(\text{bpy})_3^0$  and  $\text{Ru}(\text{bpy})_3^-$ , respectively. ECL emission occurred when  $\text{Ru}(\text{bpy})_3^{2+}$  was reduced, and continued at the potential where  $\text{Ru}(\text{bpy})_3^0$  and  $\text{Ru}(\text{bpy})_3^-$  were generated. However, only the first ECL produced at the potential of the  $\text{Ru}(\text{bpy})_3^{2+/+}$  couple is considered here for proposing the related ECL mechanism.



## 1.4 Luminophores of ECL

Generally, ECL luminophores can be divided into three categories: 1) inorganic complexes, mainly consisting of different organometallic complexes; 2) organic molecules, which include polycyclic aromatic hydrocarbons; and 3) nanoparticles, such as semiconductor quantum dots (QDs), gold nano-clusters, and carbon dots (CDs). However, there are still a lot of efforts focusing on exploiting new types of ECL luminophores to meet the fast developing analytical applications.

### 1.4.1 Inorganic complexes

$\text{Ru}(\text{bpy})_3^{2+}$  and its derivatives are the well-known and most used ECL luminophores. This can be attributed to their excellent luminescent properties and tunable solubility in a variety of aqueous and non-aqueous solvents at room temperature, and more

importantly the capability to undergo reversible one electron-transfer reactions at mild potentials.<sup>4</sup>

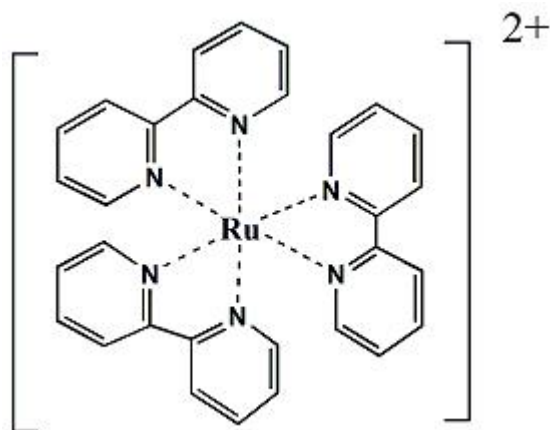


Figure 7. Chemical structure of Ru(bpy)<sub>3</sub><sup>2+</sup>.

Ru(bpy)<sub>3</sub><sup>2+</sup> complex exhibits a yellow-orange colour with the typical absorption wavelength  $\lambda_{\text{Abs}}$  at 454 nm and the emission wavelength  $\lambda_{\text{em}}$  at 610 nm.<sup>62</sup> In the Ru(bpy)<sub>3</sub><sup>2+</sup> structure, Ru is surrounded by coordination bonding with three bidentate polypyridine ligands (bpy). These ligands are colorless molecules possessing  $\sigma$ -donor orbitals localised on the nitrogen atoms and  $\pi$ -donor and  $\pi^*$ -acceptor orbitals more or less delocalised on aromatic rings.<sup>78</sup> Ru<sup>2+</sup> is a  $d^6$  system with electron configuration [Kr]4d<sup>6</sup>. The electronic situation for this configuration in octahedral symmetry (D<sub>3</sub>) is depicted as in the simplified molecular orbital diagram. One electron excitation from a  $\pi_{\text{M}}$  metal orbital to the  $\pi_{\text{L}}$  ligand orbitals gives rise to the metal-to-ligand charge transfer (MLCT) excited states, whereas promotion of an electron from  $\pi_{\text{M}}$  to  $\sigma_{\text{M}}$  orbitals produce the metal centered (MC) excited states. The ligand centered (LC) excited states are obtained by promoting an electron from  $\pi_{\text{L}}$  to  $\pi^*_{\text{L}}$ .<sup>54,78</sup>

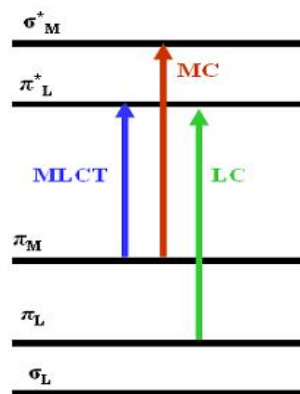


Figure 8. Simplified representation of molecular orbital diagram for  $\text{Ru}(\text{LL})^{2+}$  complexes in octahedral symmetry for the three types of electronic transitions occurring at low energies.

But it is difficult to tune the PL properties of Ru complexes due to the limited ligand-field splitting energies of central metal ions of Ru complexes.<sup>1</sup> Most of the Ru complexes have a maximum emission wavelength between 600 and 650 nm. By introducing two reactive acrylate moieties on the bidentate polypyridine ligands, the emission wavelength can be tuned ranging from 640 to 700 nm.<sup>79</sup> The large red shift in the emission wavelength is probably related to a decrease in their ligand based lowest unoccupied molecular orbital (LUMO) value and the resulting lower energy triplet MLCT excited state transitions. On the other hand, these two reactive acrylate moieties allows the polymerization of insoluble film upon thermal cross-linking, which makes them promising materials for electrochromic devices.

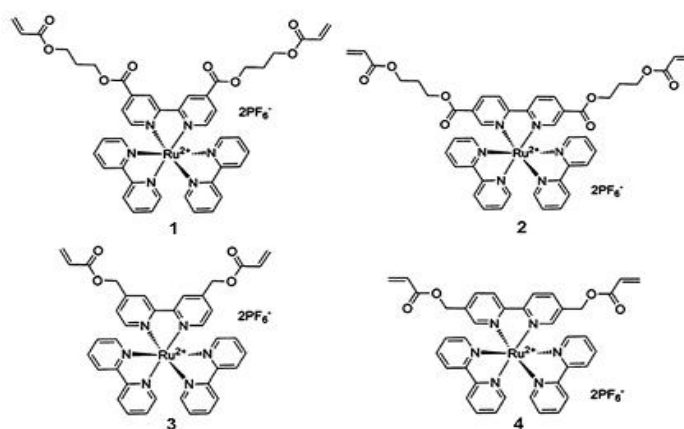


Figure 8. Structures of Ru complexes containing acrylate groups.<sup>79</sup>

Besides, many attempts have been made in designing or modifying the ligands of Ru

complexes to improve its molecular recognition ability for inorganic, organic, or bio-molecular detections. For examples, a new type of  $\text{Ru}(\text{bpy})_2(\text{CE-bpy})^{2+}$  complex was prepared by grafting the crown ether moiety in one (bpy).<sup>80</sup> The recognition reaction between  $\text{Na}^+$  and crown ether moiety could result in a significant increase in ECL intensity. The enhancement of ECL intensity was said to be due to decreased steric repulsion within the disubstituted bipyridine upon binding of  $\text{Na}^+$ . In the same time, another  $(\text{bpy})_2\text{Ru}(\text{AZA-bpy})^{2+}$  (AZA-bpy = 4-(N-aza-18-crown-6-methyl-2,2'-bipyridine) was also reported that its ECL efficiency could be tuned with the presence of  $\text{Pb}^{2+}$ ,  $\text{Hg}^{2+}$ ,  $\text{Cu}^{2+}$ ,  $\text{Ag}^+$  and  $\text{K}^+$ , respectively.<sup>81</sup>

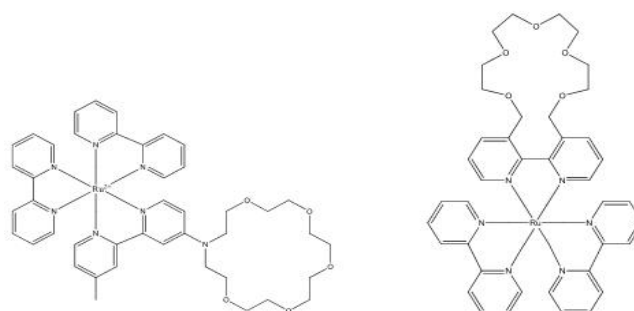


Figure 9.  $\text{Ru}(\text{bpy})_2(\text{CE-bpy})^{2+}$  (left) and  $(\text{bpy})_2\text{Ru}(\text{AZA-bpy})^{2+}$  (right).<sup>80,81</sup>

ECL label  $[\text{Ru}(\text{bpy})_2\text{dppz}]^{2+}$  for bio-molecules was also developed for DNA detection by Xu *et al.*<sup>82</sup> The ECL intensity of  $[\text{Ru}(\text{bpy})_2\text{dppz}]^{2+}$  / oxalate system increased about 1000 times when the complex intercalates to DNA while it exhibited negligible ECL without DNA. Such switch behavior could attribute to the intercalation that shielded the phenazine nitrogens from the solvent and resulted in an excited state.

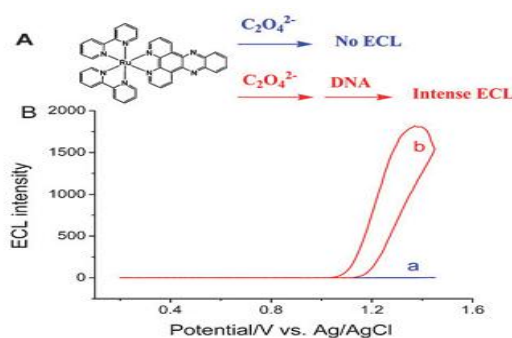


Figure 10. A) Scheme of ECL switch based on  $[\text{Ru}(\text{bpy})_2\text{dppz}]^{2+}$  and DNA; B) ECL curves of

[Ru(bpy)<sub>2</sub>dppz]<sup>2+</sup> / oxalate system without DNA(a) and with DNA(b).<sup>82</sup>

Despite of the great success of Ru complexes in most of the ECL applications, iridium (Ir) complexes have gained a lot of attentions in the past few years. The advantage over Ru complexes is that they have higher ligand-field splitting energies of the trivalent iridium ion. As a result, multi-colored ECL systems can be realized upon Ir complexes due to the versatility for color tuning.<sup>1</sup> Depending on ligands and the structure, Ir complexes can be classified into three different groups. The first group of complexes have a common formula of (pq)<sub>2</sub>Ir(L), in which pq is a 2-phenylquinoline anion and L is either acetylacetonate (acac) or picolinate (pico).<sup>83</sup> In electrochemistry, these Ir complexes show one electron oxidation wave around +1.0 V vs. SCE and the first reduction wave ranging from -1.45 to -1.70 V vs. SCE in MeCN. Since most oxidized and reduced forms of these Ir complexes are stable, ECL can be produced by either annihilation pathway or co-reactant pathway. Some of them exhibit extremely high ECL efficiency. For example, the ECL of (pq)<sub>2</sub>Ir(acac) / TPrA system is up to 77 times higher than that of the Ru(bpy)<sub>3</sub><sup>2+</sup> / TPrA system under the same conditions.<sup>83</sup> But emission wavelength is similar to Ru(bpy)<sub>3</sub><sup>2+</sup>. The second group of complexes consist of [(ppy)<sub>2</sub>Ir(L)]<sup>+</sup> configuration.<sup>84</sup> By different chemical modifications on the ligands of this group, many blue/green ECL emitters were reported.<sup>85,86</sup> The introducing of electron withdrawing fluorine into the cyclometalated ligand can stabilize the highest occupied molecular orbital (HOMO), resulting in efficient blue-shifted emission, but at the same time decreasing the stability of the complexes. To overcome this drawback, methoxy and methyl-substituted 2,3'-bipyridine as the cyclometalated ligands were used.<sup>87</sup> These new compounds have maximum emission wavelength at around 450 nm. Green ECL emitters was firstly reported on Ir(ppy)<sub>3</sub> complexes in 2002.<sup>88</sup> But ECL intensity of Ir(ppy)<sub>3</sub> complexes is lower than Ru(bpy)<sub>3</sub><sup>2+</sup> under the same conditions. To improve ECL efficiency, bpy and phen ligands were introduced to form [(ppy)<sub>2</sub>Ir(bpy)]<sup>+</sup> and [(ppy)<sub>2</sub>Ir(phen)]<sup>+</sup> complexes.<sup>84</sup> ECL intensities for these complexes were found to be six and twelve times greater than that of Ir(ppy)<sub>3</sub> in polar organic solvents using TPrA as a co-reactant due to

accelerating the generation of TPrA<sup>•+</sup>. The third group of the structure configuration can be described as L<sub>2</sub>Ir(acac). Emission wavelengths of the L<sub>2</sub>Ir(acac) complexes ranges widely from 490 nm to 640 nm with color from fairly green to deep red.<sup>89,90</sup> As a result, they are useful for the fabrication of display devices and multiplexing analysis based on ECL. In addition to changing the nature of ligands, multi-colors ECL system can also be achieved by changing frequency of the applied current or assembling a self-co-reactant.<sup>91-93</sup>

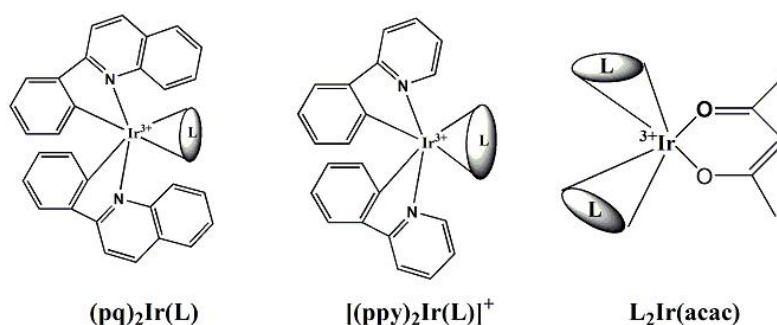


Figure 11. Iridium complexes for ECL.<sup>3</sup>

ECL of other organometallic complexes have also been reported, containing different metal core such as Ag, Al, Au, Cd, Cr, Cu, Eu, Hg, Mo, W, Os, Pd, Pt, Re, Tb, and Tl.<sup>4</sup> The major challenges for using the organometallic complexes are the toxicity to the environment and the cost for intense uses in analysis.

## 1.4.2 Organic molecules

The first detailed ECL was actually performed on 9,10-diphenylanthracene (DPA).<sup>5,6,94</sup> DPA, rubrene and pyrene, are termed as polycyclic aromatic hydrocarbons (PAHs) that have been used widely for early ECL theories investigations. Interestingly, organic nanoparticles of DPA and rubrene were also prepared in an aqueous phase using a simple reprecipitation method for ECL studies.<sup>95,96</sup> ECL emission from these NPs was produced by oxidative–reduction way in aqueous solutions containing co-reactant tri-n-propylamine for rubrene NPs and oxalate for DPA NPs. It was found that ECL intensity of rubrene NPs was much

higher than that from DPA NPs due the smaller size of rubrene NPs so that a higher diffusion coefficient on rubrene NPs. Recently, new polycyclic aromatic hydrocarbons (**FDF**, **FPF**, **FAF**) were prepared by capping a DPA derivative, pyrene and anthracene, with two spirobifluorene derivatives.<sup>97</sup> These new aromatic hydrocarbons presented very interesting ECL behaviors with blue emission. The ECL measured for FDF was almost as intense as that of DPA under the same conditions. Such efficient ECL in the organic compounds is related to the introduction of spirobifluorene groups, which can stabilize the PAH core.

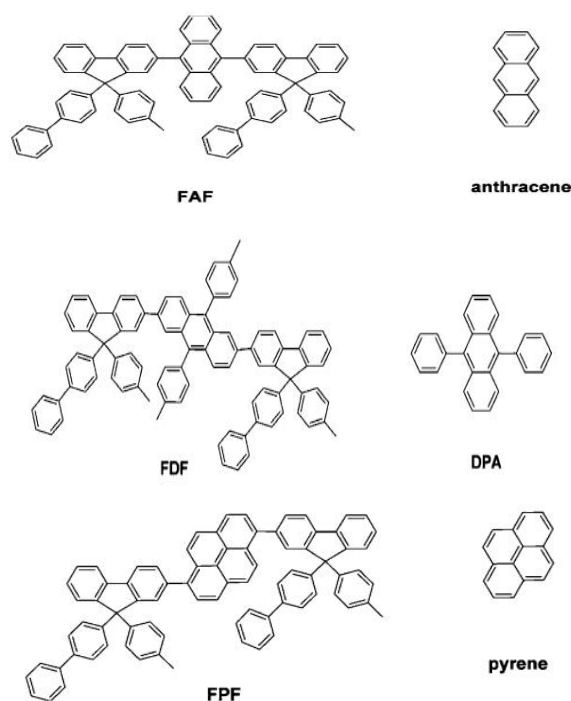


Figure 12. Chemical structures of new aromatic compounds and PAH core.<sup>97</sup>

Indeed, spirobifluorene has two fluorene units connected through the spiro-carbon atom. This spatial configuration results in strong rigidity and increasing the stability of the system. Many other spirobifluorene based molecules were synthesized upon the spirobifluorene as the  $\pi$ -bridge core, and then attaching different acceptors (A) and donors (D) to the core symmetrically to tune the emission of the molecular system. Blue emission spirobifluorene derivatives were synthesized by capping directly two triphenylamine groups as donors to the core forming a D- $\pi$ -D configuration.<sup>98</sup> ECL

emission from annihilation reaction was higher than DPA under the similar conditions in DMF solution. Intense ECL emission was also observed by using BPO as co-reactant. On the contrary, the emission color can be tuned to the green region by introducing the two electron-deficient 2,1,3-benzothiadiazole (BTA) groups as acceptors into the spirobifluorene core forming a A- $\pi$ -A configuration.<sup>99</sup> This spirobifluorene-based molecule shows interesting electrochemical behaviors in CV, which exhibits two reversible oxidation peaks and three reversible reduction peaks. Thus strong annihilation ECL was produced by applying an alternating pulsing potential. Its intensity is almost the same as that of the reference compound DPA. Further tuning the emission to red color ( $\lambda_{em}=621\text{nm}$ ) was also reported by end-capping two triphenylamine groups as donors to BAT forming the overall D-A- $\pi$ -A-D structure.<sup>100</sup> The anion radical and cation radical of the molecule is highly stable existing in the mixed MeCN/benzene solution upon electrochemical reduction and oxidation. ECL with red emission is so intense that it could be seen in a well-lit room upon annihilation reaction. Well-dispersed organic nanoparticles of this compound were also prepared by the reprecipitation in water. Then ECL of these organic nanoparticles was generated *via* the oxidation of both TPrA coreactant and nanoparticles simultaneously.

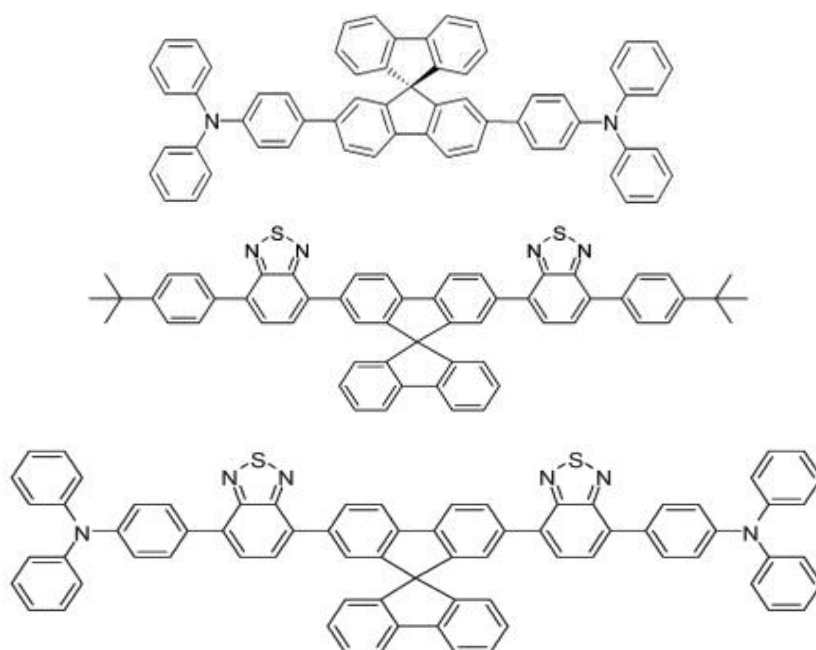


Figure 13. Spirobifluorene based molecules with D- $\pi$ -D, A- $\pi$ -A and D-A- $\pi$ -A-D configurations (From top to bottom).<sup>98-100</sup>

Boron dipyrromethene (BODIPY) dyes are also important organic compounds for ECL investigations due to their unique spectroscopic and electrochemical properties comparable to those of aromatic hydrocarbons.<sup>101</sup> Some of BODIPY dyes have been commercialized for the applications as laser dyes and for biological labeling experiments of DNA, proteins, and lipids.<sup>102,103</sup> The electrochemical, PL and ECL properties of these BODIPY dyes can be tuned easily by the nature of the substituent in the *meso*,  $\alpha$  and  $\beta$  positions of the core structure.<sup>101</sup>

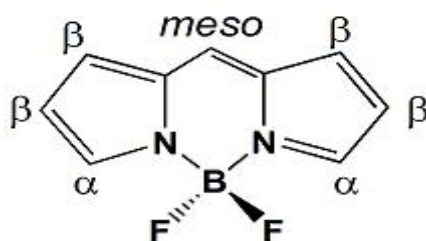


Figure 14. Core structure of BODIPY.

The reversibility of the electrochemical oxidation or reduction of BODIPY strongly depends on the substituent. Basically, the oxidation of BODIPY dyes occurs at mild potentials ranging from +0.72 V to +1.57 V vs. SCE, while the reduction takes place at potentials from -0.37 V to -1.57 V vs. SCE.<sup>101</sup> So the generation of ECL on BODIPY dyes can be done by either annihilation or sacrificial co-reactant method according to the stabilities of their cation radicals and anion radicals. The ECL emission of BODIPY dyes has maximum wavelength in a wide range from 540 nm to 752 nm. In contrast with Ru(bpy)<sub>3</sub><sup>2+</sup> as reference, some BODIPY dyes present higher ECL efficiencies under the same conditions.<sup>104-106</sup>

ECL of organic compounds is still an attracting hot topic in recent years. The advantages over other materials are that relative abundant element components and diversity in electrochemical, PL properties. Because most of the ECL experiments on organic compounds are performed in non-aqueous system, it will be a very interesting field to exploit water-soluble organic dyes for ECL studies.

### 1.4.3 Nanoparticles

Silicon nanoparticles (NPs) were the first nanomaterials reported for ECL in 2002.<sup>107</sup> After that, miscellaneous nanomaterials including CdSe, CdS, CdTe, PbS, ZnSe, and Ag<sub>2</sub>Se quantum dots (QDs) with various sizes and shapes, have been prepared and used as ECL nano-emitters.<sup>2</sup> In recent years, carbon based nanomaterials have attracted significant scientific attention due to their interesting PL properties, particularly their excitation wavelength-dependent emission.<sup>108</sup> Carbon nanodots (CDs) and graphene quantum dots (G-QDs) are promising luminophores for ECL studies because of their low toxicity, good photo stability, tunable electron-transferring, wide working potential window and chemical inertness.<sup>109</sup> A novel ECL nano-emitter C-dot@Ag core-shell hybrid nanoparticle has been prepared for label free detection of cancer cells.<sup>110</sup> The Ag passivation layer on C-dot could greatly enhance the ECL intensity and provide a platform for the further functionalization with amino, thiol groups. Moreover, the ECL signal generated by using persulfate as co-reactant was amplified by graphene nanosheets modified on GC, which make the C-dot@Ag nanoparticle very sensitive for the detection. This kind of nanoparticle has also been used for the detection of sulfide ions.<sup>111</sup> Nitrogen (N) doped CDs were reported for the detection of intracellular lead ions. ECL intensity of N-doped CDs enhanced by Pd-Au hexoctahedrons was so strong that it very sensitive to intracellular Pb<sup>2+</sup> with the detection limit of 0.33 ng / mL.<sup>112</sup>

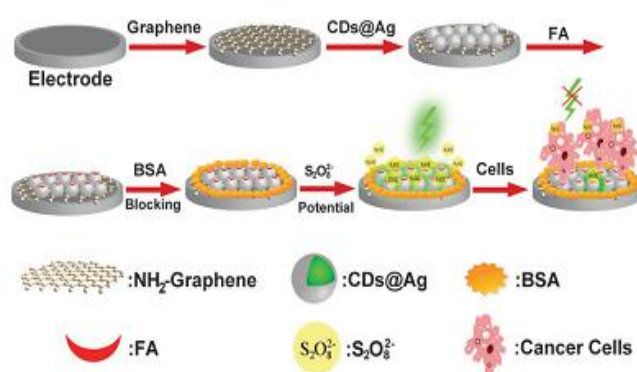


Figure 15. Profile of a label-free electrochemiluminescent cytosensor based on C-dot@Ag

nanoparticles.<sup>112</sup>

(G-QDs) with greenish-yellow have been prepared by a simultaneous cleaving and reduction approach in the mixture of  $\text{HNO}_3$  and  $\text{H}_2\text{SO}_4$  accomplished under the microwave treatment.<sup>113</sup> The emission color of these G-QDs could be tuned to bright blue by further reduction with  $\text{NaBH}_4$ . Both G-QDs show relative high PL quantum yield up to 11.7% and 22.9%, respectively. Then the ECL properties of these G-QDs were demonstrated by using potassium persulfate as the coreactant for the first time. The greenish-yellow G-QDs then were used to develop novel ECL sensor for  $\text{Cd}^{2+}$ . Up to 92 % of quenching in ECL intensity was observed due to the interaction between  $\text{Cd}^{2+}$  and G-QDs. The ECL could be recovered again by adding a stronger ion chelator ethylenediaminetetraacetic acid (EDTA). This indicates that the G-QDs are promising ECL luminophores for ECL detection.

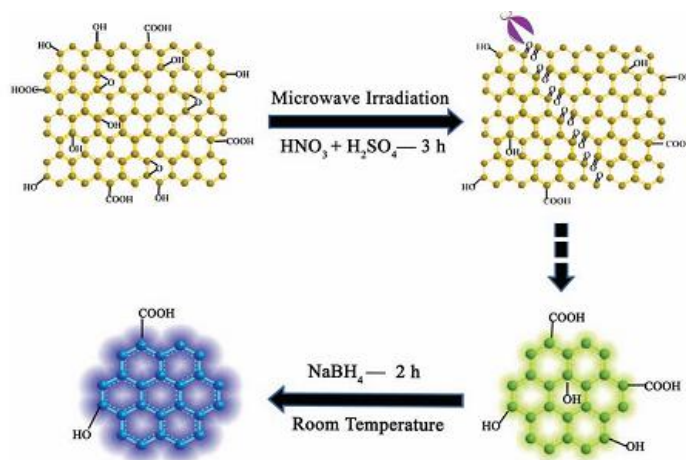


Figure 16. Schematic representation for the preparation of graphene QDs.<sup>113</sup>

Carbon Nitride ( $\text{C}_3\text{N}_4$ ) nanosheet is another carbon based material that was reported for ECL due to its special structure and properties. ECL emission of  $\text{C}_3\text{N}_4$  nanosheet can be generated with different co-reactants in aqueous solution by applying an anodic potential or a cathodic one. It was reported that ECL intensity of the  $\text{C}_3\text{N}_4$  luminophore could be used to fabricate ECL sensor due to the efficient quenching effect by trace amounts of  $\text{Cu}^{2+}$ .<sup>114</sup> The chemical structures of  $\text{C}_3\text{N}_4$  nanosheet were

further modulated by liquid-exfoliation of facile accessible bulk CN with different polymerization degree, resulting in different ECL behaviors and distinctive ECL response to different metal-ions, such as  $\text{Cu}^{2+}$ ,  $\text{Ni}^{2+}$ , and  $\text{Cd}^{2+}$ .<sup>115</sup> Gold NPs functionalized  $\text{C}_3\text{N}_4$  nanosheet nanohybrids ( $\text{Au-C}_3\text{N}_4$  NHs), which exhibit improved ECL stability and ECL intensity compared to graphite-like carbon nitride, were also prepared and used to develop an ECL immunosensor for detection of carcinoembryonic antigen (CEA).<sup>116</sup> Recently, ECL sensor for sensitive detection of microRNA was developed based on the ECL resonance energy transfer (ECL-RET) from  $\text{Au-C}_3\text{N}_4$  NHs to  $\text{Ru}(\text{bpy})_3^{2+}$ .<sup>117</sup>

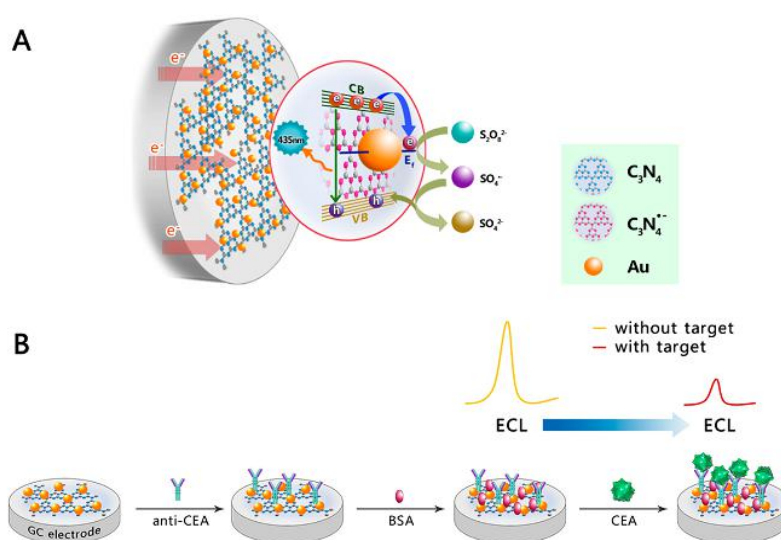


Figure 17. Schematic representation of the improving stable ECL emission mechanism on the  $\text{Au-C}_3\text{N}_4$  NHs–Coreactant System (A) and its related ECL Immunosensor (B).<sup>117</sup>

## 1.5 ECL applications

Analytical application is the most important feature of ECL, because the light intensity is proportional to the concentration of the ECL luminophore or the concentration of co-reactant. In comparison with other techniques, the ECL technology has many distinct characteristics, such as a very low detection limit (at sub-picomolar concentrations), an extremely wide dynamic range (greater than six

orders of magnitude), fast analysis process and simple instrumentation. All these properties make it widely use in clinical diagnostics, food and water testing and bio-warfare agent detection.

### **1.5.1 ECL immunoassays**

Immunoassays based on ECL detection are the most common and most important commercial applications of ECL. Since no radioactive isotopes are used in ECL immunoassays, sample preparation is much easier during the storage, handling and disposal. A large number of biomolecules, including protein, DNA and peptide, have no co-reactant functionalities or they can give very poor ECL signal. However, the ECL detections of these biomolecules are realized on the solid phase ECL assay formats in which the model ECL labels  $\text{Ru}(\text{bpy})_3^{2+}$  or its derivatives are linked to the biomolecules. Then, the ECL signals are generated in the presence of a co-reactant, typically TPrA. Many commercial systems have been developed based on  $\text{Ru}(\text{bpy})_3^{2+}$  labeled target / TPrA system because it is highly efficient for generating ECL and performs optimally in aqueous solutions at neutral pH. Over the past few years, many attempts have been done on this system to extend the applications of ECL immunoassays.<sup>1</sup>

The sandwich format is widely used in ECL immunoassays based on recognition properties and antibody/antigen binding. A bead-based ECL platform has been exploited to simultaneously detect three antigens. The microspheres modified with capture antibodies were loaded into the wells of an electrode, prepared from etched fiber optic bundles coated with thin gold films. Then microspheres with different antibodies were encoded with different concentration of  $\text{Eu}^{3+}$  to enable surface mapping. The bead-based assays were performed by incubating the array first in a sample containing antigen and then in a solution of biotinylated detection antibody that was finally attached to streptavidin-modified  $\text{Ru}(\text{bpy})_3^{2+}$  as an ECL label. The ECL imaging of the beads on the platform was recorded by a CCD camera as an alternative readout mechanism to detect multiple antigens.<sup>118</sup>

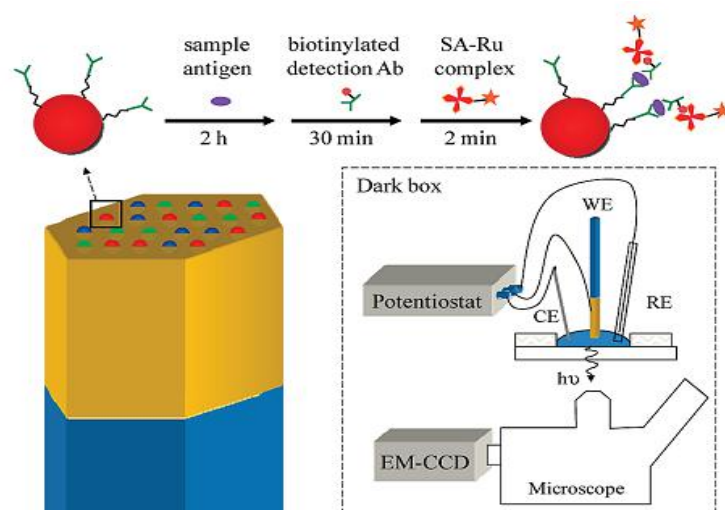


Figure 18. Schematic representation of a multiplexed bead-based immunoassay based on an etched gold-coated fiber-optic bundle.<sup>118</sup>

Another sandwich type ECL immunoassay was fabricated based on single-walled carbon nanotube (SWCNT) forest microwells formed by the surrounding of a hydrophobic polymer on the chip. Then, SWCNT forest functionalized with primary antibodies in the bottom of the well offered a large conductive surface area for the attachment of capture antibodies of the prostate-specific antigen (PSA) and interleukin-6 (IL-6). After incubation with PSA and IL-6 in the SWCNT forest microwells, silica nanoparticles containing  $\text{Ru}(\text{bpy})_3^{2+}$  and secondary antibodies were added to generate ECL due to the antibody/antigen binding. The ECL imaging signals were recorded by a CCD camera with the simultaneous detection limits of 1 pg / mL for PSA and 0.25 pg / mL for IL-6, respectively.<sup>119</sup>



Figure 19. Schematic representation of ECL immunoarray based on the SWCNT forest

A novel sandwich type ECL immunoassay was also reported for the determination of pseudorabies virus (PrV) antibody.<sup>120</sup> In this case, they proposed a stretch–stowage–growth strategy to fabricate the nonenzymatic, triply amplified and tunable ECL immunoassay, where the gold nanoparticle graphene nanosheets (Au–GN) were used as the matrix, silicon nanoparticles (SNPs) as the Ru(bpy)<sub>3</sub><sup>2+</sup> carries, and “biotin–streptavidin–biotin” (B–SA–B) structure as the bridges, respectively. Moreover, the sensitivity toward the detected target could be enhanced by repeating the combination of B–Ru@SNPs and SA to form the B–SA–B structure. Such ECL immunoassay provided a highly sensitive way for the detection of PrV antibody in a low linear range from 50 ng/mL to 1 pg/mL (LOD= 0.40 pg/mL) in not only in the calibration solution but also in real serum. The comparison with the traditional enzyme-linked immunosorbent assay (ELISA) and emerging fluorescence analysis shows that the proposed method has a higher sensitivity, wider linear range and better specificity, reproducibility, and stability. These advantages make it potential tool for clinical diagnosis and immunological efficiency evaluation.

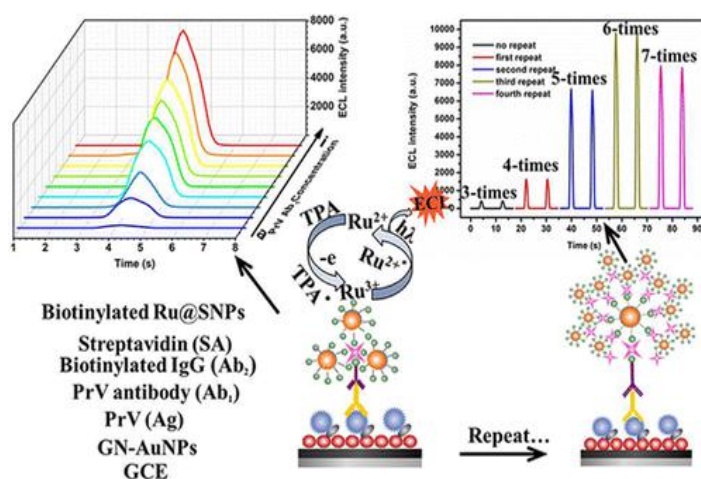


Figure 20. Schematic representation of the stretch–stowage–growth strategy created ECL immunoarray for PrV.<sup>120</sup>

## 1.5.2 Commercialized ECL instrumentation

Since ECL instrumentation was commercially available in 1994, it has been fast developed and used widely for clinical, industrial and research detection. IGEN International Inc.<sup>3</sup> invented the first ECL instrument the Origen-1 Analyzer which was presented by Carter and Bard in their work.<sup>121</sup> The Origen-1 Analyzer has been used for the clinical immunoassay testing based on the magnetic responsive functionalized beads. Like in the sandwich immunoassay format, the antibody coated magnetic beads are usually used to bind the detection antigen and secondary ECL labeled antibody. The recognition bindings on the beads are usually done before drawing into the flow cell. Then, the beads are magnetically captured on the electrode surface during the flowing in the cell, which could increase the amount of ECL labels attached to the beads on the electrode surface. When a solution containing TPrA is introduced into the flowing cell to wash the beads and supply co-reactant, ECL is produced by applying an anodic potential on the working electrode, where the emission is detected by a PMT. Finally, the beads can be washed away from the cell, and further clean the cell with pure water thoroughly so the surface of the electrode can be used again.

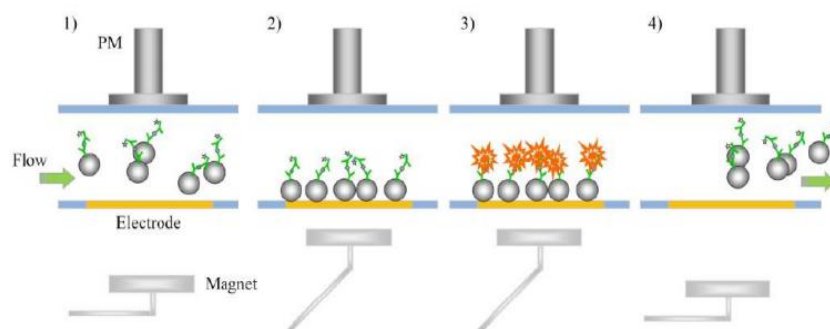


Figure 21. Generic process of ECL immunoassays based on the magnetic beads in the flowing cell.<sup>2</sup>

ECL technology is also Roche's highly innovative detection technology for heterogeneous immunoassays. Based on magnetic beads systems, they launched the first Elecsys 2010 analyzer for small to mid-range laboratories in 1996.<sup>122</sup> Since then,

the extraordinary success story of the Elecsys platform and ECL technology has continued to set the standard in immunoassay. More than 30,000 instruments were sold around the world, illustrating the outstanding success of Elecsys systems, assays and the ECL technology. Every second, 30 results are reported in laboratories all over the world. These tests offered over 150 types of inexpensive immunoassay tests in the area including cardiology, thyroid function, oncology, anemia, fertility, infection diseases and osteoporosis.<sup>123</sup>



Figure 22. Elecsys 2010 system commercialized by Roche Inc.<sup>124</sup>

Another type of commercialized ECL system (SECTOR imager 6000) is provided by Meso Scale Discovery Inc.<sup>125</sup> ECL measurements are carried out on the disposable solid phase assay electrodes. These assay electrodes are the screen-printed carbon ink electrodes within the wells of multi-well plates that can be called as Multi-Array plates. A variety of plate formats have been developed with 96-, 384-, and 1536-well formats for high throughput analysis. Another type assays are performed on the Multi-Spot plates with patterned microarrays within each plate well, which can enable multiplexed detections. The emission detector of the instrument is ultra-low noise CCD camera, so it is suitable to use in the multiplexed and high throughput assays base on the ECL images.

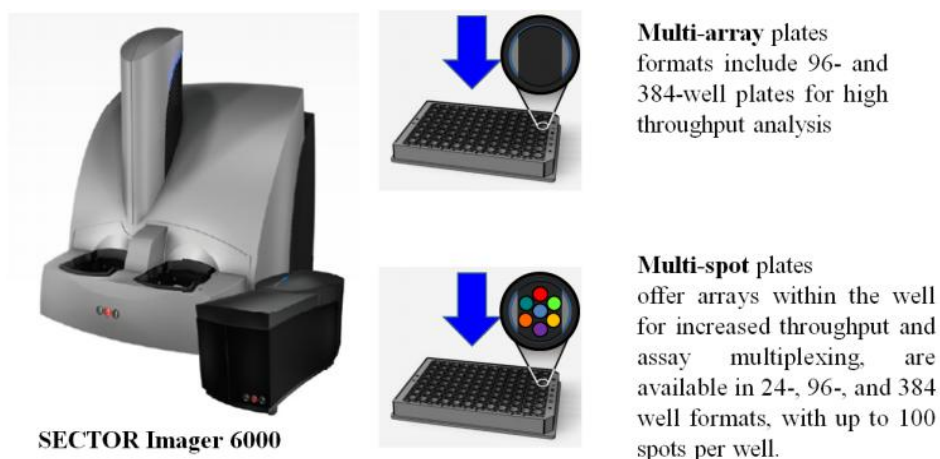


Figure 23. Commercial ECL imager from Meso Scale Discovery.<sup>125</sup>

ECL is easy to combine with other analytical systems such as capillary electrophoresis (CE), high performance liquid chromatography (HPLC) and flow injection analysis (FIA) for the special applications.<sup>2</sup> Among these combinations, CE-ECL is a typical commercialized system that has been realized by collaboration of the Changchun Institute of Applied Chemistry (China) and Xi'an Remex Electronic Co. Ltd(Figure 24). It integrated CE with the electrochemical and ECL system together controlled by a computer, where data acquisition and treatment are done. CE current, electrochemical current, electrochemical potential and ECL intensity *versus* time can be presented simultaneously at operation interface.<sup>126</sup> So it has been used in drug analysis and bio-molecules detections, such as amino acids, peptides, proteins and nucleic acid.



Figure 24. Commercial MPI-A CE-ECL detector system from Xi'an Remex Electronic Co. Ltd.<sup>127</sup>

## 1.6 Conclusion

Light emissions initiated from the electrochemically produced excited states of the luminophores are the analytical signals in ECL. Over the past decades, ECL has been demonstrated as a powerful detection tool due to its high sensitivity, good selectivity, insensitivity to matrix effects and high dynamic range. ECL can be easily produced by applying either a step potential or scanning potential with a potentiostat. This provides the possibilities to control the time and position for generating ECL according to the experimental purposes. Faradaic current and ECL curves are the two major parameters in ECL, and usually recorded simultaneously to analysis the electrochemical and ECL behaviors. The mechanisms for ECL are formally classified into two pathways: annihilation and co-reactant ECL. Although ECL is firstly demonstrated through annihilation pathway, rigorous experimental conditions such as oxygen free, non-aqueous system and highly stable oxidized/reduced forms are mandatory to produced strong ECL *via* annihilation reactions. These limitations somehow hinder the real applications of annihilation ECL. However, ECL in aqueous system can be produced by introducing a sacrificial co-reactant. Ru(bpy)<sub>3</sub><sup>2+</sup> and TPrA is the most studied system that has been successfully commercialized for designing ECL immunoassays. For examples, different detection kits provided by Roche Diagnostic and Mesosale Discovery companies offer a large number of fast, reliable and inexpensive assays for clinical diagnosis. More and more efforts have been made to design new ECL luminorhpores/co-reactants system, improve the ECL efficiency and combine ECL with other techniques to extend the applications of ECL. These are also the goals of the present work as illustrated in the following chapters.

## References

- (1) Liu, Z.; Qi, W.; Xu, G. Recent advances in electrochemiluminescence. *Chem. Soc. Rev.* **2015**, *44*, 3117-3142.
- (2) Bard, A. J.: *Electrogenerated chemiluminescence*; CRC Press, 2004.
- (3) Miao, W. Electrogenerated chemiluminescence and its biorelated applications. *Chem. Rev.* **2008**, *108*, 2506-2553.
- (4) Richter, M. M. Electrochemiluminescence (ECL). *Chem. Rev.* **2004**, *104*, 3003-3036.
- (5) Visco, R. E.; Chandross, E. A. Electroluminescence in solutions of aromatic hydrocarbons. *J. Am. Chem. Soc.* **1964**, *86*, 5350-5351.
- (6) Santhanam, K.; Bard, A. J. Chemiluminescence of electrogenerated 9, 10-Diphenylanthracene anion radical. *J. Am. Chem. Soc.* **1965**, *87*, 139-140.
- (7) Silverstein, T. P. Marcus theory: Thermodynamics can control the kinetics of electron transfer reactions. *J. Chem. Edu.* **2012**, *89*, 1159-1167.
- (8) Tokel, N. E.; Bard, A. J. Electrogenerated chemiluminescence IX: Electrochemistry and emission from systems containing tris (2, 2'-bipyridine) ruthenium (II) dichloride. *J. Am. Chem. Soc.* **1972**, *94*, 2862-2863.
- (9) Rubinstein, I.; Bard, A. J. Electrogenerated chemiluminescence 37: Aqueous ECL systems based on tris (2, 2'-bipyridine) ruthenium (2+) and oxalate or organic acids. *J. Am. Chem. Soc.* **1981**, *103*, 512-516.
- (10) Leland, J. K.; Powell, M. J. Electrogenerated chemiluminescence: an oxidative-reduction type ECL reaction sequence using tripropyl amine. *J. Am. Chem. Soc.* **1990**, *112*, 3127-3131.
- (11) Miao, W.; Choi, J.-P.; Bard, A. J. Electrogenerated Chemiluminescence 69: The Tris (2, 2'-bipyridine) ruthenium (II), (Ru (bpy)<sub>3</sub><sup>2+</sup>)/Tri-n-propylamine (TPrA) System Revisited A New Route Involving TPrA<sup>+</sup> Cation Radicals. *J. Am. Chem. Soc.* **2002**, *124*, 14478-14485.
- (12) Li, J.; Jia, X.; Wang, E. Electrochemiluminescence of ruthenium complex and its application in biosensors. *Spectrosc. Prop. Inorg. Organomet. Compd.* **2013**, *44*, 1-27.
- (13) Hu, L.; Xu, G. Applications and trends in electrochemiluminescence. *Chem. Soc. Rev.* **2010**, *39*, 3275-3304.
- (14) Bertoncello, P.; Forster, R. J. Nanostructured materials for electrochemiluminescence (ECL)-based detection methods: recent advances and future perspectives. *Biosens. Bioelectron.* **2009**, *24*, 3191-3200.
- (15) Dennany, L.; Forster, R. J.; Rusling, J. F. Simultaneous direct electrochemiluminescence and catalytic voltammetry detection of DNA in ultrathin films. *J. Am. Chem. Soc.* **2003**, *125*, 5213-5218.
- (16) Zamolo, V. A.; Valenti, G.; Venturelli, E.; Chaloin, O.; Marcaccio, M.; Boscolo, S.; Castagnola, V.; Sosa, S.; Berti, F.; Fontanive, G. Highly sensitive electrochemiluminescent nanobiosensor for the detection of palytoxin. *ACS nano* **2012**, *6*, 7989-7997.
- (17) Shan, Y.; Xu, J.-J.; Chen, H.-Y. Distance-dependent quenching and enhancing of electrochemiluminescence from a CdS: Mn nanocrystal film by Au nanoparticles for highly sensitive detection of DNA. *Chem. Commun.* **2009**, 905-907.
- (18) Lakowicz, J. R.: *Principles of fluorescence spectroscopy*; Springer Science &

Business Media, 2013.

(19) Montalti, M.; Credi, A.; Prodi, L.; Gandolfi, M. T.: *Handbook of photochemistry*; CRC press, 2006.

(20) Potrawa, T.; Langhals, H. Fluorescent dyes with large stokes shifts-soluble dihydropyrrolopyrrolediones. *Chem. Inform.* **1987**, *42*, 18.

(21) Samanta, A. Solvation dynamics in ionic liquids: what we have learned from the dynamic fluorescence stokes shift studies. *J. Phys. Chem. Lett.* **2010**, *1*, 1557-1562.

(22) Vollmer, F.; Rettig, W.; Birckner, E. Photochemical mechanisms producing large fluorescence Stokes shifts. *J. Fluoresc.* **1994**, *4*, 65-69.

(23) Vij, D.: *Handbook of electroluminescent materials*; CRC Press, 2004.

(24) Ivey, H. F.: *Electroluminescence and related effects*; Academic Press, 1963; Vol. 1.

(25) Destriau, G. Experimental studies on the action of an electric field on phosphorescent sulfides. *J. Chem. Phys.* **1936**, *33*, 620.

(26) Lehovc, K.; Accardo, C.; Jamgochian, E. Light emission produced by current injected into a green silicon-carbide crystal. *Phys. Rev.* **1953**, *89*, 20.

(27) Ouyang, J.; Fan, F. R. F.; Bard, A. J. Semiconductor electrodes 62: Photoluminescence and electroluminescence from manganese-doped ZnS and CVD ZnS electrodes. *J. Electrochem. Soc.* **1989**, *136*, 1033-1039.

(28) Garcia-Campana, A. M.: *Chemiluminescence in analytical chemistry*; CRC Press, 2001.

(29) Zhang, X.; Baeyens, W.; Van der Weken, G.; Calokerinos, A.; Nakashima, K. Chemiluminescence determination of captopril based on a Rhodamine B sensitized cerium (IV) method. *Anal. Chim. Acta.* **1995**, *303*, 121-125.

(30) Luo, M.; Chen, X.; Zhou, G.; Xiang, X.; Chen, L.; Ji, X.; He, Z. Chemiluminescence biosensors for DNA detection using graphene oxide and a horseradish peroxidase-mimicking DNAzyme. *Chem. Commun.* **2012**, *48*, 1126-1128.

(31) Lee, J. S.; Joung, H.-A.; Kim, M.-G.; Park, C. B. Graphene-based chemiluminescence resonance energy transfer for homogeneous immunoassay. *ACS nano* **2012**, *6*, 2978-2983.

(32) Zhao, L.; Sun, L.; Chu, X. Chemiluminescence immunoassay. *TrAC Trends in Anal. Chem.* **2009**, *28*, 404-415.

(33) Roda, A.: *Chemiluminescence and bioluminescence: past, present and future*; RSC, 2011.

(34) Haapakka, K. E.; Kankare, J. J. The mechanism of the electrogenerated chemiluminescence of luminol in aqueous alkaline solution. *Anal. Chim. Acta* **1982**, *138*, 263-275.

(35) Gosser, D. K.: *Cyclic voltammetry: simulation and analysis of reaction mechanisms*; VCH New York, 1993; Vol. 43.

(36) Zoski, C. G.: *Handbook of electrochemistry*; Elsevier, 2006.

(37) Beideman, F. E.; Hercules, D. M. Electrogenerated chemiluminescence from 9, 10-diphenylanthracene cations reacting with radical anions. *J. Phys. Chem.* **1979**, *83*, 2203-2209.

(38) Faulkner, L. R.; Tachikawa, H.; Bard, A. J. Electrogenerated chemiluminescence VII: Influence of an external magnetic field on luminescence intensity. *J. Am. Chem. Soc.* **1972**, *94*,

691-699.

(39) Faulkner, L. R.; Bard, A. J. Electrogenerated chemiluminescence IV: Magnetic field effects on the electrogenerated chemiluminescence of some anthracenes. *J. Am. Chem. Soc.* **1969**, *91*, 209-210.

(40) Ritchie, E. L.; Pastore, P.; Wightman, R. M. Free energy control of reaction pathways in electrogenerated chemiluminescence. *J. Am. Chem. Soc.* **1997**, *119*, 11920-11925.

(41) Kim, J.; Faulkner, L. R. Environmental control of product states in the chemiluminescent electron transfer between rubrene radical ions. *J. Am. Chem. Soc.* **1988**, *110*, 112-119.

(42) Tachikawa, H.; Bard, A. J. Electrogenerated chemiluminescence: Effect of solvent and magnetic field on ECL of rubrene systems. *Chem. Phys. Lett.* **1974**, *26*, 246-251.

(43) Chandross, E. A.; Longworth, J. W.; Visco, R. E. Excimer formation and emission via the annihilation of electrogenerated aromatic hydrocarbon radical cations and anions. *J. Am. Chem. Soc.* **1965**, *87*, 3259-3260.

(44) Park, S.-M.; Paffett, M. T.; Daub, G. H. Electrogenerated chemiluminescence of naphthalene derivatives: Steric effects on exciplex emissions. *J. Am. Chem. Soc.* **1977**, *99*, 5393-5399.

(45) Zweig, A.; Maurer, A. H.; Roberts, B. G. Oxidation, reduction, and electrochemiluminescence of donor-substituted polycyclic aromatic hydrocarbons. *J. Org. Chem.* **1967**, *32*, 1322-1329.

(46) Oyama, M.; Mitani, M.; Okazaki, S. Formation of  $\pi$ -excimer or  $\pi$ -exciplex in electrogenerated chemiluminescence involving perylene molecule revealed using a dual-electrolysis stopped-flow method. *Electrochem. Commun.* **2000**, *2*, 363-366.

(47) Bard, A.; Debad, J.; Leland, J.; Sigal, G.; Wilbur, J.; Wohlsatdter, J.; Meyers, R.: Encyclopedia of analytical chemistry: applications, theory and instrumentation. Meyers, RA, Ed, 2000.

(48) Chang, M.-M.; Saji, T.; Bard, A. J. Electrogenerated chemiluminescence 30: Electrochemical oxidation of oxalate ion in the presence of luminescers in acetonitrile solutions. *J. Am. Chem. Soc.* **1977**, *99*, 5399-5403.

(49) Kanoufi, F.; Cannes, C.; Zu, Y.; Bard, A. J. Scanning electrochemical microscopy 43: Investigation of oxalate oxidation and electrogenerated chemiluminescence across the liquid-liquid interface. *J. Phys. Chem. B* **2001**, *105*, 8951-8962.

(50) Rubinstein, I.; Martin, C. R.; Bard, A. J. Electrogenerated chemiluminescent determination of oxalate. *Anal. Chem.* **1983**, *55*, 1580-1582.

(51) Kanoufi, F.; Bard, A. J. Electrogenerated chemiluminescence 65: An investigation of the oxidation of oxalate by tris (polypyridine) ruthenium complexes and the effect of the electrochemical steps on the emission intensity. *J. Phys. Chem. B* **1999**, *103*, 10469-10480.

(52) Ege, D.; Becker, W. G.; Bard, A. J. Electrogenerated chemiluminescent determination of tris (2, 2'-bipyridine) ruthenium ion ( $\text{Ru}(\text{bpy})_3^{2+}$ ) at low levels. *Anal. Chem.* **1984**, *56*, 2413-2417.

(53) Bard, A. J.; Choi, J.-P.; Miao, W.: Coreactants. In *Electrogenerated Chemiluminescence*; CRC Press, 2004; pp 213-271.

(54) Zu, Y.; Bard, A. J. Electrogenerated chemiluminescence. 66. The role of direct

coreactant oxidation in the ruthenium tris (2, 2') bipyridyl/triethylamine system and the effect of halide ions on the emission intensity. *Anal. Chem.* **2000**, *72*, 3223-3232.

(55) Gross, E. M.; Pastore, P.; Wightman, R. M. High-frequency electrochemiluminescent investigation of the reaction pathway between tris (2, 2'-bipyridyl) ruthenium (II) and triethylamine using carbon fiber microelectrodes. *J. Phys. Chem. B* **2001**, *105*, 8732-8738.

(56) Kanoufi, F.; Zu, Y.; Bard, A. J. Homogeneous oxidation of trialkylamines by metal complexes and its impact on electrogenerated chemiluminescence in the trialkylamine/Ru(bpy)<sub>3</sub><sup>2+</sup> system. *J. Phys. Chem. B* **2001**, *105*, 210-216.

(57) Sentic, M.; Milutinovic, M.; Kanoufi, F.; Manojlovic, D.; Arbault, S.; Sojic, N. Mapping electrogenerated chemiluminescence reactivity in space: mechanistic insight into model systems used in immunoassays. *Chem. Sci.* **2014**, *5*, 2568-2572.

(58) Collinson, M. M.; Taussig, J.; Martin, S. A. Solid-state electrogenerated chemiluminescence from gel-entrapped ruthenium (II) tris (bipyridine) and triethylamine. *Chem. Mater.* **1999**, *11*, 2594-2599.

(59) Rubinstein, I.; Bard, A. J. Polymer films on electrodes. 5. Electrochemistry and chemiluminescence at Nafion-coated electrodes. *J. Am. Chem. Soc.* **1981**, *103*, 5007-5013.

(60) Hu, L.; Xu, G. Applications and trends in electrochemiluminescence. *Chem. Soc. Rev.* **2010**, *39*, 3275-3304.

(61) Miao, W.; Bard, A. J. Electrogenerated chemiluminescence 77: DNA hybridization detection at high amplification with [Ru(bpy)<sub>3</sub>]<sup>2+</sup>-containing microspheres. *Anal. Chem.* **2004**, *76*, 5379-5386.

(62) Factor, B.; Muegge, B.; Workman, S.; Bolton, E.; Bos, J.; Richter, M. M. Surfactant chain length effects on the light emission of tris (2, 2'-bipyridyl) ruthenium (II)/triethylamine electrogenerated chemiluminescence. *Anal. Chem.* **2001**, *73*, 4621-4624.

(63) Xu, G.; Pang, H.-L.; Xu, B.; Dong, S.; Wong, K.-Y. Enhancing the electrochemiluminescence of tris (2, 2'-bipyridyl) ruthenium (II) by ionic surfactants. *Analyst* **2005**, *130*, 541-544.

(64) Okajima, T.; Ohsaka, T. Electrogenerated chemiluminescence of lucigenin enhanced by the modifications of electrodes with self-assembled monolayers and of solutions with surfactants. *J. Electroanal. Chem.* **2002**, *534*, 181-187.

(65) Forster, R. J.; Bertocello, P.; Keyes, T. E. Electrogenerated chemiluminescence. *Annu. Rev. Anal. Chem.* **2009**, *2*, 359-385.

(66) Zheng, H.; Zu, Y. Emission of tris (2, 2'-bipyridine) ruthenium (II) by coreactant electrogenerated chemiluminescence: from O<sub>2</sub>-insensitive to highly O<sub>2</sub>-sensitive. *J. Phys. Chem. B* **2005**, *109*, 12049-12053.

(67) Vinyard, D. J.; Richter, M. M. Enhanced electrogenerated chemiluminescence in the presence of fluorinated alcohols. *Anal. Chem.* **2007**, *79*, 6404-6409.

(68) Noffsinger, J. B.; Danielson, N. D. Generation of chemiluminescence upon reaction of aliphatic amines with tris (2, 2'-bipyridine) ruthenium (III). *Anal. Chem.* **1987**, *59*, 865-868.

(69) Knight, A. W.; Greenway, G. M. Relationship between structural attributes and observed electrogenerated chemiluminescence (ECL) activity of tertiary amines as potential analytes for the tris (2, 2'-bipyridine) ruthenium (II) ECL reaction: A review. *Analyst* **1996**,

121, 101R-106R.

(70) Liu, X.; Shi, L.; Niu, W.; Li, H.; Xu, G. Environmentally friendly and highly sensitive ruthenium (II) Tris (2, 2'-bipyridyl) electrochemiluminescent system using 2-(dibutylamino) ethanol as co-reactant. *Angew. Chem. Int. Ed.* **2007**, *119*, 425-428.

(71) Xue, L.; Guo, L.; Qiu, B.; Lin, Z.; Chen, G. Mechanism for inhibition of/DBAE electrochemiluminescence system by dopamine. *Electrochem. Commun.* **2009**, *11*, 1579-1582.

(72) Hu, T.; Liu, X.; Liu, S.; Wang, Z.; Tang, Z. Toward understanding of transfer mechanism between electrochemiluminescent dyes and luminescent quantum dots. *Anal. Chem.* **2014**, *86*, 3939-3946.

(73) Bolleta, F.; Ciano, M.; Balzani, V.; Serpone, N. Polypyridine transition metal complexes as light emission sensitizers in the electrochemical reduction of the persulfate ion. *Inorg. Chim. Acta.* **1982**, *62*, 207-213.

(74) White, H. S.; Bard, A. J. Electrogenerated chemiluminescence 41: Electrogenerated chemiluminescence and chemiluminescence of the Ru(2, 2'-bpy)<sub>3</sub><sup>2+</sup>-S<sub>2</sub>O<sub>8</sub><sup>2-</sup> system in acetonitrile-water solutions. *J. Am. Chem. Soc.* **1982**, *104*, 6891-6895.

(75) Hu, L.; Li, H.; Zhu, S.; Fan, L.; Shi, L.; Liu, X.; Xu, G. Cathodic electrochemiluminescence in aqueous solutions at bismuth electrodes. *Chem. Commun.* **2007**, 4146-4148.

(76) Choi, J.-P.; Bard, A. J. Electrogenerated chemiluminescence 73: acid-base properties, electrochemistry, and electrogenerated chemiluminescence of neutral red in acetonitrile. *J. Electroanal. Chem.* **2004**, *573*, 215-225.

(77) Chandross, E. A.; Sonntag, F. I. Chemiluminescent electron-transfer reactions of radical anions. *J. Am. Chem. Soc.* **1966**, *88*, 1089-1096.

(78) Bruce, D.; McCall, J.; Richter, M. M. Effects of electron withdrawing and donating groups on the efficiency of tris (2, 2'-bipyridyl) ruthenium (II)/tri-n-propylamine electrochemiluminescence. *Analyst* **2002**, *127*, 125-128.

(79) Puodziukynaite, E.; Oberst, J. L.; Dyer, A. L.; Reynolds, J. R. Establishing dual electrogenerated chemiluminescence and multicolor electrochromism in functional ionic transition-metal complexes. *J. Am. Chem. Soc.* **2011**, *134*, 968-978.

(80) Lai, R. Y.; Chiba, M.; Kitamura, N.; Bard, A. J. Electrogenerated chemiluminescence 68: Detection of sodium ion with a ruthenium (II) complex with crown ether moiety at the 3, 3'-positions on the 2, 2'-bipyridine ligand. *Anal. Chem.* **2002**, *74*, 551-553.

(81) Muegge, B. D.; Richter, M. M. Electrochemiluminescent detection of metal cations using a ruthenium (II) bipyridyl complex containing a crown ether moiety. *Anal. Chem.* **2002**, *74*, 547-550.

(82) Hu, L.; Bian, Z.; Li, H.; Han, S.; Yuan, Y.; Gao, L.; Xu, G. [Ru(bpy)<sub>2</sub>dppz]<sup>2+</sup> electrochemiluminescence switch and its applications for DNA interaction study and label-free ATP aptasensor. *Anal. Chem.* **2009**, *81*, 9807-9811.

(83) Shin, I.-S.; Kim, J. I.; Kwon, T.-H.; Hong, J.-I.; Lee, J.-K.; Kim, H. Efficient electrogenerated chemiluminescence from bis-cyclometalated iridium (III) complexes with substituted 2-phenylquinoline ligands. *J. Phys. Chem. C* **2007**, *111*, 2280-2286.

(84) Kim, J. I.; Shin, I.-S.; Kim, H.; Lee, J.-K. Efficient electrogenerated chemiluminescence from cyclometalated iridium (III) complexes. *J. Am. Chem. Soc.* **2005**,

127, 1614-1615.

(85) Meier, S. B.; Sarfert, W.; Junquera-Hernández, J. M.; Delgado, M.; Tordera, D.; Ortí, E.; Bolink, H. J.; Kessler, F.; Scopelliti, R.; Grätzel, M. A deep-blue emitting charged bis-cyclometallated iridium (iii) complex for light-emitting electrochemical cells. *J. Mater. Chem. C* **2013**, *1*, 58-68.

(86) Fernández-Hernández, J. M.; Ladouceur, S.; Shen, Y.; Iordache, A.; Wang, X.; Donato, L.; Gallagher-Duval, S.; de Anda Villa, M.; Slinker, J. D.; De Cola, L. Blue light emitting electrochemical cells incorporating triazole-based luminophores. *J. Mater. Chem. C* **2013**, *1*, 7440-7452.

(87) Evariste, S.; Sandroni, M.; Rees, T. W.; Roldán-Carmona, C.; Gil-Escrig, L.; Bolink, H. J.; Baranoff, E.; Zysman-Colman, E. Fluorine-free blue-green emitters for light-emitting electrochemical cells. *J. Mater. Chem. C* **2014**, *2*, 5793-5804.

(88) Bruce, D.; Richter, M. M. Green electrochemiluminescence from ortho-metallated tris (2-phenylpyridine) iridium (III). *Anal. Chem.* **2002**, *74*, 1340-1342.

(89) Muegge, B. D.; Richter, M. M. Electrogenerated chemiluminescence from polymer-bound ortho-metallated iridium (III) systems. *Luminescence* **2005**, *20*, 76-80.

(90) Kapturkiewicz, A.; Nowacki, J.; Borowicz, P. Electrochemiluminescence studies of the cyclometallated iridium (III) L 2 Ir (acetyl acetonate) complexes. *Electrochim. Acta.* **2005**, *50*, 3395-3400.

(91) Haghghatbin, M. A.; Lo, S.-C.; Burn, P. L.; Hogan, C. F. Electrochemically tuneable multi-colour electrochemiluminescence using a single emitter. *Chem. Sci.* **2016**. DOI: 10.1039/C6SC01912A

(92) Doeven, E. H.; Zammit, E. M.; Barbante, G. J.; Hogan, C. F.; Barnett, N. W.; Francis, P. S. Selective excitation of concomitant electrochemiluminophores: tuning emission color by electrode potential. *Angew. Chem. Int. Ed.* **2012**, *124*, 4430-4433.

(93) Swanick, K. N.; Ladouceur, S.; Zysman-Colman, E.; Ding, Z. Self-enhanced electrochemiluminescence of an Iridium (III) complex: Mechanistic insight. *Angew. Chem. Int. Ed.* **2012**, *51*, 11079-11082.

(94) Hercules, D. M. Chemiluminescence resulting from electrochemically generated species. *Science* **1964**, *145*, 808-809.

(95) Omer, K. M.; Bard, A. J. Electrogenerated chemiluminescence of aromatic hydrocarbon nanoparticles in an aqueous solution. *J. Phys. Chem. C* **2009**, *113*, 11575-11578.

(96) Suk, J.; Bard, A. J. Electrochemistry and electrogenerated chemiluminescence of organic nanoparticles. *J. Solid. State. Electrochem.* **2011**, *15*, 2279-2291.

(97) Omer, K. M.; Ku, S. Y.; Wong, K. T.; Bard, A. J. Efficient and stable blue electrogenerated chemiluminescence of fluorene-substituted aromatic hydrocarbons. *Angew. Chem. Int. Ed.* **2009**, *48*, 9300-9303.

(98) Polo, F.; Rizzo, F.; Veiga-Gutierrez, M.; De Cola, L.; Quici, S. Efficient greenish blue electrochemiluminescence from fluorene and spirobifluorene derivatives. *J. Am. Chem. Soc.* **2012**, *134*, 15402-15409.

(99) Omer, K. M.; Ku, S.-Y.; Wong, K.-T.; Bard, A. J. Green electrogenerated chemiluminescence of highly fluorescent benzothiadiazole and fluorene derivatives. *J. Am. Chem. Soc.* **2009**, *131*, 10733-10741.

(100) Omer, K. M.; Ku, S.-Y.; Cheng, J.-Z.; Chou, S.-H.; Wong, K.-T.; Bard, A. J.

Electrochemistry and electrogenerated Chemiluminescence of a spirobifluorene-based donor (triphenylamine)–acceptor (2, 1, 3-benzothiadiazole) molecule and its organic nanoparticles. *J. Am. Chem. Soc.* **2011**, *133*, 5492-5499.

(101) Nepomnyashchii, A. B.; Bard, A. J. Electrochemistry and electrogenerated chemiluminescence of BODIPY dyes. *Acc. Chem. Res.* **2012**, *45*, 1844-1853.

(102) Loudet, A.; Burgess, K. BODIPY dyes and their derivatives: syntheses and spectroscopic properties. *Chem. Rev.* **2007**, *107*, 4891-4932.

(103) Haugland, R. P.: *Handbook of fluorescent probes and research products: Molecular Probes*, 2002.

(104) Nepomnyashchii, A. B.; Cho, S.; Rossky, P. J.; Bard, A. J. Dependence of electrochemical and electrogenerated chemiluminescence properties on the structure of BODIPY dyes: Unusually large separation between sequential electron transfers. *J. Am. Chem. Soc.* **2010**, *132*, 17550-17559.

(105) Suk, J.; Omer, K. M.; Bura, T.; Ziessel, R.; Bard, A. J. Electrochemistry and electrogenerated chemiluminescence of some BODIPY derivatives. *J. Phys. Chem. C* **2011**, *115*, 15361-15368.

(106) Nepomnyashchii, A. B.; Bröring, M.; Ahrens, J.; Krüger, R.; Bard, A. J. Electrochemistry and electrogenerated chemiluminescence of n-pentyl and phenyl BODIPY species: Formation of aggregates from the radical ion annihilation reaction. *J. Phys. Chem. C* **2010**, *114*, 14453-14460.

(107) Ding, Z.; Quinn, B. M.; Haram, S. K.; Pell, L. E.; Korgel, B. A.; Bard, A. J. Electrochemistry and electrogenerated chemiluminescence from silicon nanocrystal quantum dots. *Science* **2002**, *296*, 1293-1297.

(108) Baker, S. N.; Baker, G. A. Luminescent carbon nanodots: emergent nanolights. *Angew. Chem. Int. Ed.* **2010**, *49*, 6726-6744.

(109) Lim, C. S.; Hola, K.; Ambrosi, A.; Zboril, R.; Pumera, M. Graphene and carbon quantum dots electrochemistry. *Electrochem. Commun.* **2015**, *52*, 75-79.

(110) Wu, L.; Wang, J.; Ren, J.; Li, W.; Qu, X. Highly sensitive electrochemiluminescent cytosensing using carbon nanodot@Ag hybrid material and graphene for dual signal amplification. *Chem. Commun.* **2013**, *49*, 5675-5677.

(111) Wang, Z.; Zheng, C.; Li, Q.; Ding, S. Electrochemiluminescence of a nanoAg–carbon nanodot composite and its application to detect sulfide ions. *Analyst* **2014**, *139*, 1751-1755.

(112) Xiong, C.; Liang, W.; Wang, H.; Zheng, Y.; Zhuo, Y.; Chai, Y.; Yuan, R. In situ electro-polymerization of nitrogen doped carbon dots and their application in an electrochemiluminescence biosensor for the detection of intracellular lead ions. *Chem. Commun.* **2016**, *52*, 5589-5592.

(113) Li, L.; Ji, J.; Fei, R.; Wang, C.; Lu, Q.; Zhang, J.; Jiang, L.; Zhu, J. A facile microwave avenue to electrochemiluminescent two-color graphene quantum dots. *Adv. Funct. Mater.* **2012**, *22*, 2971-2979.

(114) Cheng, C.; Huang, Y.; Tian, X.; Zheng, B.; Li, Y.; Yuan, H.; Xiao, D.; Xie, S.; Choi, M. M. Electrogenerated chemiluminescence behavior of graphite-like carbon nitride and its application in selective sensing Cu<sup>2+</sup>. *Analy. Chem.* **2012**, *84*, 4754-4759.

(115) Zhou, Z.; Shang, Q.; Shen, Y.; Zhang, L.; Zhang, Y.; Lv, Y.; Li, Y.; Liu, S.;

Zhang, Y. Chemically modulated carbon nitride nanosheets for highly selective electrochemiluminescent detection of multiple metal-ions. *Anal. Chem.* **2016**, *88*, 6004-6010.

(116) Chen, L.; Zeng, X.; Si, P.; Chen, Y.; Chi, Y.; Kim, D.-H.; Chen, G. Gold nanoparticle-graphite-like C<sub>3</sub>N<sub>4</sub> nanosheet nanohybrids used for electrochemiluminescent immunosensor. *Anal. Chem.* **2014**, *86*, 4188-4195.

(117) Feng, Q.; Shen, Y.; Li, M.; Zhang, Z.; Zhao, W.; Xu, J.; Chen, H. Dual-wavelength electrochemiluminescence ratiometry based on resonance energy transfer between Au nanoparticles functionalized g-C<sub>3</sub>N<sub>4</sub> nanosheet and Ru(bpy)<sub>3</sub><sup>2+</sup> for microRNA detection. *Anal. Chem.* **2015**, *88*, 937-944.

(118) Deiss, F.; LaFratta, C. N.; Symer, M.; Blicharz, T. M.; Sojic, N.; Walt, D. R. Multiplexed sandwich immunoassays using electrochemiluminescence imaging resolved at the single bead level. *J. Am. Chem. Soc.* **2009**, *131*, 6088-6089.

(119) Sardesai, N. P.; Barron, J. C.; Rusling, J. F. Carbon nanotube microwell array for sensitive electrochemiluminescent detection of cancer biomarker proteins. *Anal. Chem.* **2011**, *83*, 6698-6703.

(120) Shao, K.; Wang, J.; Jiang, X.; Shao, F.; Li, T.; Ye, S.; Chen, L.; Han, H. Stretch-stowage-growth strategy to fabricate tunable triply-amplified electrochemiluminescence immunosensor for ultrasensitive detection of pseudorabies virus antibody. *Analy. Chem.* **2014**, *86*, 5749-5757.

(121) Carter, M. T.; Bard, A. J. Electrochemical investigations of the interaction of metal chelates with DNA 3: Electrogenerated chemiluminescent investigation of the interaction of tris (1, 10-phenanthroline) ruthenium (II) with DNA. *Bioconjugate Chem.* **1990**, *1*, 257-263.

(122) Erler, K. Elecsys immunoassay systems using electrochemiluminescence detection. *Wiener Klinische Wochenschrift* **1997**, *110*, 5-10.

(123) Myers, M. B. Analyzers: Elecsys. *The Immunoassay Handbook* **2005**, 385.

(124) Roche Inc. [www.roche.com](http://www.roche.com).

(125) Meso Scale Discovery. [www.mesoscale.com](http://www.mesoscale.com).

(126) Yin, X.; Dong, S.; Wang, E. Analytical applications of the electrochemiluminescence of tris (2, 2'-bipyridyl) ruthenium and its derivatives. *TrAC Trends. Anal. Chem.* **2004**, *23*, 432-441.

(127) Xi'an Remex Electronic Co. Ltd. [www.chinaremex.com](http://www.chinaremex.com).

## **Chapter 2**

### **Electrochemiluminescence of organic molecules: from spirofluorene, triangulene and helicene luminophores to nanoparticles**

## 2.1 Introduction

Despite of the great success of  $\text{Ru}(\text{bpy})_3^{2+}$  and its derivatives in ECL investigation and application, there are still numerous findings about ECL produced with diverse organic dyes.<sup>1</sup> Current researches on organic ECL mainly focus on the fundamental of the light emission process, multi-wavelength ECL and the preparation of organic nanoparticles for ECL.<sup>2</sup> With these respects, organic dyes are usually modified with different functional groups so that it is possible to tune electrochemical and PL properties and improve the ECL efficiency.<sup>3</sup>

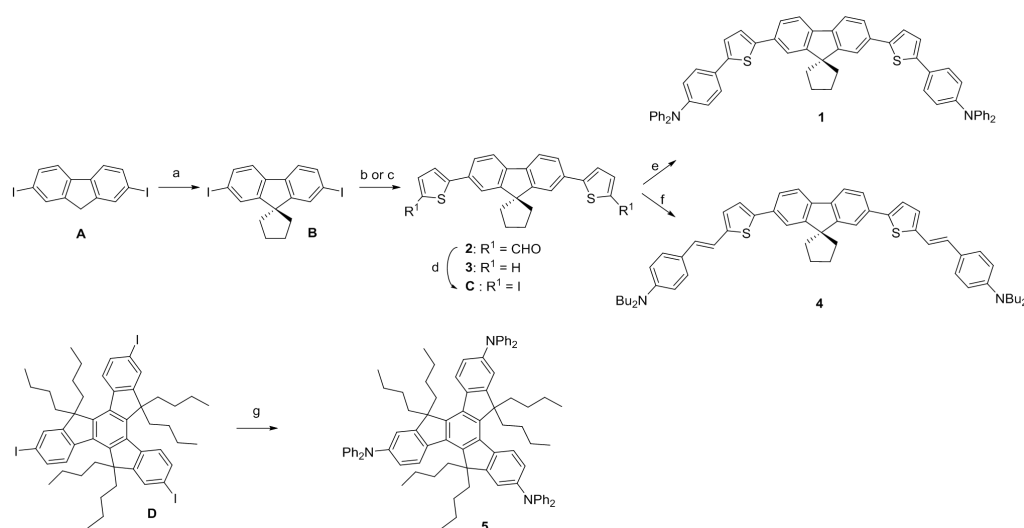
Thanks to the collaborations with two research groups, three types of organic dyes are selected for ECL investigations. Firstly, a series of symmetric fluorescent dyes built from a spirofluorene core bearing electroactive end groups and having different conjugated linkers were prepared by our colleague Dr Jonathan Daniel from the group of Mireille Blanchard-Desce (University of Bordeaux). The electrochemical, spectroelectrochemical, and ECL studies were performed on these dyes with a view to their use as building blocks for the preparation of ECL dyes and nanoparticles. Then, eight cationic triangulene dyes prepared by the group of Professor Jérôme Lacour from University of Geneva, were also used because their electrochemical and PL properties can be adjusted by tuning the heteroatoms within the core structures as well the nature of the side chains. With ECL experiments using BPO as co-reactant, the structure/activity relationship (SAR) of the triangulene dyes was demonstrated and ECL capability could be discriminated *via* the ECL “wall”.<sup>4</sup> Finally, similar organic dyes cationic helicenes provided by the same group in Geneva were selected for further ECL investigations. ECL of cationic helicene dyes can be produced by either the annihilation pathway or co-reactant pathway. By using BPO and TPrA co-reactants, we have also established an ECL “map”, which is derived from the ECL “wall” formalism, to provide a global overview of energy sufficiency required for two different co-reactants.

## 2.2 Bis-donor quadrupolar spirofluorene dye

Thiophenes and their functional derivatives based materials have been widely investigated in the fields of electroluminescence devices,<sup>5-7</sup> chemo-sensors,<sup>8,9</sup> and biosensors.<sup>10</sup> In particular, oligo/polythiophenes have been advanced to be the most frequently investigated structures.<sup>11-14</sup> Thiophene studies have been developed and well established for a long time.<sup>15</sup> Thiophenes are ideal platforms in transition metal-catalyzed cross-coupling reactions, which have provided numerous methods for the synthesis of most functionalized thiophene derivatives in the past decades.<sup>16</sup> Thiophene-based materials have many outstanding chemical and physical properties, such as their unique variety of electronic properties and easy structure variation.<sup>17-19</sup> Recently, N-perarylated aromatic amines have received intense interest due to their use in organic synthesis and structure studies.<sup>20</sup> Especially, thiophene derivatives functionalized with N-perarylated aromatic amino groups can be used in hole-transporting materials for optical and microelectronic devices, like organic light-emitting diodes (OLEDs),<sup>21-23</sup> organic field-effect transistors (OFETs),<sup>24,25</sup> solar cell<sup>26</sup> and photocopiers.<sup>27</sup> Many thiophene derivatives with N-perarylated aromatic amino moieties have been successfully prepared to investigate the interaction of both components.<sup>13,28,29</sup> Moreover, spirofluorene core is an excellent the  $\pi$ -bridge system that it can be stably linked to either an electron withdrawing acceptor or electron donating donor.<sup>28,30,31</sup> These spirofluorene based dyes have been prepared for ECL investigations. Herein, a series of symmetric fluorescent dyes built from a spirofluorene core, bearing electroactive end-groups and having different conjugated linkers were prepared in view of their use as building blocks for the preparation of ECL dyes and nanoparticles. The structure/activity relationships of these organic dyes were then demonstrated upon their electrochemical, spectroelectrochemical and ECL properties in the solution.<sup>32</sup>

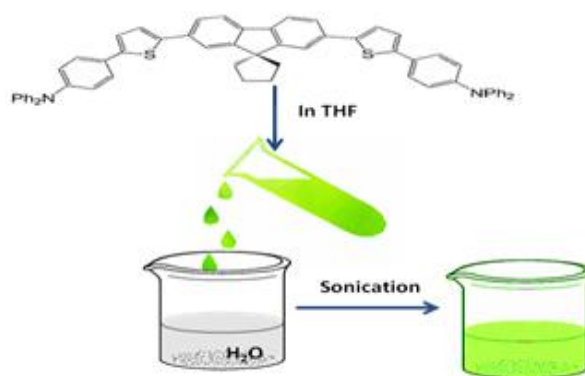
## 2.2.1 Preparation of the organic dye and its nanoparticles

The design and synthesis of a new fluorescent dye having a quadrupolar configuration are shown in Scheme 1.<sup>33-35</sup> This dye is a push-push derivative based on a spirofluorene core linked by thiophene moieties to two end-capped triphenylamine moieties as electron donating groups.<sup>34</sup> This dye shows interesting properties, including strong absorption in the violet-blue visible region and intense blue-green emission in solution. Moreover, the dye is capable to aggregate into fluorescence organic nanoparticles (FONs) in water by a simple reprecipitation method (Scheme 2). Briefly, FONs were obtained by fast addition of a minute amount of a stock solution of the corresponding dye in tetrahydrofuran (THF) into a large amount of water under sonication. Instantly after addition, colored non-turbid solutions are obtained that show intense absorption in the near-UV violet region, indicating the formation of NPs. Furthermore, under UV irradiation, FONs suspensions in water emit strong fluorescence in the visible region, thus attesting the formation of FONs.<sup>34</sup>



a) **A**, 1,4-dibromobutane, KOH, *n*-Bu<sub>4</sub>NBr, toluene, 75°C, 2h30 (80% of **B**); b) **B**, 5-formyl-2-thienylboronic acid, K<sub>2</sub>CO<sub>3</sub>, [PdCl<sub>2</sub>dppf], MeOH/Toluene, 75°C, 20 h (94% of **2**); c) **B**, 2-thienylmagnesium bromide, [PdCl<sub>2</sub>dppf], THF, reflux, 48h (75% of **3**); d) **3**, *N*-iodosuccinimide (NIS), CHCl<sub>3</sub>/glacial acetic acid, 90°C, 5 min (99% of **C**); e) **C**, 4-(*N,N'*-diphenylamino)phenylboronic acid, [PdCl<sub>2</sub>dppf], K<sub>2</sub>CO<sub>3</sub>, toluene/MeOH, 74°C, overnight (61% of **1**); f) **2**, tBuOK, 4-(*N,N'*-dibutylaminobenzyl)triphenylphosphonium iodide, DCM, rt, 24 h (71% of **4**); g) **D**, K<sub>2</sub>CO<sub>3</sub>, Cu<sub>6</sub>, 18-crown-6, diphenylamine, *o*-dichlorobenzene, reflux, 60 h (77% of **5**).

Scheme 1. Synthesis of the dyes **1**, **2**, **3**, **4**, and **5**.



Scheme 2. Preparation of FONs of the dye **1**.

During the transformation of organic dyes to organic nanoparticles, the fluorescence quantum yield could decrease from about 0.7 for dye **1** in organic solutions to 0.15 for its FONs in water. This observation is due to the decrease of the radiative rate (in relation with the red-shifted emission and excitonic coupling) and major increase in the non-radiative decay rate (most probably due to efficient vibrational deactivation processes favored by water molecules H-bonded to the nanoparticles surfaces or electron transfer reactions). However, huge brightness is still obtained due to the molecular confinement, which makes FONs of dye **1** a major interest for bioimaging application.<sup>34</sup> Similar N-perarylated aromatic amino derivatives have been reported that are able to give stable oxidized species or reduced species to generate intense ECL in organic solvents.<sup>36</sup> Due to the presence of their electron-donating end-groups, we thus anticipate that such dyes would also generate interesting ECL properties both as individual dyes and FONs. Even if the fluorene core is a good fluorescence emitting center, the unstable oxidized cation radicals could lead to an inefficient ECL. However, its stability may be improved by modifying it with appropriate redox groups such as thiophene.<sup>30,37</sup> The choice of suitable  $\pi$ -spacers and terminal groups is also crucial since they can directly influence the energies of the highest occupied molecular orbital (HOMO), the lowest unoccupied molecular orbital (LUMO), absorption spectrum, and the charge separation upon photo-excitation. In the present work, we firstly investigated the electrochemical and ECL properties of the dye **1** dissolved in organic solution and aggregated as FONs in buffered water. Then we also

investigated related dyes (Scheme 1) having a similar core but bearing electron accepting groups dye (2) or without end-groups (3). An extended version of dye 1 having elongated  $\pi$ -conjugated system was also investigated in (4) as well as a more compact version (without thiophene moieties in the  $\pi$ -conjugated system) built from a truxene (i.e. with three fused fluorene units) core having different symmetry (5). Through these comparative studies, we can have a deeper insight into the origin of these luminescence processes and in the role of the electronic structure of the dye (core,  $\pi$ -conjugated system, end-groups).

### 2.2.2 Electrochemistry

The electrochemical properties of all the spirofluorene-based and truxene-based dyes were investigated by using cyclic voltammetry (Figure 1) and the results are gathered in Table 1. These experiments were performed on platinum working electrode in dichloromethane (DCM) that contained 1 mM of each dye and 0.1 M *n*-tetrabutylammonium hexafluorophosphate (TBAPF<sub>6</sub>) as the supporting electrolyte. As shown in Figure 1, the voltammograms of 1 exhibits three reversible oxidation waves, at  $E_{1,ox} = 0.89$  V,  $E_{2,ox} = 1.24$  V, and  $E_{3,ox} = 1.50$  V vs. SCE. The peak current of the first oxidation wave is near twice that of the other two waves. This is probably related to a 2-electron transfer reaction occurring in the first wave and mono-electron transfer reactions in the next two waves. The first oxidation wave can be attributed to the dication radical formation through the oxidation of the two triphenylamine moieties simultaneously.<sup>13,28,30,37</sup> This 2-electron wave which generates triphenylaminium dication derivatives indicates that the electronic communication is negligible between the two terminal triphenylamine groups. The influence of the scan rate on the oxidation waves was varied in a broad range from 0.05 to 1 V/s (Figure 2) and the study of the current peak shows a linear evolution with respect to the square root of scan rate (Figure 3). This demonstrates a diffusion controlled process on the Pt surface in this potential window for all three well-separated anodic steps. The next two reversible anodic 1-electron waves are probably related to the oxidation of the

central spirofluorene core. However, another hypothesis that cannot be excluded is that the reversible 1-electron oxidation waves are related to the oxidation of the thiophene moieties. Nonetheless, the CV shows that the cation  $\mathbf{1}^{4+}$  is stable in solution during at least the time scale of the voltammetric experiments. We have not observed the reduction of  $\mathbf{1}$  in the explored potential window accessible in DCM. However, the reversible oxidations could give enough stable cation radicals that allows the generation ECL following the oxidative-reduction pathway with TPrA as a co-reactant.<sup>1,38,39</sup>

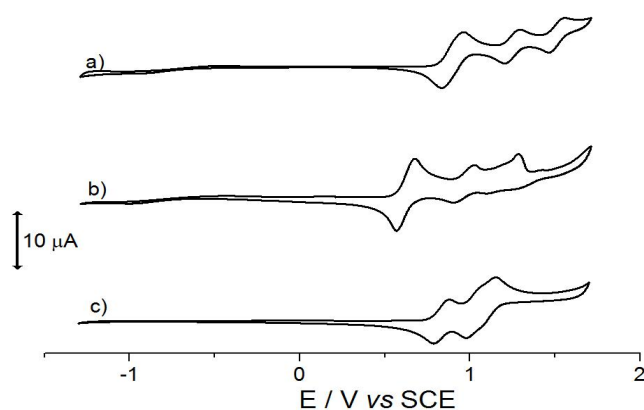


Figure 1. Cyclic voltammograms of (a) 1mM solution of  $\mathbf{1}$ , (b) 1 mM solution of  $\mathbf{4}$ , and (c) 1 mM solution of  $\mathbf{5}$  in DCM with 0.1 M TBAPF6 as supporting electrolyte. A Pt disk and Ag wire were used as working electrode and pseudo-reference electrode, respectively. The potential was calibrated with  $\text{Fc}/\text{Fc}^+$  (0.342V vs. SCE).<sup>40</sup> Scan rate: 100 mV/s.

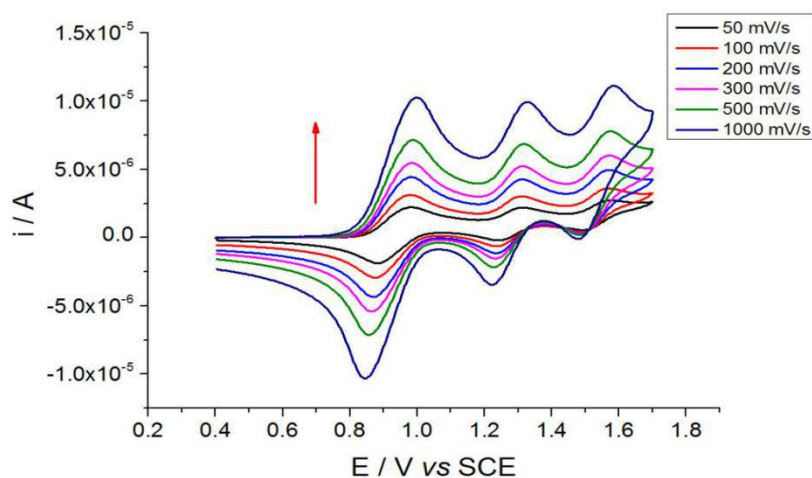


Figure 2. Cyclic voltammograms of  $\mathbf{1}$  in DCM, with different scan rates from 50 mV/s to 1000 mV/s. The arrow indicates the increasing scan rates.

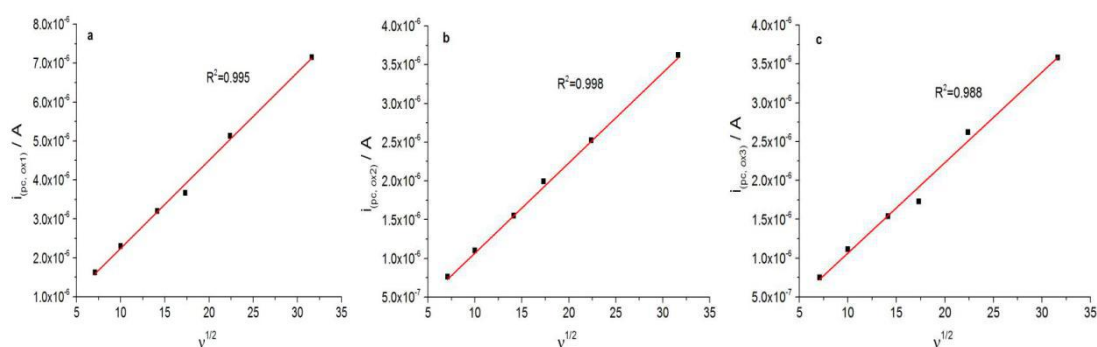


Figure 3. Plot of anodic peak current of **1** in DCM as a function of the square root of the scan rate for the (a) first, (b) second and (c) third oxidation waves.

Further electrochemical experiments were performed on the dyes **2** and **3** to investigate the influence of the end-groups on the electrochemical properties. Dye **3** is an intermediate in the synthesis of dye **1**. The cyclic voltammogram of dye **3** presents the irreversible oxidation waves of the thiophene moieties and the first anodic peak potential at 1.26 V vs. SCE (Figure 4a). Dye **2** is similar to **1** except that it is terminated by a good electron-withdrawing aldehyde group<sup>41</sup> instead of an electron-donor group (i.e. triphenylamine). By changing the nature of the end-group from a donor to an acceptor, a potential shift is supposed to occur in both the reduction and the oxidation waves at more positive (or less negative) values. As depicted on Figure 4b, the cyclic voltammogram of the dye **2** in DCM shows an irreversible oxidation at high potential ( $E_{ox} = 1.6$  V vs. SCE). The results obtained for both **2** and **3** are comparable to the wave observed at 1.31 V vs. SCE for the electropolymerization of the compounds with two thiophene moieties.<sup>42</sup> After only a single scan, polymer films were observed on the Pt surface. This kind of electropolymerization is not of interest in the present study, but provides the evidence that the two end thiophene moieties exhibit high electrochemical and chemical reactivity in **3** and also **2**. Eventually, the drastic change in oxidation behaviors between **1** and both precursors shows that the substitution with the terminal electron-donor triphenylamine moiety in the  $\alpha$  position prevents its oxidation through these positions and subsequent polymerization.

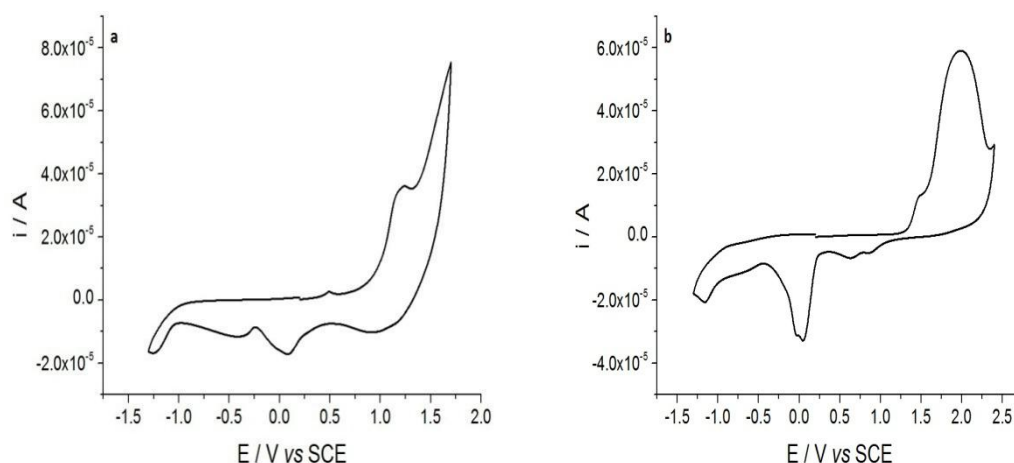


Figure 4. Cyclic voltammograms of 1 mM of a) **3** and **2** in DCM with 0.1 M TBAPF<sub>6</sub> as supporting electrolyte. Pt disk as WE, Ag wire as pseudo-reference.

Unlike dye **1**, dye **4** has an additional alkene connector between the thiophene moiety and the terminal donating groups (i.e. dibutyl-amino groups). Its CV shows a first 2-electron reversible oxidation wave and a one-electron oxidation wave. The first two oxidation potentials of **4** are shifted to less anodic potentials by about 300 mV in comparison to **1** (Table 1). Indeed, the butyl chain is known to be stronger electron-donor group compared to the diphenyl.<sup>41</sup> On the other hand, the alkene function placed between the thiophene groups and the terminal ones may contribute to reinforcing the entire donor effects. As a result, the molecule becomes easier to oxidize and its radical cation can be stabilized by the charge delocalization. The subsequent oxidation processes are more complex and exhibit irreversible oxidation waves. They consist of a shoulder at 1.18 V before a mainly irreversible wave at 1.27 V vs. SCE. Such oxidation behavior at above  $E_{2,ox}$  remains so far unclear but it reveals the instability of the corresponding electrogenerated radicals at higher potential. This is probably caused by the presence of the alkene moiety which may lead to the isomerization processes of the core structure. Whatever, this characteristic may provide some insights into the comparative studies of the ECL efficiency for the different compounds, as detailed below in the ECL section.

The electrochemical properties of the electron-donating diphenylamine groups were also examined by studying a different new dye **5**, which mainly consists of three

diphenylamine moieties grafted on a truxene core. Interestingly, the cyclic voltammogram of **5** shows three reversible oxidation waves: the first one occurs at 0.83 V vs. SCE and the last two are partially overlapped. Considering the chemical structure, these three waves are consistent with the oxidation of the terminal diphenylamine moieties. But two of them are partially separated, indicating that the electronic communication between the terminal diphenylamine groups is not negligible, in contrast to what was observed for **1**. The reversibility points out also to a good stability of the trication **5**<sup>3+</sup>.

Table 1. Electrochemical and photophysical properties of **1**, **4** and **5** in DCM.

Entry	$E_{1,ox}^{(a)}$	$E_{2,ox}^{(a)}$	$E_{3,ox}^{(a)}$	$\lambda_{max}^{Abs}$	$\lambda_{max}^{FL}$	$\lambda_{max}^{ECL}$	$E_{FL}^{(b)}$	$\Delta G^\circ$ (c)	$\Phi_{FL}^{(d)}$	$\Phi_{ECL}^{(e)}$
	[V vs. SCE]			[nm]			[eV]			
<b>1</b>	0.89	1.24	1.50	415	496	503	2.50	-0.49	0.71	4.54
<b>4</b>	0.61	0.95	1.27 <sup>(f)</sup>	447	546	549	2.27	-0.42	0.67	1.11
<b>5</b>	0.83	1.05 <sup>(g)</sup>	1.15 <sup>(g)</sup>	360	388	- <sup>(h)</sup>	3.20	0.40	0.40	0.05

[a] Oxidation potentials calculated as the mean value of the redox peaks. [b]  $E_{FL}$ , energy of the excited singlet state estimated from fluorescence emission maximum with Eq.10. [c] The values of  $\Delta G^\circ$  were calculated by using Eq. 9. [d] Fluorescence quantum yields in DCM were determined using fluorescein for **1** and using quinine bisulfate for **4** and **5**. [e] The ECL efficiency was calculated by comparison with Ru(bpy)<sub>3</sub><sup>2+</sup> as a reference ( $\Phi_{ECL} = 1$ ). [f] Anodic wave not well-defined with a loss of reversibility. [g] Partially overlapped anodic waves. [h] ECL signal too weak to allow recording the ECL spectrum.

### 2.2.3 Spectroelectrochemistry

The *in situ* spectroelectrochemistry studies of **1** were performed in solution to evaluate the spectral changes between its neutral and first oxidized state (i.e.  $E_{1,ox}$ ). It is important to study in more details of the stability of the radicals, which is essential factor for the ECL efficiency. Meanwhile, such studies allow also assessing their suitability as electrofluorochromic and electrochromic materials.<sup>43,44</sup> The dye was dissolved in DCM solution containing 0.1 M TBAPF<sub>6</sub> as supporting electrolyte, then the absorption and emission spectroelectrochemical studies were done using a Pt mesh working electrode. Upon the first oxidation potential  $E_{app} = + 0.8$  V vs. Ag/Ag<sup>+</sup>, the evolution of the UV-*vis* and fluorescence spectra with time were collected and

depicted on Figure 5. Interestingly, the monitoring of the absorption revealed a nice modification of the electronic transition when the first oxidized state is reached. As shown on Figure 5a, the periphery-to-core intramolecular charge transfer (ICT) band<sup>45</sup> of **1** in DCM at 415 nm vanished upon oxidation and a new red-shifted absorption band appeared at 610 nm in the meantime. The evolution of the fluorescence band at 496 nm is a good mirror image of the absorption one at 415 nm. This observation may be attributed to the reversal of ICT (i.e. core-to-periphery ICT transition) due to the strong electron-withdrawing character of triphenylaminium end-groups generated after loss of electrons from the triphenylamine moieties.<sup>44</sup> After approaching the equilibrium, an open circuit potential ( $E = 0$  V vs. Ag/Ag<sup>+</sup>) was applied to the system. The absorbance recovered with time until the intensity and shape of the curve were as same as the initial state. It confirms the reversibility observed by cyclic voltammetry for the oxidation process. Similar determination was done through fluorescence. The fluorescence intensity showed reversible variation during the oxidation and recovery processes by exciting at 415 nm (Figure 5b). We also excited **1** at the new absorption band that appeared at 610 nm. However, it did not lead to any fluorescence emission during the oxidation process. This is consistent with an excited state having quinoidal character (in relation with strong core-to-periphery ICT) resulting in very low fluorescence quantum yield. Therefore, the absorption and fluorescence properties of **1** also are controlled by these terminal electron-donating triphenylamine groups.

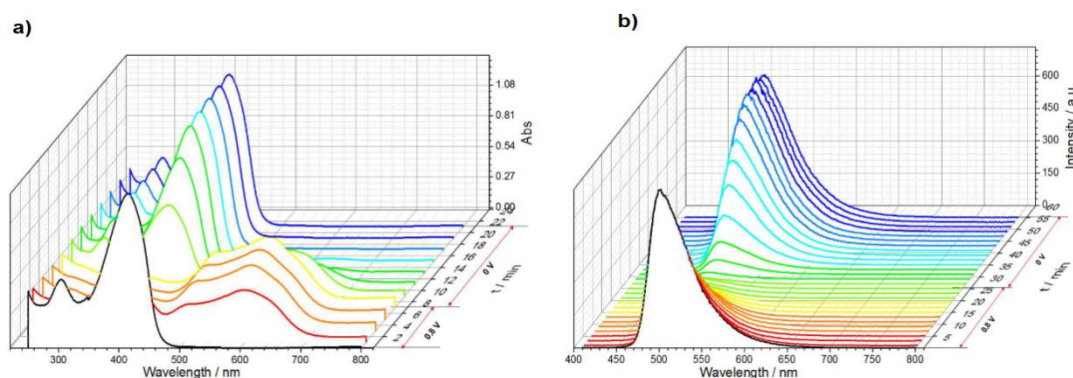


Figure 5. Time-resolved (a) UV-vis and (b) fluorescence spectra ( $\lambda_{\text{ex}} = 415$  nm) for **1** under oxidation at 0.8 V vs. Ag/Ag<sup>+</sup> and electrochemical restoration by applying  $E = 0$  V vs. Ag/Ag<sup>+</sup> in DCM solution containing 0.1 M TBAPF<sub>6</sub>.

Besides, thanks to this totally reversible oxidation behavior, a different method to determine the half-wave potential  $E_{1/2}$  and the number  $n$  of electrons for the first oxidation process was applied based on the spectroelectrochemistry studies discussed above.<sup>46,47</sup> A series of oxidation potential was applied to the thin layer cell in DCM, and individual UV-vis or fluorescence spectra were recorded after applying an anodic potential during the time necessary to obtain equilibrium. As shown on Figure 6, the absorbance and the fluorescence decay in a similar way when imposing more anodic potentials. The maximum absorbance ( $\lambda_{Abs} = 415$  nm) and the maximum fluorescence ( $\lambda_{FL} = 496$  nm) variations can be related to the ratio of the oxidized state to reduced state at different holding potentials by the following equations:

$$[R]/[O] = [A_2 - A_3]/[A_1 - A_2] \quad (1)$$

$$E_{app} = E_{1/2} - (0.0591/n) \log([R]/[O]) \quad (2)$$

In where  $A_2$  is the absorbance measured at a wavelength at a given potential, and  $A_1$  and  $A_3$  are the absorbance values of the totally reduced and oxidized species, respectively. According to the Nernst equation, a plot of  $E_{app}$  vs.  $\log([R]/[O])$  is linear with a slope  $0.0591/n$  V and an intercept of  $E_{1/2}$ . The potential-resolved UV-vis spectra were shown in Figure 6a where the inset plot represents the profile of  $E_{app}$  vs.  $\log([R]/[O])$ . The linear fitting gives a slope of -0.028 and an intercept of 0.70 V (Figure 6a, inset), indicating that the electron transfer number is 2 and the  $E_{1/2}$  is 0.70 V for the first oxidation reaction. We also performed a similar treatment of the potential-resolved fluorescence data with  $A_1$ ,  $A_2$  and  $A_3$  having the same meaning than above, except that they correspond to the fluorescence intensities measured at 496 nm (Figure 6b). For the fluorescence, a slope of -0.030 and  $E_{1/2} = 0.71$  V were found (Figure 6b, inset). These results confirmed a 2-electron transfer reaction occurring at the first oxidation wave and the stability of the oxidized resulting dications for several minutes. It also demonstrates that the two following oxidation waves correspond to a 1-electron transfer reaction.

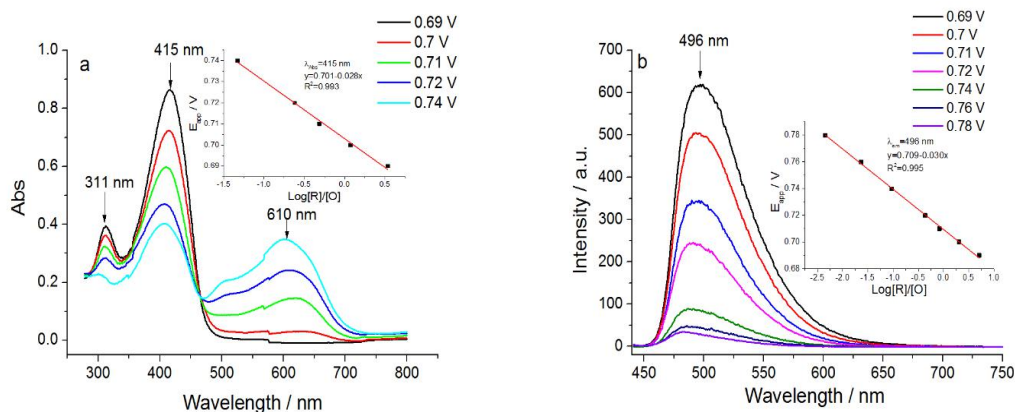


Figure 6. Evolution of the (a) UV-vis and (b) fluorescence spectra ( $\lambda_{\text{ex}} = 415 \text{ nm}$ ) for **1** when applying different potentials during the first oxidation process in DCM solution containing 0.1 M TBAPF<sub>6</sub>. Inset figures are the plots of  $E_{\text{app}}$  vs.  $\log([\text{Red}]/[\text{Ox}])$ .

## 2.2.4 ECL of the dyes

ECL of spirofluorene derivatives was generated essentially *via* the annihilation mechanism or via the reductive-oxidation pathway by applying a cathodic potential in presence of benzoyl peroxide as a cathodic co-reactant.<sup>31,48,49</sup> Since the exploited oxidized forms of **1** have the high stability in the solution, ECL of the luminophores was thus generated through an anodic sacrificial co-reactant pathway. In this case, TPrA was used as a co-reactant in order to follow the “oxidative-reduction” pathway and the excited state is generated after the simultaneous oxidation of TPrA and of the studied luminophore.

By imposing an anodic scanning potential up to 1.7 V vs. SCE, ECL signal of **1** starts to increase at 0.9 V, reaches a maximum at 1.29 V and then decreases until 1.7 V vs. SCE (Figure 7). ECL emission was very intense and extended over a large potential range compared to the reference compound, Ru(bpy)<sub>3</sub><sup>2+</sup>. In addition, it is noteworthy that ECL is generated just after the first 2-electron oxidation wave corresponding to the simultaneous oxidation of the two terminal triphenylamine moieties, but it starts before the second oxidation wave (Figure 8). Since the TPrA co-reactant is already oxidized at 0.8 V vs. SCE, it is not the limiting step in the ECL process. In a similar way, ECL signal of **4** increases at 0.75 V vs. SCE and is composed of two overlapping

peaks with a maximum at 1.1 V vs. SCE. Afterwards, it decays very rapidly. The ECL emission occurring at lower anodic potential is consistent with the shift of the first oxidation wave to less anodic potential for **4** in comparison to **1**.

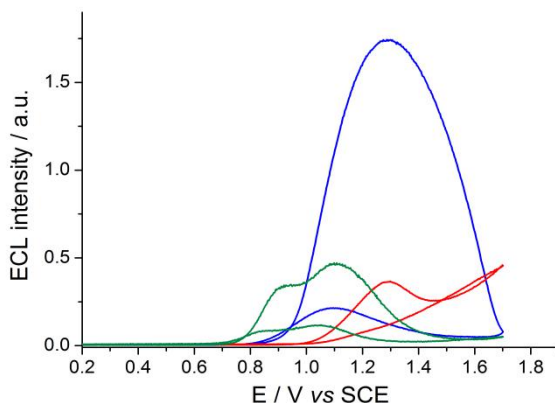


Figure 7. ECL signals for **1** (blue line), **4** (green line) and the reference Ru(bpy)<sub>3</sub><sup>2+</sup> compound (red line). ECL was recorded with a glassy carbon electrode in DCM solution containing 1 mM luminophore, 0.1 M TBAPF<sub>6</sub> and 100 mM TPrA. Scan rate: 100 mV/s.

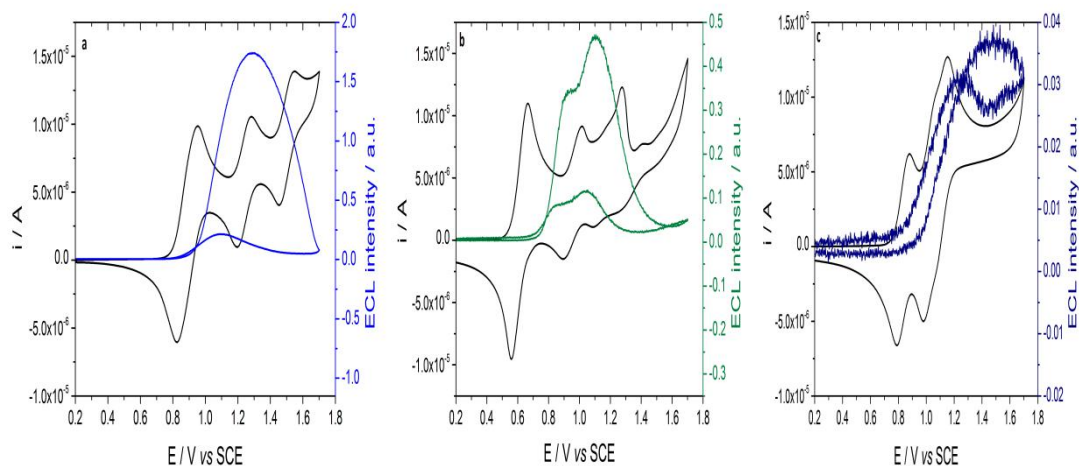


Figure 8. Comparison of the cyclic voltammograms and ECL signals of the luminophores (a) **1**, (b) **4**, and (c) **5**. Cyclic voltammograms are the same as on Figure 1 and were recorded in DCM with 0.1 M TBAPF<sub>6</sub> as supporting electrolyte. ECL signals are the same as on Figure 7 and were recorded in DCM solution containing 1 mM luminophore, 0.1 M TBAPF<sub>6</sub> with 100mM TPrA as a co-reactant.

For both **1** and **4**, ECL is thus generated after the two-electron oxidation of the end-capping donor groups, but 200 mV before the second oxidation wave (Figure 8).

The different shapes of the ECL responses displayed on Figure 7 can be evidenced by considering the width at half-maximum of the ECL peak which is 450 mV, 380 mV and 180 mV for **1**, **4** and Ru(bpy)<sub>3</sub><sup>2+</sup>, respectively. The ECL signal extends over a much larger potential range for both spirofluorene dyes in comparison with Ru(bpy)<sub>3</sub><sup>2+</sup>. There is thus a clear correlation between the oxidation behavior and both the position and the extension of the potential domain where ECL is generated. An explanation for this intriguing behavior could be that the third oxidation wave contributes partially to the ECL process giving high ECL intensity due to the remarkable stability of the corresponding cationic species. Ding *et al.* reported the self-enhanced ECL of an iridium-based complex where the ECL efficiency is increased after each oxidation steps.<sup>50</sup> But in their case, self-enhancement of ECL involved the oxidation of dimethylamino groups on the bipyridine ligands of the iridium complex which act as self-coreactant. The cascade of reactions leading *in fine* to the ECL emission could be described by the following mechanism:



where Im<sup>+</sup> is the iminium product.

Both TPrA and **1** (or **4**) are oxidized at the electrode surface. Then the cation radical TPrA<sup>•+</sup> undergoes a deprotonation step which produces a strong reducing radical TPrA<sup>•</sup>. This intermediate reacts with the oxidized **1**<sup>3+</sup> to generate the excited state **1**<sup>2+\*</sup>. Finally, it relaxes to the ground state by accompanying with light emission.<sup>38</sup> The ECL signals of the dyes are generated by scanning the potential from 0 to +1.7 V vs. SCE on a glassy carbon electrode in the tested DCM solution containing 0.5 10<sup>-3</sup> M of each dye and 100 mM of TPrA co-reactant. The ECL efficiency ( $\Phi_{\text{ECL}}$ ) relative to

$\text{Ru}(\text{bpy})_3^{2+}$  in the same conditions were calculated by integrating both the ECL intensity of ECL curve and current of CV as shown in the following equation:

$$\Phi_{(x)} = 100 \times \left[ \frac{\int_0^t ECL dt}{\int_0^t idt} \right]_x / \left[ \frac{\int_0^t ECL dt}{\int_0^t idt} \right]_{st} \quad (9)$$

where  $x$  and  $st$  correspond to the tested organic dye and the reference compound  $\text{Ru}(\text{bpy})_3(\text{PF}_6)_2$ , respectively.<sup>51</sup>

The ECL efficiency depends mainly on the generation of the excited state (Eq. 7) and subsequent radiative emission to return to the ground state (Eq. 8). Therefore, it is governed by two main contributions that are the thermodynamics of reaction 7 ( $\Delta G^\circ$ ) and the photophysics of the radiative de-excitation ( $\Phi_{\text{FL}}$ ). The free energy  $\Delta G^\circ$  may be calculated from:

$$\Delta G^\circ = E^\circ_{\text{red}}(\text{TPrA}\bullet) - E_{2,\text{ox}} + E_{\text{FL}} \quad (10)$$

$$E_{\text{FL}} = h.c / \lambda_{\text{max}}^{\text{FL}} = 1239.81 / \lambda_{\text{max}}^{\text{FL}} \quad (11)$$

where the reduction potential of the TPrA neutral radical  $E^\circ_{\text{red}}(\text{TPrA}\bullet)$  has previously been found to have a value of  $-2.1$  V.<sup>4</sup> Since ECL is mainly produced at the level of the second oxidation wave, we employed the corresponding potential  $E_{2,\text{ox}}$  and  $E_{\text{FL}}$  in Eq. 10 to calculate  $\Delta G^\circ$ . As presented in Table 1, it is clear that reaction 7 provides enough energy for dye **1** and **4** to populate the excited state, while it is not energy sufficient for **5**. This explains why **5** gives very little or no ECL. Among these dyes, **1** showed the brightest ECL and its efficiency value is 4.5-time greater than the reference compound  $\text{Ru}(\text{bpy})_3^{2+}$ . The value obtained is remarkably high as compared to those observed in other organic ECL dyes and fluorene compounds.<sup>13,30,31,37,48,49,52,53</sup> From an energetic point of view, the reaction between the dication radical **1**<sup>2+</sup> and TPrA $\bullet$  would also be exergonic enough to populate the first singlet excited state. On the contrary, if we use the value of  $E_{1,\text{ox}}$  in Eq. 10, the calculated energy is about 0.14

eV and 0.08 eV for **1** and **4**, respectively. This available energy is sufficient to populate the excited state and to generate ECL. It means that there is another photochemical process which quenches the ECL emission until both donor groups are oxidized. Since the fluorescence quantum yield are relatively similar for **1** and **4** (0.71 and 0.67, respectively), the important difference for the ECL efficiency between both dyes may be due to the more exergonic reaction generating the excited state and to the better stability of the oxidized cation radicals. Reaction 7 is actually energy sufficient by about 0.49 eV and 0.42 eV according to Eq. 10 for **1** and **4**, respectively. This slightly higher available energy cannot justify a so important difference for the efficiency of the ECL process. But the better stability of the oxidized forms in the voltammetric studies explains this remarkable ECL characteristic.<sup>54</sup>

Thanks to their strong ECL emission, ECL spectra for **1** and **4** were recorded and shown on Figure 9. ECL signal of **5** was too low to allow recording its ECL spectrum. By comparison with the corresponding fluorescence spectra, a red-shift was observed in ECL spectra, 7 nm for **1** and 3 nm for **4**, respectively. Such a red-shift is common in ECL and caused by the inner filter effect due to the high concentration of luminophore used in ECL experiments.<sup>30,55,56</sup> Nonetheless, these results confirmed that the same excited states were produced by photochemical and electrochemical excitation.

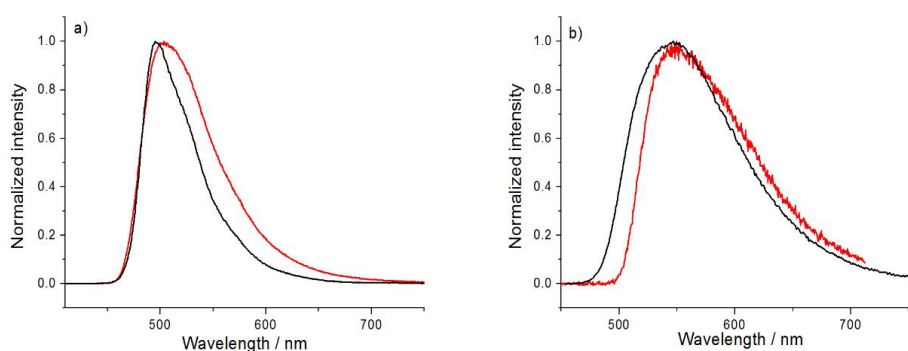


Figure 8. Normalized fluorescence (black line) and ECL spectra (red line) for (a) **1** and (b) **4** in DCM. ECL spectra were recorded in DCM solution containing 0.1 M TBAPF<sub>6</sub> with 100 mM TPrA as a co-reactant.

## 2.2.5 Electrochemistry and ECL of FONs

FONs suspensions in aqueous solution can emit strong fluorescence in the visible region.<sup>34,57</sup> FONs **[1]** emit in the green region while FONs **[4]** (Table 2) emit in the yellow region leading to ultra-bright nanoparticles with giant brightness even orders of magnitude larger than those of QDs or dye-doped silica nanoparticles.<sup>58</sup> The FONs size and morphology (spherical shape) was characterized by Transmission Electron Microscopy (TEM) (Figure 9a and Figure 10c). The good colloidal stability of the FONs is further attested by their large negative zeta potentials. We note that the hydrated radius values determined by Dynamic Light Scattering (DLS) in water are somewhat larger than those measured for “naked” nanoparticles by TEM. This difference can be ascribed to the highly negative surface potentials of both FONs responsible for the presence of a shell of H-bonded water molecules.<sup>34</sup>

Table 2. Structural and luminescence (fluorescence and ECL) characteristics of FONs

	$d_{TEM}^{(a)}$	$d_h^{(b)}$	$\zeta^{(c)}$	$\lambda_{max}^{Abs}$	$\epsilon_{max}$	$\lambda_{max}^{FL}$	$\Phi_f^{(d)}$	$\epsilon_{max} \Phi_f^{(e)}$	$\lambda_{max}^{ECL}$
	[nm]	[nm]	[mV]	[nm]	[ $10^9 \text{ M}^{-1} \text{ cm}^{-1}$ ]	[nm]		[ $10^8 \text{ M}^{-1} \text{ cm}^{-1}$ ]	[nm]
<b>[1]</b>	43	103	-70	400	1.6	507	0.14*	2.2	510
<b>[4]</b>	43	68	-50	426	2.1	560	0.02**	0.42	-

(a) Diameter of the FONs determined by TEM; (b) Hydrodynamic diameter derived from DLS experiment; (c) Zeta potential; (d) Fluorescence quantum yield were determined using fluorescein\* or cresyl violet \*\*; (e) Brightness.

Since FONs **[1]** and **[4]** are stable in water, the electrochemical characterization of these FONs was performed in 100 mM PBS solution (pH 7.4). Differential Pulse Voltammetry (DPV) of FONs **[1]** dispersed in buffer solution shows two oxidation peaks at 0.99 V and 1.20 V vs. SCE and one small shoulder at 1.33 V vs. SCE (Figure 9b). This last one is not well-defined because water oxidation starts in the same potential region. As already mentioned, **1** exhibits three oxidation waves, at  $E_{1,ox} = 0.89 \text{ V}$ ,  $E_{2,ox} = 1.24 \text{ V}$ , and  $E_{3,ox} = 1.50 \text{ V}$  vs. SCE. So there is a good agreement for **1** between its molecular and NPs forms. In addition, the current of the first anodic peak is near twice that of the second one for FONs **[1]**. It corresponds thus to sequential

2-electron and 1-electron transfer reactions for the first two peaks, respectively. It is more difficult to determine for the third peak due to its shape. In any case, the DPV results show that both the triphenylamine terminal moieties and the spirofluorene core are electrochemically-accessible in the FONs [1]. DPV of FONs [4] exhibits only a one small oxidation wave which starts at 0.9 V and finishes at 1.3 V vs. SCE (Figure 10a).

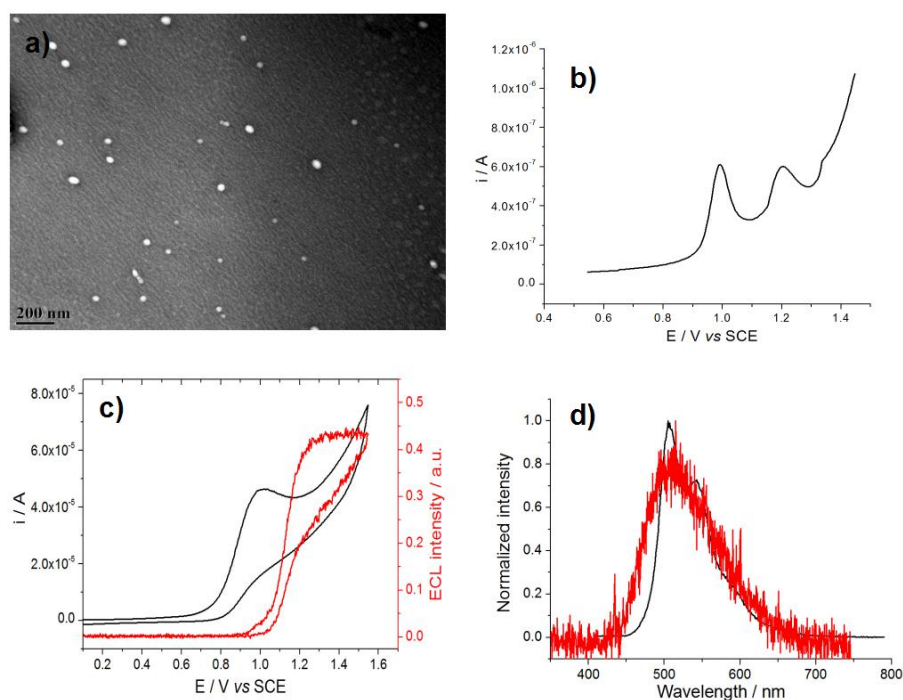


Figure 9. (a) TEM image of FONs [1] dispersed in water. (b) DPV of 0.4 nM FONs [1] in 100 mM PBS (pH 7.4) solution. (c) Voltammetric and ECL curves of 0.4 nM FONs [1] in 100 mM PBS (pH 7.4) containing 100 mM TPrA. Scan rate: 100 mV/s. (d) Fluorescence (black line) and ECL (red line) spectra of FONs [1] in 100 mM PBS (pH 7.4) solution with 100 mM TPrA.

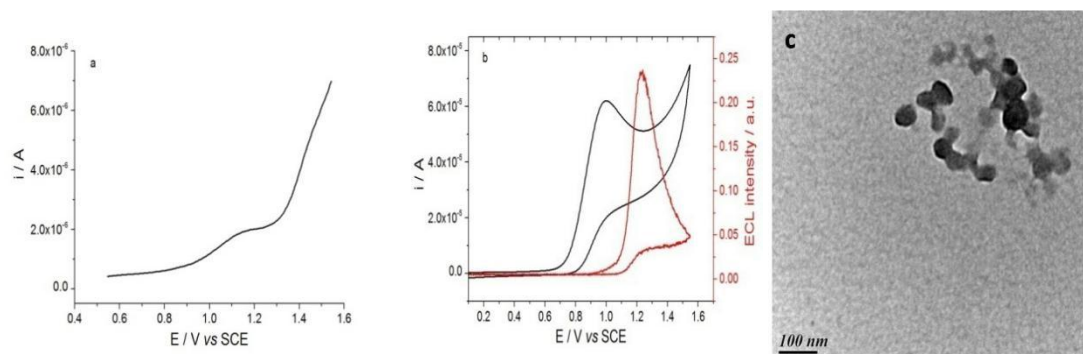


Figure 10. (a) DPV of 0.4 nM FONs [4] in 100 mM PBS (pH 7.4) solution. (b) Voltammetric and

ECL curves of 0.4 nM FONs [4] in 100 mM PBS (pH 7.4) containing 100 mM TPrA. Scan rate: 100 mV/s. (c) TEM image of FONs [4] dispersed in water.

Then ECL emission was generated in the buffer solution containing both the FONs and TPrA when the electrode potential was scanned from 0 to 1.5 V vs. SCE. As detailed in the cascade of reactions 3-8, the oxidized NPs reacted with the strong reducing radical TPrA• to populate the excited state and eventually emit the ECL signal. As shown on Figure 9c for FONs [1], ECL intensity started to increase at 0.95 V and reached a plateau up to 1.5 V vs. SCE. FONs made from 1 thus behave in water as 1 in organic solution and generate ECL after the oxidation of the triphenylamine terminal moieties. It means that FONs<sup>2+</sup> react with the neutral TPrA• radical to generate the excited state in the NPs. For FONs made from dye 4, after a similar initial increase, the ECL intensity decreases very rapidly (Figure 10b). This behavior is consistent with the ECL study of the molecular species where ECL of 4 decreases rapidly whereas it lasted over a larger potential range for 1.

The ECL efficiency of the FONs was calculated by comparison with Ru(bpy)<sub>3</sub><sup>2+</sup>/TPrA as a reference ( $\Phi_{\text{ECL}} = 100\%$ ). At a scan rate of 100 mV/s, the values of  $\Phi_{\text{ECL}}$  were 20.8 % and 5.5 % for the FONs [1] and [4], respectively. Such a ratio between both FONs is consistent with the ECL efficiencies of the molecular compounds reported in Table 1. It shows that the nano-confinement did not modify their respective ECL properties in comparison with the initial molecular forms. The ECL efficiency depends on the scan rate and the reported values are particularly high. For example, Hesari et al. reported recently the ECL efficiency of BODIPY-capped PbS.<sup>59</sup> At the same scan rate (i.e. 100 mV/s), they obtained values comprised between 8 and 10 %, which are the highest ECL efficiencies observed from the semiconductor nanocrystals. Au nanoclusters provided even higher ECL efficiency of 103 %.<sup>60</sup>

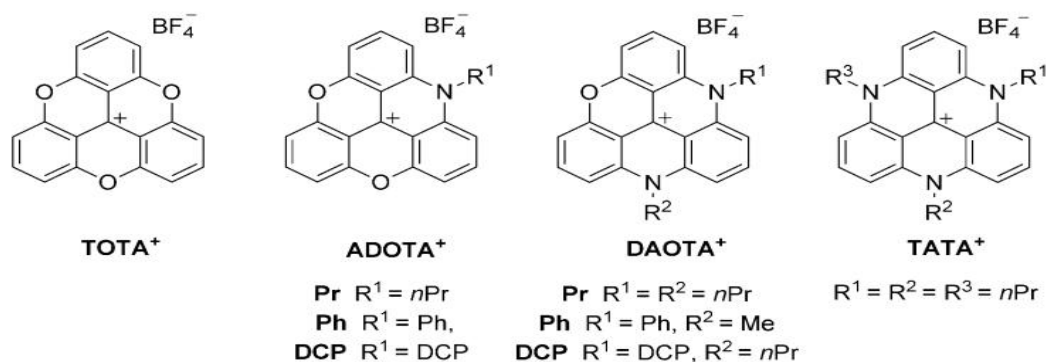
The ECL signal of FONs [1] was strong enough to allow recording the ECL spectrum (Figure 9d). Comparison with the corresponding fluorescence spectrum clearly shows the similarity between photoluminescence and ECL spectra (Figure 9d), confirming that the same excited state is reached *via* both excitation methods. Unfortunately, ECL

intensity of FONs [4] is too weak to allow acquiring an ECL spectrum for these FONs. This emphasizes that the choice of suitable dye subunits is critical to achieve stable and ultrabright FONs for the generation of ECL in water. As such, the fully organic nanoparticles easily prepared from **1** offer major promises for bioimaging and sensing purposes.

## 2.3 Cationic triangulene dyes

Since ECL has found a large number of applications in the development of variety analytical fields,<sup>61</sup> more and more researches have been turned to find new family of luminophores in order to tune the wavelength and capability of the ECL reporter to meet the fast demands for highly stable and efficient ECL emission. An excellent ECL luminophore with the following remarkable features is highly expected: low oxidation potential, high emission efficiency and good chemical stability.<sup>38,62,63</sup> Recently, stabilized cations such as triphenyl carbocations have been widely employed as luminophores due to their remarkable spectroscopic properties. But these structures show a major drawback due to the non-planarity of the twisted phenyl rings that lead to a poor electron delocalization efficiency. To overcome this limitation, cationic triangulene derivatives have been developed and exhibit an improved planarity thanks to the ring closure constraining the triphenyl carbocation in space.<sup>64</sup> The oxygen derivative TOTA (standing for trioxotriangulenium) has been first described by Russell G. Smith in 1964.<sup>65</sup> After that, diverse analogues triazatriangulenium with mixed O/N atoms in the core were synthesized through a stepwise regioselective nucleophilic aromatic substitution.<sup>66-68</sup> These trianguleniums are indeed very promising molecules, especially thanks to high stability and superior electronic properties.<sup>69</sup> Particularly, they exhibit red fluorescence emission which is of major interest for *in-vitro* imaging because it matches the spectral “open window” where the biological tissues show no auto-fluorescence and a good transparency.<sup>70</sup> Trianguleniums have been successfully used for many applications such as phase transfer catalyst,<sup>71</sup> reporter of surface modification,<sup>72</sup> metal-enhanced fluorescence

probe,<sup>73</sup> and DNA intercalator.<sup>74,75</sup> Besides, the central carbocation core can be further post-functionalized<sup>76</sup> with the desired ligands for the development of supramolecular structures, or for the creation of well-ordered columnar structures stabilized by  $\pi$  stacking.<sup>77,78</sup> Such molecular configurations exhibit very interesting electrochemical and photoluminescent properties that can be adjusted by tuning the nature of the heteroatoms in the core structure, as well as the pendant chemical substitutions.<sup>64,69</sup> However, ECL of triangulenium luminophores has never been reported so far. In this section, a series of eight triangulenium luminophores (Scheme 3) have been prepared according to the previous reports and are employed for ECL studies.<sup>56</sup> Depending on the heteroatoms situation in the core, these luminophores are divided and termed as three groups: (1) oxygen derivate, trioxotriangulenium ion **TOTA**<sup>+</sup>; (2) mixed oxygen/nitrogen derivate, azadioxotriangulenium ion **ADOTA**<sup>+</sup>, or diazoxotriangulenium ion **DAOTA**<sup>+</sup>; (3) nitrogen derivate, triazotriangulenium ion **TATA**<sup>+</sup>. Moreover, a comparison between the ECL and photoluminescence behaviour is drawn as well as a thermodynamic rationalization of the ECL efficiency.



Scheme 3. Chemical structures of the cationic triangulene dyes: trioxotriangulenium (**TOTA**<sup>+</sup>), azadioxotriangulenium (**ADOTA**<sup>+</sup>), diazoxotriangulenium (**DAOTA**<sup>+</sup>) and triazotriangulenium (**TATA**<sup>+</sup>). DCP stands for 3,5-dichloro-2-hydroxyphenyl.

### 2.3.1 Electrochemistry of cationic triangulene dyes

The electrochemical properties of the triangulenium molecules were investigated by CV as depicted in Figure 11, and the electrochemical data are gathered in Table 3. All

the CVs have been performed in deaerated CH<sub>3</sub>CN solutions containing 0.1 M TBAPF<sub>6</sub> as supporting electrolyte and 1 mM of each triangulene dye. Both oxidation and reduction waves are determined in the potential window. Among these dyes, **TATA**<sup>+</sup> has the most negative reduction potential at the value of  $E^{\circ}_{\text{red}} = -1.20 \text{ V vs. Fc/Fc}^+$ . The reduction of **TATA**<sup>+</sup> is a reversible monoelectronic transfer process with the production of a neutral species from the cation. However, the repetitive cleaning and polishing of the electrode surface is mandatory to record accurate and reproducible CVs as these compounds show a strong tendency to adsorb at the working electrode. On the contrary, the oxidation process of **TATA**<sup>+</sup> is more complex exhibiting three partially-reversible waves with the corresponding anodic peaks centred at  $E_{1,\text{ox}} = 1.34$ ,  $E_{2,\text{ox}} = 1.68$  and  $E_{3,\text{ox}} = 1.87 \text{ V vs. Fc/Fc}^+$ , respectively. The first oxidation was assigned to the removal of an electron to generate the corresponding dication. The other two oxidation waves indicate the capability to form highly oxidized species by losing another two of electrons. By changing either the nature of the heteroatoms or the pending substituent modulates significantly both oxidation and reduction potentials of the dye. The presence of an electron donating group brings a larger electron density and renders the reduction more difficult. As shown in Figure 11, the reduction becomes easier when successively replacing the electron donating nitrogen atoms by 1, 2 or 3 oxygen atoms in the core. It is obvious that the reduction potential becomes sequentially more positive along the series **TATA**<sup>+</sup>, **DAOTA**<sup>+(Pr)</sup>, **ADOTA**<sup>+(Pr)</sup>, and **TOTA**<sup>+</sup>(Table 3) with  $E^{\circ}_{\text{red}} = -0.73 \text{ V}$ ,  $-0.33 \text{ V}$  and  $-0.12 \text{ V vs. Fc/Fc}^+$ , respectively.

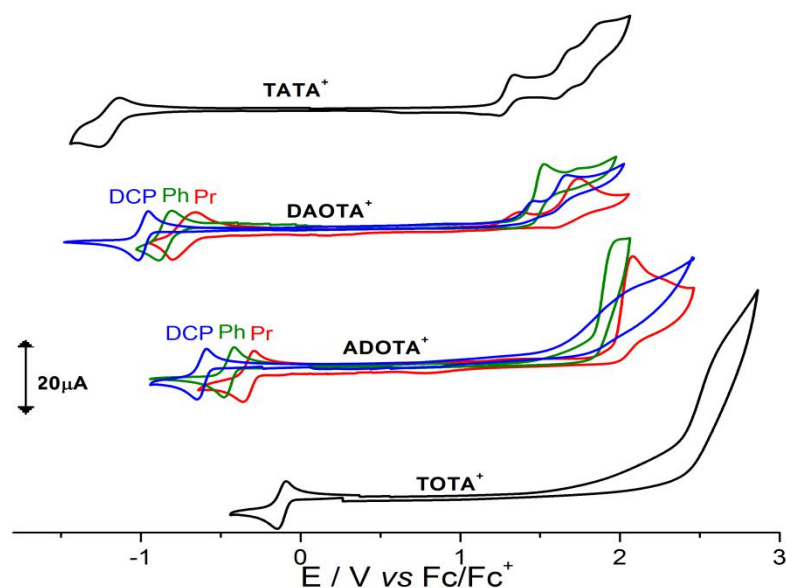


Figure 11. Cyclic voltammograms of 1 mM of each triangulene dye recorded in CH<sub>3</sub>CN solutions with 0.1 M TBAPF<sub>6</sub> as supporting electrolyte, scan rate: 100 mV/s.

Table 3. Electrochemical characterisation, fluorescence and electrochemiluminescence data in CH<sub>3</sub>CN.

	$E / V \text{ vs. Fc/Fc}^+$		FL	ECL <sup>[c]</sup>	$\Phi_{\text{FL}}^{\text{[d]}}$	Relative $\Phi_{\text{ECL}}^{\text{[e]}}$	$\Delta G^\circ$ <sup>[f]</sup>
	$E^\circ_{\text{red}}^{\text{[a]}}$	$E_{\text{ox}}^{\text{[b]}}$	$\lambda_{\text{max}} / \text{nm}$		%	%	[eV]
<b>TATA<sup>+</sup></b>	-1.20	1.34	558	585	19	35.3	-0.48
<b>DAOTA<sup>+</sup> (Pr)</b>	-0.73	1.37	591	598	47	15.4	-0.13
<b>DAOTA<sup>+</sup> (Ph)</b>	-0.84	1.53	590	598	36	21.1	-0.24
<b>DAOTA<sup>+</sup> (DCP)</b>	-0.99	1.47	599	606	40	46.5	-0.42
<b>ADOOTA<sup>+</sup> (Pr)</b>	-0.33	2.08	558	566	52	< 10 <sup>-4</sup>	0.39
<b>ADOOTA<sup>+</sup> (Ph)</b>	-0.45	~ 2	563	567	48	10 <sup>-4</sup>	0.25
<b>ADOOTA<sup>+</sup> (DCP)</b>	-0.62	n.d.	570	579	31	0.002	0.06
<b>TOTA<sup>+</sup></b>	-0.12	n.d.	524	<i>n.d.</i>	11	< 10 <sup>-4</sup>	0.75

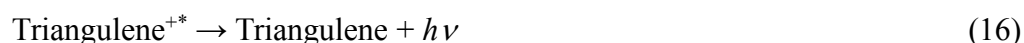
[a] Reduction potentials calculated as the mean value of the cathodic and anodic peaks for the monoelectronic reduction process. [b] Oxidations processes are mostly irreversible therefore the potential value refers to the anodic peak. [c] ECL spectra were collected in CH<sub>3</sub>CN containing 1 mM of each cationic triangulene dye and 10 mM of BPO co-reactant. [d] The quantum yield ( $\Phi_{\text{FL}}$ ) values were measured in CH<sub>3</sub>CN that contained 50  $\mu\text{M}$  each cationic triangulene dye and 0.1M TBAPF<sub>6</sub>. [e] The ECL yield or efficacy has been calculated by comparison with Ru(bpy)<sub>3</sub><sup>2+</sup> as a reference ( $\Phi_{\text{ECL}} = 100\%$ ). [f] The values of  $\Delta G^\circ$  were calculated by using Eq.17.

However, such structure/activity relationship (SAR) for the oxidation of the **DAOTA<sup>+</sup>**, **ADOOTA<sup>+</sup>** and **TOTA<sup>+</sup>** is not straightforward because the oxidation waves appear to be irreversible at higher potentials by comparison to **TATA<sup>+</sup>**, which are consistent

with the ones reported in the literature.<sup>64,79,80</sup> The SAR of both **ADOTA**<sup>+</sup> and **DAOTA**<sup>+</sup> sub-families are also verified respectively by the substitution of three different chemical groups on one nitrogen atom for each series: *n*-propyl (**Pr**), phenyl (**Ph**), or 3,5-dichloro-2-hydroxyphenyl (**DCP**) appendages. A similar trend was observed in both families as the reduction potential becomes more negative in the order of **Pr** to **Ph** to **DCP** groups. The reduction potential difference  $\Delta E^{\circ}_{\text{red}}$  between Pr and DCP groups is about 290 mV for **ADOTA**<sup>+</sup>, and about 260 mV for **DAOTA**<sup>+</sup>. This could be explained by the electron-donating capability of substituent following the increase trend: **Pr** < **Ph** < **DCP**. All these results demonstrated that substituting oxygen by nitrogen progressively has a major influence on the electrochemical properties. The further tuning of the redox properties can also be achieved by a careful choice of the nature of pending groups on the nitrogen heteroatoms.

### 2.3.2 ECL of cationic triangulene dyes

The CVs of all triangulene dyes show systematically well-reversible reduction waves. These mean that the reduced species are stable in the explored potential window. As a result, the reductive-oxidative pathway has been chosen to generate ECL. In that case, both triangulene dye and benzoyl peroxide (BPO) co-reactant are reduced simultaneously at the surface of the electrode when scanning toward cathodic direction (Figure 12). After dissociation, BPO produces a strong oxidant which can react with the reduced neutral specie to generate the excited state as illustrated by the following sequence of reactions.<sup>2,48,49</sup>



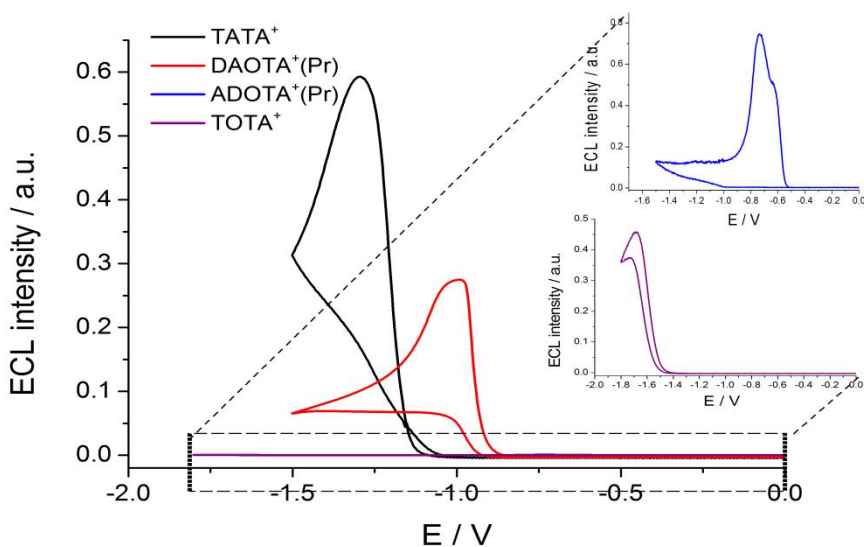


Figure 12. Overlapped ECL intensity of 1 mM **TATA<sup>+</sup>**, 1mM **DAOTA<sup>+</sup>(Pr)**, 1mM **ADOTA<sup>+</sup>(Pr)** and 1mM **TOTA<sup>+</sup>** when 10 mM BPO co-reactant was used for each dye in CH<sub>3</sub>CN containing 0.1 M TBAPF<sub>6</sub> as supporting electrolyte, scan rate:100 mV/s. Insets are the ECL curves for **ADOTA<sup>+</sup>(Pr)** and **TOTA<sup>+</sup>** recorded at high sensitivity range.

As shown in Figure 12, **TATA<sup>+</sup>** and **DAOTA<sup>+</sup>** do exhibit much stronger ECL emission than that of **ADOTA<sup>+</sup>** and **TOTA<sup>+</sup>** which show well-defined ECL curves only at high sensitivity scale at the same conditions (Inset figures). ECL was also generated by using each dye of the **ADOTA<sup>+</sup>** and **DAOTA<sup>+</sup>** sub-families when same co-reactant BPO was used. Then ECL efficiencies of all the studied cationic triangulene were calculated based on the comparisons the ECL intensities between each triangulene dye and the reference compound Ru(bpy)<sub>3</sub><sup>2+</sup> at the same conditions(Eq.9). As seen from Table 3, **TATA<sup>+</sup>** has a very good relative ECL efficiency of 35 %, whereas the **DAOTA<sup>+</sup>** sub-family presents interesting ECL with efficiencies values following the similar trend as in its reduction potential: 15 % (**Pr**) < 21 % (**Ph**) < 46 % (**DCP**). This indicates that the ECL abilities of these four dyes are quite high when compared with other organic luminophores. On the contrary, **ADOTA<sup>+</sup>** sub-family and **TOTA<sup>+</sup>** show very low ECL emission that could only be detected at the high sensitivity scale. The corresponding relative ECL yields are typically four to five orders of magnitude smaller, with **ADOTA<sup>+</sup>(DCP)** exhibiting a yield of only  $2 \times 10^{-4}$  %. The ECL decreased to  $10^{-4}$  % in the case of **ADOTA<sup>+</sup>(Ph)** and is even lower for **ADOTA<sup>+</sup>(Pr)**

and **TOTA**<sup>+</sup>.

It was possible to record the ECL spectra corresponding to such a reductive-oxidative pathway for the whole series of compounds except **TOTA**<sup>+</sup>. The comparisons between the fluorescence and ECL spectra show similar maximum emission wavelengths and shapes. As shown in Figure 13, fluorescence of **TATA**<sup>+</sup> and **ADOTA**<sup>+</sup> were found to emit at around  $\lambda = 560$  nm, and in the latter case, another marked shoulder at approximately  $\lambda = 610$  nm is observed in both the fluorescence and ECL spectra of the **ADOTA**<sup>+</sup> sub-family.<sup>81-83</sup> For **DAOTA**<sup>+</sup> compounds, the emission is centered at around  $\lambda = 590$  nm.<sup>70</sup> Even though **TOTA**<sup>+</sup> has the most energetic luminescence irradiated at  $\lambda_{\text{max}} = 524$  nm, its ECL spectra is not recordable due to very low ECL intensity. The introduction of the **DCP** group induces emission a red shift of approximately 10 nm in both the sub-families **ADOTA**<sup>+</sup> and **DAOTA**<sup>+</sup>. Finally, when comparing the maximum emission in the fluorescence and ECL spectra, a small red shift is noticeable most of the time, typically between 5 and 25 nm. Such a shift is classically observed when comparing ECL and fluorescence spectra. It is mainly attributed to the inner-filter effects of the solution due to the relative high concentration of the triangulene dyes used in ECL and fluorescence experiments. Besides, different devices are used to collect ECL and PL data which could also contribute to such wavelength shift.<sup>30,55,84</sup>

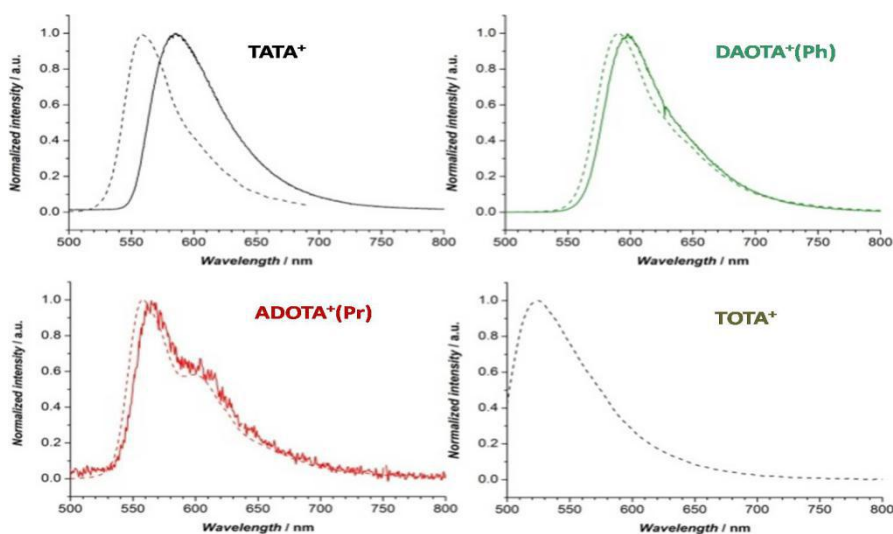


Figure 13. Representative normalized PL (dashed lines) and ECL (solid lines) spectra of

triangulene dyes. ECL was recorded under electrochemical control in CH<sub>3</sub>CN solutions containing 1 mM of each triangulene dye and 10 mM BPO co-reactant. 0.1 M TBAPF<sub>6</sub> was used as supporting electrolyte.

### 2.3.3 ECL efficiency discriminated by ECL “wall”

As demonstrated in the above ECL experiments, the cationic triangulene dyes can be divided into two distinctive categories that show either very strong or very low ECL capability. This dramatic variation in ECL efficiency can be explained upon the threshold energetic requirements which are rationalized by considering the free energy  $\Delta G^\circ$  associated with the homogeneous reaction to give the excited state (Eq.17):

$$\Delta G^\circ = E^\circ_{\text{red}}(\text{triangulene}) - E^\circ_{\text{ox}}(\text{Ph-CO}_2^\bullet / \text{Ph-CO}_2^-) + E_{\text{FL}} \quad (17)$$

The electron transfer reaction between the reduced triangulene species and the strongly oxidizing benzoyloxy radical (Ph-CO<sub>2</sub>•) results in the formation of the excited state, and its energy is given by Eq. 17, in which  $E^\circ_{\text{ox}}(\text{Ph-CO}_2^\bullet / \text{Ph-CO}_2^-)$  has been reported to be either +0.8 V or +1.5 V vs. SCE<sup>85-87</sup> and  $E_{\text{FL}}$  is the energy required to populate the singlet excited state. It is important to stress here that,  $E^\circ_{\text{ox}}(\text{Ph-CO}_2^\bullet / \text{Ph-CO}_2^-)$ , is indeed difficult to determine accurately. Whatever, the latter value of was used in the calculations (i.e., 1.36 V vs. Fc/Fc<sup>+</sup>) because it is so far the one classically admitted.<sup>1,30</sup> Since the maximum emission wavelengths have been determined in Table 3, the latter one could be calculated from the fluorescence emission data (Eq. 18). The corresponding estimated values for the lowest singlet excited state of all the studied triangulene dyes vary in a narrow range between  $E_{\text{FL}} = 2.1$  and 2.4 eV. By contrast, the cathodic potentials of triangulenes  $E^\circ_{\text{red}}(\text{triangulene})$  show drastically change from -0.12 to -1.2 V vs. Fc/Fc<sup>+</sup>. Thus,  $E^\circ_{\text{red}}(\text{triangulene})$  is the major factor that governs the free energy  $\Delta G^\circ$  as indicated by wide evolution range observed from -0.48 eV to 0.75 eV among these triangulene dyes, also in consistent with their corresponding ECL efficiency variation (Table 3). Recently, the

threshold energetic requirement for ECL has been a simple dynamic plot, namely ECL “wall”, by Barnard, Hogan *et al.*<sup>4</sup> In their work, the energetic criterion for ECL is established to discriminate ECL capability of Ir complex series with N-heterocyclic carbene ligands when TPrA used as co-reactant. In our study, we developed the same formalism which strongly support this simple thermodynamic requirement by using organic dyes instead of organometallic ones and also with BPO co-reactant in the context of a reductive-oxidative pathway (Figure 13). Moreover, it has been found from the ECL “wall” that allows qualitatively predicting ECL capability from the electrochemical and fluorescence data without conducting ECL experiments. The energetic distance between each data point and the threshold limit represented by the dotted line directly represents the capability for the generation of the excited state according to Eq. 15. Same trend of ECL efficiency in the experimental sequence: **TOTA<sup>+</sup> < ADOTA<sup>+</sup>(Pr) < ADOTA<sup>+</sup>(Ph) < ADOTA<sup>+</sup>(DCP) < DAOTA<sup>+</sup>(Pr) < DAOTA<sup>+</sup>(Ph) < DAOTA<sup>+</sup>(DCP)  $\approx$  TATA<sup>+</sup>** has also been observed directly from the ECL “wall”.

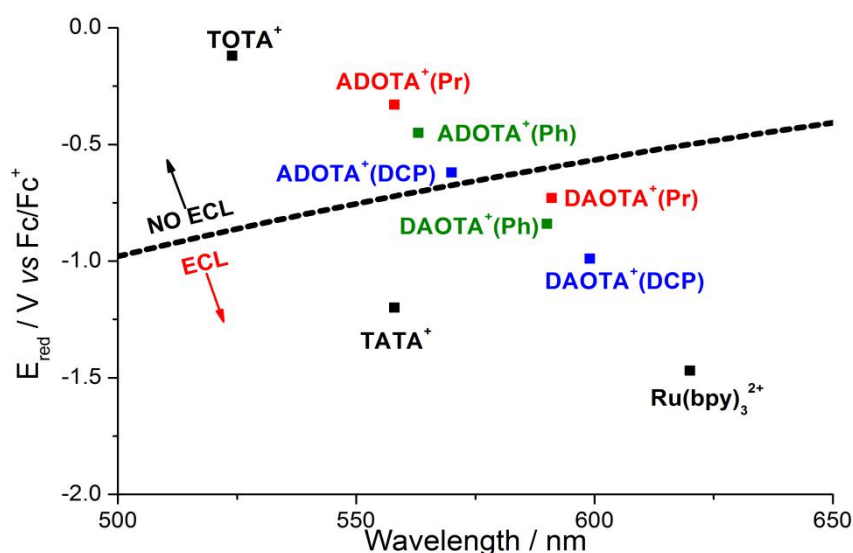
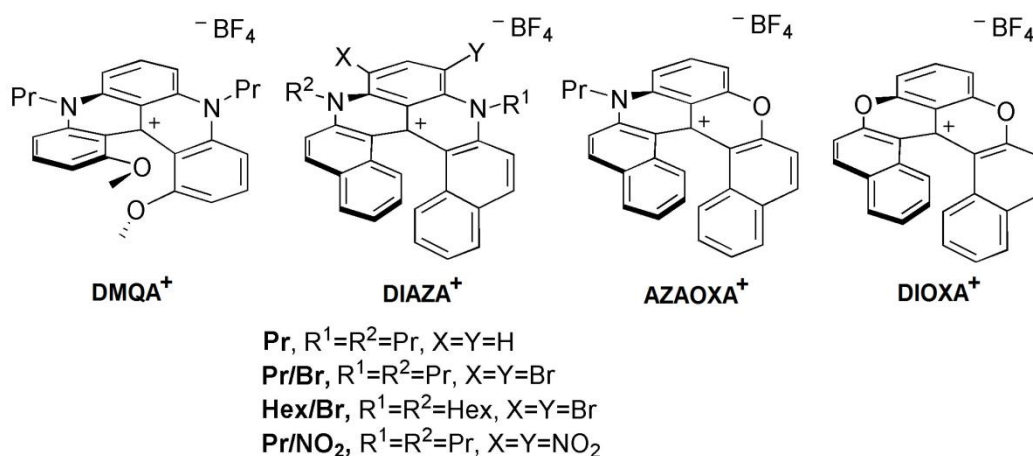


Figure 14. ECL wall showing the energy sufficiency for the BPO co-reactant. The dashed line indicates the reduction potential threshold value necessary for a given emission wavelength. Each data point represented the molecule is defined as ECL-active when located beneath the dashed line, while above the dashed line is ECL-inactive.

## 2.4 Cationic helicene dyes

Helicenes are polyaromatic compounds with a helical structure formed by fused benzene or other hetero-aromatic rings.<sup>88</sup> Since the very first helicenes were synthesized as early as in 1903,<sup>89</sup> helicenes with different aromatic rings have been developed and widely used in chirality, organic chemistry, catalysis, optoelectronic and biology fields due to their helical structure, high barrier to racemization and high luminescent efficiency.<sup>90</sup> For simplicity and clarity, the number in brackets [*n*] before the helicene name is used to denote the number of conjugated aromatic rings directly involved in the helical backbone. A new [6]helicene series was prepared from a single common precursor as it is rather difficult to introduce heteroatoms to helical core or post-functionalize the helicenes with exocyclic substituents regioselectively.<sup>91</sup> Diaza[6]helicene derivatives were synthesized by further selective functionalization of the initial diaza[6]helicene core. All these reactions were readily achieved to enhance the molecular diversity of the helicene dyes (Scheme 4). Therefore, the luminescent and redox properties could be easily tuned by modulating their chemical structure. As a leading model and reference compound, a [4]helicene quinacridinium (**DMQA<sup>+</sup>**) was used. It is noteworthy that **DMQA<sup>+</sup>** is also configurationally stable and exhibits relatively high luminescence quantum yields.<sup>92-94</sup>



Scheme 4. Chemical structures of dimethoxyquinacridinium (**DMQA<sup>+</sup>**), diaza[6]helicene (**DIAZA<sup>+</sup>**), azaoxa[6]helicene (**AZAOXA<sup>+</sup>**) and dioxa[6]helicene (**DIOXA<sup>+</sup>**).

The electrochemical and ECL properties of the helicene dyes are reported in the present study. Cyclic voltammetry was used to investigate their electrochemical behaviors in acetonitrile. The stability of the helicene radical ions was also compared in order to draw a structure/activity relationship depending on the nature of the heteroatoms included in the helical core as well as the pending substituents. The ECL emission of these helicene dyes was recorded in both annihilation and co-reactant pathways, respectively. The data for the ECL efficiency were collected by comparison with  $\text{Ru}(\text{bpy})_3^{2+}$  as a standard under the same experimental conditions. Finally, the threshold energetic requirement for generating ECL in the helicene/co-reactant systems was demonstrated by using a full ECL “map” with two thermodynamic plot representation for the anodic and cathodic regions.<sup>4</sup>

### 2.4.1 Electrochemistry of cationic helicene dyes

The series of chiral [6]helicene dyes was investigated by recording the cyclic voltammograms and the corresponding electrochemical behavior was compared to  $\text{DMQA}^+$  as a leading model [4]helicene compound (Figure 15).  $\text{DMQA}^+$  shows a relatively simple redox behavior. It is typically reduced at  $-0.7 \text{ V vs. Fc/Fc}^+$  with a peak to peak separation ( $\Delta E_{\text{peaks}}$ ) of  $\sim 56 \text{ mV}$  evidencing a reversible monoelectronic transfer (Table 1). The oxidation also shows a reversible behavior and is centered at  $1.4 \text{ V vs. Fc/Fc}^+$  generating a dicationic species from the initial cationic form. The voltammetric characteristics of  $\text{DIAZA}(\text{Pr})^+$  have been reported recently.<sup>95</sup> Briefly, it shows very similar electrochemical behaviors as  $\text{DMQA}^+$ , exhibiting also reversible redox monoelectronic processes at  $-0.72 \text{ V}$  and  $+1.4 \text{ V vs. Fc/Fc}^+$ , respectively. Another irreversible process is also observed at more positive potentials and starts at about  $2 \text{ V}$ . This was assigned to an irreversible oxidative decomposition of the diaza[6]helicene core but it was not further investigated. The similar electrochemical behaviors of  $\text{DMQA}^+$  and  $\text{DIAZA}(\text{Pr})^+$  indicate that substituting methoxy groups in the [4]helicene family by additional benzene rings (*i.e.* [6]helicene) marginally affects the redox potentials thanks to comparable donating ability.

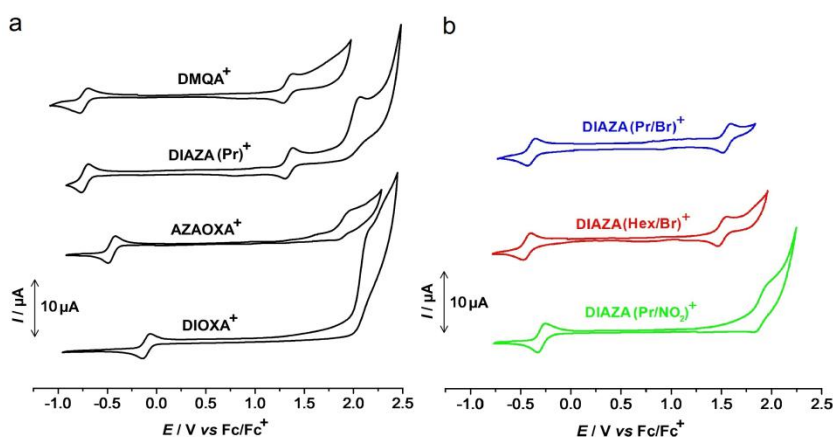


Figure 15. a) Influence of the nature of the heteroatoms in the helical core on the voltammetric behavior of helicenes: **DMQA<sup>+</sup>**, **DIAZA(Pr)<sup>+</sup>**, **AZAOXA<sup>+</sup>** and **DIOXA<sup>+</sup>**. b) Influence of the pending ligands on the electrochemistry of **DIAZA<sup>+</sup>** derivatives. Cyclic voltammogram of 1 mM each helicene was recorded in degassed CH<sub>3</sub>CN solution containing 0.1 M TBAPF<sub>6</sub> as supporting electrolyte. Scan rate 100 mV / s.

By contrast, changing the N atoms to O ones in the cationic core drastically modified the corresponding voltammograms. Indeed, on one hand, by comparing **DIAZA(Pr)<sup>+</sup>** to **DIOXA<sup>+</sup>**, the reductive behavior is apparently unchanged with a single reversible one-electron process, but occurring at a much milder cathodic potential. On the other hand, no reversible oxidation was observed with the compound **DIOXA<sup>+</sup>** with only a fully irreversible process occurring at large anodic overpotentials (2.14 V vs. Fc/Fc<sup>+</sup>). This directly highlights the structure/activity influence of the nature of the heteroatoms involved inside the cationic core of the [6]helicene as it strongly modulates the stabilization of a dicationic structure. Finally, the electrochemical characterization of the asymmetric **AZAOXA<sup>+</sup>** derivate reveals a strong analogy with the behavior of **DIOXA<sup>+</sup>** ( $E_{\text{red}} = -0.45$  vs. Fc/Fc<sup>+</sup> with  $\Delta E_{\text{peaks}} \sim 58$  mV, and  $E_{\text{ox}} = 1.93$  V vs. Fc/Fc<sup>+</sup>). The electrochemical mechanisms are perfectly comparable for both [6]helicenes **AZAOXA<sup>+</sup>** and **DIOXA<sup>+</sup>** demonstrating that the replacement of a single N atom by an O one perturbs irreversibly the oxidation process. As previously observed for cationic triangulene structures,<sup>56</sup> the replacement of N heteroatoms by O ones decreases the corresponding donor effect. Therefore the reduction becomes easier for **AZAOXA<sup>+</sup>** and **DIOXA<sup>+</sup>** compared to **DMQA<sup>+</sup>** and **DIAZA(Pr)<sup>+</sup>** and the voltammetric waves appear at less cathodic potential values (Figure 15a).

Table 4. Electrochemical characterisation, fluorescence and electrochemiluminescence data in CH<sub>3</sub>CN.

Compound	$E / V$ vs. Fc/Fc <sup>+</sup>		FL	ECL <sup>[c]</sup>	$\Phi_{FL}$ <sup>[e]</sup>	$\Phi_{ECL} / \%$		$E_s$ <sup>[g]</sup>	$\Delta H_{ann}$ <sup>[h]</sup>
	$E_{red}^\circ$ <sup>[a]</sup>	$E_{ox}$ <sup>[a,b]</sup>	$\lambda_{max} / nm$		%	BPO <sup>[f]</sup>	TPrA <sup>[f]</sup>	[eV]	
<b>DMQA<sup>+</sup></b>	-0.70	1.40	670	670	7.6	46.2	231	1.85	2.00
<b>DIAZA(Pr)<sup>+</sup></b>	-0.72	1.40	657	664	27.4	37.9	100	1.89	2.02
<b>DIAZA(Pr/Br)<sup>+</sup></b>	-0.38	1.56	680	686	3.9	8.3	236	1.82	1.84
<b>DIAZA(Hex/Br)<sup>+</sup></b>	-0.43	1.51	682	689	4.8	12.5	264	1.82	1.84
<b>DIAZA(Pr/NO<sub>2</sub>)<sup>+</sup></b>	-0.30	1.98	600	n.d.	38.6	<10 <sup>-4</sup>	n.d.	2.07	2.18
<b>AZAOXA<sup>+</sup></b>	-0.45	1.93	616	616 <sup>[d]</sup>	21.6	0.0026	n.d.	2.01	2.28
<b>DIOXA<sup>+</sup></b>	-0.12	2.14	592	602 <sup>[d]</sup>	7.6	<10 <sup>-4</sup>	n.d.	2.09	2.16

[a] Redox potentials calculated as the mean value of the cathodic and anodic peaks for the monoelectronic redox process. [b] For those with irreversible oxidations processes, the potential value refers to the anodic peak. [c] ECL spectra were collected in solution containing 1 mM helicenes, 0.1 M TBAPF<sub>6</sub> and 10 mM of BPO used as a co-reactant. [d] ECL spectra were collected in an annihilation pathway. [e] The quantum yield ( $\Phi_{FL}$ ) values were measured in CH<sub>3</sub>CN that contained 10  $\mu$ M helicenes and 0.1 M TBAPF<sub>6</sub> taking DMQA<sup>+</sup> as a reference.<sup>94</sup> [g] The ECL efficiency was calculated by comparison with Ru(bpy)<sub>3</sub><sup>2+</sup> as a reference ( $\Phi_{ECL} = 100\%$ ) using either BPO or TPrA as co-reactant and corrected for the quantum efficiency of the PMT at the different wavelengths.<sup>96</sup> [g] The values of  $E_{FL}$  were calculated by using Eq.11. [h] The values of  $\Delta H_{ann}$  were calculated by using Eq.18.

Further pending substitution on the aromatic rings of diaza[6]helicene core were developed and the corresponding cyclic voltammograms were recorded to investigate the influence on the electrochemical behavior caused by various functional groups, such as -Br or -NO<sub>2</sub> (Figure 15b). As observed previously with **DIAZA(Pr)<sup>+</sup>**, all the other diaza[6]helicene compounds displayed a reversible monoelectronic reduction at less cathodic potential (see Table 4). The presence of the -Br group in the core does not affect the reversibility of the oxidation process. However, the introduction of -NO<sub>2</sub> into the [6]helicene core strongly affects the oxidation behavior which becomes irreversible. In summary, the electrochemical investigation reveals for all [6]helicenes a reversible monoelectronic reduction whereas the oxidation could be either reversible (**DIAZA<sup>+</sup>**) or irreversible (**DIOXA<sup>+</sup>** and **AZAOXA<sup>+</sup>**). Due to the donor effect, N heteroatoms within the helicene core (**DMQA<sup>+</sup>** and **DIAZA(Pr)<sup>+</sup>**) also stabilize more efficiently the dicationic species generated during the oxidation process by

comparison to the compounds containing O atoms (**AZAOXA**<sup>+</sup> and **DIOXA**<sup>+</sup>). Therefore, the oxidation waves of these latter compounds are shifted to higher potentials and become irreversible. The fine tuning of the redox properties can also be achieved through a careful choice of the nature of chemical functions pending on the nitrogen heteroatoms or aromatic ring as exemplified in the **DIAZA**<sup>+</sup> series. Such diverse electrochemical features may lead to dissimilar ECL capability in the annihilation mode because these [6]helicenes exhibit different values for the potential difference  $\Delta E$  between the reduction and oxidation processes;  $\Delta E$  values ranging between 1.9 and 2.4 V.

## 2.4.2 ECL of cationic helicene dyes

### 2.4.2.1 Annihilation pathway

As already illustrated in Chapter 1, the ECL emitting excited state could be reached *via* annihilation pathway including direct the “S-route” or indirect the “T-route”. In the first case, the energy of the system is high enough to populate the singlet state. For the second case, the triplet state is produced first and the triplet-triplet annihilation generates the singlet emitting state. To clarify the involved route for our systems, we compared the energy of the electronically singlet excited state,  $E_{FL}$ (Eq. 11) obtained from the fluorescence spectra with the enthalpy provided by the annihilation reaction  $-\Delta H_{ann}$  is given by Eq.18.

$$-\Delta H_{ann} \text{ (in eV)} = E^\circ(A^{2+}/A^+) - E^\circ(A^+/A) - T.\Delta S \quad (18)$$

where  $\lambda$  is the wavelength at the maximum fluorescence intensity. The calculated values of  $E_s$  span from 1.80 to 2.06 eV for the analyzed compounds (Table 4). The enthalpy of the annihilation reaction depends on the difference between the oxidation and reduction potentials of the helicenes (i.e.  $E^\circ(A^{2+}/A^+)$  and  $E^\circ(A^+/A)$ ).  $T.\Delta S$  is an estimated entropy effect of 0.1 eV. By comparing both values in Table 4, one can see

that the energy of the annihilation reaction is greater than the energy required to populate directly the first singlet excited states for these helicene dyes. Therefore all studied helicenes can be defined as energy sufficient systems following the “S-route”. To further investigate the stability of the ECL and radical ions of the [6]helicenes, potential pulsing ECL transients were recorded. Transient ECL for **DIAZA(Pr)<sup>+</sup>** depicted in Figure 16b shows that a constant ECL emission is observed upon each individual pulsing step, indicating that almost the same quantities of neutral (i.e. **DIAZA(Pr)**) and cation (i.e. **DIAZA(Pr)<sup>2+</sup>**) radicals are generated per pulse and both species appear to be stable during the timescale of the annihilation reaction (Eq. 19-21). Besides, the ECL transient process of **DIAZA(Pr)<sup>+</sup>** is comparable to the ones recorded for **DMQA<sup>+</sup>** as the model helicene with similar electrochemical reactions and redox potentials (Figure 16a).

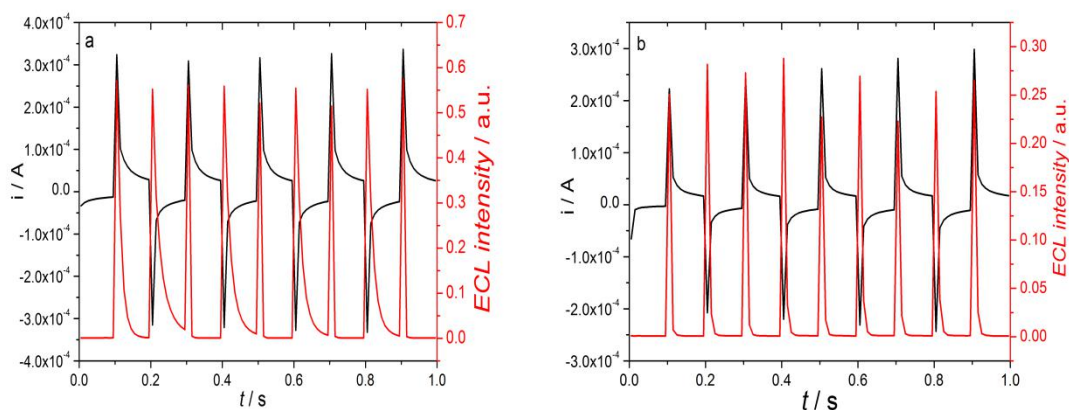
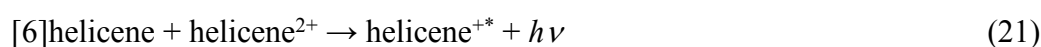


Figure 16. Chronoamperometric curves and ECL transients of (a) 1 mM **DMQA<sup>+</sup>** and (b) 1 mM **DIAZA(Pr)<sup>+</sup>** in degassed CH<sub>3</sub>CN solution containing 0.1 M TBAPF<sub>6</sub> pulsed between the first reduction potential ( $E_{(1/2, \text{red})} - 100 \text{ mV}$ ) and the first oxidation potential ( $E_{(1/2, \text{ox})} + 100 \text{ mV}$ ), respectively. Pulse duration: 0.1 s.



However, **AZAOXA<sup>+</sup>** and **DIOXA<sup>+</sup>** also gave some ECL emission by annihilation

even though their anodic wave appears irreversible. It means that the annihilation reaction is kinetically in competition with the follow-up chemical reaction and that the oxidized intermediate is stable enough to react with the reduced form and thus to yield the excited state. As shown in Figure 17a, the annihilation of **AZAOXA**<sup>+</sup> performed by potential pulses shows asymmetric ECL transients in which the intensity corresponding to the cathodic pulse is always much smaller than the anodic one. This kind of ECL transient reveals that the oxidized form (**AZAOXA**<sup>2+</sup>) is unstable and depleted in solution, as already mentioned, leaving only a small fraction available for generating ECL when the following anodic pulse occurs. For the annihilation of **DIOXA**<sup>+</sup>, the shape and intensity of ECL maximum intensity is very different to the other compounds. ECL does not occur immediately after the anodic pulse but with a time delay and increases steadily until the reduction pulse (Figure 17b). This behavior may possibly involve an adsorption step with formation of an emitting film on the electrode.<sup>28,97</sup>

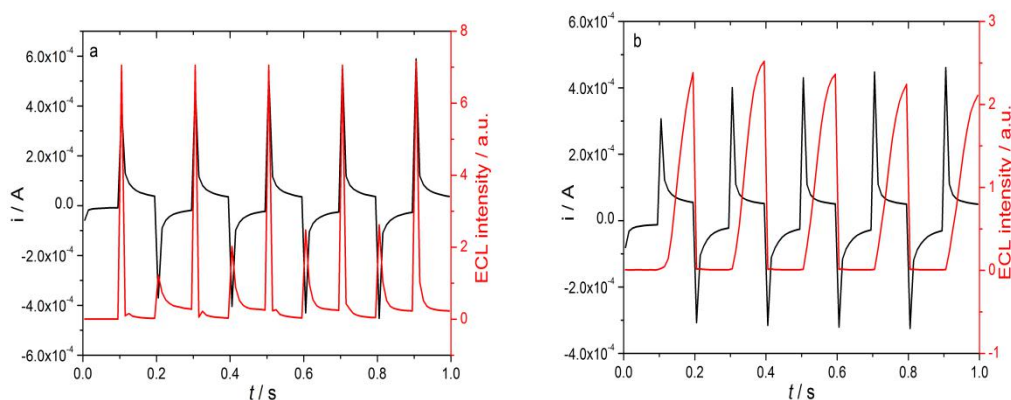


Figure 17. Chronoamperometric curves and ECL transients of (a) 1 mM **AZAOXA**<sup>+</sup> and (b) 1 mM **DIOXA**<sup>+</sup> in degassed CH<sub>3</sub>CN solution containing 0.1 M TBAPF<sub>6</sub> pulsed between the first reduction potential ( $E_{(1/2, \text{red})} - 100$  mV) and the first oxidation potential ( $E_{(1/2, \text{ox})} + 100$  mV), respectively. Pulse duration: 0.1 s.

Moreover, ECL emission recorded for the four studied compounds was stable with time and strong enough to collect ECL spectra using the annihilation method. ECL spectra of **DMQA**<sup>+</sup> and **DIAZA(Pr)**<sup>+</sup> are very similar with their band centered around

650-670 nm (Figure 18a-b). It is not surprising since, as already discussed, their oxidation and reduction potentials are almost the same and therefore the energy gap is similar. By comparison, **DIOXA**<sup>+</sup> shows a hypsochromic shift with a band centered at 600 nm, similarly to the fluorescence spectrum (Figure 18d). Therefore, the same excited state is generated by photoexcitation and by the annihilation between the electrogenerated neutral and dication radicals. The behavior of **AZAOXA**<sup>+</sup> is similar to **DIOXA**<sup>+</sup> and its emission is shifted to a longer wavelength of 616 nm (Figure 18c). But considering the ECL spectra of **DIAZA(Pr)**<sup>+</sup> and **DIOXA**<sup>+</sup>, a red-shift of ~10 nm in comparison to the fluorescence ones was observed experimentally and attributed to an inner-filter effect caused by the higher concentration used in ECL.<sup>30,55,84</sup>

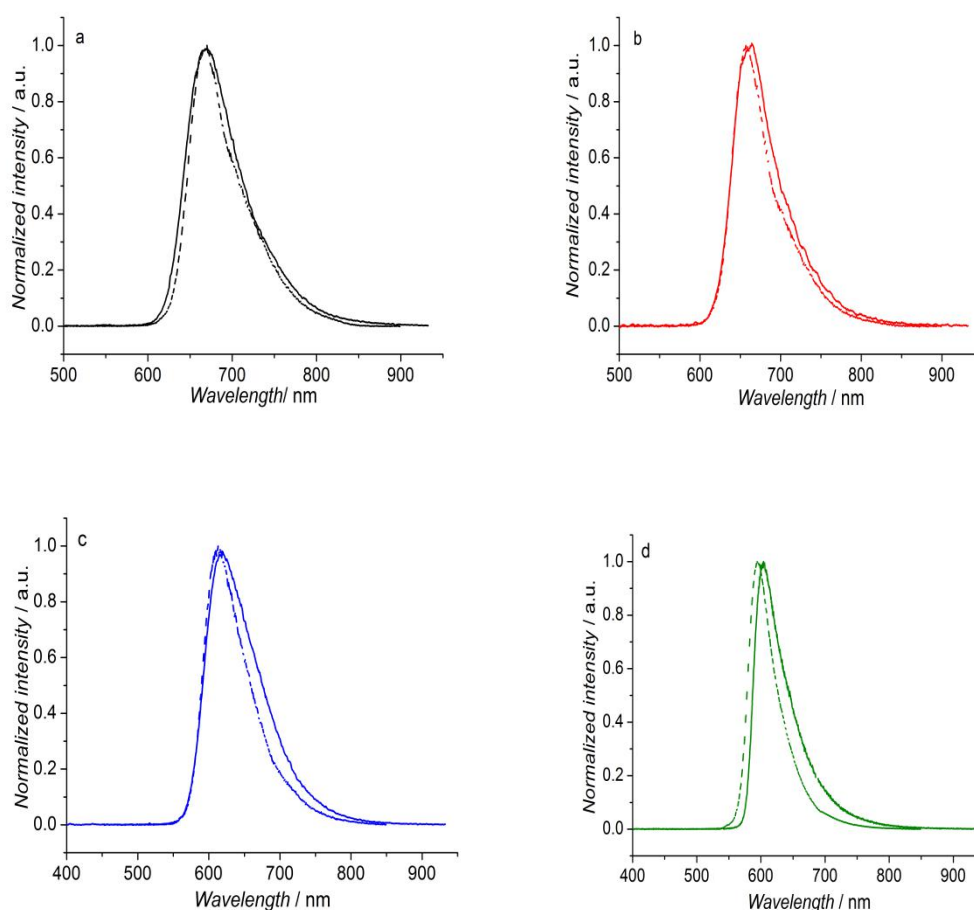
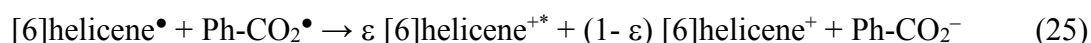


Figure 18. Typical fluorescence (dashed line) and annihilation ECL (solid line) spectra for (a) **DMQA**<sup>+</sup>, (b) **DIAZA(Pr)**<sup>+</sup>, (c) **AZAOXA**<sup>+</sup> and (d) **DIOXA**<sup>+</sup> in CH<sub>3</sub>CN solution.

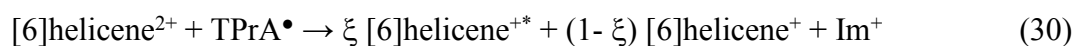
### 2.4.2.2 Co-reactant pathway

Using sacrificial co-reactant species, ECL can also be produced by applying a single anodic or cathodic potential step at an electrode.<sup>39</sup> In the “oxidative-reduction” process, the luminophore and the co-reactant are both oxidized.<sup>1</sup> The oxidized co-reactant undergoes then a chemical decomposition to form a strong reducing intermediate which can react with the oxidized luminophore to generate the excited state. By comparison, in the “reductive-oxidation” process, the reduction of the co-reactant generates a strong oxidizing intermediate that react with the reduced luminophore to produce ECL. Both mechanisms involve the formation of powerful reducing or oxidizing radicals that react with the luminophore to induce the ECL emission. ECL spectra of [6]helicenes were also successfully collected using two typical co-reactants for the illustration of the oxidative-reduction and reductive-oxidation pathways, respectively.

All the studied compounds exhibit a reversible cathodic wave. It indicates that the electrogenerated neutral radical is stable and that ECL may be obtained with a co-reactant which follows a reductive-oxidation pathway. In a first set of experiments, we used BPO which is irreversibly reduced. During the cathodic reaction, it forms a benzoyloxy radical ( $\text{Ph-CO}_2^\bullet$ ) which is a strongly oxidizing intermediate.<sup>85</sup> Therefore, by applying  $-1.5$  V at the working electrode, the reduced helicene and the benzoyloxy radical are both generated simultaneously in the reaction layer close to the electrode surface. Then they may react together to produce the ECL emission according to the following sequence of reactions:



The competition between the formation of the excited state and the ground state (reaction 25) is here materialized by the factor  $\varepsilon$  which reflects the ECL efficiency. To further study the ECL behavior of the helicenes, we tested another typical co-reactant, TPrA which follows an oxidative-reduction mechanism.<sup>98</sup> TPrA is oxidized at the electrode surface and, after a deprotonation step, a strong reducing radical is generated. This intermediate may react with the oxidized helicene (i.e. [6]helicene<sup>2+</sup>) since its reversible anodic wave indicates the formation of a stable species.



where  $\text{Im}^+$  is the iminium product.

As shown in Figure 19 a-d, it was possible to record ECL spectra using both co-reactants with **DMQA<sup>+</sup>**, **DIAZA(Pr)<sup>+</sup>**, **DIAZA(Pr/Br)<sup>+</sup>** and **DIAZA(Hex/Br)<sup>+</sup>** according to their reversible cathodic and anodic waves. By comparing with the corresponding fluorescence spectra, ECL spectra show almost the same maximum emission wavelength confirming that the same excited state is produced when using two different co-reactants. Substitution with bromide in diaza[6]helicene core makes its emission red-shifted to a longer wavelength, as for **DIAZA(Pr/Br)<sup>+</sup>** to 680 nm, **DIAZA(Hex/Br)<sup>+</sup>** to 682 nm. The substitution of propyl (Pr/Br) by a longer alkyl chain (Hex/Br) increases steric hindrance but does not change the emission wavelength. Finally, it was not possible to collect the ECL spectra for compounds exhibiting an irreversible oxidation (**DIOXA<sup>+</sup>** and **DIAZA(Pr/NO<sub>2</sub>)<sup>+</sup>**) and very low ECL intensity except for **AZAOXA<sup>+</sup>**(Figure 19e)

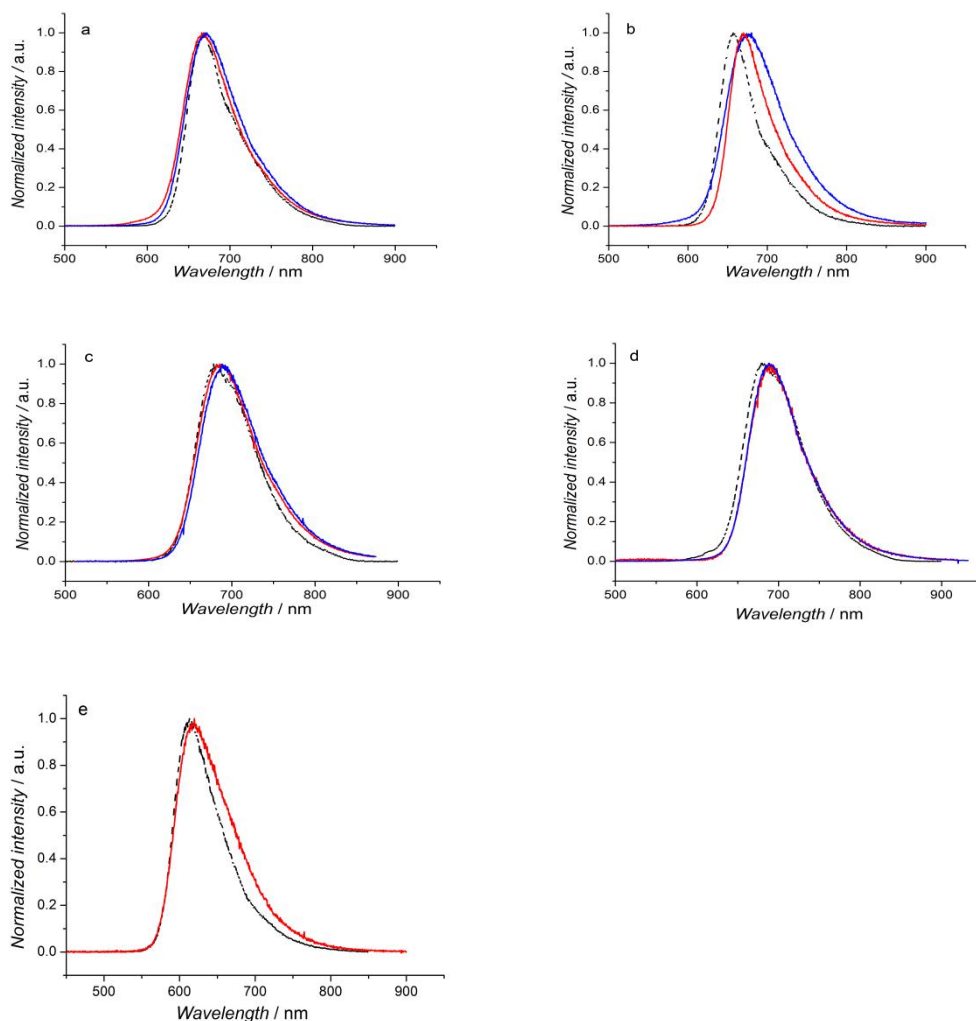


Figure 19. Typical fluorescence (dashed line) and ECL (solid lines) spectra for (a) **DMQA**<sup>+</sup>, (b) **DIAZA(Pr)**<sup>+</sup>, (c) **DIAZA(Pr/Br)**<sup>+</sup>, (d) **DIAZA(Hex/Br)**<sup>+</sup> and **AZAOXA**<sup>+</sup> in CH<sub>3</sub>CN solution. ECL spectra were recorded in degassed solution containing 0.1 M TBAPF<sub>6</sub> with either 0.05 M TPrA (blue line) or 0.01 M BPO (red line) used as co-reactants.

### 2.4.3 ECL efficiency discriminated by ECL “map”

As shown in Table 4, some [6]helicene compounds show strong ECL whereas the others do exhibit very weak ECL intensity even though ECL was performed by using the same concentration of BPO co-reactant under the similar conditions. According to Eq. 9, the corresponding ECL efficiency is referred to Ru(bpy)<sub>3</sub><sup>2+</sup> as a reference ECL-active compound<sup>99</sup> exhibiting arbitrary an ECL efficiency of 100% with BPO as a co-reactant (Table 4). As expected, **DMQA**<sup>+</sup> and **DIAZA(Pr)**<sup>+</sup> have very similar high ECL efficiency (46.2 % vs. 37.9 %). On the other hand, **AZAOXA**<sup>+</sup> has a very

low ECL efficiency about  $2.6 \times 10^{-3}$  % and the ECL intensity of **DIOXA**<sup>+</sup> is so low (ECL efficiency less than  $10^{-4}$  %) that light could only be detected on a very high sensitive calibration range. The **DIAZA**<sup>+</sup> series shows a drastic variation in ECL efficiency ranging from 37.9 % (**Pr**), 12.5 % (**Hex/Br**), 8.3 % (**Pr/Br**) down to  $10^{-4}$  % (**Pr/NO2**). In summary, not only the single replacement of a N atom by an O in the [6]helicene core would result in an irreversible oxidation, but also greatly reduce the ECL efficiency. Furthermore, introducing different substituent groups to the aromatic ring in the [6]helicene core can also lead to dramatic change of the ECL intensity. Such comparison of ECL intensities for all the studied helicenes reveals very interesting feature for the cathodic behavior.

With TPrA as the anodic co-reactant, all the helicenes exhibiting a reversible oxidation behavior (*i.e.* **DIAZA(Pr/Br)**<sup>+</sup>, **DIAZA(Hex/Br)**<sup>+</sup>, **DIAZA(Pr)**<sup>+</sup> and **DMQA**<sup>+</sup>) are energy-sufficient (Figure 20). Considering their position on the anodic side of the ECL map, they should generate very efficiently ECL emission. Indeed, their oxidation potentials are more anodic than those of the reference Ru(bpy)<sub>3</sub><sup>2+</sup> compound. More precisely, they are located further from the ECL-wall of TPrA than Ru(bpy)<sub>3</sub><sup>2+</sup>. These energetic considerations are verified by the ECL efficiency values determined experimentally. The ECL efficiencies are much higher than that of the reference compound Ru(bpy)<sub>3</sub><sup>2+</sup> (Table 4). For example, **DIAZA(Hex/Br)**<sup>+</sup>, **DIAZA(Pr/Br)**<sup>+</sup> and **DMQA**<sup>+</sup> showed very bright ECL and its efficiency is between 2.3 and 2.6 times greater than that of the reference compound. This high efficiency is due to the very anodic oxidation potentials of these compounds and thus to the resulting very exergonic reactions with the TPrA• radical. The ECL efficiency value of **DIAZA(Pr/Br)**<sup>+</sup> is very similar to those of **DMQA**<sup>+</sup>, even if its quantum yield is higher ( $\Phi_{FL} = 5.6$  and 13% for **DIAZA(Pr/Br)**<sup>+</sup> and **DMQA**<sup>+</sup>, respectively). However, **DIAZA(Pr/Br)**<sup>+</sup> is located further from the TPrA ECL-wall than **DMQA**<sup>+</sup>, illustrating the higher exergonicity of reaction 30 and thus falling deeper in the inverted Marcus region. But it was surprising to us that **DIAZA(Pr)**<sup>+</sup> gave lower ECL efficiency than the just above mentioned compounds since its quantum yield is at least 4 times higher. A possible explanation is that the ECL process is mainly governed by the energetics of

the process. Whatever, It is noteworthy that such values are remarkably high by compare with the other organic luminophores.<sup>1</sup>

The resulting ECL efficiencies are mainly determined by two factors: the free energy ( $\Delta G^\circ$ ) associated to the generation of the excited state (reactions 25 and 30) and the photophysics ( $\Phi_{\text{FL}}$ ) of the radiative de-excitation (reactions 26 and 31). The homogeneous electron-transfer reaction occurring between the electrogenerated reactive species (reactions 25 and 30) leads competitively to the population of the electronically excited state with a low exergonicity or to the formation of the ground state with a high exergonicity.<sup>100</sup> Even if this latter path is thermodynamically favored, it is kinetically inhibited during the ECL phenomenon as a consequence of the inverted Marcus region.<sup>101</sup> Such a competition in the ECL process is therefore a suitable way to study experimentally the inverted Marcus region. Therefore, we first considered the photophysical contribution in the overall ECL process by measuring the fluorescence quantum yields ( $\Phi_{\text{FL}}$ ) of the different compounds in the same experimental conditions (solvent, concentration, supporting electrolyte, co-reactant) as the previous study on structurally-related triangulenes. No noticeable quenching effects were observed with the presence of co-reactant BPO or TPrA and the supporting electrolyte. The values show that these helicenes are moderately fluorescent with quantum yields varying between 5.6 and 83.6 %. The variation of  $\Phi_{\text{FL}}$  in this range cannot explain the dramatic difference of the ECL efficiency ( $\Phi_{\text{ECL}}$ ) observed for the studied compounds. It means that the ECL efficiency is solely governed by the energetics of the reactions producing the excited state. Then the dependence relationship of  $\Phi_{\text{ECL}}$  *versus* the electron-transfer reaction exergonicity<sup>102</sup> was also investigated on this series of helicene cations. In the present study, a full ECL map of energy sufficiency was defined for the promotion of ECL in the cathodic region *via* the co-reactant reductive-oxidation pathway by using BPO and the anodic region *via* the oxidative-reduction pathway with TPrA. In the case of the co-reactant ECL, the free energy  $\Delta G^\circ$  values (in eV) for both cathodic and anodic regions may be calculated through the following equations:

$$\Delta G^{\circ}_{\text{cath}} = E^{\circ}_{\text{red}}(\text{helicene}^+) - E^{\circ}_{\text{ox}}(\text{Ph-CO}_2\bullet) + E_{\text{FL}}, \quad (32)$$

where the  $E^{\circ}_{\text{ox}}(\text{Ph-CO}_2\bullet)$  equal to + 1.36 V vs. Fc/Fc<sup>+</sup> was used here.

or

$$\Delta G^{\circ}_{\text{anod}} = E^{\circ}_{\text{red}}(\text{TPrA}\bullet) - E^{\circ}_{\text{ox}}(\text{helicene}^+) + E_{\text{FL}}, \quad (33)$$

where the  $E^{\circ}_{\text{red}}(\text{TPrA}\bullet)$  has been reported to be – 2.1 V vs. Fc/Fc<sup>+</sup>.<sup>4,38</sup>

By employing the electrochemical and fluorescent data (see Table 4) in these two formalisms, a full ECL “map” of energy sufficiency for excited state formation using two model co-reactants, BPO and TPrA was established. As shown in Figure 20, it displays the dependence of the energetic criteria on the emission wavelength and on the oxidation/reduction potentials that a luminophore should fulfill to reach the excited state and emit ECL. If its reduction/oxidation potentials are respectively more cathodic/anodic than the values determined by the corresponding dashed line, then the free energy  $\Delta G^{\circ}$  is negative enough so that the pathway leading to the ground-state formation is kinetically inhibited in accordance with the Marcus model of electron transfer processes.<sup>103</sup> It thus leads preferentially to the excited state which relaxes to the ground with ECL emission. If not, the compounds fall in the grey zone delimited by both dashed lines where they are energy deficient for excited state formation. As expected, this grey zone is widening for bluer emission, meaning that the required free energy is larger for these wavelengths. As shown in Figure 20, the electrochemical HOMO–LUMO gap ( $E^{\circ}_{\text{ox}} - E^{\circ}_{\text{red}}$ ) is almost constant for the helicene compounds presenting reversible oxidation and reduction waves.

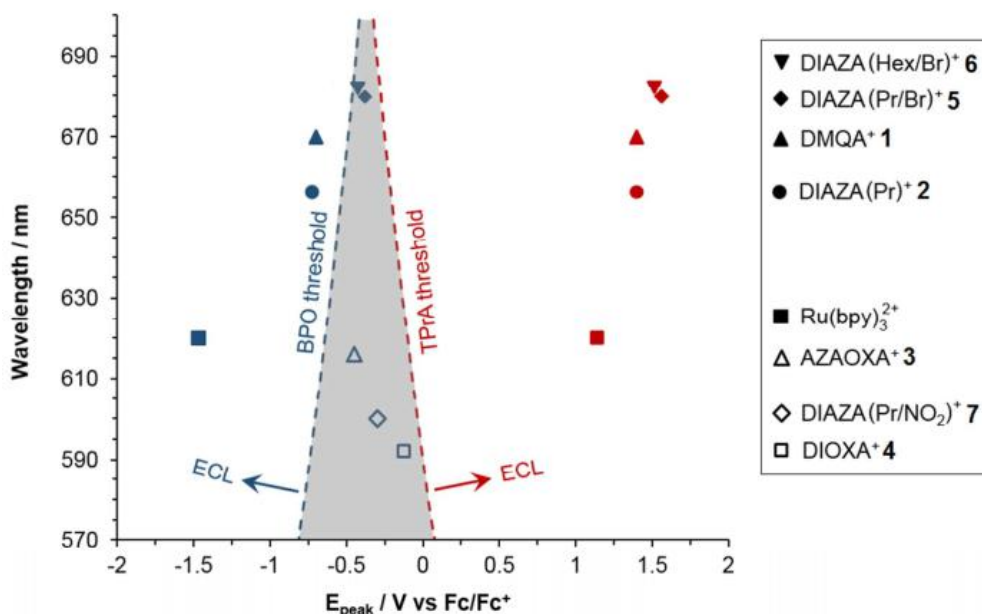


Figure 20. ECL map of energy sufficiency for the [6]helicene dyes with TPrA (red markers) and BPO (blue markers) co-reactants. The dashed lines show the reduction/oxidation potential threshold values of the luminophores required for a given emission wavelength using both co-reactants. The system is defined as energy sufficient when it is located on the right/left of the red/blue dashed lines, respectively.

Considering the ECL efficiency (Table 4) calculated from the experiments with BPO as co-reactant, it is obvious that the trend of ECL efficiencies of [6]helicenes follows the order  $\text{DIOXA}^+ < \text{DIAZA(Pr/NO}_2\text{)}^+ < \text{AZAOXA}^+ < \text{DIAZA(Pr/Br)}^+ < \text{DIAZA(Hex/Br)}^+ < \text{DIAZA(Pr)}^+ \approx \text{DMQA}^+$ . However, the ECL map provides a more convenient way to qualitatively discriminate the ECL capabilities of [6]helicenes. In this map, ECL capability could be predicted by directly calculating the distance between each data point to the plot. As expected, the points of  $\text{DIAZA(Pr)}^+$  and  $\text{DMQA}^+$  locate in ECL zone with a relative long bias from the dashed line, which indicates relative high ECL efficiency. On the other hand,  $\text{DIOXA}^+$ ,  $\text{DIAZA(Pr/NO}_2\text{)}^+$  and  $\text{AZAOXA}^+$  are clearly in the grey region and cannot generate strong ECL as shown in the experiments. This map also provides another clue for understanding why it was impossible to record the ECL spectra in the co-reactant pathway for these [6]helicenes exhibiting a dramatically low ECL efficiency. However, the situation appears less clear for both  $\text{DIAZA(Pr/Br)}^+$  and  $\text{DIAZA(Hex/Br)}^+$ . Indeed, both fall at the limit of the grey region and should not

produce ECL with BPO whereas they gave intermediate values for ECL yields between 8.3 and 12.5 %. This could be explained by the fact that they are very close to the threshold defined and that the value of the oxidation potential of the Ph-CO<sub>2</sub>• radical used in the calculations is not accurate enough. It is noteworthy that such ECL map formalism does not take into account the contribution of the fluorescence quantum yields  $\Phi_{\text{FL}}$ . Therefore, even if it illustrates the energetic criterion necessary to generate ECL, it can be used for predicting the ECL efficiency only for compounds with similar  $\Phi_{\text{FL}}$  values. Meanwhile, it will be essential to confirm the oxidation potential of the Ph-CO<sub>2</sub>• radical because BPO is largely used as a co-reactant in organic solvents. For the helicenes exhibiting a reversible oxidation behavior (i.e. **DIAZA(Pr/Br)<sup>+</sup>**, **DIAZA(Hex/Br)<sup>+</sup>**, **DIAZA(Pr)<sup>+</sup>** and **DMQA<sup>+</sup>**), they occupy the high energy-sufficient positions with TPrA as co-reactant in the anodic region and thus facilitate the generation of stronger ECL than the reference Ru(bpy)<sub>3</sub><sup>2+</sup>. Finally, the two threshold lines will cross each other in the “north part” of this ECL map with extending emission wavelength in the far away infrared region ( $\lambda > 715$  nm). It will be very interesting to explore the new types of ECL luminophores with suitable redox potentials in this crossed-threshold zone.

## 2.5 Conclusion

In summary, we have demonstrated the electrochemistry and ECL properties of three types of organic dyes, respectively. For the bis-quinone quadrupolar spirofluorene dyes, only the derivatives having donor end groups (dye **1** and **4**) show reversible oxidation waves. In contrast, a related dye **5** based on direct grafting of three diarylamino groups to a truxene core shows three successive one-electron oxidation steps. The most efficient ECL is achieved with green-emitting dye **1**, which exhibits three reversible oxidation waves with highly stable oxidized states (**1<sup>2+</sup>**, **1<sup>3+</sup>**, **1<sup>4+</sup>**). Dye **1** exhibits very intense and large ECL signal (4.5 times higher than that of the model compound Ru(bpy)<sub>3</sub><sup>2+</sup>) due to the high stability of the radicals at the high oxidized states. In addition, thanks to its molecular structure, dye **1** retains fluorescence after

nano-precipitation in water, which leads to fluorescent organic nanoparticles (FONs). ECL from FONs made of dye **1** was recorded in water and strong ECL nanoemitters are thus obtained. Then, a series of cationic triangulene dyes is selected for the electrochemistry and ECL investigations. It has been found that the nature of the heteroatoms in the core structure strongly influences the ECL capability. By only using BPO as co-reactant, dyes that contain two and three nitrogen atoms, **DAOTA**<sup>+</sup> and **TATA**<sup>+</sup>, respectively, exhibited high relative ECL yields, whereas **ADOTA**<sup>+</sup> (one nitrogen atoms) and **TOTA**<sup>+</sup> (none) showed dramatically small ECL intensities. Such dichotomy was rationalized and illustrated by using a new ECL “wall” presentation that can predict the ECL capability of triangulene dyes simply based on the redox and fluorescence data. Finally, another series of cationic helicene dyes, which have similar configuration to triangulene dye, was selected for further studies. ECL of these helicene dyes could be produced by either annihilation pathway or co-reactant pathway with BPO or TPrA depending on the redox behaviors. Helicenes **DMQA**<sup>+</sup> and **DIAZA(Pr)**<sup>+</sup> exhibit similar electrochemical redox behaviors and have almost the same high ECL efficiency generated through the co-reactant pathway. Similar decrease in ECL was also observed by progressively changing the heteroatoms in the core from **DIAZA(Pr)**<sup>+</sup>, to **AZAOXA**<sup>+</sup>, to **DIOXA**<sup>+</sup> with BPO as co-reactant. But the helicene dyes with reversible oxidation waves (*i.e.* **DIAZA(Pr/Br)**<sup>+</sup>, **DIAZA(Hex/Br)**<sup>+</sup>, **DIAZA(Pr)**<sup>+</sup> and **DMQA**<sup>+</sup>) present very high ECL efficiencies with TPrA as co-reactant. Thus similar formalism for rationalizing the ECL efficiencies was then advanced to a full ECL “map” by taking account both cathodic and anodic regions. Such a systematic overview based on the photophysical and electrochemical properties may guide the conception and the synthesis of new helicene compounds with a strong ECL.

Indeed, some of the organic dyes present ECL efficiencies than Ru(bpy)<sub>3</sub><sup>2+</sup> in the organic solvent system. In this study, we have demonstrated that the electrochemical, PL and ECL properties of organic dyes can be tuned in different way: 1) the two end-capped triphenylamine on the spirofluorene dyes enhance the stability of the oxidized species, thus enlarge the ECL signal; 2) progressively replacement of the

heteroatom in the core structures of triangulene and helicene dyes can tune reversibility of redox behaviors as well as the ECL efficiencies of the dyes; 3) the substitution of electron rich groups on the molecules could be another way to improve the ECL efficiency. However, most of the organic ECL has been performed in organic solvents. Such limitation can somehow hinder its analytical application in aqueous system. In our study, the conversion of spirofluorene dye to organic nanoparticles allows the preparation ECL nano-emitter in aqueous system. Moreover, all these triangulene and helicene dyes consist of two ionic partners (an organic cation and a fluoroborate anion) that allow an easy dissolution in organic solvents, like acetonitrile, acetone or dichloromethane. Such molecular configuration provides us the opportunity to potentially exchange the anionic part with other anions and prepare water-soluble helicenes which may be suitable for bioanalytical applications. Also, the ability to tune the luminescence of the chromophores makes them attractive candidates for multiple wavelength ECL labels.

## References

- (1) Miao, W. Electrogenerated chemiluminescence and its biorelated applications. *Chem. Rev.* **2008**, *108*, 2506-2553.
- (2) Bard, A. J. *Electrogenerated Chemiluminescence*; M. Dekker: New-York, 2004.
- (3) Nepomnyashchii, A. B.; Bard, A. J. Electrochemistry and electrogenerated chemiluminescence of BODIPY dyes. *Acc. Chem. Res.* **2012**, *45*, 1844-1853.
- (4) Stringer, B. D.; Quan, L. M.; Barnard, P. J.; Wilson, D. J. D.; Hogan, C. F. Iridium complexes of N-heterocyclic carbene ligands: Investigation into the energetic requirements for efficient electrogenerated chemiluminescence. *Organometallics* **2014**, *33*, 4860-4872.
- (5) Kanitz, A.; Schumann, J.; Scheffel, M.; Rajoelson, S.; Rogler, W.; Hartmann, H.; Rohde, D. Arylated mono-and bifunctional 2-aminothiophenes and 2-aminothiazoles as a new class of hole transport materials. *Chem. Lett.* **2002**, 896-897.
- (6) Welsh, D. M.; Kumar, A.; Meijer, E.; Reynolds, J. Enhanced contrast ratios and rapid switching in electrochromics based on poly (3, 4 - propylenedioxythiophene) derivatives. *Adv.Mater.* **1999**, *11*, 1379-1382.
- (7) Kumar, A.; Welsh, D. M.; Morvant, M. C.; Piroux, F.; Abboud, K. A.; Reynolds, J. R. Conducting poly (3, 4-alkylenedioxythiophene) derivatives as fast electrochromics with high-contrast ratios. *Chem. Mater.* **1998**, *10*, 896-902.
- (8) Goldenberg, L. M.; Bryce, M. R.; Petty, M. C. Chemosensor devices: voltammetric molecular recognition at solid interfaces. *J. Mater. Chem.* **1999**, *9*, 1957-1974.
- (9) Swager, T. M. The molecular wire approach to sensory signal amplification. *Acc. Chem. Res.* **1998**, *31*, 201-207.
- (10) Röckel, H.; Huber, J.; Gleiter, R.; Schuhmann, W. Synthesis of functionalized poly (dithienylpyrrole) derivatives and their application in amperometric biosensors. *Adv. Mater.* **1994**, *6*, 568-571.
- (11) Barbarella, G.; Favaretto, L.; Sotgiu, G.; Zambianchi, M.; Fattori, V.; Cocchi, M.; Cacialli, F.; Gigli, G.; Cingolani, R. Modified oligothiophenes with high photo- and electroluminescence efficiencies. *Adv. Mater.* **1999**, *11*, 1375-1379.
- (12) Cazzato, A.; Capobianco, M. L.; Zambianchi, M.; Favaretto, L.; Bettini, C.; Barbarella, G. Oligothiophene molecular beacons. *Bioconjug. Chem.* **2007**, *18*, 318-322.
- (13) Nepomnyashchii, A. B.; Ono, R. J.; Lyons, D. M.; Bielawski, C. W.; Sessler, J. L.; Bard, A. J. Electrochemistry and electrogenerated chemiluminescence of thiophene and fluorene oligomers: Benzoyl peroxide as a coreactant for oligomerization of thiophene dimers. *Chem. Sci.* **2012**, *3*, 2628-2638.
- (14) Capobianco, M. L.; Barbarella, G.; Manetto, A. Oligothiophenes as fluorescent markers for biological Applications. *Molecules* **2012**, *17*, 910.
- (15) Perepichka, I. F.; Perepichka, D. F. *Handbook of thiophene-based materials: applications in organic electronics and photonics*; Wiley Online Library, 2009.
- (16) Diederich, F.; Stang, P. J. *Metal-catalyzed cross-coupling reactions*; John Wiley & Sons, 2008.
- (17) Bäuerle, P. End - capped oligothiophenes—new model compounds for polythiophenes. *Adv. Mater.* **1992**, *4*, 102-107.

- (18) Rapta, P.; Haubner, K.; Machata, P.; Lukeš, V.; Rosenkranz, M.; Schiemenz, S.; Klod, S.; Kivelä, H.; Kvarnström, C.; Hartmann, H. Charged states in diphenylamino endcapped thiophenes with a 1, 4-phenylene core: In situ electron spin resonance/ultraviolet–visible–near infrared and nuclear magnetic resonance spectroelectrochemistry and quantum chemical study. *Electrochim. Acta* **2013**, *110*, 670-680.
- (19) Mitschke, U.; Bauerle, P. Synthesis, characterization, and electrogenerated chemiluminescence of phenyl-substituted, phenyl-annulated, and spirofluorenyl-bridged oligothiophenes. *J. Chem. Soc., Perkin Trans. 1* **2001**, 740-753.
- (20) Rohde, D.; Dunsch, L.; Tabet, A.; Hartmann, H.; Fabian, J. Radical ions of  $\alpha$ ,  $\alpha'$ -bis (diphenylamino)-capped oligothiophenes: A combined spectroelectrochemical and theoretical study. *J. Phys. Chem. B* **2006**, *110*, 8223-8231.
- (21) Fichou, D. Structural order in conjugated oligothiophenes and its implications on opto-electronic devices. *J. Mater. Chem.* **2000**, *10*, 571-588.
- (22) Mitschke, U.; Bäuerle, P. The electroluminescence of organic materials. *J. Mater. Chem.* **2000**, *10*, 1471-1507.
- (23) Perepichka, I. F.; Perepichka, D. F.; Meng, H.; Wudl, F. Light-emitting polythiophenes. *Adv. Mater.* **2005**, *17*, 2281-2306.
- (24) Garnier, F.; Hajlaoui, R.; Yassar, A.; Srivastava, P. All-polymer field-effect transistor realized by printing techniques. *Science* **1994**, *265*, 1684-1686.
- (25) Ong, B. S.; Wu, Y.; Liu, P.; Gardner, S. High-performance semiconducting polythiophenes for organic thin-film transistors. *J. Am. Chem. Soc.* **2004**, *126*, 3378-3379.
- (26) Sariciftci, N.; Smilowitz, L.; Heeger, A. J.; Wudl, F. Photoinduced electron transfer from a conducting polymer to buckminsterfullerene. *Science* **1992**, *258*, 1474-1476.
- (27) Getautis, V.; Stanisauskaite, A.; Paliulis, O.; Uss, S.; Uss, V. Influence of methyl substituents in phenylenediamine derivatives on the properties of electrophotographic layers. *J. Prakt. Chem.* **2000**, *342*, 58-62.
- (28) Omer, K. M.; Ku, S.-Y.; Cheng, J.-Z.; Chou, S.-H.; Wong, K.-T.; Bard, A. J. Electrochemistry and electrogenerated chemiluminescence of a spirobifluorene-based donor (triphenylamine)–acceptor (2,1,3-Benzothiadiazole) molecule and its organic nanoparticles. *J. Am. Chem. Soc.* **2011**, *133*, 5492–5499.
- (29) Mangione, M. I.; Spanevello, R. A.; Rumero, A.; Heredia, D.; Marzari, G.; Fernandez, L.; Otero, L.; Fungo, F. Electrogenerated conductive polymers from triphenylamine end-capped dendrimers. *Macromolecules* **2013**, *46*, 4754-4763.
- (30) Polo, F.; Rizzo, F.; Veiga-Gutierrez, M.; De Cola, L.; Quici, S. Efficient greenish blue electrochemiluminescence from fluorene and spirobifluorene derivatives. *J. Am. Chem. Soc.* **2012**, *134*, 15402-15409.
- (31) Omer, K. M.; Ku, S.-Y.; Wong, K.-T.; Bard, A. J. Green electrogenerated chemiluminescence of highly fluorescent benzothiadiazole and fluorene derivatives. *J. Am. Chem. Soc.* **2009**, *131*, 10733-10741.
- (32) Li, H.; Daniel, J.; Verlhac, J. B.; Blanchard - Desce, M.; Sojic, N. Bright Electrogenerated chemiluminescence of a bis - donor quadrupolar spirofluorene dye and its nanoparticles. *Chem. Eur. J.* **2016**, *22*, 12702-12714.
- (33) Bansal, R. C.; Eisenbraun, E. J.; Ryba, R. J. The Iodination of fluorene to 2,7-diiodofluorene. *Org. Prep. Proced. Int.* **1987**, *19*, 258-260.

- (34) Daniel, J.; Godin, A. G.; Palayret, M.; Lounis, B.; Cognet, L.; Blanchard-Desce, M. Innovative molecular-based fluorescent nanoparticles for multicolor single particle tracking in cells. *J. Phys. D.* **2016**, *49*, 084002.
- (35) Yuan, S.-C.; Chen, H.-B.; Zhang, Y.; Pei, J. Rigid linear and star-shaped  $\pi$ -conjugated 2,2':6',2''-terpyridine ligands with blue emission. *Org. Lett.* **2006**, *8*, 5701-5704.
- (36) Omer, K. M.; Ku, S.-Y.; Chen, Y.-C.; Wong, K.-T.; Bard, A. J. Electrochemical behavior and electrogenerated chemiluminescence of star-shaped D-A compounds with a 1,3,5-triazine core and substituted fluorene arms. *J. Am. Chem. Soc.* **2010**, *132*, 10944-10952.
- (37) Fungo, F.; Wong, K.-T.; Ku, S.-Y.; Hung, Y.-Y.; Bard, A. J. Electrogenerated chemiluminescence 81: Influence of donor and acceptor substituents on the ECL of a spirobifluorene-bridged bipolar system. *J. Phys. Chem. B* **2005**, *109*, 3984-3989.
- (38) Miao, W.; Choi, J.-P.; Bard, A. J. Electrogenerated chemiluminescence 69: The tris(2, 2'-bipyridine) ruthenium (II), (Ru(bpy)<sub>3</sub><sup>2+</sup>)/tri-n-propylamine (TPrA) system revisited—a new route involving TPrA<sup>+</sup> cation radicals. *J. Am. Chem. Soc.* **2002**, *124*, 14478-14485.
- (39) Yuan, Y.; Han, S.; Hu, L.; Parveen, S.; Xu, G. Coreactants of tris(2,2'-bipyridyl)ruthenium(II) electrogenerated chemiluminescence. *Electrochim. Acta.* **2012**, *82*, 484-492.
- (40) Pavlishchuk, V. V.; Addison, A. W. Conversion constants for redox potentials measured versus different reference electrodes in acetonitrile solutions at 25 °C. *Inorg. Chim. Acta.* **2000**, *298*, 97-102.
- (41) Hansch, C.; Leo, A.; Taft, R. W. A survey of hammett substituent constants and resonance and field parameters. *Chem. Rev.* **1991**, *91*, 165-195.
- (42) Diaz, A.; Crowley, J.; Bargon, J.; Gardini, G.; Torrance, J. Electrooxidation of aromatic oligomers and conducting polymers. *J. Electroanal. Chem.* **1981**, *121*, 355-361.
- (43) Audebert, P.; Miomandre, F. Electrofluorochromism: from molecular systems to set-up and display. *Chem. Sci.* **2013**, *4*, 575-584.
- (44) Quinton, C.; Alain-Rizzo, V.; Dumas-Verdes, C.; Miomandre, F.; Clavier, G.; Audebert, P. Redox-controlled fluorescence modulation (electrofluorochromism) in triphenylamine derivatives. *RSC Adv.* **2014**, *4*, 34332-34342.
- (45) Katan, C.; Tretiak, S.; Werts, M. H. V.; Bain, A. J.; Marsh, R. J.; Leonczek, N.; Nicolaou, N.; Badaeva, E.; Mongin, O.; Blanchard-Desce, M. Two-photon transitions in quadrupolar and branched chromophores: Experiment and theory. *J. Phys. Chem. B* **2007**, *111*, 9468-9483.
- (46) Bi, Y.-H.; Huang, Z.-L.; Liu, B.; Zou, Q.-J.; Yu, J.-H.; Zhao, Y.-D.; Luo, Q.-M. Two-photon-excited fluorescence and two-photon spectrofluorochemistry of riboflavin. *Electrochem. Commun.* **2006**, *8*, 595-599.
- (47) Yilmaz, I. In situ monitoring of metallation of metal-free phthalocyanine via UV-Vis and steady-state fluorescence techniques. Thin-layer UV-Vis and fluorescence spectroelectrochemistry of a new non-aggregating and electrochromic manganese(3+) phthalocyanine. *New J. Chem.* **2008**, *32*, 37-46.
- (48) Choi, J.-P.; Wong, K.-T.; Chen, Y.-M.; Yu, J.-K.; Chou, P.-T.; Bard, A. J. Electrogenerated chemiluminescence 76: Excited singlet state emission vs excimer emission in ter(9,9-diarylfuorene)s. *J. Phys. Chem. B* **2003**, *107*, 14407-14413.

- (49) Omer, K. M.; Ku, S.-Y.; Wong, K.-T.; Bard, A. J. Efficient and stable blue electrogenerated chemiluminescence of fluorene-substituted aromatic hydrocarbons. *Angew. Chem. Int. Ed.* **2009**, *48*, 9300-9303.
- (50) Swanick, K. N.; Ladouceur, S.; Zysman-Colman, E.; Ding, Z. Self-enhanced electrochemiluminescence of an Iridium(III) complex: mechanistic insight. *Angew. Chem. Int. Ed.* **2012**, *51*, 11079-11082.
- (51) Swanick, K. N.; Ladouceur, S.; Zysman-Colman, E.; Ding, Z. Bright electrochemiluminescence of iridium (III) complexes. *Chem. Commun.* **2012**, *48*, 3179-3181.
- (52) Kapturkiewicz, A.; Grabowski, Z. R.; Jasny, J. Electrochemical generation of excited TICT states. Part I. *J. Electroanal. Chem.* **1990**, *279*, 55-65.
- (53) Kapturkiewicz, A. Electrochemical generation of excited TICT states V: Evidence of inverted Marcus region. *Chem. Phys.* **1992**, *166*, 259-273.
- (54) Oh, J.-W.; Lee, Y. O.; Kim, T. H.; Ko, K. C.; Lee, J. Y.; Kim, H.; Kim, J. S. Enhancement of electrogenerated chemiluminescence and radical stability by peripheral multidonors on alkynylpyrene derivatives. *Angew. Chem. Int. Ed.* **2009**, *48*, 2522-2524.
- (55) Shen, M.; Zhu, X.-H.; Bard, A. J. Electrogenerated chemiluminescence of solutions, films, and nanoparticles of dithienylbenzothiadiazole-based donor-acceptor-donor red fluorophore: Fluorescence quenching study of organic nanoparticles. *J. Am. Chem. Soc.* **2013**, *135*, 8868-8873.
- (56) Adam, C.; Wallabregue, A.; Li, H.; Gouin, J.; Vanel, R.; Grass, S.; Bosson, J.; Bouffier, L.; Lacour, J.; Sojic, N. Electrogenerated chemiluminescence of cationic triangulene dyes: Crucial influence of the core heteroatoms. *Chem. Eur. J.* **2015**, *21*, 19243-19249.
- (57) Masuhara, H.; Nakanishi, H.; Sasaki, K.: *Single Organic Nanoparticles*; Springer, 2003.
- (58) Bonacchi, S.; Genovese, D.; Juris, R.; Montalti, M.; Prodi, L.; Rampazzo, E.; Zaccheroni, N. Luminescent silica nanoparticles: Extending the frontiers of brightness. *Angew. Chem. Int. Ed.* **2011**, *50*, 4056-4066.
- (59) Hesari, M.; Swanick, K. N.; Lu, J.-S.; Whyte, R.; Wang, S.; Ding, Z. Highly Efficient dual-color electrochemiluminescence from BODIPY-capped PbS nanocrystals. *J. Am. Chem. Soc.* **2015**, *137*, 11266-11269.
- (60) Hesari, M.; Workentin, M. S.; Ding, Z. Thermodynamic and kinetic origins of Au<sub>250</sub> nanocluster electrochemiluminescence. *Chem. Eur. J.* **2014**, *20*, 15116-15121.
- (61) Knight, A. W. A review of recent trends in analytical applications of electrogenerated chemiluminescence. *TrAC Trend. Anal. Chem.* **1999**, *18*, 47-62.
- (62) Richter, M. M. Electrochemiluminescence (ECL). *Chem. Rev.* **2004**, *104*, 3003-3036.
- (63) Hu, L.; Xu, G. Applications and trends in electrochemiluminescence. *Chem. Soc. Rev.* **2010**, *39*, 3275-3304.
- (64) Bosson, J.; Gouin, J.; Lacour, J. Cationic triangulenes and helicenes: synthesis, chemical stability, optical properties and extended applications of these unusual dyes. *Chem. Soc. Rev.* **2014**, *43*, 2824-2840.
- (65) Martin, J.; Smith, R. G. Factors influencing the basicities of triarylcarbinols. The synthesis of sesquixanthidrol. *J. Am. Chem. Soc.* **1964**, *86*, 2252-2256.
- (66) Laursen, B. W.; Krebs, F. C. Synthesis of a triazatriangulenium salt. *Angew.*

*Chem. Int. Ed.* **2000**, *112*, 3574-3576.

(67) W Laursen, B.; C Krebs, F. Synthesis, structure, and properties of azatriangulenium salts. *Chem. Eur. J.* **2001**, *7*, 1773-1783.

(68) Krebs, F. C. On the synthesis and functionalisation of the 4-aza-8, 12-dioxa-4, 8, 12, 12c-tetrahydrodibenzo [cd, mn] pyrenium system. *Tetrahedron. Lett.* **2003**, *44*, 17-21.

(69) Thyraug, E.; Sørensen, T. J.; Gryczynski, I.; Gryczynski, Z.; Laursen, B. W. Polarization and symmetry of electronic transitions in long fluorescence lifetime triangulenium dyes. *J. Phys. Chem. A* **2013**, *117*, 2160-2168.

(70) Maliwal, B. P.; Fudala, R.; Raut, S.; Kokate, R.; Sørensen, T. J.; Laursen, B. W.; Gryczynski, Z.; Gryczynski, I. Long-lived bright red emitting azaoxa-triangulenium fluorophores. *PLoS one* **2013**, *8*, e63043.

(71) Nicolas, C.; Lacour, J. Triazatriangulenium cations: Highly stable carbocations for phase-transfer catalysis. *Org. Lett.* **2006**, *8*, 4343-4346.

(72) Gejo, J. L.; Manoj, N.; Sumalekshmy, S.; Glieman, H.; Schimmel, T.; Wörner, M.; Braun, A. M. Vacuum-ultraviolet photochemically initiated modification of polystyrene surfaces: morphological changes and mechanistic investigations. *Photochem. Photobiol. Sci.* **2006**, *5*, 948-954.

(73) Sørensen, T. J.; Laursen, B. W.; Luchowski, R.; Shtoyko, T.; Akopova, I.; Gryczynski, Z.; Gryczynski, I. Enhanced fluorescence emission of Me-ADOTA<sup>+</sup> by self-assembled silver nanoparticles on a gold film. *Chem. Phys. Lett.* **2009**, *476*, 46-50.

(74) Reynisson, J.; Schuster, G. B.; Howerton, S. B.; Williams, L. D.; Barnett, R. N.; Cleveland, C. L.; Landman, U.; Harrit, N.; Chaires, J. B. Intercalation of trioxatriangulenium ion in DNA: binding, electron transfer, x-ray crystallography, and electronic structure. *J. Am. Chem. Soc.* **2003**, *125*, 2072-2083.

(75) Pothukuchy, A.; Mazzitelli, C. L.; Rodriguez, M. L.; Tuesuwan, B.; Salazar, M.; Brodbelt, J. S.; Kerwin, S. M. Duplex and quadruplex DNA binding and photocleavage by trioxatriangulenium ion. *Biochemistry* **2005**, *44*, 2163-2172.

(76) Baisch, B.; Raffa, D.; Jung, U.; Magnussen, O. M.; Nicolas, C.; Lacour, J.; Kubitschke, J.; Herges, R. Mounting freestanding molecular functions onto surfaces: The platform approach. *J. Am. Chem. Soc.* **2008**, *131*, 442-443.

(77) Simonsen, J. B.; Kjær, K.; Howes, P.; Nørgaard, K.; Bjørnholm, T.; Harrit, N.; Laursen, B. W. Close columnar packing of triangulenium ions in langmuir films. *Langmuir* **2009**, *25*, 3584-3592.

(78) Haketa, Y.; Sasaki, S.; Ohta, N.; Masunaga, H.; Ogawa, H.; Mizuno, N.; Araoka, F.; Takezoe, H.; Maeda, H. Oriented salts: dimension - controlled charge - by - charge assemblies from planar receptor-anion complexes. *Angew. Chem. Int. Ed.* **2010**, *49*, 10079-10083.

(79) Němcová, I.; Němec, I. The voltammetry of triarylmethane dyes in acetonitrile. *J. Electroanal. Chem. Interf. Electrochem.* **1971**, *30*, 506-510.

(80) Laursen, B. W.; Krebs, F. C.; Nielsen, M. F.; Bechgaard, K.; Christensen, J. B.; Harrit, N. 2, 6, 10-Tris (dialkylamino) trioxatriangulenium ions: Synthesis, structure, and properties of exceptionally stable carbenium ions. *J. Am. Chem. Soc.* **1998**, *120*, 12255-12263.

(81) Sørensen, T. J.; Laursen, B. W.; Luchowski, R.; Shtoyko, T.; Akopova, I.

Gryczynski, Z.; Gryczynski, I. Enhanced fluorescence emission of Me-ADOTA<sup>+</sup> by self-assembled silver nanoparticles on a gold film. *Chem. Phys. Lett.* **2009**, *476*, 46-50.

(82) Rich, R. M.; Stankowska, D. L.; Maliwal, B. P.; Sørensen, T. J.; Laursen, B. W.; Krishnamoorthy, R. R.; Gryczynski, Z.; Borejdo, J.; Gryczynski, I.; Fudala, R. Elimination of autofluorescence background from fluorescence tissue images by use of time-gated detection and the AzaDiOxaTriAngulenium (ADOTA) fluorophore. *Anal. Bioanal. Chem.* **2013**, *405*, 2065-2075.

(83) Dileesh, S.; Gopidas, K. R. Photoinduced electron transfer in azatriangulenium salts. *J. Photochem. Photobiol. A* **2004**, *162*, 115-120.

(84) Lai, R. Y.; Fleming, J. J.; Merner, B. L.; Vermeij, R. J.; Bodwell, G. J.; Bard, A. J. Electrogenerated chemiluminescence 74: Photophysical, electrochemical, and electrogenerated chemiluminescent studies of selected nonplanar pyrenophanes. *J. Phys. Chem. A* **2004**, *108*, 376-383.

(85) Choi, J.-P.; Bard, A. J. Electrogenerated chemiluminescence 73: acid-base properties, electrochemistry, and electrogenerated chemiluminescence of neutral red in acetonitrile. *J. Electroanal. Chem.* **2004**, *573*, 215-225.

(86) Chandross, E. A.; Sonntag, F. I. Chemiluminescent electron-transfer reactions of radical anions. *J. Am. Chem. Soc.* **1966**, *88*, 1089-1096.

(87) Akins, D. L.; Birke, R. L. Energy transfer in reactions of electrogenerated aromatic anions and benzoyl peroxide: chemiluminescence and its mechanism. *Chem. Phys. Lett.* **1974**, *29*, 428-435.

(88) Shen, Y.; Chen, C.-F. Helicenes: synthesis and applications. *Chem. Rev.* **2012**, *112*, 1463-1535.

(89) Meisenheimer, J.; Witte, K. Reduction von 2-nitronaphtalin. *Ber. Dtsch. Chem. Ges.* **1903**, *36*, 4153-4164.

(90) Herse, C.; Bas, D.; Krebs, F. C.; Bürgi, T.; Weber, J.; Wesolowski, T.; Laursen, B. W.; Lacour, J. A highly configurationally stable [4]heterohelicinium cation. *Angew. Chem. Int. Ed.* **2003**, *42*, 3162-3166.

(91) Torricelli, F.; Bosson, J.; Besnard, C.; Chekini, M.; Bürgi, T.; Lacour, J. Modular synthesis, orthogonal post-functionalization, absorption, and chiroptical properties of cationic [6]helicenes. *Angew. Chem. Int. Ed.* **2013**, *52*, 1796-1800.

(92) Laursen, B. W.; Krebs, F. C. Synthesis of a triazatriangulenium salt. *Angew. Chem. Int. Ed.* **2000**, *39*, 3432-3434.

(93) W. Laursen, B.; C. Krebs, F. Synthesis, structure, and properties of azatriangulenium salts. *Chem. Eur. J.* **2001**, *7*, 1773-1783.

(94) Kel, O.; Sherin, P.; Mehanna, N.; Laleu, B.; Lacour, J.; Vauthey, E. Excited-state properties of chiral [4]helicene cations. *Photochem. Photobiol. Sci.* **2012**, *11*, 623-631.

(95) Bosson, J.; Labrador, G. M.; Pascal, S.; Miannay, F.-A.; Yushchenko, O.; Li, H.; Bouffier, L.; Sojic, N.; Tovar, R. C.; Muller, G.; Jacquemin, D.; Laurent, A. D.; Le Guennic, B.; Vauthey, E.; Lacour, J. Physicochemical and electronic properties of cationic[6]helicenes: from chemical and electrochemical stabilities to far-red (polarized) luminescence. *Chem. Eur. J.* **2016**, *22*, 18394-18403..

(96) Natarajan, P.; Schmittl, M. Photoluminescence, redox properties, and electrogenerated chemiluminescence of twisted 9, 9'-bianthryls. *J. Org. Chem.* **2013**, *78*,

10383-10394.

(97) Suk, J.; Wu, Z.; Wang, L.; Bard, A. J. Electrochemistry, electrogenerated chemiluminescence, and excimer formation dynamics of intramolecular  $\pi$ -Stacked 9-naphthylanthracene derivatives and organic nanoparticles. *J. Am. Chem. Soc.* **2011**, *133*, 14675-14685.

(98) Kanoufi, F.; Zu, Y.; Bard, A. J. Homogeneous oxidation of trialkylamines by metal complexes and its impact on electrogenerated chemiluminescence in the trialkylamine/Ru(bpy)<sub>3</sub><sup>2+</sup> system. *J. Phys. Chem. B* **2001**, *105*, 210-216.

(99) McCord, P.; Bard, A. J. Electrogenerated chemiluminescence. Part 54: Electrogenerated chemiluminescence of ruthenium(II) 4,4'-diphenyl-2,2'-bipyridine and ruthenium(II) 4,7-diphenyl-1,10-phenanthroline in aqueous and acetonitrile solutions. *J. Electroanal. Chem.* **1991**, *318*, 91-99.

(100) Kapturkiewicz, A.; Szrebowaty, P.; Angulo, G.; Grampp, G. Electron transfer quenching and electrochemiluminescence comparative studies of the systems containing N-methylpyridinium cations and Ru(2,2'-bipyridine)<sub>3</sub><sup>2+</sup> or Ru(1,10-phenanthroline)<sub>3</sub><sup>2+</sup> complexes. *J. Phys. Chem. A* **2002**, *106*, 1678-1685.

(101) Kapturkiewicz, A.: Marcus theory in the qualitative and quantitative description of electrochemiluminescence phenomena. In *advances in electrochemical science and engineering*; Alkire, R. C., Gerischer, H., Kolb, D. M., Tobias, C. W., Eds.; Wiley-VCH; Vol. 5; pp 1-60.

(102) Szrebowaty, P.; Kapturkiewicz, A. Free energy dependence on tris( 2,2'-bipyridine) ruthenium(II) electrochemiluminescence efficiency. *Chem. Phys. Lett.* **2000**, *328*, 160-168.

(103) Marcus, R. A. Electron transfer reactions in chemistry: theory and experiment (Nobel Lecture). *Angew. Chem. Int. Ed.* **1993**, *32*, 1111-1121.

## **Chapter 3**

# **Electrochemiluminescence of stimuli-responsive hydrogel films**

### 3.1 Introduction

The preparation of stimuli-responsive polymer materials at the solid surface is of great interest for many practical applications,<sup>1-3</sup> such as drug delivery, temperature-induced switching, biosensor, tissue engineering and separation.<sup>4</sup> All these successful applications highly depend on the responsive phase transition in the material when exposed to an external stimulus (e.g. temperature, pH, biorecognition event, light, etc.).<sup>5-7</sup> Such transition occurs rapidly with the switching of their chemical and physical properties. Among these smart polymer materials, the most prominent example is the poly(*N*-isopropylacrylamide) (pNIPAM), exhibiting the reversible coil-to-globule transition near the room temperature in the aqueous solution.<sup>8</sup> The coil-to-globule transition could induce many changes including optical properties, conductivity, permeability, etc.<sup>9</sup> The mechanism of such phase transition is widely investigated considering its importance in many biological aspects such as protein folding, DNA packing, and interchain complexation.<sup>10-12</sup> Moreover, pNIPAM hydrogels with cross-linked networks can largely amplify the sensitiveness at a molecular level, which is translated into macroscopic effects such as a change in swelling degree.<sup>13</sup> Finally, hydrogel films of pNIPAM are very promising in the drug release and diagnostics, chemical separation, catalysis, and surface modification.<sup>8</sup> Recently, the responsive hydrogel materials incorporated with different classes of luminophores have also been widely studied for the luminescent sensing.<sup>14-23</sup> In this case, hydrogel materials are usually miniaturized into micro- or nanogels, which not only considerably improve their response time<sup>24</sup> but also bring spatial resolution to be used at the scale of biological cells.<sup>25</sup> On the other hand, the hydrogels have also been decorated on the electrode, so that the effects of coil-to-globule transition on electrochemical properties of the modified electrode can be studied. The modified responsive polymers, which are either a hydrogel layer<sup>26-28</sup> or polymer brush grafted on the electrode surface,<sup>29-34</sup> provide a unique switchable interface to manipulate the electrochemical properties.<sup>29,35-37</sup> There are two major factors that can affect the

diffusion of the electroactive species through the polymer interface:<sup>30</sup> firstly, the coil-to-globule transition may alter the permeability of the membrane by making a dense collapsed layer; secondly, the ionization state of the layer can also control the diffusion of a charged species. The charged polymer interface would strongly hinder the species with the same charge, whereas allow the opposite charged ones pass through the polymer layer. Such behavior has been nicely exploited to build a “smart” switch at the electrode surface by using a mixture of two pH-responsive polymers, which display either positive or negative charges in different pH regions.<sup>38</sup> Thus, discrimination of the positively charged and negatively charged species was achieved on the electrode. Recently, these signal-responsive thin hydrogel layers are further coupled with enzyme-based biocatalytic systems to yield “smart” multi-signal-responsive hybrid systems with built-in logic. They can be interfaced with electronic systems resulting in novel bioelectronic devices switchable by logically processed biomolecular signals.<sup>39</sup>

This chapter mainly deals with the combination of ECL technology with stimuli-responsive hydrogel films, which can be electrochemically deposited on two conductive objects. Firstly, the mechanism of the generation of the amplified ECL will be demonstrated upon the pNIPAM-Ru hydrogel films deposited on a glassy carbon electrode (GCE).<sup>40</sup> Then, such deposition can be employed to a carbon fiber which serves as bipolar electrode (BE) for the formation of the same hydrogel films by using bipolar electrochemistry (BPE) strategy.<sup>41</sup> ECL of carbon fiber was also produced by BPE mode at only the extremity where the films were deposited. Thus, this method allows the preparation of the electrochemiluminescent thermoresponsive Janus objects.<sup>41</sup>

### **3.2 ECL of hydrogel films on GCE**

The combination of ECL<sup>42-44</sup> with stimuli-responsive hydrogels offers the opportunity to design novel materials whose electrochemistry, luminescence and ECL are not only manipulated by the electrode potential but also by an external stimulus. The first ECL

microgels were reported recently in 2013.<sup>45</sup> Those microgels were based on thermo-responsive poly(N-isopropylacrylamide) (pNIPAM) hydrogels covalently incorporating Ru(bpy)<sub>3</sub><sup>2+</sup> redox centers<sup>46,47</sup> and exhibited a strong amplification of the ECL signal upon collapse of the microgels above the volume phase transition temperature (VPTT) (Figure 1). It was reported that such amplification of ECL could reach 2 orders of the magnitude. Interestingly, it was found that the ECL enhancement process was not due to the photoluminescent properties of the ruthenium complex, but probably related to a hydrophilic–hydrophobic transition and the decrease of the average distance between adjacent ruthenium centers in the microgels.

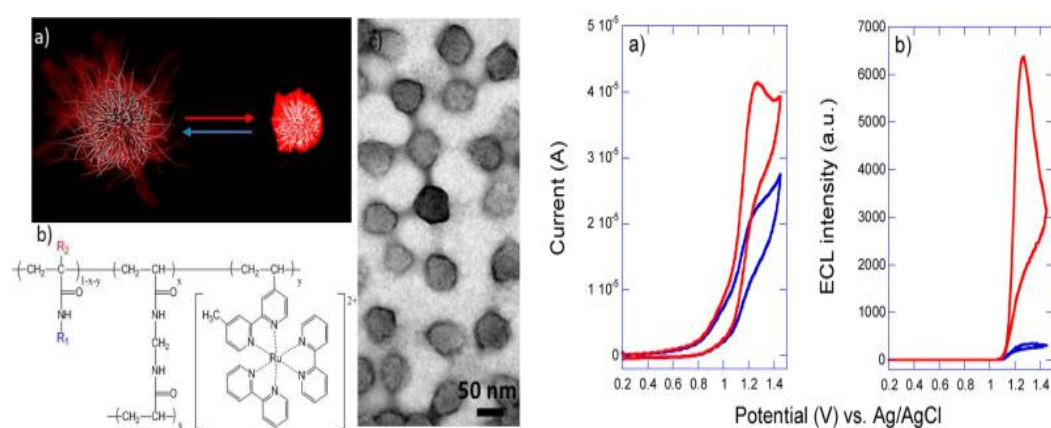


Figure 1. Left: (a) Scheme representation of ECL microhydrogel in the swollen (left) and collapsed (right) states, (b) Chemical composition of the cross-linked microgels functionalized with chemical group R<sub>2</sub> and R<sub>2</sub>, (c) Transmission electron microscopy (TEM) of the ECL microgels in dry state. Right: Cyclic voltammograms (a) and the corresponding ECL curves (b) of the microgels/TPrA system when the microgels were in the swollen (blue line) and collapsed (red line) states.<sup>45</sup>

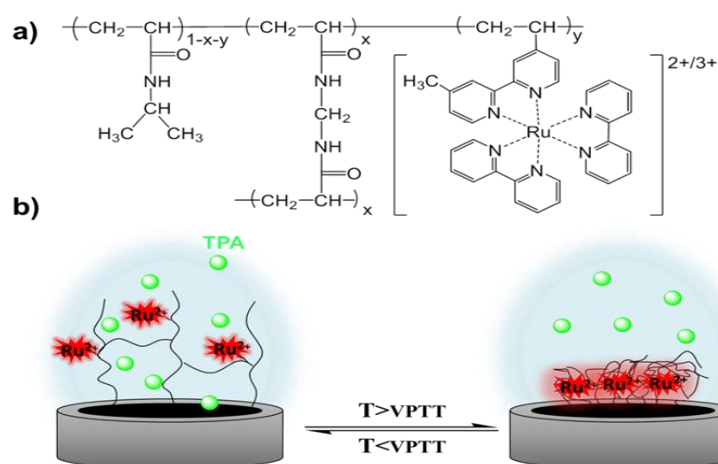


Figure 2. a) Chemical structure of the thermoresponsive pNIPAM-Ru hydrogel film. b) Schematic representation of the electrode modified with the ECL-active film in the swollen (left: below VPTT) and collapsed (right: above VPTT) states.<sup>40</sup>

However, those explanations for the ECL enhancement process are not fully testified, because the process involves too many parameters which could not be excluded separately in the microgel system. Indeed, the collapse occurring at the phase transition results in the decrease of the average distance between adjacent ruthenium centers in the microgels, which affects the electron-exchange reactions between the ruthenium sites and at the electrode. Besides, a hydrophilic-hydrophobic transition would occur due to the dehydration of the hydrogels above the VPTT, which may also contribute partially to the ECL enhancement. The hydrophobic environment of the collapsed hydrogel films was found to promote ECL process because of the absorption of neutral TPrA on the hydrophobic surface,<sup>48,49</sup> but on the other hand could block the diffusion of the co-reactant through hydrogels. Based on this previous study, the experimental proposal of pNIPAM hydrogel films incorporating covalently-attached Ru(bpy)<sub>3</sub><sup>2+</sup> luminophore were implemented here in order to figure out the ECL enhancement mechanism in the pNIPAM hydrogel films at the collapsed state (Figure 2). This study allows deciphering the key factor governing the ECL enhancement.

### 3.2.1 Preparation of the hydrogel films

Hydrogel films have been attached to the solid substrate *via* various techniques, including photo-cross-linking of polymer chains,<sup>50</sup> polymerization from a self-assembled monolayer,<sup>51</sup> plasma polymerization,<sup>52</sup> and electrochemical assisted polymerization.<sup>30,34,53</sup> In this work, the preparation of the thin redox hydrogel films is achieved by electrochemically assisted free radical polymerization. This method requires a conductive solvent and a polymer that can be synthesized *via* free-radical polymerization.<sup>54</sup> Moreover it is simple, flexible and it has been used previously for different acrylic monomers.<sup>55,56</sup> For example, the polymerization of acrylamide on a silver electrode or aluminium alloy was initiated through the electrochemical decomposition of potassium persulfate.<sup>57</sup> Sodium perchlorate was also utilized instead of persulfate salts in the recent work for the preparation of microgels.<sup>58</sup> Johannsmann and his co-workers have done several pioneering studies on the preparation of hydrogel films.<sup>28,34,53,59</sup> In their reports, pNIPAM hydrogel films with thickness between 25 and 250 nm were produced on a gold electrode. It was proved that the hydrogel films were permeable to small ions. The influence of the added salts on thickness and morphology was also investigated in the same films. It was found that the thickness and surface morphology of pNIPAM hydrogel films produced by electrochemically induced polymerization depend on the nature and the concentration of the supporting electrolyte. The film thickness increased with increasing salt concentration as well as increasing salting-out capability of the electrolyte, while the surface morphology showed small-scale globules in the case of low salting-out capability.<sup>34</sup> However, the adding of reversible addition-fragmentation chain transfer (RAFT) agent could strongly enhance the homogeneity of the film surfaces because of a reduced amount of hydrogel formation.<sup>59</sup>

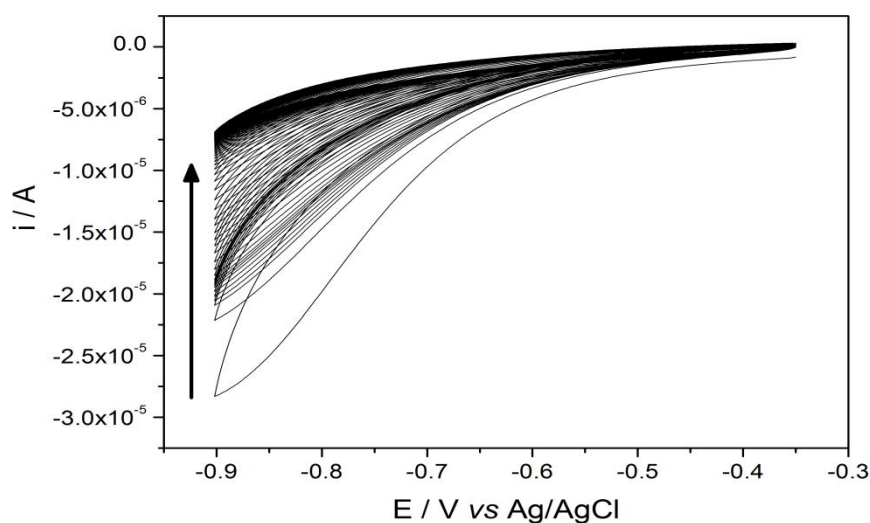


Figure 3. Electrodeposition of a pNIPAM-Ru hydrogel film by cyclic voltammetry.

Electrochemically assisted free radical polymerization was performed in a degassed solution containing 70 mM NIPAM, 0.14 mM Ru(bpy)<sub>3</sub> monomer, 1.5 mM K<sub>2</sub>S<sub>2</sub>O<sub>8</sub>, 1.75 mM BIS and 0.2M KNO<sub>3</sub>. The potential was scanned 60 times at a scan rate of 100 mV/s between -0.35 and -0.9 V vs. Ag/AgCl. The arrow indicates the increasing scan number.

Herein, thermo-responsive pNIPAM hydrogel films with surface-confined redox sites were prepared by electrochemically assisted free radical polymerization on GCE. The hydrogel films compose of pNIPAM matrix with Ru(bpy)<sub>3</sub> complex moieties covalently bounding to the polymeric network. Ru(bpy)<sub>3</sub> derivative containing 4-vinyl and 4'-methyl on one of the 2,2'-bipyridine ring was synthesized according to the procedure described by Spiro *et al.*<sup>60</sup> Free-radical polymerization of NIPAM monomer, BIS as cross-linker and ruthenium luminophore was triggered by electrochemically reduced sulfate radicals from persulfate ions at the electrode surface. All these reactions were performed in the degassed solution containing 0.2 M KNO<sub>3</sub> as supporting electrolyte. As shown in Figure 3, the potential applied to the system was cycled between -0.35 and -0.9 V vs. Ag/AgCl at a scan rate of 100 mV / s. The current decreased over the cycles, due to the growth of the resulting pNIPAM-Ru hydrogel film which is insulating in this potential window. Indeed, even if it incorporates redox centers, the ruthenium complexes are electro-inactive in this cathodic potential range and the reduction of the initiator is progressively blocked because of the diffusion

hindering. This process results not only in linear chain formation but also in branched and cross-linked structures for the formation of insoluble, water-permeable hydrogel films.

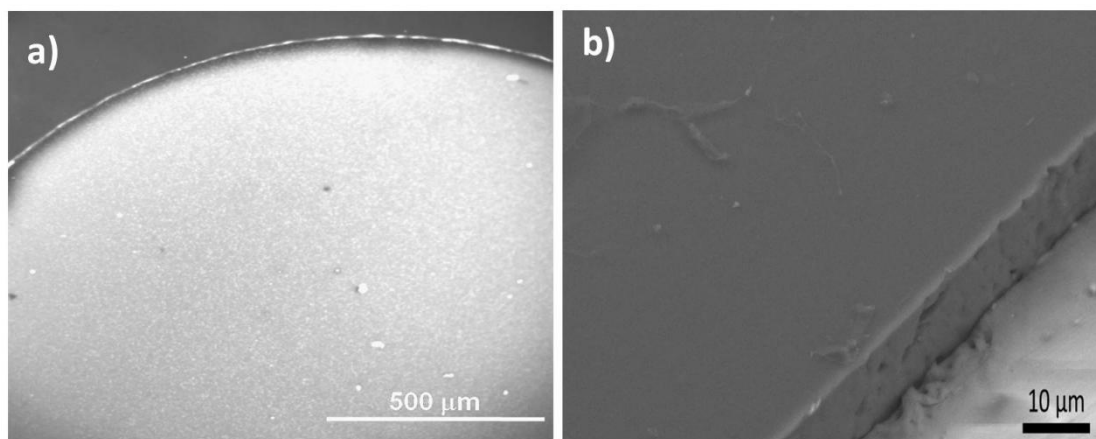


Figure 4. a) Photoluminescent image of the hydrogel film at swollen state in water recorded by a CCD camera, b) Scanning electron microscopy (SEM) image of lyophilized hydrogel films on GCE.

The electrodeposited pNIPAM-Ru hydrogel film presents a uniform morphology over the entire electrode surface (Figure 4). This observation is consistent with the work of Bünsow *et al.*<sup>34</sup> who studied the polymerization of pNIPAM hydrogels in similar conditions on a gold electrode. They showed that the layers should lead to homogeneous films, because the polymerization occurs in conditions below the lower critical solution temperature (LCST) (typically, 32 °C for pNIPAM). The SEM pictures are recorded with the film after freeze drying. The film appears covering homogeneously the entire electrode surface. The thickness of the hydrogel film is clearly visible and is 8 μm in the swollen state. When the temperature is raised above the VPTT, the film would collapse as a result of a decrease in the film thickness by a factor of 2. Related experimental details will be described in the third section. It is noteworthy that this value is also in good agreement with the diameter variation measured by dynamic light scattering (DLS) for pNIPAM-Ru microgels with similar composition.<sup>45</sup> The photoluminescent image reflects a homogeneous distribution of ruthenium sites over the entire electrode surface, indicating that Ru(bpy)<sub>3</sub> moieties

were successfully incorporated into the pNIPAM matrix by covalent bonding. This ensures the feasibility of the following electrochemical and ECL studies.

### 3.2.2 Electrochemical properties of the hydrogel films

Electrochemical properties of the pNIPAM-Ru film at the electrode were characterized by differential pulse voltammetry (DPV) in the phosphate buffer solution (PBS, 100 mM, pH7.4). When temperature was controlled at 25 °C below the VPTT of pNIPAM, the redox hydrogel was in the swollen state and it exhibited a well-defined anodic peak at 1.15 V *vs.* Ag/AgCl (Figure 5), which corresponds to the oxidation of the ruthenium centers incorporated into the pNIPAM hydrogel film network. The oxidation potential was identical to those of free Ru(bpy)<sub>3</sub><sup>2+</sup> in solution. In addition, DPV characterization of the pNIPAM films electropolymerized without the Ru(bpy)<sub>3</sub> moieties did not display any obvious oxidation peak at this potential. It indicates that the pure pNIPAM matrix is not electroactive in the explored potential window. Thus, DPV also proves the successful grafting of the Ru(bpy)<sub>3</sub> moieties in the film. Those ruthenium centers or a fraction of them are therefore electrochemically accessible in the swollen pNIPAM-Ru hydrogel film. When the temperature was raised to 40 °C (*i.e.* above the VPTT), the hydrogel film collapses and the coil-to-globule transition event affects the electrochemical signal (Figure 5). The oxidation peak current of the pNIPAM-Ru film rises from 1.2 μA to 1.9 μA below and above VPTT, respectively (Figure 5). DPV signal is directly proportional to the amount of redox complex incorporated in the hydrogel films. It means that a higher number of ruthenium sites are electroactive in the collapsed state of the film than in the swollen state.

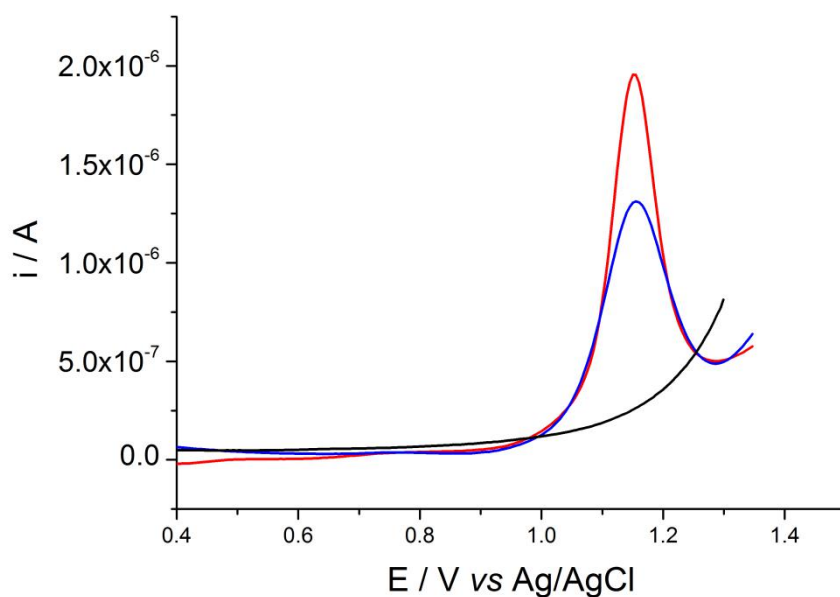


Figure 5. Differential pulse voltammograms of the pNIPAM hydrogel film at 25°C (black line) and the pNIPAM-Ru film from the swollen state at 25°C (blue curve) to the collapsed state at 40°C (red curve) in 100 mM PBS (pH 7.4).

However, this result could be counterintuitive because, on one hand, the flexibility of the polymer chain bearing the ruthenium centers is more constraint in the collapsed state. As a result, the diffusion of the charge in redox hydrogels involving an electron-hopping process from site to site should be less efficient.<sup>61</sup> In addition, the diffusion of the counter-ion in the film which is required to compensate the charge movement is more difficult in the collapsed state.<sup>62</sup> On the other hand, the efficiency of the electron-transfer processes is governed by the distance between the adjacent redox centers. The rate of electron transfer decays exponentially with the distance between the redox centers in the transition state. It has been reported by Heller *et al.* that electron-transferring collisions are effective in hydrogels when the distance between the redox sites is in the 1–3 nm range.<sup>63</sup> The natural inference is that the collapse of the pNIPAM-Ru film enhances significantly the electrochemical signal by decreasing the redox intersites distance. In other words, more ruthenium sites are addressed electrochemically in the collapsed state where the average distance between adjacent redox centers is smaller than in the swollen state. It indicates that the

distance between adjacent ruthenium sites is the key factor governing the electrochemical response of the pNIPAM-Ru films.

### 3.2.3 ECL of the hydrogel films

As shown in Figure 1, ECL of the microgel was generated by using TPrA as co-reactant. ECL enhancement up to 26 times was observed below and above the VPTT, while the CV peak current shows a much smaller increase by a 1.7 fold factor. Therefore, electrochemical process seems to be uncorrelated with the ECL enhancement in the microgels. In the present study, the pNIPAM-Ru films contained the same positively charge Ru(bpy)<sub>3</sub> centers as in the microgels. Then the ECL properties of the films were studied by using three prototypical oxidative-reduction co-reactants: tri-*n*-propylamine (TPrA), 2-(dibutylamino)ethanol (DBAE) and oxalate. TPrA and DBAE belong to organic bases and become positively charged tertiary amines after the protonation in PBS solution.<sup>64-66</sup> But DBAE is more hydrophilic than TPrA. Oxalate is negatively charged in PBS and follows different mechanistic pathways.<sup>67</sup> Electrochemical behaviors of the hydrogel film and TPrA were investigated first by using cyclic voltammetry in PBS solution that contained 100 mM of TPrA (Figure 6). As shown in Figure 6a, irreversible oxidation of TPrA started at 0.7 V and then occurred mainly at 1.1 V vs. Ag/AgCl, which is also the oxidation potential of the Ru(bpy)<sub>3</sub> centers in the film. This indicates that the oxidation process occurs predominantly by the electro-catalytic pathway where the ruthenium centers are oxidized by electron-hopping and then mediates the subsequent oxidation of the TPrA reagent.

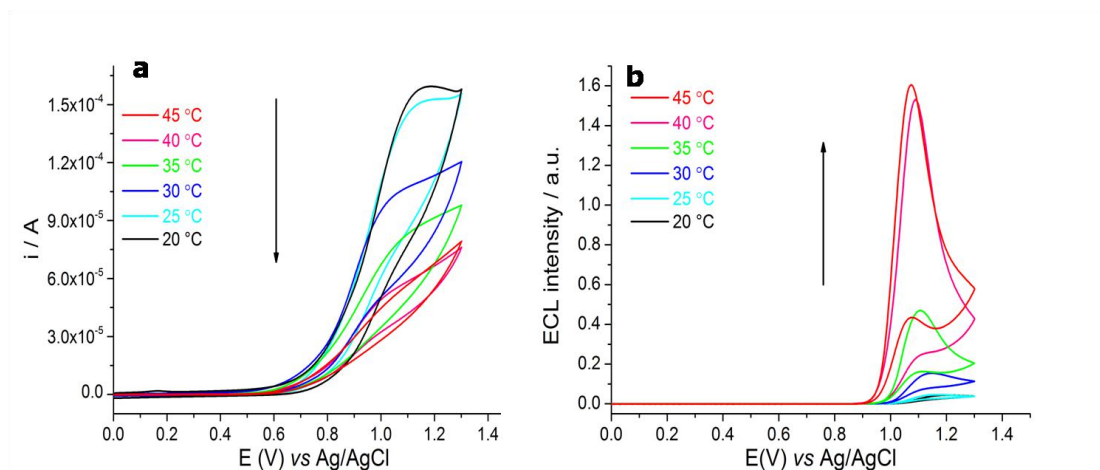


Figure 6. Influence of temperature on the electrochemical (a) and ECL (b) signals of the pNIPAM-Ru films. Experiments were performed at different temperatures in 100 mM PBS (pH 7.4) solution containing 100 TPrA mM. The arrows indicate the increasing temperatures. Scan rate: 100 mV/s.

The temperature increase caused drastic effects on both the voltammetric wave and the ECL response of the films (Figure 6). Both evolve with temperature in non-monotonic ways. When we increased progressively the temperature from 20 °C to 45 °C, the oxidation current decreased significantly at the VPTT of pNIPAM and then remained constant. The collapse of the polymeric matrix hinders the diffusion<sup>62</sup> of the TPrA into the film where it is oxidized. Such a behavior could be expected considering, on one hand, that the diffusion coefficient of free species in the collapsed gels is much smaller than in the swollen gels. But on the other hand, the favored electron-hopping process in the collapsed state could promote the electrocatalytic oxidation of the coreactant. Considering these antagonistic effects, the limiting role of the coreactant diffusion in the collapsed state has been demonstrated by experiments performed with pNIPAM films that do not contain Ru(bpy)<sub>3</sub> centers (Figure 7). In this case, both the oxidation current of TPrA and ECL intensity were decreased due to the blocked diffusion in the collapsed state of the hydrogel films. It means that a much lower amount of coreactant radicals are electrogenerated above the VPTT. In a first approximation, we can consider that the current is proportional to the amount of coreactant radicals produced at a given potential. But the faradaic charge  $Q$  (i.e. the integration of the TPrA oxidation current observed on Figure 6a) is a more relevant

parameter describing the total amount of electrogenerated TPrA radicals than the peak current. Similarly, the global ECL emission is better represented by integrating the ECL intensity (Figure. 6b). Therefore, in further plots and table, we considered the faradaic charge  $Q$  and the integrated ECL signal  $I_{ECL}$ , although a very similar trend is observed if we consider just the current intensity or the ECL intensity. Whatever, ECL emission of pNIPAM-Ru films is also remarkably modified by the swell-collapse transition occurring at 32°C for pNIPAM network. ECL signal increased at the VPTT and then remained constant. Such a behavior is consistent with the ECL enhancement observed on microgels.<sup>45</sup>

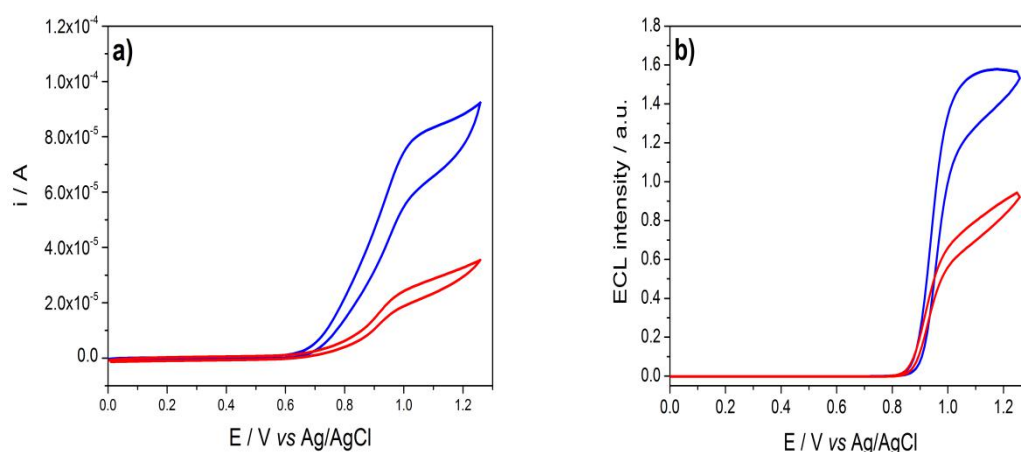


Figure 7. CVs and ECL signals of a pNIPAM-modified GCE recorded in a 100 mM PBS (pH7.4) solution containing 0.5 mM  $\text{Ru}(\text{bpy})_3^{2+}$  and 100 mM TPrA at 25 °C (red curve) and at 40 °C (blue curve). The film were prepared as in Figure 3 but without  $\text{Ru}(\text{bpy})_3$  monomer in the electrodeposition solution.

To check the precise evolution of the faradaic charge and ECL emission around the VPTT, we plotted both signals as a function of the temperature (Figure 8). The charge and ECL intensity were stable from 20 to 25 °C and then they evolved in opposite ways with film collapse between 25 and 40 °C: charge  $Q$  decreased by a factor 3 and  $I_{ECL}$  is enhanced by a factor 38 (Table 1). Finally, both reached a plateau above the VPTT. Both charge and ECL intensity are correlated to the volume phase transition of the hydrogel, since their evolution exhibit a marked evolution at the phase transition. However, both properties evolve with antagonistic effects. We also investigated the

ECL properties of the pNIPAM films without covalently-bound ruthenium complexes but with free  $\text{Ru}(\text{bpy})_3^{2+}$  and TPrA in solution (Figure 7b). pNIPAM films present a completely different ECL behavior in comparison to pNIPAM-Ru films. As expected, and similarly to the current variations, ECL intensity decreased with the hydrogel collapse. The blocked diffusion of free  $\text{Ru}(\text{bpy})_3^{2+}$  and TPA inside the collapsed films limited their oxidation at the electrode surface and thus the ECL process which leads to lower ECL emission. In brief, the collapse at the VPTT affected differently the ECL emission: it decreased for the pNIPAM films whereas it is enhanced for the pNIPAM-Ru ones.

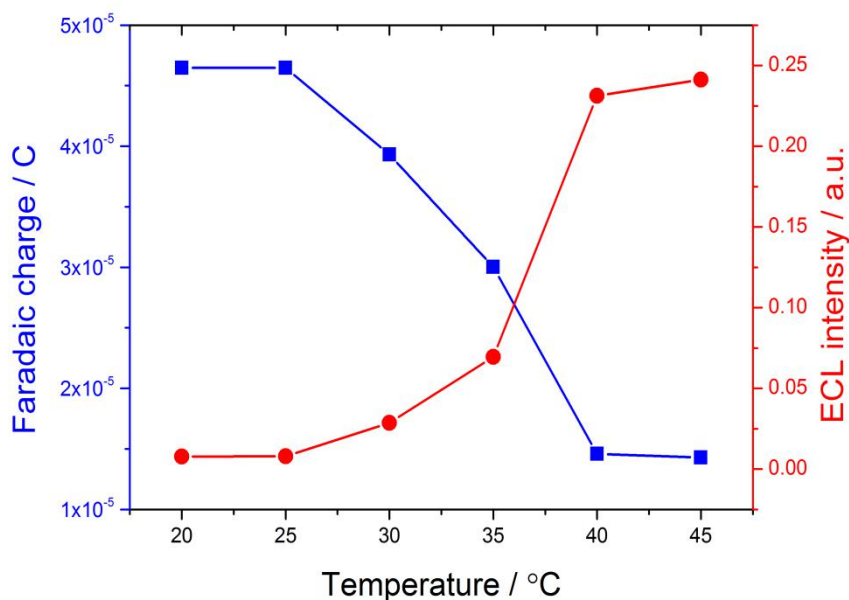


Figure 8. Evolution of the faradaic charge (blue curve) and ECL signal (red curve) as a function of temperature. Faradaic charge  $Q$  and ECL signal  $I_{\text{ECL}}$  are defined as the integration of the current under the voltammograms and of the ECL light intensity, respectively. Data are extracted from Figure 6

One can observe unambiguously that the oxidation of the coreactant and the ECL emission are not cross-correlated in the pNIPAM-Ru films (Figure 8). It demonstrates thus that the variation of the ECL intensity is not governed by the oxidation of the TPrA co-reactant. ECL enhancement is demonstrated even if antagonist effects due to the blocked diffusion of the co-reactant species were observed. Indeed, in this case, a

lower amount of TPrA radicals leads in fine to enhanced ECL intensity. A similar behavior is observed with DBAE as a coreactant (Figure 9). With the hydrogel transition, the charge is divided by a factor 3 ( $Q^{40^{\circ}\text{C}}/Q^{25^{\circ}\text{C}} = 0.31$ ) whereas the ECL signal ( $I$ ) is amplified by 40-fold after the VPTT (Table 1).

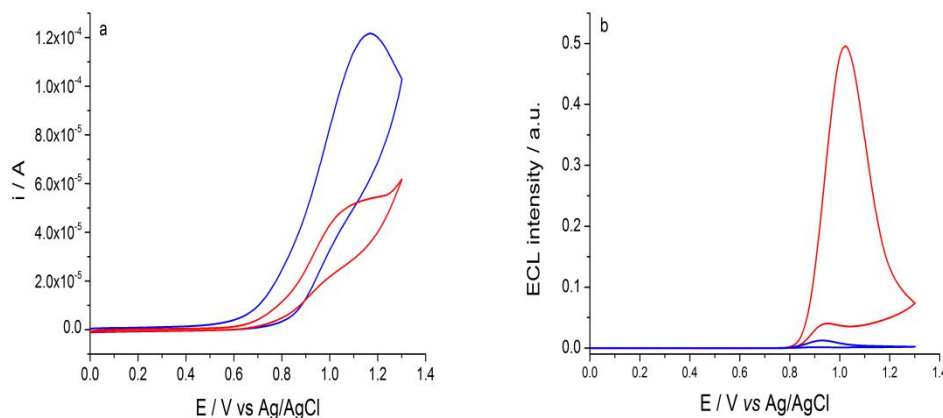


Figure 9. CVs (a) and ECL signals (b) of a GCE modified with a pNIPAM-Ru films in a 100 mM PBS solution containing 20 mM DBAE at 25°C (blue curve) and at 40°C (red curve). Scan rate: 100 mV/s.

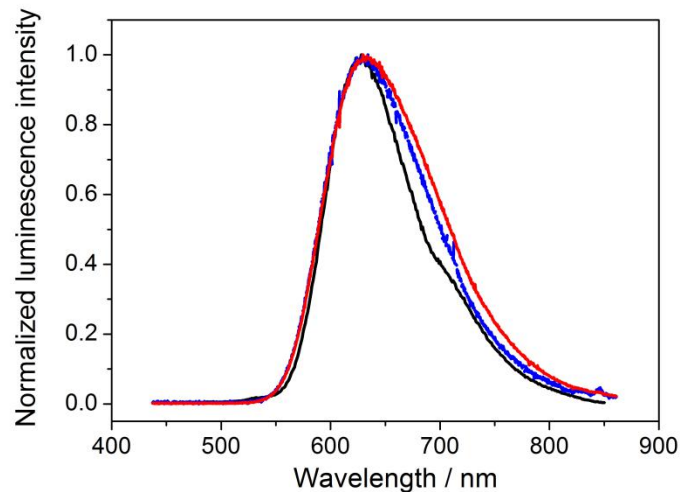


Figure 10. ECL spectra of the pNIPAM-Ru hydrogel film in the swollen state at 25 °C (blue curve) and in the collapsed state at 40 °C (red curve). Comparison with the photoluminescent spectrum (black curve) of the 10  $\mu\text{M}$   $\text{Ru}(\text{bpy})_3^{2+}$  complex in aqueous solution at 25 °C. ECL spectra were acquired in 100 mM PBS solution (pH 7.4) containing 100 mM TPrA during cyclic voltammetry experiments. The potential was scanned from 0.2 V to 1.45 V at a scan rate 50 mV/s.

To investigate further the luminescence properties of the thermoresponsive films, we recorded the ECL spectra of the pNIPAM-Ru films in the swollen and collapsed states

(Figure 10). Identical ECL and photoluminescent spectra were obtained showing that the photochemical properties of the luminophore were not affected neither by the pNIPAM matrix nor the film collapse, in agreement with previous results obtained with microgels.<sup>23,45</sup> It means also that the ECL enhancement observed at the VPTT is not controlled by the photochemical step.

Further electrochemical and ECL experiments were performed on the negatively charged oxalate coreactant to investigate the influence of the charge on the properties of such pNIPAM-Ru hydrogels. Indeed, the charge of the coreactant has a strong influence on the film permeability. Figure 11a presents the CV results obtained with oxalate at 25 °C and 40 °C. The cyclic voltammograms showed that the oxidation current of oxalate is more important in collapsed state than in the swollen state. However, we observed the opposite voltammetric behavior for positively-charge coreactants (i.e. TPrA and DBAE). It can be explained by the positive charge of the hydrogel films, which facilitated the transport of anionic coreactants, despite its collapsed state. Using oxalate as coreactant, ECL intensity is also remarkably increased with hydrogel collapse (Figure 11b). We measured a 58-fold amplification factor for the ECL intensity at the VPTT with oxalate (Table 1). The slight increase in the oxidation of the oxalate could explain the slight increase in the ECL ratio using this coreactant compared to TPrA or DBAE.

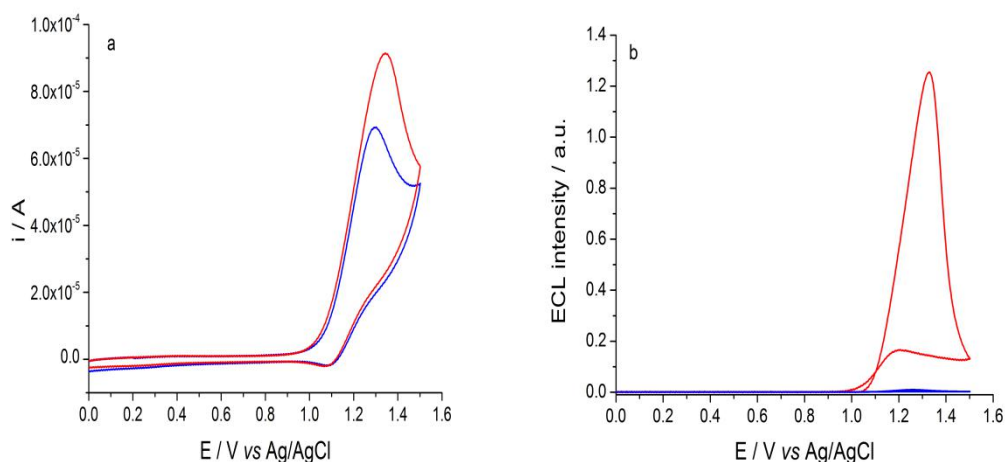


Figure 11. Cyclic voltammograms (a) and ECL signals (b) of the pNIPAM-Ru film in a PBS

solution containing 30 mM oxalate at 25 °C (blue curve) and at 40 °C (red curve). Scan rate: 100 mV/s.

The phase transition event induces the strong enhancement of the ECL intensity for all three co-reactants used. Therefore the turn-on effect is not specific of the nature or of the charge of the co-reactant. This remarkable phenomenon is not related to the oxidation efficiency of the co-reactant since a lower amount of co-reactant radicals is produced in the collapsed state due to hindered diffusion of TPrA and DBAE. But even this antagonist effect leads to an amplification of the ECL signal. It is an intriguing observation because it is classically believed that the higher oxidation rate of the co-reactant the stronger the ECL emission.<sup>66,68</sup> It has been nicely demonstrated in solution,<sup>69,70</sup> but here the pNIPAM matrix plays a key role. As already mentioned, the film collapse occurring at the VPTT provokes a hydrophilic–hydrophobic transition and a decrease of the film thickness. Using the film format, the ECL experiments performed with the pNIPAM hydrogels (i.e. without covalently-bound ruthenium centers) demonstrated that the hydrophilic–hydrophobic transition does not induce the ECL turn-on. It was an important result that could not be obtained with the microgel particles.<sup>45</sup> It was also confirmed with the DBAE coreactant which is more hydrophilic but gave similar ECL signal ratio to TPrA (Table 1).

**Table 1.** Variations of the faradaic charge ratio and of the ECL signal ratio for different coreactants between 25 °C (swollen state) and 40 °C (collapsed state).

Coreactant	Faradaic charge at 25°C $Q^{25°C}(\mu\text{C})$	Faradaic charge at 40°C $Q^{40°C}(\mu\text{C})$	ECL signal at 25°C ( $10^3$ a.u.)	ECL signal at 40°C ( $10^3$ a.u.)	Faradaic charge ratio $Q^{40°C}/Q^{25°C}$	ECL signal ratio $I_{ECL}^{40°C}/I_{ECL}^{25°C}$
TPrA	46±3	14.3±13	5±0.4	188±53	0.31±0.28	38±12
DBAE	39±2	13.7±3	1.7±0.07	67±3	0.31±0.1	40±1
Oxalate	13.7±0.4	17.5±0.7	2.68±0.07	155±4	1.28±0.06	58±3

The film shrinking induces the decrease of the average distance between adjacent ruthenium sites since they are covalently-bound to the pNIPAM matrix. The decrease of this distance in the collapsed state favors the charge diffusion by electron-hopping in the hydrogels and more ruthenium sites were addressed electrochemically above

VPTT (Figure 5). It is the main parameter governing the electrochemical response of the pNIPAM-Ru films. It can also explain the ECL amplification by promoting the ECL annihilation pathway. Indeed, the very exergonic reaction between  $\text{Ru}(\text{bpy})_3^+$  and  $\text{Ru}(\text{bpy})_3^{3+}$  in close enough proximity in the pNIPAM-Ru film can generate the excited state  $\text{Ru}(\text{bpy})_3^{2+*}$ .  $\text{Ru}(\text{bpy})_3^+$  could be produced by the highly-reducing co-reactant radicals following different mechanistic pathways and  $\text{Ru}(\text{bpy})_3^{3+}$  is generated by electron-hopping process in the film. The film collapse decreases the average distance between the ruthenium centers and thus increases exponentially the rate of the annihilation reaction which produces the excited state. This effect could also contribute to the enhanced ECL emission observed in such thermo-responsive hydrogel films.

### 3.3 ECL of hydrogel films on BE

Conventional electrochemistry is performed by using three electrodes system, where the potential of the working electrode is directly controlled by a potentiostat.<sup>71</sup> Alternatively, the polarization potential can be induced on the electrode to drive electrochemical reactions in a wireless manner. BPE is terminology to define such electrochemical reactions at the extreme poles of conductive objects placed in electrolyte solution when applying an electric field.<sup>72</sup> This electric field is established in the solution by applying an external potential ( $E_{\text{tot}}$ ) between two feeder electrodes. If the conductive object is sufficiently long and the electric potential is high enough, then faradaic reactions will occur at both poles of the object.<sup>73</sup> This conductive object acting like anode and cathode is called as bipolar electrode (BE). When an external potential ( $E_{\text{tot}}$ ) applied between the two feeder electrodes, the electric field ( $\varepsilon$ ) is given by the following equation:<sup>74</sup>

$$\varepsilon = \frac{E_{\text{tot}}}{d} \quad (1)$$

where  $d$  is the distance between the two feeder electrodes.

The potential difference ( $\Delta E$ ) between the two extreme ends of BE is given by:

$$\Delta E = \varepsilon \cdot l \quad (2)$$

where  $l$  is the length of BE. To trigger the electrochemical reactions on the bipolar electrode, a minimum potential difference ( $\Delta E_{min}$ ) between the extremities of the bipolar electrode is required. In a first order approximation,  $\Delta E$  has to be at least equal to the standard potential difference of the two redox reactions. Due to its wireless characteristics, BPE has been widely utilized for functional material preparation, inducing specific motion of micro object, generation of surface gradients or analytical applications.<sup>74-77</sup>

Therefore, BPE route was proposed for asymmetrically modifying a micro object (i.e. carbon fiber was used as BE here) with thermo-responsive hydrogel films as a further study.<sup>41</sup> By adding an electric field to the system, polymer deposition would occur only at the induced cathodic pole of the carbon fiber in the similar solution containing the same monomers as in the second section. This method allows not only the deposition of hydrogel films on a micro object, but also the generation of ECL on hydrogel films in the following experiment in a wireless manner.

### 3.3.1 Wireless deposition of the hydrogel films

As depicted in Figure 12, the BPE cell consist of two compartments, containing the feeder electrodes (graphite rods), connected with a glass capillary (outer diameter: 2 mm, inner diameter: 1.12 mm; length: 25 mm), A carbon fiber (diameter = 10  $\mu\text{m}$ , length: 2mm or 10 mm) was placed in the middle of the glass capillary. The degassed  $\text{KNO}_3$  solution containing also NIPAM monomer, BIS as cross-linker, and  $\text{Ru}(\text{bpy})_3$  monomer as ECL luminophore was injected into the BPE cell. By applying an appropriate external potential to the feeder electrodes, the electric field was created

linearly along the carbon fiber to drive the electrochemical reactions on both poles of the carbon fiber. At the cathodic pole, the initiator persulfate ions were firstly reduced to sulfate anion radicals, which then triggered the polymerization of monomers. On the contrary, the concomitant generation of oxygen occurred by water oxidation at the anodic pole of the BE. The length and thickness of the hydrogel films are controllable by applying different electric fields and deposition time. And the best conditions were selected for the best performance of ECL in this case.

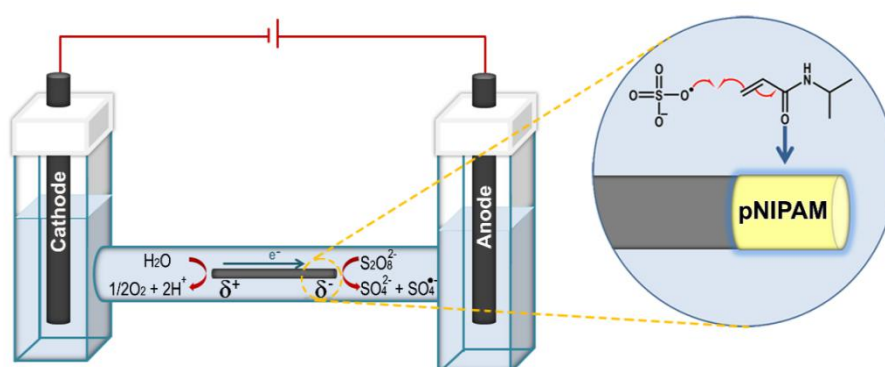


Figure 12. Schematic representation of BE setup for the deposition of pNIPAM-Ru hydrogel films on a carbon fiber.

To verify the swollen to collapsed transition caused by the temperature, *in-situ* optical images of the hydrogel films (Figure 13) on the carbon fiber were recorded at room temperature (i.e. 25 °C) and above the VPTT of the hydrogel films (i.e. 37 °C), respectively. Hydrogel films on the carbon fiber were clearly visible and strongly adhered to the carbon fiber surface without any noticeable deflections. The diameter of the modified carbon fiber was measured to be 18  $\mu\text{m}$  in the swollen state (Figure 13a) and 14  $\mu\text{m}$  in the collapsed state. It means that thickness of the hydrogel films decrease by a factor of 2.

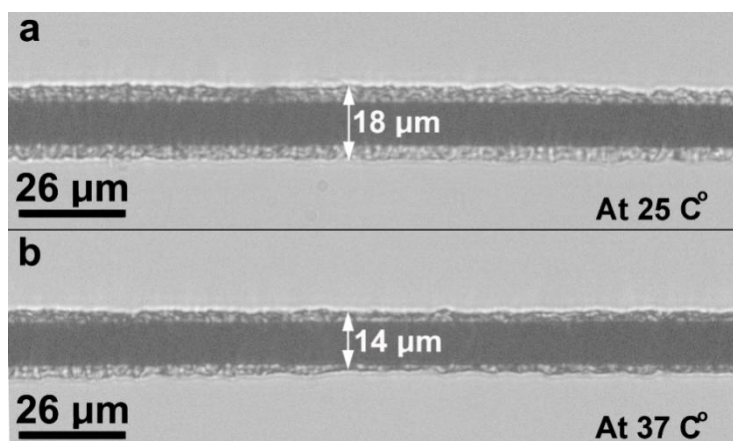


Figure 13. *In-situ* optical images of the hydrogel films on the carbon fiber a) 25 °C and b) at 37 °C.

As demonstrated in the second section, hydrogel films in the collapsed state could decrease the distance between the adjacent ruthenium sites, which promoted significantly ECL production. The average distance between the Ru(bpy)<sub>3</sub> centers in the hydrogel films was found to be only parameter that responsible for the ECL enhancement. Such parameter is subjected the swelling capacity of the hydrogel films, also described in terms of the swelling ratio ( $\alpha$ ):

$$\alpha = \frac{V_T}{V_0} = \left[ \frac{d_T}{d_0} \right]^3 \quad (3)$$

where  $V_T$  and  $V_0$  are the volumes of the hydrogel at temperature T in the fully swollen state and in the collapsed state, respectively.  $d_T$  and  $d_0$  are corresponding diameter that can also be used to determine  $\alpha$ . The swelling ratio of the hydrogel films is calculated from the average diameter and equal to 8, which is consistent with swelling ratios obtained with pNIPAM hydrogels having similar cross-linking ratios.<sup>78</sup> It is obvious that bigger swelling ratio should also result in wider range of the average distance for the Ru(bpy)<sub>3</sub> centers, which might improve the sensitivity for the ECL enhancement.

### 3.3.2 Wireless generation of ECL on the hydrogel films

PL images (Figure 14) of the carbon fiber shows that only the modified part exhibits strong emission. This indicates that the Ru(bpy)<sub>3</sub> monomers as ECL luminophores were successfully attached to pNIPAM network. Recently, the combinations of BPE and (ECL) has attracted many interests in fields of theory study for bipolar reactions, fabrication of large scale ECL array, wireless ECL swimmers and sensors.<sup>79-82</sup> As demonstrated in the second part of the chapter, ECL of the pNIPAM-Ru hydrogel films can be produced by either positively charged co-reactants (i.e. TPrA and DBAE) or a negatively charged one (i.e. oxalate). Indeed, ECL enhancement produced with oxalate is higher than the other two in the collapsed state of the films. But TPrA and DBAE are used commonly for the analytical purposes.<sup>43</sup> In this case, ECL of the hydrogel films was generated in a BPE mode, where the modified carbon fiber was just placed in the solution between two feeder electrodes without any connections. By switching the polarity of the external potentials applied to the feeder electrodes, an anodic potential can be induced at the pole where the hydrogel films were deposited. So the ECL can be produced by oxidative reduction pathway, where the co-reactant and ECL luminophores are oxidized simultaneously at the induced anodic pole of the carbon fiber.<sup>80</sup>

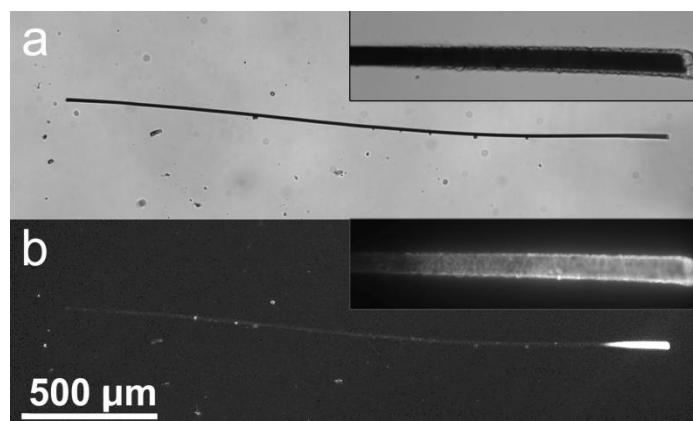


Figure 14. PL images of the carbon fiber a) Bright field and b) Fluorescent mode. Insets are the amplified images of the hydrogel films at the extremity of the carbon fiber.

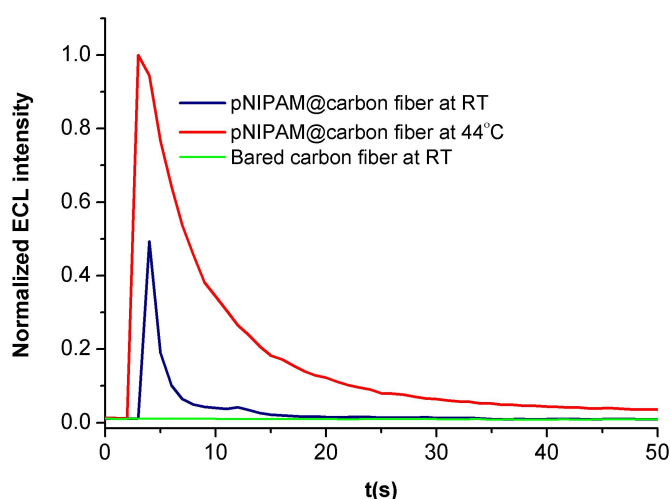


Figure 15. ECL signal of pNIPAM-Ru hydrogel films on the carbon fiber in its swollen state at room temperature (blue line), in the collapsed state at 44 °C (red line), and a bare carbon fiber (i.e. without the pNIPAM-Ru film) at room temperature (green line) in 100 mM TPrA solution.

ECL of the hydrogel films on the carbon fiber was generated in the similar setup but with 100 mM TPrA solution filled inside, and its intensity was firstly detected by a photomultiplier tube (PMT) in front of the modified part as shown in Figure 15. The intensity increased abruptly when an electric field of 3.5 V / cm was applied to BPE system, and then decreased rapidly with time. As already discussed, the oxidation of TPrA occurs predominantly by the electro-catalytic pathway in this kind of hydrogel films where the TPrA reagent is oxidized by the oxidized ruthenium (III) centers.<sup>64</sup> The resulted radical of TPrA can react directly with the un-oxidized ruthenium (II) centers to produce either the excited state of the ruthenium centers or the ruthenium (I) centers in the films at the swollen state. When raising the temperature above the VPTT, the films collapsed and made the average distance between the adjacent ruthenium centers close enough that annihilation of the ruthenium (II) centers and the ruthenium (I) centers occurred to produce the excited state of the ruthenium centers. Therefore, more ruthenium centers in the excited state were generated at higher temperature. This explains why the integrated ECL intensity of the films in the collapsed state is 5.7 times higher than that of the swollen state. However, the fast decreasing ECL intensity with time at both temperatures may relate to the fact that the

ruthenium centers became inactive after few turnovers. It is noteworthy that a bare carbon fiber gives no ECL signal in 100 mM TPrA solution as the control experiment.

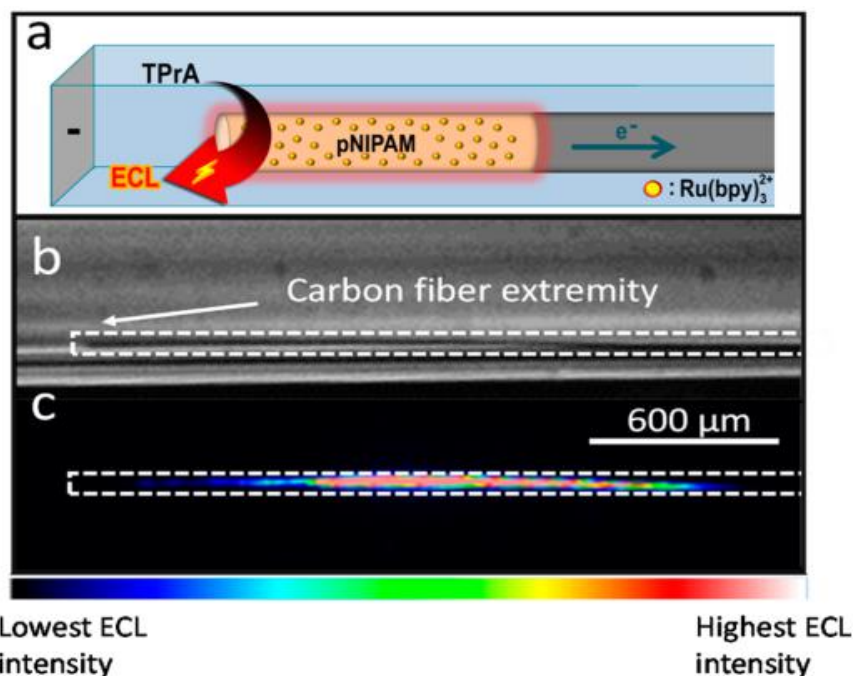


Figure 16. a) Schematic representation of the ECL generation on the pNIPAM-Ru hydrogel films@carbon fiber in a BPE mode, b) PL image recorded by CCD camera without applying potential at room temperature, c) ECL image recorded by CCD camera during application of an electric field of 3.5 V/cm at room temperature. On the bar color, the dark blue color represents the lowest ECL intensity and the red color the highest.

ECL images of the pNIPAM-Ru hydrogel films@carbon fiber were also recorded by using an EMCCD camera (Figure 16) in the same experimental setup. Figure 16b shows the image taken under white light, which the extremity of the carbon fiber with the deposited pNIPAM-Ru hydrogel films is indicated with a white arrow. By applying the same electric field as in the previous experiment, ECL images of the same object was recorded in a black box under the dark (Figure 16c). The presented ECL image was recorded during 4 seconds. Electrogenerated pH gradients lead to a decrease of the ECL signal at the extremity of the carbon fiber, which reduces the size of the ECL-emitting region over time.<sup>80,83</sup> As a result, ECL intensity mainly concentrated in the middle region was observed. Nevertheless, a constant ECL signal could be observed over one minute.

### 3.4 Conclusion

Thermoresponsive pNIPAM films incorporating covalently-attached Ru(bpy)<sub>3</sub> luminophores were fabricated by two pathways. In the conventional three-electrode system, pNIPAM-Ru hydrogel films were prepared on GCE based on electrochemically induced free radical polymerization. ECL emission up to a 58-fold is demonstrated at the pNIPAM-Ru hydrogel due to the swell-to-collapse transition. We found that the collapse of the films triggered by the temperature affects antagonistically electrochemical and ECL processes. On one hand, the diffusion of positively-charged free coreactant species which are required to generate ECL is hindered by the decrease of the gel permeability. On the other hand, the swell-to-collapse transition increases the local concentration of grafted redox species within the film. These two effects were revealed for the pNIPAM-Ru films. Strikingly, the ECL signal exhibited a strong enhancement in spite of the lower amount of electrogenerated co-reactant radicals. Thanks to the study of film format, it was demonstrated that the turn-on of the ECL intensity was neither correlated to the oxidation of the co-reactant nor to the hydrophilic–hydrophobic transition, but solely promoted by the shrinking of the hydrogel film. The decrease of the distance between adjacent ruthenium centers at the swell-collapse transition is the main parameter governing the generation of ECL. Thus it favors the electron-hopping process and the generation of the excited state Ru(bpy)<sub>3</sub><sup>2+\*</sup> by annihilation pathway, which involves adjacent Ru(bpy)<sub>3</sub><sup>+</sup> and Ru(bpy)<sub>3</sub><sup>3+</sup> sites. In the BPE system, asymmetric pNIPAM-Ru hydrogel films deposition was achieved by using carbon microfibers as BE in wireless manner. By changing the temperature, *in-situ* swell-to-collapse transition was observed on the hydrogel films by optical imaging. The swelling capability of this transition was calculated and presented as the swelling ratio with a value of 8. Thus it provided a direct evidence for the decreasing of average distance of the ruthenium centers above the VPTT. Furthermore, the asymmetric reactivity induces by bipolar electrochemistry are also exploited to promote ECL in a wireless manner on one side

of the modified object. The asymmetric carbon fiber shows an ECL signal in TPrA solutions which can be enhanced upon hydrogel films collapsed at higher temperatures. We believe that this approach will allow the development of smart hybrid micro objects that show potential use in sensing applications.

In this work, it was possible to prove that the concept of ECL amplification using responsive redox hydrogel materials is a general process, which can be applied to a wide class of materials including hydrogel films. It could be extended to other types of stimuli in order to design new biosensors taking advantage of bio-responsive hydrogels. For example, glucose-responsive hydrogels could be designed by incorporating simultaneously glucose-sensitive moieties and luminophores in the hydrogel layer.<sup>23</sup> Moreover, in the collapsed state, the ECL process efficiency does not depend on the amount of co-reactant radicals electrogenerated. It can be hoped that new ultrasensitive assays could be designed using less efficient coreactants. Finally, the ECL amplification translates the high efficiency of the electron-transfer processes, due to the proximity of the redox centers. Such efficiency could be applied to many redox centers and advantageously used in electrode materials to promote biocatalytic processes with enzyme-catalyzed redox reactions.

## References

- (1) Jochum, F. D.; Theato, P. Temperature- and light-responsive smart polymer materials. *Chem. Soc. Rev.* **2013**, *42*, 7468-7483.
- (2) Roy, D.; Cambre, J. N.; Sumerlin, B. S. Future perspectives and recent advances in stimuli-responsive materials. *Prog. Polym. Sci.* **2010**, *35*, 278-301.
- (3) Stuart, M. A. C.; Huck, W. T.; Genzer, J.; Müller, M.; Ober, C.; Stamm, M.; Sukhorukov, G. B.; Szleifer, I.; Tsukruk, V. V.; Urban, M. Emerging applications of stimuli-responsive polymer materials. *Nat. Mater.* **2010**, *9*, 101-113.
- (4) Urban, M. W.: *Handbook of stimuli-responsive materials*; Wiley Online Library, 2011; Vol. 69469.
- (5) Hendrickson, G. R.; Lyon, L. A. Bioresponsive hydrogels for sensing applications. *Soft Matter* **2009**, *5*, 29-35.
- (6) Dong, L.; Agarwal, A. K.; Beebe, D. J.; Jiang, H. Adaptive liquid microlenses activated by stimuli-responsive hydrogels. *Nature* **2006**, *442*, 551-554.
- (7) Ma, X.; Tian, H. Stimuli-responsive supramolecular polymers in aqueous solution. *Acc. Chem. Res.* **2014**, *47*, 1971-1981.
- (8) Schild, H. G. Poly (N-isopropylacrylamide): experiment, theory and application. *Prog. Polym. Sci.* **1992**, *17*, 163-249.
- (9) García, T. A.; Gervasi, C. A.; Rodríguez Presa, M. a. J.; Otamendi, J. I.; Moya, S. E.; Azzaroni, O. Molecular transport in thin thermoresponsive poly (N-isopropylacrylamide) brushes with varying grafting density. *J. Phys. Chem. C* **2012**, *116*, 13944-13953.
- (10) Yamamoto, K.; Mizutani, Y.; Kitagawa, T. Nanosecond temperature jump and time-resolved Raman study of thermal unfolding of ribonuclease A. *Biophys. J.* **2000**, *79*, 485-495.
- (11) Füllbrandt, M.; Ermilova, E.; Asadujjaman, A.; Hölzel, R.; Bier, F. F.; von Klitzing, R.; Schönhals, A. Dynamics of linear poly (N-isopropylacrylamide) in water around the phase transition investigated by dielectric relaxation spectroscopy. *J. Phys. Chem. B* **2014**, *118*, 3750-3759.
- (12) Katsumoto, Y.; Tanaka, T.; Sato, H.; Ozaki, Y. Conformational change of poly (N-isopropylacrylamide) during the coil-globule transition investigated by attenuated total reflection/infrared spectroscopy and density functional theory calculation. *J. Phys. Chem. A* **2002**, *106*, 3429-3435.
- (13) Buenger, D.; Topuz, F.; Groll, J. Hydrogels in sensing applications. *Prog. Polym. Sci.* **2012**, *37*, 1678-1719.
- (14) Li, C.; Hu, J.; Liu, S. Engineering FRET processes within synthetic polymers, polymeric assemblies and nanoparticles via modulating spatial distribution of fluorescent donors and acceptors. *Soft Matter* **2012**, *8*, 7096-7102.
- (15) Wang, D.; Liu, T.; Yin, J.; Liu, S. Stimuli-responsive fluorescent poly(N-isopropylacrylamide) microgels labeled with phenylboronic acid moieties as multifunctional ratiometric probes for glucose and temperatures. *Macromolecules* **2011**, *44*, 2282-2290.
- (16) Li, Y.; Huang, G.; Zhang, X.; Li, B.; Chen, Y.; Lu, T.; Lu, T. J.; Xu, F. Magnetic

- hydrogels and their potential biomedical applications. *Adv. Funct. Mater.* **2013**, *23*, 660-672.
- (17) Wu, W.; Zhou, T.; Shen, J.; Zhou, S. Optical detection of glucose by CdS quantum dots immobilized in smart microgels. *Chem. Commun.* **2009**, 4390.
- (18) Zhou, M.; Xie, J.; Yan, S.; Jiang, X.; Ye, T.; Wu, W. Graphene@Poly(phenylboronic acid)s microgels with selectively glucose-responsive volume phase transition behavior at a physiological pH. *Macromolecules* **2014**, *47*, 6055-6066.
- (19) Wu, W.; Zhou, T.; Berliner, A.; Banerjee, P.; Zhou, S. Glucose-mediated assembly of phenylboronic acid modified CdTe/ZnTe/ZnS quantum dots for intracellular glucose probing. *Angew. Chem. Int. Ed.* **2010**, *49*, 6554-6558.
- (20) Wu, W.; Zhou, T.; Aiello, M.; Zhou, S. Construction of optical glucose nanobiosensor with high sensitivity and selectivity at physiological pH on the basis of organic-inorganic hybrid microgels. *Biosens. Bioelectron.* **2010**, *25*, 2603.
- (21) Zenkl, G.; Mayr, T.; Klimant, I. Sugar-responsive fluorescent nanospheres. *Macromol. Biosci.* **2008**, *8*, 146.
- (22) Zenkl, G.; Klimant, I. Fluorescent acrylamide nanoparticles for boronic acid based sugar sensing - from probes to sensors. *Microchim. Acta* **2009**, *166*, 123.
- (23) Denisov, S. A.; Pinaud, F.; Chambaud, M.; Lapeyre, V.; Catargi, B.; Sojic, N.; McClenaghan, N. D.; Ravaine, V. Saccharide-induced modulation of photoluminescence lifetime in microgels. *Phys. Chem. Chem. Phys.* **2016**, *18*, 16812-16821.
- (24) Tanaka, T.; Fillmore, D. J. Kinetics of swelling of gels. *J. Chem. Phys.* **1979**, *70*, 1214.
- (25) Okabe, K.; Inada, N.; Gota, C.; Harada, Y.; Funatsu, T.; Uchiyama, S. Intracellular temperature mapping with a fluorescent polymeric thermometer and fluorescence lifetime imaging microscopy. *Nat. Commun.* **2012**, *3*, 705.
- (26) Kaniewska, K.; Karbarz, M.; Stojek, Z. Electrochemical attachment of thermo- and pH sensitive interpenetrating-polymers-network hydrogel to conducting surface. *Electrochim. Acta.* **2015**, *179*, 372-378.
- (27) Karbarz, M.; Lukaszek, A.; Stojek, Z. Electrochemical properties of micro- and regular electrodes modified with environmentally sensitive poly(n-isopropylacrylamide) gel via electrochemically induced free-radical polymerization. *Electroanal.* **2013**, *25*, 875-880.
- (28) Bünsow, J.; Enzenberg, A.; Pohl, K.; Schuhmann, W.; Johannsmann, D. Electrochemically induced formation of surface-attached temperature-responsive hydrogels. amperometric glucose sensors with tunable sensor characteristics. *Electroanal.* **2010**, *22*, 978-984.
- (29) Fandrich, A.; Buller, J.; Wischerhoff, E.; Laschewsky, A.; Lisdat, F. Electrochemical detection of the thermally induced phase transition of a thin stimuli-responsive polymer film. *ChemPhysChem* **2012**, *13*, 2020-2023.
- (30) Zhou, J.; Wang, G.; Hu, J.; Lu, X.; Li, J. Temperature, ionic strength and pH induced electrochemical switching of smart polymer interfaces. *Chem. Comm.* **2006**, 4820-4822.
- (31) Tam, T. K.; Pita, M.; Trotsenko, O.; Motornov, M.; Tokarev, I.; Halánek, J.; Minko, S.; Katz, E. Reversible "closing" of an electrode interface functionalized with a polymer brush by an electrochemical signal. *Langmuir* **2010**, *26*, 4506-4513.
- (32) Zhang, K. Y.; Liu, S.; Zhao, Q.; Huang, W. Stimuli-responsive metallopolymers. *Coord. Chem. Rev.* **2016**, *319*, 180-195.

- (33) Motornov, M.; Kin Tam, T.; Pita, M.; Tokarev, I.; Katz, E.; Minko, S. Switchable selectivity for gating ion transport with mixed polyelectrolyte brushes: Approaching 'smart' drug delivery systems. *Nanotechnology* **2009**, *20*, 434006
- (34) Bünsow, J.; Johannsmann, D. Electrochemically produced responsive hydrogel films: Influence of added salt on thickness and morphology. *J. Colloid. Interface. Sci.* **2008**, *326*, 61-65.
- (35) Fandrich, A.; Buller, J.; Schäfer, D.; Wischerhoff, E.; Laschewsky, A.; Lisdat, F. Electrochemical characterization of a responsive macromolecular interface on gold. *Phys. Status Solidi A* **2015**, *212*, 1359-1367.
- (36) Zhang, J.; Riskin, M.; Tel-Vered, R.; Tian, H.; Willner, I. Photochemical switching of the phase-transition temperatures of p-NIPAM–Pt nanoparticles thermosensitive polymer composites associated with electrodes: Functional electrodes for switchable electrocatalysis. *Chem. Eur. J.* **2011**, *17*, 11237-11242.
- (37) Pita, M.; Katz, E. Switchable Electrodes: how can the system complexity be scaled up? *Electroanal.* **2009**, *21*, 252-260.
- (38) Tam, T. K.; Pita, M.; Motornov, M.; Tokarev, I.; Minko, S.; Katz, E. Modified electrodes with switchable selectivity for cationic and anionic redox species. *Electroanal.* **2010**, *22*, 35-40.
- (39) Katz, E.; Minko, S. Enzyme-based logic systems interfaced with signal-responsive materials and electrodes. *Chem. Commun.* **2015**, *51*, 3493-3500.
- (40) Li, H.; Sentic, M.; Ravaine, V.; Sojic, N. Antagonistic effects leading to turn-on electrochemiluminescence in thermoresponsive hydrogel films. *Phys. Chem. Chem. Phys.* **2016**, *18*, 32697–32702.
- (41) Phuakkong, O.; Sentic, M.; Li, H.; Warakulwit, C.; Limtrakul, J.; Sojic, N.; Kuhn, A.; Ravaine, V.; Zigah, D. Wireless synthesis and activation of electrochemiluminescent thermoresponsive Janus objects using bipolar electrochemistry. *Langmuir*, **2016**, *32*, 12995–13002.
- (42) Bard, A. J.: *Electrogenerated Chemiluminescence*; M. Dekker: New-York, 2004.
- (43) Miao, W. Electrogenerated chemiluminescence and its biorelated applications. *Chem. Rev.* **2008**, *108*, 2506-2553.
- (44) Liu, Z.; Qi, W.; Xu, G. Recent advances in electrochemiluminescence. *Chem. Soc. Rev.* **2015**, *44*, 3117-3142.
- (45) Pinaud, F.; Russo, L.; Pinet, S.; Gosse, I.; Ravaine, V.; Sojic, N. Enhanced electrogenerated chemiluminescence in thermoresponsive microgels. *J. Am. Chem. Soc.* **2013**, *135*, 5517-5520.
- (46) Suzuki, D.; Sakai, T.; Yoshida, R. Self-flocculating/self-dispersing oscillation of microgels. *Angew. Chem. Int. Ed.* **2008**, *47*, 917-920.
- (47) Suzuki, D.; Yoshida, R. Temporal control of self-oscillation for microgels by cross-linking network structure. *Macromolecules* **2008**, *41*, 5830-5838.
- (48) Zu, Y.; Bard, A. J. Electrogenerated chemiluminescence 67: Dependence of light emission of the tris (2, 2') bipyridylruthenium (II)/tripropylamine system on electrode surface hydrophobicity. *Anal. Chem.* **2001**, *73*, 3960-3964.
- (49) Bruce, D.; McCall, J.; Richter, M. M. Effects of electron withdrawing and donating groups on the efficiency of tris (2, 2'-bipyridyl) ruthenium (II)/tri-n-propylamine

electrochemiluminescence. *Analyst* **2002**, *127*, 125-128.

(50) Kuckling, D.; Adler, H. J. P.; Arndt, K. F.; Hoffmann, J.; Plötner, M.; Wolff, T. Photocrosslinking of thin films of temperature - sensitive polymers. *Polym. Adv. Technol.* **1999**, *10*, 345-352.

(51) Ista, L. K.; Mendez, S.; Pérez-Luna, V. H.; López, G. P. Synthesis of poly (N-isopropylacrylamide) on initiator-modified self-assembled monolayers. *Langmuir* **2001**, *17*, 2552-2555.

(52) Pan, Y. V.; Wesley, R. A.; Luginbuhl, R.; Denton, D. D.; Ratner, B. D. Plasma polymerized N-isopropylacrylamide: synthesis and characterization of a smart thermally responsive coating. *Biomacromolecules* **2001**, *2*, 32-36.

(53) Reuber, J.; Reinhardt, H.; Johannsmann, D. Formation of surface-attached responsive gel layers via electrochemically induced free-radical polymerization. *Langmuir* **2006**, *22*, 3362-3367.

(54) Plamper, F. A. Polymerizations under electrochemical control. *Colloid. Polym. Sci.* **2014**, *292*, 777-783.

(55) Baute, N.; Jérôme, C.; Martinot, L.; Mertens, M.; Geskin, Viktor M.; Lazzaroni, R.; Brédas, J.-L.; Jérôme, R. Electrochemical strategies for the strengthening of polymer-metal interfaces. *Eur. J. Inorg. Chem.* **2001**, *2001*, 1097-1107.

(56) Lee, C. S.; Bell, J. Kinetic study of the aqueous electropolymerization of acrylamide, acrylonitrile and N, N'-methylene-bisacrylamide on an aluminium alloy cathode. *J. Mater. Sci.* **1995**, *30*, 3827-3833.

(57) Yildiz, G.; Çatalgil-Giz, H.; Kadirgan, F. Electrochemically prepared acrylamide/N, N'-methylene bisacrylamide gels. *J. Appl. Electrochem.* **2000**, *30*, 71-75.

(58) Yan, S.; Wu, Q.; Chang, A.; Lu, F.; Xu, H.-C.; Wu, W. Electrochemical synthesis of polymer microgels. *Polym. Chem.* **2015**, *6*, 3979-3987.

(59) Bünsow, J.; Mänz, M.; Vana, P.; Johannsmann, D. Electrochemically induced RAFT polymerization of thermoresponsive hydrogel films: Impact on film thickness and surface morphology. *Macromol. Chem. Phys.* **2010**, *211*, 761-767.

(60) Ghosh, P.; Spiro, T. G. Photoelectrochemistry of tris (bipyridyl) ruthenium (II) covalently attached to n-type tin (IV) oxide. *J. Am. Chem. Soc.* **1980**, *102*, 5543-5549.

(61) Mergel, O.; Gelissen, A. P. H.; Wünnemann, P.; Böker, A.; Simon, U.; Plamper, F. A. Selective packaging of ferricyanide within thermoresponsive microgels. *J. Phys. Chem. C* **2014**, *118*, 26199-26211.

(62) Zhang, W.; Gaberman, I.; Ciszowska, M. Diffusion and concentration of molecular probes in thermoresponsive poly(N-isopropylacrylamide) hydrogels: Effect of the volume phase transition. *Anal. Chem.* **2002**, *74*, 1343-1348.

(63) Heller, A. Electron-conducting redox hydrogels: design, characteristics and synthesis. *Curr. Opin. Chem. Biol.* **2006**, *10*, 664-672.

(64) Miao, W. J.; Choi, J. P.; Bard, A. J. Electrogenerated chemiluminescence 69: The tris(2,2'-bipyridine)ruthenium(II), (Ru(bpy)<sub>3</sub><sup>2+</sup>)/tri-n-propylamine (TPrA) system revisited - A new route involving TPrA<sup>+</sup> cation radicals. *J. Am. Chem. Soc.* **2002**, *124*, 14478-14485.

(65) Sentic, M.; Milutinovic, M.; Kanoufi, F.; Manojlovic, D.; Arbault, S.; Sojic, N. Mapping electrogenerated chemiluminescence reactivity in space: mechanistic insight into model systems used in immunoassays. *Chem. Sci.* **2014**, *5*, 2568-2572.

- (66) Liu, X.; Shi, L.; Niu, W.; Li, H.; Xu, G. Environmentally friendly and highly sensitive ruthenium(II) tris(2,2'-bipyridyl) electrochemiluminescent system using 2-(dibutylamino)ethanol as co-reactant. *Angew. Chem. Int. Ed.* **2007**, *46*, 421-424.
- (67) Kanoufi, F.; Bard, A. J. Electrogenerated chemiluminescence 65: An investigation of the oxidation of oxalate by tris(polypyridine) ruthenium complexes and the effect of the electrochemical steps on the emission intensity. *J. Phys. Chem. B* **1999**, *103*, 10469-10480.
- (68) Kebede, N.; Francis, P. S.; Barbante, G. J.; Hogan, C. F. Electrogenerated chemiluminescence of tris(2,2'-bipyridine)ruthenium(ii) using common biological buffers as co-reactant, pH buffer and supporting electrolyte. *Analyst* **2015**, *140*, 7142-7145.
- (69) Workman, S.; Richter, M. M. The effects of nonionic surfactants on the tris(2,2'-bipyridyl)ruthenium(II)-tripropylamine electrochemiluminescence system. *Anal. Chem.* **2000**, *72*, 5556-5561.
- (70) Zu, Y.; Bard, A. J. Electrogenerated chemiluminescence 67: Dependence of light emission of the tris(2,2')bipyridylruthenium(II)/tripropylamine system on electrode surface hydrophobicity. *Anal. Chem.* **2001**, *73*, 3960-3964.
- (71) Zoski, C. G.: *Handbook of electrochemistry*; Elsevier, 2006.
- (72) Loget, G.; Zigah, D.; Bouffier, L.; Sojic, N.; Kuhn, A. Bipolar electrochemistry: From materials science to motion and beyond. *Acc. Chem. Res.* **2013**, *46*, 2513-2523.
- (73) Fosdick, S. E.; Knust, K. N.; Scida, K.; Crooks, R. M. Bipolar electrochemistry. *Angew. Chem. Int. Ed.* **2013**, *52*, 10438-10456.
- (74) Bouffier, L.; Doneux, T.; Goudeau, B.; Kuhn, A. Imaging redox activity at bipolar electrodes by indirect fluorescence modulation. *Anal. Chem.* **2014**, *86*, 3708-3711.
- (75) Loget, G.; Roche, J.; Kuhn, A. True bulk synthesis of Janus objects by bipolar electrochemistry. *Adv. Mater.* **2012**, *24*, 5111-5116.
- (76) Loget, G.; Kuhn, A. Electric field-induced chemical locomotion of conducting objects. *Nat. Commun.* **2011**, *2*, 535.
- (77) Loget, G.; Roche, J. r.; Gianessi, E.; Bouffier, L.; Kuhn, A. Indirect bipolar electrodeposition. *J. Am. Chem. Soc.* **2012**, *134*, 20033-20036.
- (78) Destribats, M.; Lapeyre, V.; Wolfs, M.; Sellier, E.; Leal-Calderon, F.; Ravaine, V.; Schmitt, V. Soft microgels as Pickering emulsion stabilisers: Role of particle deformability. *Soft Matter* **2011**, *7*, 7689-7698.
- (79) Chow, K.-F.; Mavr e, F.; Crooks, J. A.; Chang, B.-Y.; Crooks, R. M. A large-scale, wireless electrochemical bipolar electrode microarray. *J. Am. Chem. Soc.* **2009**, *131*, 8364-8365.
- (80) Sentic, M.; Loget, G.; Manojlovic, D.; Kuhn, A.; Sojic, N. Light - emitting electrochemical "Swimmers" . *Angew. Chem. Int. Ed.* **2012**, *51*, 11284-11288.
- (81) Bouffier, L.; Zigah, D.; Adam, C.; Sentic, M.; Fattah, Z.; Manojlovic, D.; Kuhn, A.; Sojic, N. Lighting up redox propulsion with luminol electrogenerated chemiluminescence. *ChemElectroChem* **2014**, *1*, 95-98.
- (82) Sentic, M.; Arbault, S.; Goudeau, B.; Manojlovic, D.; Kuhn, A.; Bouffier, L.; Sojic, N. Electrochemiluminescent swimmers for dynamic enzymatic sensing. *Chem. Commun.* **2014**, *50*, 10202-10205.
- (83) de Poulpiquet, A.; Diez-Buitrago, B.; Milutinovic, M.; Goudeau, B.; Bouffier, L.; Arbault, S.; Kuhn, A.; Sojic, N. Dual-color electrogenerated chemiluminescence from

dispersions of conductive microbeads addressed by bipolar electrochemistry.  
*ChemElectroChem* **2015**, 3, 404-409.

## **Chapter 4**

### **New electrochemiluminescence sensing methods**

## 4.1 Introduction

Diverse ECL assays have been elaborately designed and widely studied in the clinical diagnostics in the past decades.<sup>1,2</sup> Some of them have been commercialized as ECL immunoassays.<sup>3</sup> To date, there are still a great of efforts that have been made to improve sensitivity, stability and applicability of the ECL detection.<sup>4</sup> Indeed, analytical application is one of the intrinsic characteristics of ECL as its light intensity is proportional to the concentrations of the ECL luminophore or co-reactant.<sup>5</sup> Therefore, the ECL luminophore has been used as labels in numerous bioassays<sup>3</sup> or as molecular probes with different receptor sites.<sup>6-11</sup> For example, ruthenium and iridium complexes have been modified with crown ether moiety to measure different metal cations.<sup>6-9</sup> In this case, the co-reactant is kept in constant relative high concentration so that it could provide sufficient radicals to react with the ECL luminophore. ECL intensity produced in the system will linearly depend on the concentration of ECL luminophore in a wide dynamic range. The labeled target or binding analyte is determined according to the linearity between light intensity and ECL luminophore. Alternatively, if the detection is performed in the presence of constant ECL luminophore concentration, ECL intensity will present dependence toward the concentration of co-reactant. In this context, the analyte usually serves as co-reactant directly involving in the ECL reactions. It means that the analyte has to be electro-active and capable to generate strong reducing or oxidizing radicals to bring the ECL luminophore to the excited state. Oxalate<sup>12,13</sup> and peroxydisulfate<sup>14,15</sup> are two typical analytes that can be used directly as co-reactants and determined based on the produced ECL intensity. Another popular type of analyte that act as co-reactants is amines or its derivates,<sup>16</sup> because the amine group exists in many pharmacological compounds such as as antibiotics, anti-histamines, opiates, *etc.*<sup>3,17,18</sup> Meanwhile, it has been proved that the system consist of  $\text{Ru}(\text{bpy})_3^{2+}$  as luminophore and TPrA as co-reactant exhibits high ECL efficiency and has become the commercial benchmark for ECL immunoassays and DNA analysis.<sup>3,5</sup> However, it is still difficult to detect

those analytes which are not competent to the role as co-reactant in this approach. Such limitation has hindered its further analytical application. To solve this problem, we proposed here to confer recognition properties to the coreactant by integrating a receptor site to its chemical structure. The recognition of the target analyte would then modulate its electrochemical properties and the resulting ECL emission of the luminophore. Related details will be demonstrated in the second part of the chapter.<sup>19</sup> Currently, ECL generation can be achieved by either a conventional three electrode system or a wireless bipolar electrode (BE) system.<sup>20,21</sup> The latter has provided a power tool for ECL investigations such as the theoretical understanding of bipolar reactions, the fabrication of large scale ECL arrays, and wireless light-emitting swimmers and sensors.<sup>22-29</sup> ECL generation on BE occurs at one extremity of the electrode where ECL signals are directly detected so far only with classic photomultipliers or cameras.<sup>30</sup> On the other hand, the BE is not directly connected to any external device, the transmission of ECL signals through a long distance are difficult. Therefore, to circumvent this impediment, the utilization of optical fiber bundle has been chosen due to their intrinsic characteristics of transmitting light over long distances. With this respect, a thin film of gold or transparent indium tin oxide (ITO) can be deposited onto the one end of fiber bundle, which plays dual roles as BE to locally generate ECL, and as light collector to capture then transmit ECL emission to the remote end, where ECL signals are detected. This strategy will be illustrated in the third part of the chapter.<sup>31</sup>

## **4.2 Boronic acid-modified co-reactants**

Boronic acid is a kind of Lewis acids and can react with Lewis base to form boronate anions known as the acid-base equilibrium reaction.<sup>32</sup> Boronic acid is also recognized well as a saccharide receptor due to its capability to bind with diol units to form cyclic boronate esters.<sup>33</sup> In 1959, Lorand and coworkers reported the first quantitative evaluation of the interaction between various diol-containing compounds and

phenylboronic acid.<sup>34</sup> It was found that the activity is increased due to the covalent reactions with 1,2-, 1,3-, or 1,4-diols to form cyclic boronic esters (5, 6, or 7 membered rings) in aqueous solution.<sup>35</sup> The complexation of diols group with boronic acid is reversible under certain conditions, but also relies on an interaction between a Lewis acidic boronic acid and a proximal tertiary amine as Lewis base, because the N-B interaction enhances the binding at neutral pH and controls the fluorescence properties of nearby luminophores.<sup>35,36</sup> Therefore, many organic molecules were designed and synthesized by finely tuning the N-B interaction for the development of saccharide chemo-sensors.<sup>37</sup> Tertiary amine containing boronic acid compounds means that they are the potential candidates as co-reactants,<sup>5</sup> which might be useful to explore new ECL assays of saccharides.

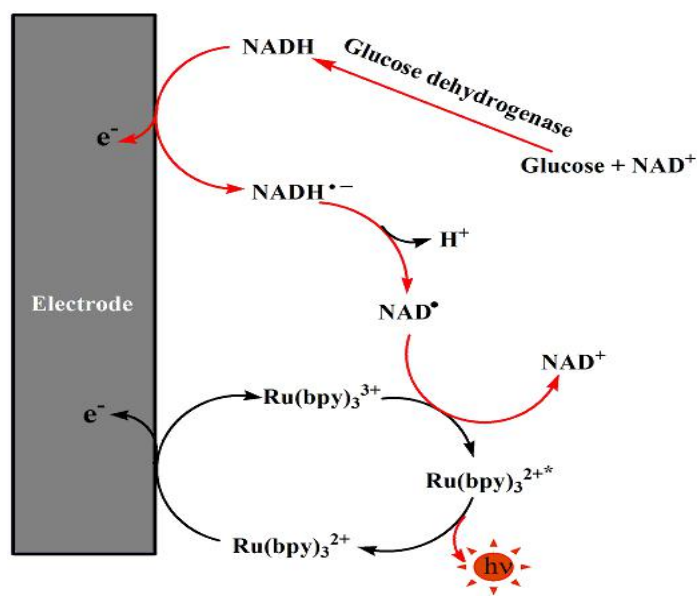
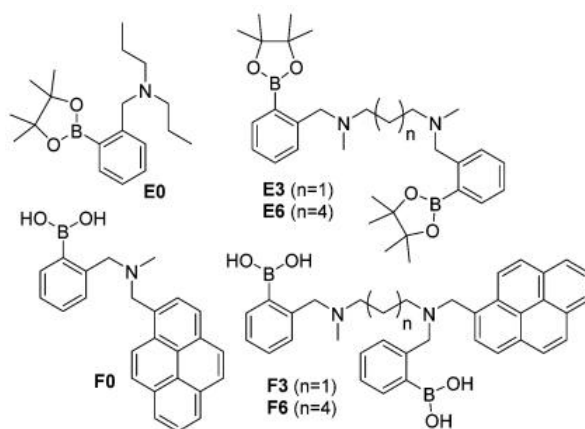


Figure 1. Schematic representation of enzymatic ECL mechanism for the determination of glucose.<sup>17</sup>

Glucose determination is one of attractive topics in ECL technology.<sup>28,38,39</sup> The model system of this kind of ECL assays involves both enzymatic and electrochemical reactions at the same electrode (Figure 1). The addition of  $\beta$ -nicotinamide adenine dinucleotide ( $\text{NAD}^+$ ) in the glucose substrate is required as a co-factor. Glucose dehydrogenase (GDH) oxidizes glucose to gluconolactone with the concomitant

conversion of  $\text{NAD}^+$  to  $\text{NADH}$ . Then, the generated  $\text{NADH}$  acting as an ECL co-reactant is oxidized to energetic reducing forms, which reacts with the ruthenium luminophore to produce the light emission. It is noteworthy that the presences of  $\text{NAD}^+$  and  $\text{GDH}$  do not produce any ECL emission with the luminophore unless glucose is added. By setting the amount of  $\text{NAD}^+$  and  $\text{GDH}$ , the light intensity should vary with the glucose concentration. Like many other enzymatic assays, catalytic activities of  $\text{GDH}$  are susceptible to experimental conditions such as  $\text{pH}$ , temperature and toxic chemicals,<sup>40</sup> because there is a possible deformation during fabrication, storage or use in some harsh environments, leading to denaturing the enzyme.<sup>41</sup> Therefore, the pursuing of enzymeless sensing is an important area for the development of robust, highly sensitive and reproducible sensors. With this respect, numerous saccharide sensors based on boronic acids receptors have been fabricated and attracted much attention because of their strong interaction with diol moieties.<sup>42</sup> Herein, inspired by the remarkable structure/reactivity relationship of this very efficient biomolecules, a series of tertiary amine containing compounds with boronic acid integrating function units were synthesized by the group of Professor Tony D. James at University of Bath (Scheme 1). Then these compound were used as co-reactants to generate ECL with  $\text{Ru}(\text{bpy})_3^{2+}$ , meanwhile as a receptor for sensing saccharides.



Scheme 1. Chemical structures of the boronic acid based coreactants **E0**, **E3** and **E6** and fluorescent boronic based saccharide sensors **F0**, **F3** and **F6**.<sup>43</sup>

For the first time, we demonstrated that the recognition of the saccharide modifies both the structure and the reactivity of the coreactant and thus the resulting ECL emission (Figure 2). With the presented approach, ECL generation depends on target molecules that are electro-inactive and do not to change the conformation of the luminophore as classically performed with molecular probes. Moreover, differential selectivity for D-glucose and D-fructose is achieved by tuning the number of boronic acid groups and the spacer length.

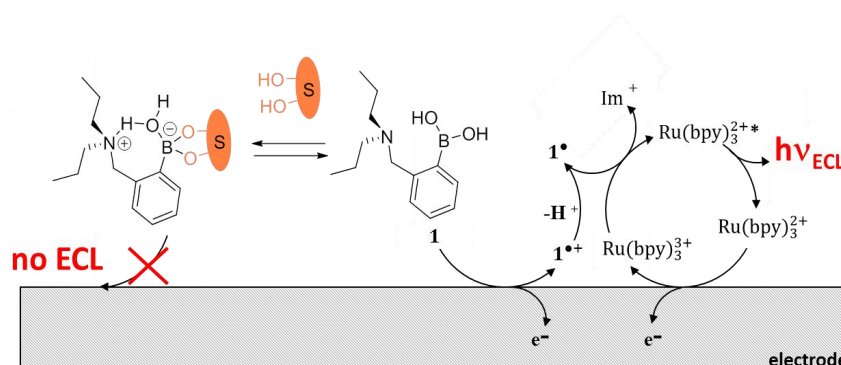
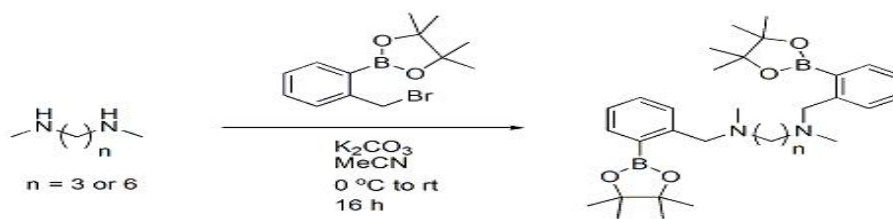


Figure 2. Influence of the binding equilibrium of phenylboronic acid to the saccharides (either D-fructose or D-glucose) on the ECL mechanism of the system  $\text{Ru}(\text{bpy})_3^{2+}/\text{E0}$ .  $\text{Im}^+$  is the iminium product. Under the measurement conditions the pinacol protecting group is removed.

#### 4.2.1 ECL produced with boronic acid-modified co-reactants

To explore the usefulness of the above strategy, we selected the prototypical  $\text{Ru}(\text{bpy})_3^{2+}$  complex as a luminophore and modified tertiary amines as oxidative-reduction co-reactants because such a model system leads very efficiently to strong ECL emission.<sup>44</sup> As a test case, we designed and prepared compound **E0** which is similar to the TPrA structure but containing a boronic acid as recognition unit. **E0** and the other coreactants shown in Scheme 2 (**E3** and **E6**) were synthesised through the alkylation of their corresponding amine using 2-(2-(bromomethyl)phenyl)-4,4,5,5-tetramethyl-1,3,2-dioxaborolane (Scheme 2).



Scheme 2. Synthesis of the boronic acid based coreactants **E3** and **E6**. Reaction conditions— $\text{K}_2\text{CO}_3$  (3 eq), BPinBnBr (2 eq), amine, MeCN, 0 °C to rt, 16 h,  $n = 3$  (92 %),  $n = 6$  (16 %).

Once isolated, electrochemical and ECL properties of these boronic acid-modified co-reactants were investigated by using cyclic voltammetry in PBS solution that contained 10  $\mu\text{M}$  of  $\text{Ru}(\text{bpy})_3^{2+}$  and 0.1 mM of each co-reactant (Figure 3). The co-reactant concentration was in excess in comparison to the luminophore, as very classically employed in ECL experiments because it is consumed during the ECL process. As shown in Figure 3a, irreversible oxidation of **E0** occurred at 0.77 V vs. Ag/AgCl and the oxidation wave is shifted to less anodic potentials by 100 mV in comparison to the model TPrA reagent. It indicates that the phenylboronic acid group is a better donor than ethyl group. This donor effect makes the molecule much easier to oxidize and can also stabilize the radical cation by charge delocalization.

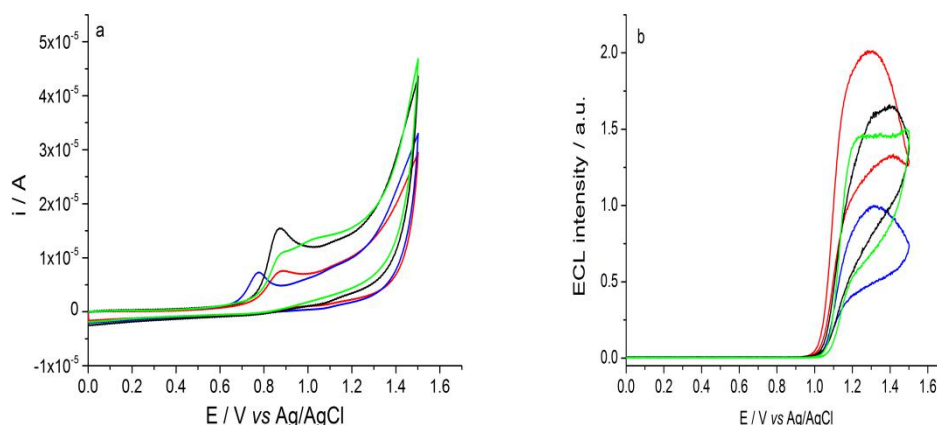


Figure 3. Comparison of the (a) voltammetric and (b) ECL signals of  $\text{Ru}(\text{bpy})_3^{2+}$  with either the co-reactant TPrA (red line), **E0** (blue line), **E6** (black line) or **E3** (green line). Experiments were performed in 100 mM PBS solution (pH 7.4) containing 10  $\mu\text{M}$   $\text{Ru}(\text{bpy})_3^{2+}$  and 0.1 mM of each co-reactant with a GCE as a working electrode. Scan rate 100 mV/s.

ECL emission occurred at the oxidation potential of  $\text{Ru}(\text{bpy})_3^{2+}$  (Figure 3b), as for TPrA in the same experimental condition (*i.e.* low  $\text{Ru}(\text{bpy})_3^{2+}$  concentration). It follows an oxidative-reduction mechanism where both the luminophore and the coreactant are oxidized (Figure 2). After a deprotonation step, the cation radical gives a highly reducing neutral radical that react with the oxidized  $\text{Ru}(\text{bpy})_3^{3+}$  to generate the excited state of the luminophore. This one relaxes *in fine* to the ground state by emitting ECL light. In comparison to TPrA, ECL response with **E0** is divided by a factor 2 (Figure 3b). Indeed, the nature of substituents attached to nitrogen or  $\alpha$ -carbon on the amine coreactant can also affect the ECL efficiency<sup>3,45</sup> and it has been reported that aromatic-substituted amines that can conjugate the radical intermediates consistently lead to lower ECL emission response.<sup>46</sup> Further ECL investigations were also performed on the new symmetric tertiary bis amino reagents bearing boronic acid end-groups containing linkers with different lengths (*i.e.* **E3** and **E6**, respectively). We investigated first the properties of the compound **E6** with a hexyl linker between both amino groups. The cyclic voltammogram of **E6** presents the irreversible oxidation waves of the amino moieties at the same potential as the TPrA. The peak current is increased by approximately 2.1-fold indicating that both amino groups are simultaneously oxidized. However, ECL signal is 15% lower with **E6** than with TPrA (Figure 3b), even if two amino groups were oxidized and may participate to the ECL process. This low ECL response is probably related to the lower stability of the electrogenerated dication radicals. In contrast with **E6**, **E3** has the shorter linker between both amino group and the phenyl boronic acid moieties. The cyclic voltammetric experiment showed that the oxidation process of **E3** is more complex exhibiting a first anodic wave at 0.87 V *vs.* Ag/AgCl and a second at 0.95 V *vs.* Ag/AgCl (Figure 3a). Both oxidation waves of **E3** partially separated in contrast to what was observed for **E6**. Such oxidation behaviors can be explained by the fact that the shorter linker can facilitate the two electronic communications between both amino groups. ECL signal produced with **E3** is slightly weaker than that of **E6** under the same conditions.

## 4.2.2 ECL response induced by binding saccharides

The addition of D-glucose caused a notable effect on both the voltammetric wave and the ECL response with **E0**. As shown in Figure 4, the binding D-glucose on the **E0** resulted in a dramatic decrease of the oxidation current along with its shift to more anodic potentials (Figure 4b). Correspondingly, ECL intensity decreases progressively with the addition of D-glucose (Figure 4c). Under these conditions, the effects of D-fructose were qualitatively similar to the ones of D-glucose but with a much stronger decrease of both anodic wave and ECL intensity for a given concentration (Figure 5). Indeed, the oxidation wave almost vanished and the ECL peak decreased by 57% with 50 mM of D-fructose (Figure. 7a). The same limit values for the ECL intensity and for the current were reached with 200 mM of D-glucose than with 50 mM of D-fructose. Such a difference was expected because the complexation constant of phenylboronic acid with D-fructose is much higher than with D-glucose.<sup>47</sup>

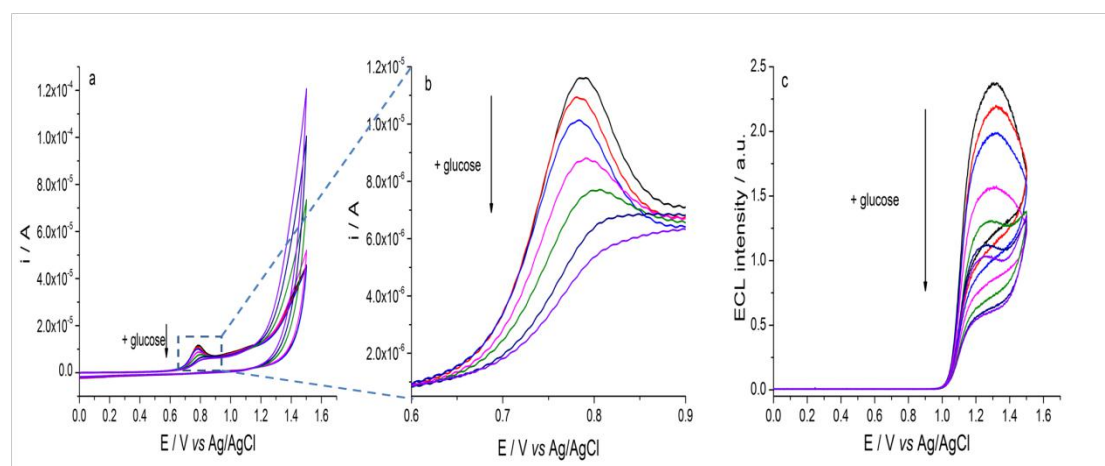


Figure 4. Effect of D-glucose addition on electrochemical oxidation of **E0** and on the corresponding ECL response. (a-b) Cyclic voltammetry and (c) ECL signal of a PBS solution (pH 7.4) containing 10  $\mu$ M Ru(bpy)<sub>3</sub><sup>2+</sup>, 0.2 mM **E0** and different concentrations of D-glucose. The arrow indicates increasing concentrations of D-glucose (0, 0.5, 1, 10, 50, 100 and 200 mM). Experiments were performed on glassy carbon electrode (GCE) at a scan rate of 100 mV/s.

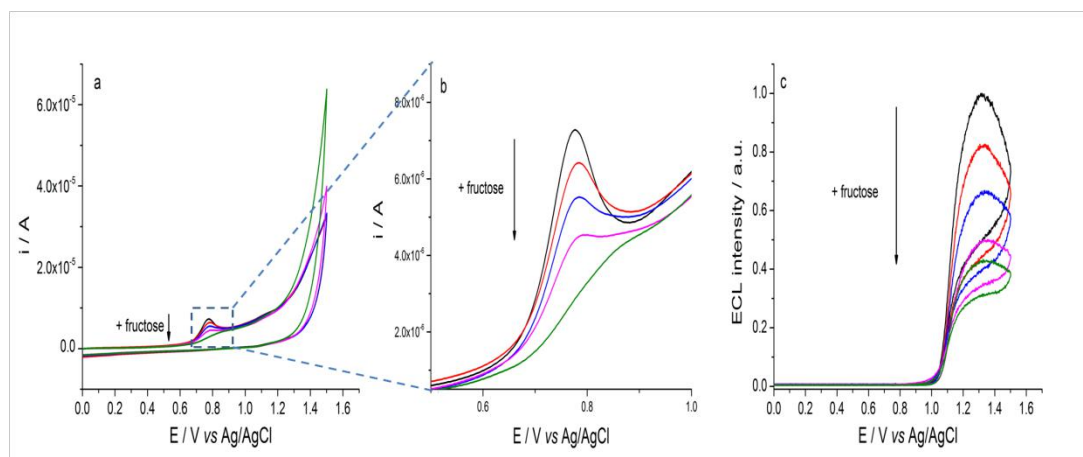


Figure 5. Effect of D-fructose addition on electrochemical oxidation of **E0** and on the corresponding ECL response. (a-b) Cyclic voltammetry and (c) ECL signal of a PBS solution (pH 7.4) containing 10  $\mu\text{M}$   $\text{Ru}(\text{bpy})_3^{2+}$ , 0.1 mM **E0** and different concentrations of D-fructose. The arrow indicates increasing concentrations of D-fructose (0, 0.5, 1, 10, and 50 mM). Experiments were performed on glassy carbon electrode (GCE) at a scan rate of 100 mV/s.

To check that the observed decrease was related to the complexation of the saccharides by the phenylboronic acid from **E0** and not to some photochemical or quenching effects, we compared firstly the ECL and photoluminescent (PL) spectra recorded with same solution (Figure 6a). Identical ECL and PL spectra were obtained meaning that the same excited state was reached. Then the evolution of PL spectra was tested with increasing concentrations of D-fructose (Figure 6b). The obtained PL spectra shows that the intensity of  $\text{Ru}(\text{bpy})_3^{2+}$  remains constant even adding D-fructose with concentration up to 3 orders of magnitude. This indicates that the photochemical properties of the luminophore were not affected neither by D-fructose nor D-glucose. Besides, the electrochemical and ECL signals of the model  $\text{Ru}(\text{bpy})_3^{2+}/\text{TPrA}$  in presence of D-fructose was studied and the effects of D-fructose addition led to minute changes (data not shown).

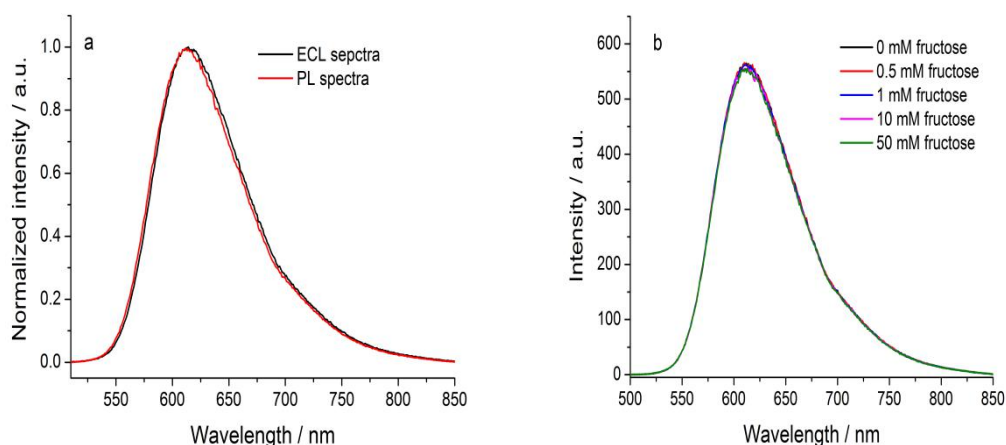


Figure 6. (a) Comparison of the ECL and PL spectra recorded in PBS (pH 7.4) solution with 10  $\mu\text{M}$   $\text{Ru}(\text{bpy})_3^{2+}$  and 0.1 mM  $\text{E0}$ , respectively. (b) PL spectra were recorded in PBS (pH 7.4) solution with 10  $\mu\text{M}$   $\text{Ru}(\text{bpy})_3^{2+}$ , 0.1 mM  $\text{E0}$  and different concentrations of D-fructose (0, 0.5, 1, 10 and 50 mM).  $\lambda_{\text{exc}} = 452$  nm.

In order to determine the rate controlling step in the global ECL process, we plotted the variations of the normalized ECL peak (*i.e.* final readout signal) as a function of the normalized peak current (*i.e.* first step in the ECL process) with increasing concentration of D-fructose or D-glucose (Figure 7). One can observe unambiguously that both signals are cross-correlated for both saccharides. It demonstrates thus that the variation of the ECL intensity is governed by the oxidation process of the co-reactant. The electrochemical step, and more specifically the heterogeneous oxidation of  $\text{E0}$ , controls the efficiency of the ECL process. In other words, the decrease of the ECL intensity observed with increasing concentration of saccharides is due to the direct oxidation of the  $\text{E0}$  at the electrode surface when it binds the saccharides.

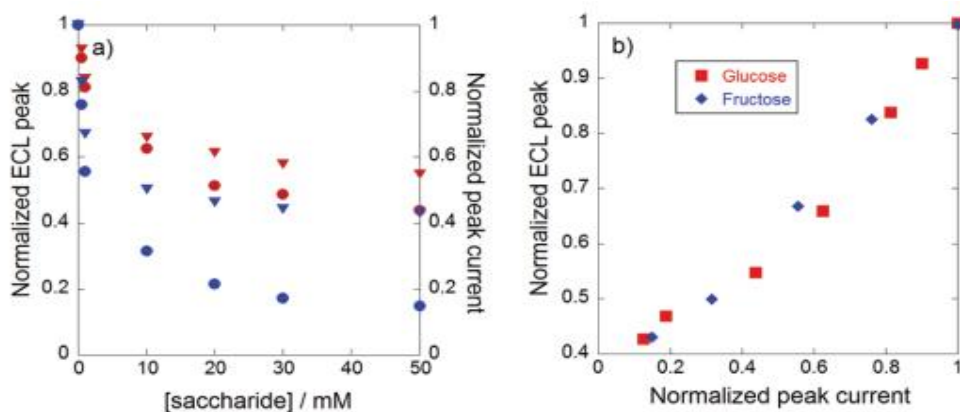


Figure 7. (a) Variation of the normalized ECL peak intensity (triangles) and of the oxidation peak current (dots) for the system Ru(bpy)<sub>3</sub><sup>2+</sup>/E0 as a function of the concentration of D-glucose (red markers) or of D-fructose (blue markers). (b) Correlation between the ECL signals and the peak current corresponding to the E0 oxidation for the addition of different concentrations of D-glucose or of D-fructose.

The oxidation behavior of tertiary amines at glassy carbon electrodes has been examined in aqueous solutions.<sup>16,48-50</sup> It is known that oxidation of a tertiary amine occurs when it is in the deprotonated form.<sup>48</sup> When protonation of the tertiary amines becomes important at acidic pH, its oxidation peak decreases in intensity and shifts toward more positive potentials.<sup>10</sup> As illustrated in Figure 2, the complexation of the saccharide by E0 induces a solvent-inserted B-N bond which behaves in a very similar fashion to protonation of the nitrogen atom.<sup>47,51</sup> Therefore, heterogeneous oxidation of the co-reactant in presence of saccharide becomes a very inefficient process that limits drastically the ECL signal. However, even at high D-fructose concentrations where almost all the E0 is bound, we still observe an ECL signal. Since ECL is obtained at the oxidation potential of Ru(bpy)<sub>3</sub><sup>2+</sup>, the remaining ECL intensity resulted probably from the electrocatalytic mechanism where E0 is homogeneously oxidized by the electrogenerated Ru(bpy)<sub>3</sub><sup>3+</sup>.

### 4.2.3 ECL response induced by selectively binding saccharides

To further assess our approach and to improve the selectivity, we designed and prepared new symmetric tertiary bis amino reagents bearing boronic acid end-groups

and having linkers with different lengths (Scheme 2). Previous, research has demonstrated that saccharide selectivity can be achieved in systems with two boronic acid groups.<sup>43,47</sup> We investigated first the binding properties of the compound **E6** with a hexyl linker between both amino groups. The addition of D-fructose or D-glucose induces the decrease of the oxidation current and the shift of the corresponding anodic wave, as reported for **E0**, which resulted in a decrease of the ECL response in the presence of both saccharides (Figure 8).

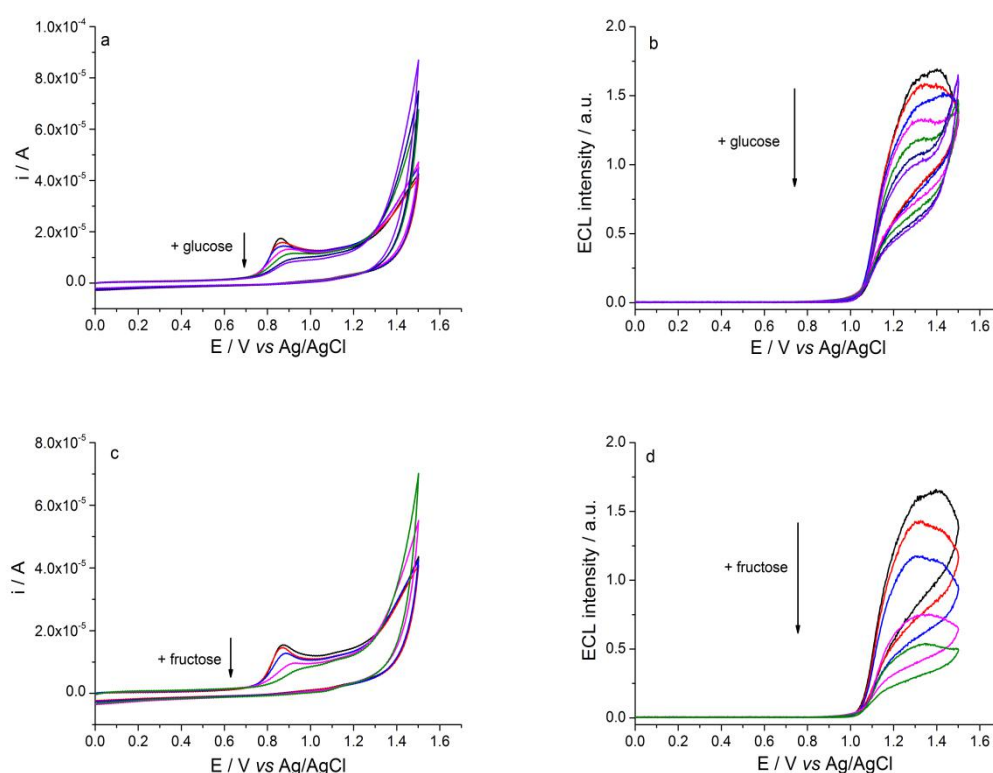


Figure 8. Effect of (a-b) D-glucose or (c-d) D-fructose addition on electrochemical oxidation of **E6** and on the corresponding ECL responses. Cyclic voltammograms and ECL signals of a PBS solution (pH 7.4) containing 10  $\mu\text{M}$   $\text{Ru}(\text{bpy})_3^{2+}$ , 0.1mM **E6** and different concentrations of D-glucose or of D-fructose. The arrow indicates increasing concentrations of D-glucose (0, 0.5, 1, 10, 50, 100 and 200 mM) or of D-fructose (0, 0.5, 1, 10 and 50 mM).

Similar plots as in **E0** were established upon the ECL peak intensity and oxidation peak current data. As shown in Figure 9, both ECL peak intensity and oxidation peak current are decreasing progressively with the increasing concentration of either glucose or fructose. Moreover, the ECL peak intensity decrease caused by fructose is

greater than that of glucose at the same concentration. It is noteworthy that such phenomenon in ECL is coherent to the case in oxidation peak current, as the oxidation process of co-reactant has proven to govern the ECL efficiency of the system.

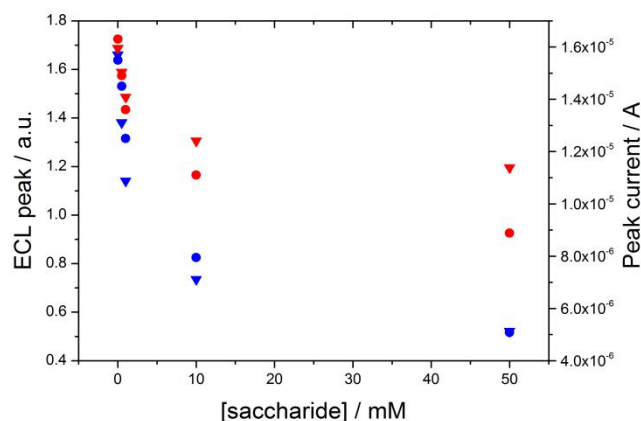


Figure 9. Variation of the ECL peak intensity (triangles) and of the oxidation peak current (dots) for the system  $\text{Ru}(\text{bpy})_3^{2+}/\mathbf{E6}$  as a function of the concentration of D-glucose (red markers) or of D-fructose (blue markers). Values are extracted from Figure 8.

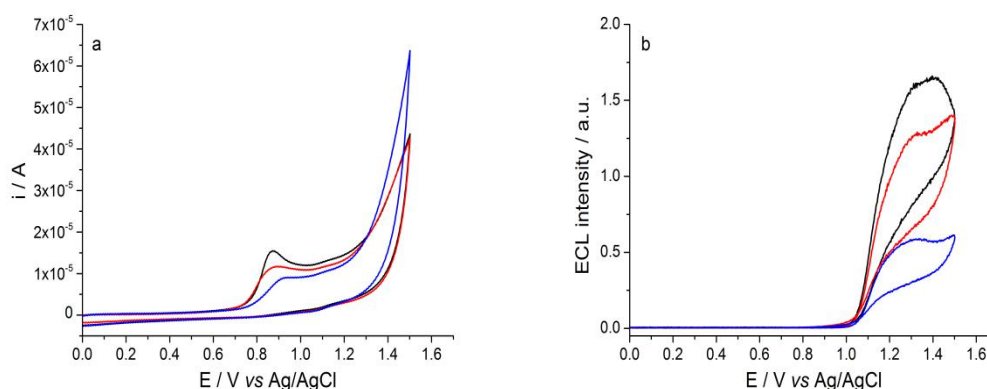


Figure 10. Variation of the (a) voltammetric response and (b) ECL peak intensity for the system  $\text{Ru}(\text{bpy})_3^{2+}/\mathbf{E6}$  in a competitive assay. Cyclic voltammograms and ECL signals of a PBS solution (pH 7.4) containing  $10 \mu\text{M}$   $\text{Ru}(\text{bpy})_3^{2+}$ ,  $0.1 \text{mM}$   $\mathbf{E6}$  (black curve) after adding first  $10 \text{mM}$  D-glucose (red curve) and then  $10 \text{mM}$  D-fructose (blue curve).

To further investigate the properties of  $\mathbf{E6}$ , additional competitive assays were performed. They clearly showed that D-fructose and D-glucose caused notable modification of the current and of the ECL signal (Figure 10). The detection limits of D-glucose and of D-fructose for  $\mathbf{E6}$  were  $20 \mu\text{M}$  and  $10 \mu\text{M}$ , respectively. Initially, it was somewhat surprising to us that  $\mathbf{E6}$  could not discriminate between D-fructose and

D-glucose and detect them selectively. However, according to our previous fluorescence work for **F6** (Scheme 1), the measured binding constants for D-fructose and D-glucose are very similar  $784 \pm 44$  and  $962 \pm 70 \text{ dm}^3 \text{ mol}^{-1}$ .<sup>43</sup>

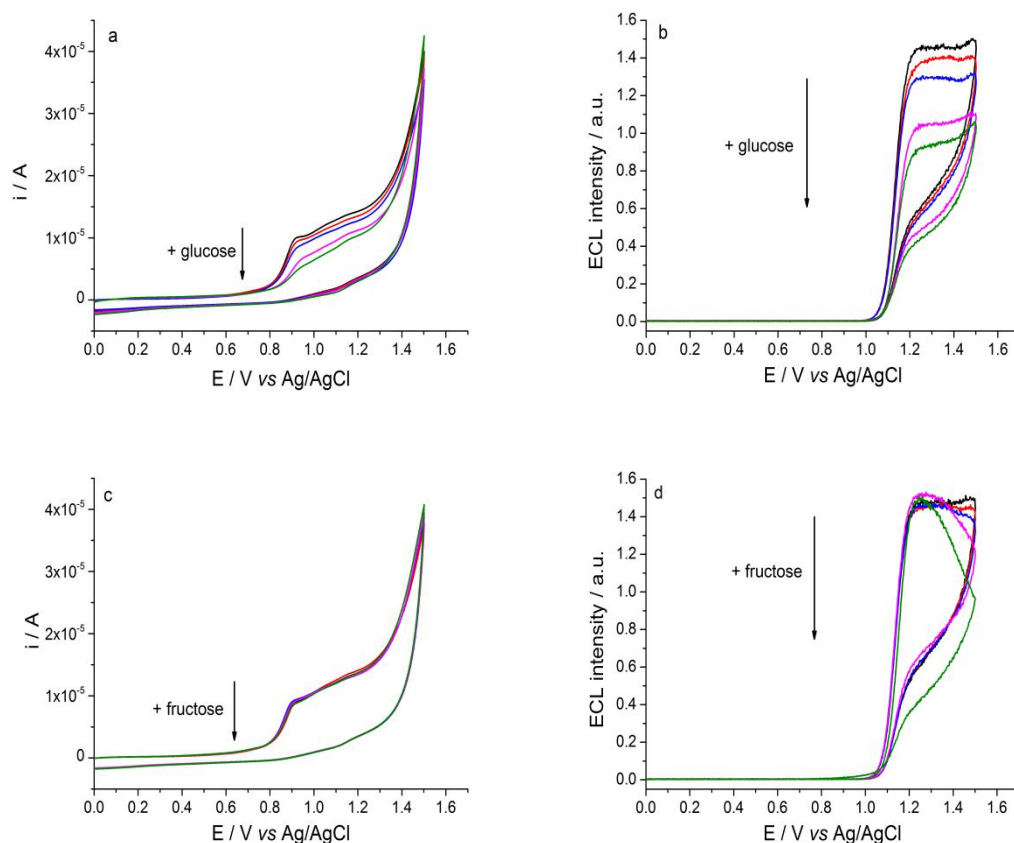


Figure 11. Effect of (a-b) D-glucose or (c-d) D-fructose addition on electrochemical oxidation of **E3** and on the corresponding ECL responses. Cyclic voltammograms and ECL signals of a PBS solution (pH 7.4) containing  $10 \mu\text{M Ru}(\text{bpy})_3^{2+}$ ,  $0.1 \text{ mM E3}$  and different concentrations of D-glucose or of D-fructose. The arrow indicates increasing concentrations of D-glucose or of D-fructose (0, 0.5, 1, 10 and 50 mM).

Further ECL assays were performed on **E3** which has a shorter the linker between both amino group and the phenylboronic acid moieties to investigate the influence of the linker length on the selective recognition of both saccharides. Figure 11 presents the results obtained with **E3**. Adding D-glucose induces the decrease of the current for both oxidation waves as well as the parallel decrease of the ECL response (Figure 11a-b). Remarkably, a characteristic stability of the voltammetric signal and of the ECL response (Figure 11c-d) was found for D-fructose, allowing discriminating

between both saccharides (Figure 12). While this result seems quite strange, our observations with similar fluorescence systems<sup>43</sup> can help explain the observed selectivity. Since, the binding of **F3** with D-fructose is significantly impaired when compared with the model system **F0** evidenced by a 4-fold reduction in binding for D-fructose from  $395 \pm 11 \text{ dm}^3 \text{ mol}^{-1}$  for **F0** to  $95 \pm 9 \text{ dm}^3 \text{ mol}^{-1}$  for **F3**. However, for D-glucose the binding is enhanced 2-fold from  $44 \pm 3 \text{ dm}^3 \text{ mol}^{-1}$  for **F0** to  $103 \pm 3 \text{ dm}^3 \text{ mol}^{-1}$  for **F3**.<sup>43</sup> The proportional decrease of the ECL readout signal with the D-glucose concentration allowed for facile quantification. Finally, the correlation of the ECL variation with the current for **E3** confirmed that the oxidation step of the co-reactant is the one determining the efficiency of the ECL process.

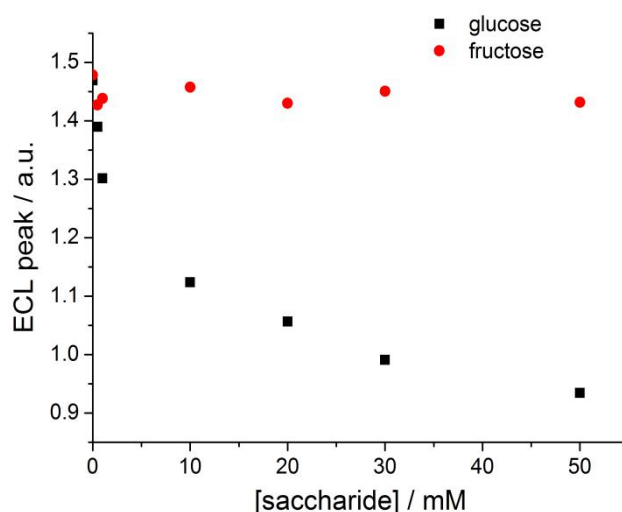


Figure 12. Variation of the ECL peak intensity for the system  $\text{Ru}(\text{bpy})_3^{2+}/\mathbf{E3}$  as a function of the concentration of D-glucose or of D-fructose.

### 4.3 Optical fiber bundle

Optical fiber bundle is well-established tools in analytical chemistry.<sup>52</sup> Their intrinsic characteristic of transmitting light over long distances makes them very useful tools for remote sensing in confined or hazardous environments.<sup>53</sup> Optical fiber consists of two different components: a glass core surrounding by a clad with lower refractive index (Figure 13).<sup>54</sup> However, it is difficult to transmit image via a single optical fiber

due to its incapability to maintain spatial information.<sup>55</sup> To obtain such information, optical fiber bundle are created by bundling and fusing of thousands of fibers. It is an ideal platform integrated with other strategies for specific use. The applications of such devices pervade in many diverse areas, such chemical sensor, biosensor, environmental surveillance and clinical monitoring.<sup>52,56,57</sup> For instance, etched fiber bundles have been developed as suitable templates for randomly ordered sensing arrays,<sup>58-61</sup> for surface-enhanced Raman imaging<sup>62-66</sup> and for single molecule detection.<sup>67-69</sup> They are also recognized as very convenient platforms that can be further integrated with other techniques for specific tasks. Moreover, the ability to intimately combine optical fiber bundles with electrochemical methods provides an opportunity to develop miniaturized and flexible opto-electrochemical arrays.<sup>70-75</sup>

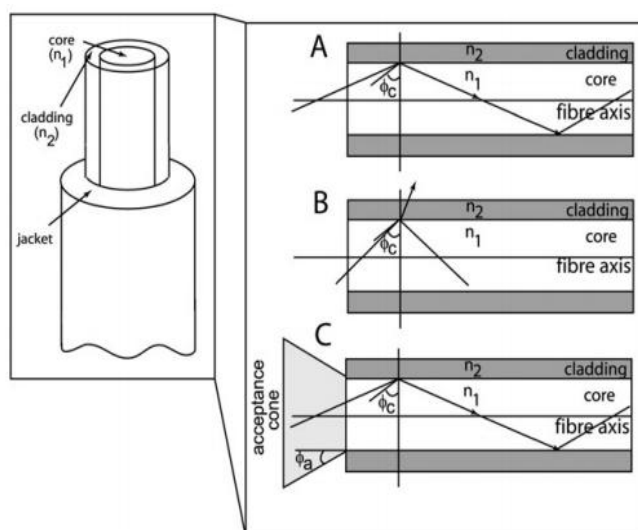


Figure 13. Configuration of an optical fiber with a core and cladding layer.<sup>54</sup>

The remote electrochemical addressing of conducting (micro) objects in order to locally trigger different chemical reactions at their surface has attracted increasing interests during the last decade, leading to the renaissance of bipolar electrochemistry (BPE).<sup>21</sup> In most of the examples reported in the literature, objects made out of conventional conducting<sup>20</sup> or at least semi-conducting materials<sup>76</sup> have been used in this context. A very popular family of reactions that has been explored for this

wireless type of electrochemistry is ECL. Indeed, the combinations of BPE and ECL has attracted many interests in fields for the fabrication of large scale ECL array, wireless ECL swimmers and sensors.<sup>22-24</sup> However the detection of the generated light has been achieved so far only by classic photomultipliers or cameras. A more straightforward approach would be the utilization of an optical fiber based platform, where not only ECL generation of ECL occurs very locally at the tip optical fiber, but also to guide ECL signal directly to the remote end of the optical fiber. This would open up interesting new applications because optical fibers are well-established tools serving in many domains, ranging from information transmission to analytical chemistry.<sup>54,58</sup> To this end, a thin film of gold or transparent indium tin oxide (ITO) can be deposited onto the fiber bundle, which can then be used as a working electrode. Further modification of the conducting layer can be achieved by coating for example either a molecular layer or thin polymer layer with specific functionality.<sup>10,74,77</sup>

### **4.3.1 Gold coated optical fiber bundle tip as BE**

In the present case, gold coated fiber bundle serves as BE, meaning that a polarization potential can be induced alongside the unconnected object submitted to an electric field within an electrolyte phase. A sufficiently large polarization potential allows then driving electrochemical reactions in a wireless manner with anodic and cathodic electrochemical reactions taking place simultaneously at the extreme poles of the same conductive object.<sup>20,21</sup> Practically, the electric field is established in the electrolyte by applying an external potential difference ( $E_{tot}$ ) between two feeder electrodes. If the conductive object is sufficiently long and  $E_{tot}$  is high enough, Faradaic reactions will occur at both poles of the object making it a BE. The polarization potential difference between its two ends ( $\Delta E_{elec}$ ) is the fraction of  $E_{tot}$  which drops over the length of the electrode (Figure 14).

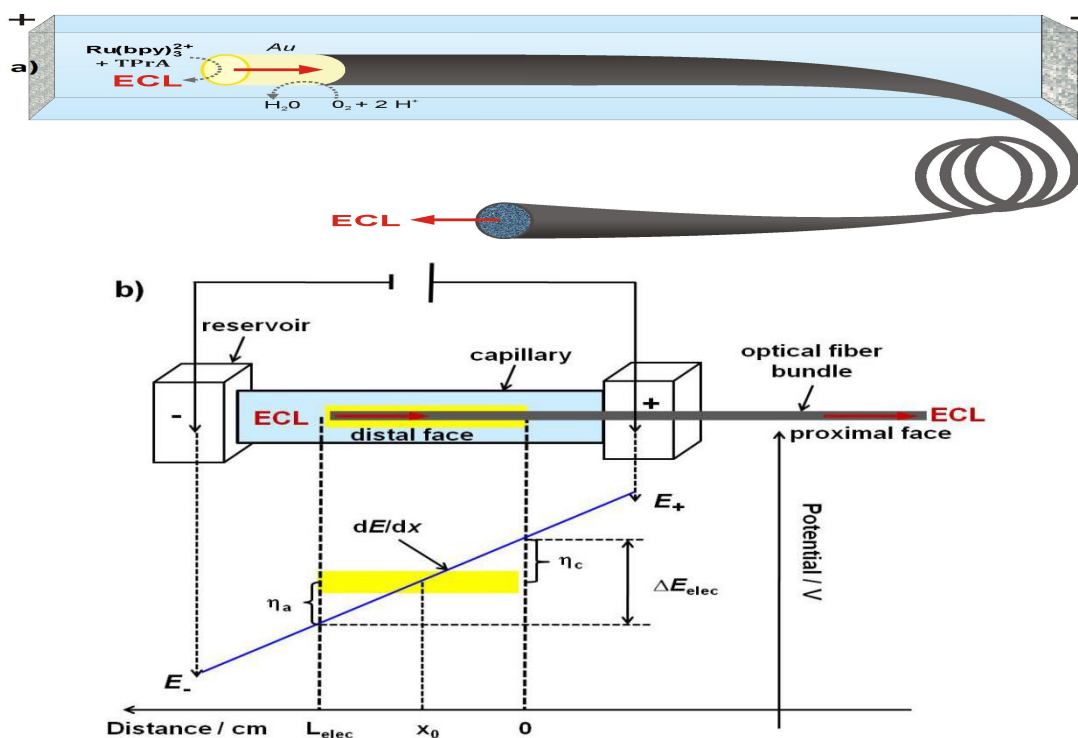


Figure 14. (a) Principle of the double remote electrochemical generation and optical readout of ECL. (b) Schematic illustration of the experimental setup which combines BPE and ECL imaging at the level of an optical fiber bundle. The gold-coated distal face of the optical fiber bundle is placed in a capillary between 2 feeder electrodes and it acts as a bipolar opto-electrode. The concomitant reduction of O<sub>2</sub> at the cathodic pole (side of the bundle) and oxidation of the ECL reagents at the anodic pole (extremity of the distal face) induces light generation. The corresponding ECL light is transmitted by the waveguide and remotely monitored at the proximal face of the bundle.

As mentioned above, BPE has been widely used so far not only for the elaboration of functional materials or devices, but also for inducing specific motion of micro-objects, generation of surface gradients or also for performing various analytical tasks.<sup>23,78-82</sup> However, as the BEs are not directly connected to any external device, the readout of the electrochemical information is not easy. To overcome this problem, Manz and co-workers introduced ECL as a reporting signal for BPE.<sup>83</sup> Thus the electrochemical activity of the BE is directly related to the ECL intensity,<sup>26,84</sup> transducing the Faradaic current into an optical signal which is detected in a wireless manner. In the present study, we explore this powerful combination of BPE and ECL for generating light directly at the tip of an optical fiber bundle in a highly controlled way, associated with its transmission through the fiber and a remote readout at the opposite end (Figure

14a).

### 4.3.2 Direct ECL imaging on a optical fiber bundle

ECL is a very sensitive method that is initiated by electron-transfer reactions to generate the excited state of a redox-active luminophore.<sup>4,5</sup> The most common method to generate ECL is based on the simultaneous oxidation of the luminophore  $\text{Ru}(\text{bpy})_3^{2+}$  and TPrA on the electrode surface to produce the excited state of  $\text{Ru}(\text{bpy})_3^{2+}$ .<sup>3</sup> A specific homemade bipolar electrochemical cell was constructed by using two individual reservoirs connected together by a capillary. Two feeder electrodes were placed separately in the reservoirs, while the gold-coated distal face of the optical fiber bundle is used as BE when positioned in the capillary. ECL reactions take place at the anodic pole of the gold-coated fiber bundle when the external potential is applied. The ECL emission which is produced in a wireless manner at the distal face of the fiber is then captured and transmitted to the proximal end (Figure 14b).

The experiments reported here provide the possibility to monitor ECL emission in a double remote mode (i.e. electrochemical addressing and optical sensing). To the best of our knowledge, this is the first time that such optical fibers modified with a conducting layer are used as BE. Figure. 15a displays an optical image recorded under white light illustrating the position of the optical fiber bundle placed in a capillary filled with PBS solution containing both, the luminophore and the co-reactant ( $\text{Ru}(\text{bpy})_3^{2+}$  and TPrA, respectively). It is noteworthy that the exact position of the optical fiber bundle in the capillary is not an essential criterion because the polarization potential only depends on the length of the gold coating. As already discussed, electrochemical reactions can be promoted at the two extreme poles of the BE by applying a sufficient electric field. In the present case, only the gold-coated part of the distal end of the bundle acts as a BE. ECL is produced by the simultaneous oxidation of  $\text{Ru}(\text{bpy})_3^{2+}$  and TPrA at the anodic pole and the concomitant oxygen and

eventual water reduction occurring at the cathodic end of the BE. Figure 15b shows an intense visible orange/red ECL emission localized at the distal end of the gold-coated fiber when an external electric field of 0.8 V/cm is applied across the bipolar cell. One can clearly observe that ECL is produced along the side of the bundle and also at its tip. In a first approximation, these conditions correspond to a polarization potential  $\Delta E_{elec}$  equal to 1.6 V according to eq. 1:

$$\Delta E_{elec} = \frac{dE}{dx} \times L_{elec} \quad (1)$$

with  $dE/dx$  being the external electric field applied by the feeder electrodes. The length of the BE ( $L_{elec}$ ) is 2 cm (length of the gold coated part of the fiber). ECL emission is observed over a length of  $\sim 1.2$  mm and is so strong that it is visible by the naked eye, thus providing a straightforward readout. High quality images were also recorded with a commercial camera (Figure. 15). The effect of the external electric field strength on ECL emission was studied on the same BE. Further increase of the electric field to 1.2 V/cm results indeed in increasing the length of the ECL emission profile alongside the gold-coated fiber bundle ( $\sim 6.3$  mm in length when  $\Delta E_{elec}$  increases to 2.4 V, see Figure 15c). Since  $\Delta E_{elec}$  depends linearly on the electrode length and the external electric field, a stronger electric field can thus lead to a higher  $\Delta E_{elec}$  on the BE. As a result, this will immediately extend the part of the BE where it is thermodynamically possible to drive ECL generation.<sup>82</sup> Compared to Figure 15b, ECL intensity becomes also higher for a given position on the BE, for instance at the extreme end of the distal part, due to a higher potential difference  $\eta(x)$  allowing driving ECL reactions (see eq. 2):

$$\eta(x) = \frac{\Delta E_{elec}}{L_{elec}} (x_0 - x) \quad (2)$$

$\eta(x)$  being the difference in potential between the BE and the solution at a given position ( $x$ ) of the electrode.  $x_0$  is the particular position where the solution potential is

equal to the mixed potential of the BE. By assuming that the electric field is constant through the entire capillary,  $\eta(x)$  is linearly decreasing as  $x$  approaches  $x_0$ .<sup>26</sup> Thus, ECL emission on the gold-coated fiber is driven by different potential values along the BE, depending on the  $x$  position. This is why the ECL intensity decreases when moving from the edge of the BE towards the center.<sup>85</sup> This also explains the tail-like ECL emission which is observed on the gold coated fiber (Figure 15c). However, these results reveal also that the gold layer deposited by sputtering is robust and conductive enough to support the electrochemical reactions that are driven by the external electric field in the bipolar mode.



Figure 15. Side-view of ECL emission at the distal part of a gold-coated optical fiber bundle. (a) White light image of the bundle placed in a capillary, filled with 10 mM PBS (pH 7.4) containing 1 mM of  $\text{Ru}(\text{bpy})_3^{2+}$  and 100 mM TPrA. The arrow shows the extremity of the distal face of the gold-coated bundle. Optical images recorded in the dark, show the BE emitting ECL when exposed to an external electric field of (b) 0.8 V/cm or (c) 1.2 V/cm. Feeder electrodes are symbolically represented.

### 4.3.3 Remote ECL sensing through an optical fiber bundle

Although ECL emission produced on a BE has been directly observed and studied in many systems,<sup>26,86-89</sup> the use of optical fibers in BPE allows to remotely monitor the electrochemical reactions on the BE. In this case, ECL is generated at the distal face of the bipolar opto-electrode and a fraction of the ECL emission is concomitantly captured by the waveguide. Therefore, a thinner gold layer has to be present at the distal face of the optical fiber bundle in order to transmit the largest remote optical

signal. The gold thickness should be a compromise to ensure a sufficient conductivity for BPE as well as to remain quasi-transparent to allow enough light being transmitted through the gold layer.

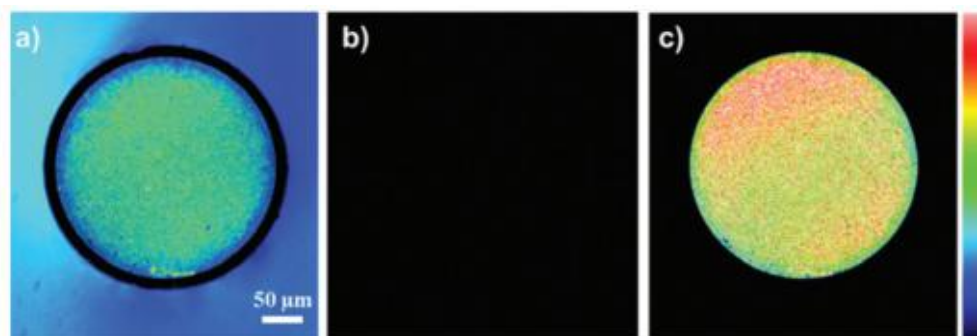


Figure 16. Remote imaging of the proximal face of the optical fiber bundle. These images were acquired through the bundle. (a) A halogen lamp illuminates the gold-coated distal face of the bundle. The white light is transmitted through it and recorded with a CCD camera. Images of the proximal face (b) when no electric field is applied and (c) when ECL is generated at the distal face by applying an external electric field of 0.8 V/cm.

Figure 16a presents a remote image of the proximal face of the optical fiber bundle recorded by a CCD camera, when the white light emitted from a halogen lamp is captured at the gold coated distal face and guided through the bundle. Each individual fiber is clearly visible even though its distal surface is covered by a gold layer, indicating good light-transmission efficiency. As demonstrated above, light can be produced easily at the gold-coated distal face using ECL reactions driven by the external electric field. Figure 15 has already shown that ECL emission occurs not only along the side of the optical fiber bundle but also at its tip. Since the gold layer is relatively thick ( $\sim 500$  nm) on the sidewall and consequently non-transparent, it prevents the collection of the ECL emission which is generated in this region. Only the ECL light produced at the very tip, where the gold layer is thin enough is collected by the fibers and transmitted to the proximal face as shown in Figure 16c. The thicker gold coating along the fiber is essential to allow the opposite reaction, a reduction herein, to occur in the bipolar mode. In addition, it means also that much stronger ECL might be generated and transmitted by using a transparent conductive coating

such as ITO. It is noticeable that in Figure 16c there is absolutely no residual light surrounding the fiber in contrast to Figure 16a. This is because the ECL signal is intense enough to be specifically collected and guided through the fiber. This provides a very interesting signal to noise ratio for instance for sensing applications. A negative control is displayed in Figure 16b revealing that there is obviously no recordable remote ECL signal without external electric field. The ECL intensity is lower at the periphery of the bundle (Figure 16c). This “edge effect” may also be observed on Figure 16a (*i.e.* the white light image). It is indeed related to the optics of the optical fiber bundle and also classically observed for epifluorescence measurements. It is mainly due to the numerical aperture and also to the position of each single fiber in the bundle. The fibers located in the center collect and transmit more light than the ones at the periphery.

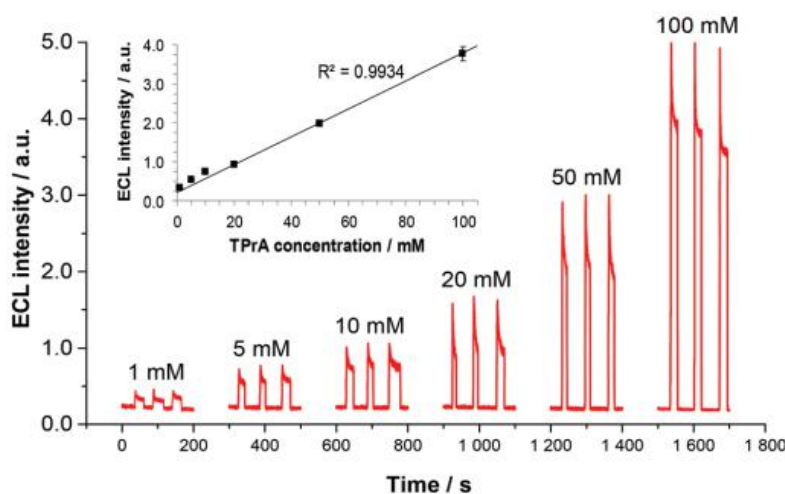


Figure 17. Remote ECL intensity generated at the gold-coated distal face of the optical fiber bundle and recorded at the proximal end with a PMT, when the cell is filled with 0.1 mM Ru(bpy)<sub>3</sub><sup>2+</sup> and increasing concentrations of TPrA in 10 mM PBS solution (pH 7.4). External electric field is 0.8 V/cm.

The Ru(bpy)<sub>3</sub><sup>2+</sup>/TPrA system exhibits very high ECL efficiency, and it is well-known that the ECL light intensity is proportional to the concentration of both Ru(bpy)<sub>3</sub><sup>2+</sup> and TPrA in a large dynamic range with potentially very low detection limits.<sup>16</sup> Many commercial immunoassays and DNA assays are developed based on the use of this

benchmark ECL system.<sup>90</sup> As shown in Figure 17, ECL intensity recorded at the proximal end with a PMT increases linearly with increasing TPrA concentration. The concentration range tested in this proof-of-principle determination of co-reactant concentration spreads between 1 mM and 100 mM. ECL increases abruptly, and then tends to be stable with time when the external electric field is applied across the BPE cell. Following, ECL signal disappears rapidly after turning off the power supply. Also, the correlation coefficient obtained in this dynamic range demonstrates a very good linearity ( $R^2 = 0.9934$ , Figure 17 inset). The bipolar opto-electrode exhibits good reproducibility for three consecutive measurements.

## 4.4 Conclusion

Two original pathways for ECL sensing have been demonstrated in this chapter, respectively. In the first pathway, we have selected a series of bearing boronic acids bearing tertiary amine groups as ECL co-reactant for saccharides sensing. This unprecedented approach is based on the boronic acid as the receptor group due to its ability to bind saccharides in water. The recognition of the saccharide moiety modulate the electrochemical reactivity of the coreactant, resulting the response of direct ECL readout from a classical luminophore  $\text{Ru}(\text{bpy})_3^{2+}$ . Excellent selectivity for D-glucose was achieved by tuning the linker length of a bis-boronic acid amine coreactant. Whatever, such pathway allows manipulating the ECL readout signal with an additional parameter and not by playing only with the structure of the luminophore and the electrode potential. The simplicity of the system ensures that it will find many applications from biological and chemical sensing to incorporation in molecular logic circuits. In the second pathway, ECL double remote sensing system has been designed by combining advantageously the intrinsic characteristics of BPE and the remote imaging properties of optical fiber bundles. ECL emission is generated and detected *in-situ* at the tip of the bipolar opto-electrode in a wireless manner. A fraction of the ECL signal is collected at the distal face of the fiber bundle when the electric field is

applied. Then, the captured ECL is transmitted to the proximal end of the optical fiber bundle, where the luminescent signal is recorded by a CCD camera or a PMT. Therefore both remote functions (*i.e.* bipolar generation and guiding of ECL) can be integrated at the level of a single device. The coherent structure of the fiber array used in this study allows transmission of an image through the dual opto-electrochemical platform. Successful recording of ECL demonstrates that the conducting gold layer deposited on the fiber bundle allows using the opto-electrode as a BE, thus enabling wireless ECL generation and collection. The concept of double remote ECL sensing is then reported for the first time and provides new opportunities to record data from the collected images. The powerful features of this simultaneous generation, collection and transmission of ECL are demonstrated with the model system  $\text{Ru}(\text{bpy})_3^{2+}/\text{TPrA}$ . The linearity between ECL intensity and TPrA was successfully verified based on double remote signal processing. This new approach broadens significantly the applicability of BPE and of optical fibers and could be potentially used for remote multiplex ECL sensing in the future. Finally, since microwell and nanotip arrays have been developed based on etched optical fiber bundles,<sup>91,92</sup> the reported strategy could also be extended to fabricate a variety of bipolar ECL devices with interesting high throughput features.

## References

- (1) Blackburn, G. F.; Shah, H. P.; Kenten, J. H.; Leland, J.; Kamin, R. A.; Link, J.; Peterman, J.; Powell, M. J.; Shah, A.; Talley, D. B.; Tyagi, S. K.; Wilkins, E.; Wu, T.-G.; Massey, R. J. Electrochemiluminescence detection for development of immunoassays and DNA probe assays for clinical diagnostics. *Clin. Chem.* **1991**, *37*, 1534-1539.
- (2) Chen, X.-M.; Su, B.-Y.; Song, X.-H.; Chen, Q.-A.; Chen, X.; Wang, X.-R. Recent advances in electrochemiluminescent enzyme biosensors. *Trends Anal. Chem.; TrAC* **2011**, *30*, 665-676.
- (3) Miao, W. Electrogenerated chemiluminescence and its biorelated applications. *Chem. Rev.* **2008**, *108*, 2506-2553.
- (4) Liu, Z.; Qi, W.; Xu, G. Recent advances in electrochemiluminescence. *Chem. Soc. Rev.* **2015**, *44*, 3117-3142.
- (5) Bard, A. J.: *Electrogenerated Chemiluminescence*; M. Dekker: New-York, 2004.
- (6) Lai, R. Y.; Chiba, M.; Kitamura, N.; Bard, A. J. Electrogenerated chemiluminescence 68: detection of sodium ion with a ruthenium(II) complex with crown ether moiety at the 3,3'-positions on the 2,2'-bipyridine ligand. *Anal. Chem.* **2002**, *74*, 551-553.
- (7) Muegge, B. D.; Richter, M. M. Electrochemiluminescent detection of metal cations using a ruthenium(II) bipyridyl complex containing a crown ether moiety. *Anal. Chem.* **2002**, *74*, 547-550.
- (8) Schmittl, M.; Lin, H.-W. Quadruple-channel sensing: a molecular sensor with a single type of receptor site for selective and quantitative multi-ion analysis. *Angew. Chem. Int. Ed.* **2007**, *46*, 893-896.
- (9) Lin, H.; Cinar, M. E.; Schmittl, M. Comparison of ruthenium(II) and cyclometalated iridium(III) azacrown ether phenanthroline hybrids for the detection of metal cations by electrochemiluminescence. *Dalton Trans.* **2010**, *39*, 5130-5138.
- (10) Shu, Q.; Adam, C.; Sojic, N.; Schmittl, M. Electrochemiluminescent polymer films with a suitable redox "turn-off" absorbance window for remote selective sensing of Hg<sup>2+</sup>. *Analyst* **2013**, *138*, 4500-4504.
- (11) Berni, E.; Gosse, I.; Badocco, D.; Pastore, P.; Sojic, N.; Pinet, S. Differential photoluminescent and electrochemiluminescent detection of anions with a modified ruthenium(II) bipyridyl complex. *Chem. Eur. J.* **2009**, *15*, 5145-5152.
- (12) Rubinstein, I.; Martin, C. R.; Bard, A. J. Electrogenerated chemiluminescent determination of oxalate. *Anal. Chem.* **1983**, *55*, 1580-1582.
- (13) Skotty, D. R.; Lee, W.-Y.; Nieman, T. A. Determination of dansyl amino acids and oxalate by HPLC with electrogenerated chemiluminescence detection using tris (2, 2'-bipyridyl) ruthenium (II) in the mobile phase. *Analy. Chem.* **1996**, *68*, 1530-1535.
- (14) Yamashita, K.; Yamazaki-Nishida, S.; Harima, Y.; Segawa, A. Direct current electrogenerated chemiluminescent microdetermination of peroxydisulfate in aqueous solution. *Anal. Chem.* **1991**, *63*, 872-876.
- (15) Xu, G.; Dong, S. Electrochemiluminescent determination of peroxydisulfate with Cr (bpy)<sub>3</sub><sup>3+</sup> in purely aqueous solution. *Anal. Chim. Acta* **2000**, *412*, 235-240.

- (16) Zu, Y.; Bard, A. J. Electrogenerated chemiluminescence 66: The role of direct coreactant oxidation in the ruthenium tris(2,2')bipyridyl/triethylamine system and the effect of halide ions on the emission intensity. *Anal. Chem.* **2000**, *72*, 3223-3232.
- (17) Jameison, F.; Sanchez, R. I.; Dong, L.; Leland, J. K.; Yost, D.; Martin, M. T. Electrochemiluminescence-based quantitation of classical clinical chemistry analytes. *Anal. Chem.* **1996**, *68*, 1298-1302.
- (18) Liang, P.; Sanchez, R. I.; Martin, M. T. Electrochemiluminescence-based detection of  $\beta$ -lactam antibiotics and  $\beta$ -lactamases. *Anal. Chem.* **1996**, *68*, 2426-2431.
- (19) Li, H.; Sedgwick, A. C.; Li, M.; Blackburn, R. A. R.; Bull, S. D.; Arbault, S.; James, T. D.; Sojic, N. Selective electrochemiluminescent sensing of saccharides using boronic acid-modified coreactant. *Chem. Commun.* **2016**, *52*, 12845-12848.
- (20) Loget, G.; Zigah, D.; Bouffier, L.; Sojic, N.; Kuhn, A. Bipolar Electrochemistry: from materials science to motion and beyond. *Acc. Chem. Res.* **2013**, *46*, 2513-2523.
- (21) Fosdick, S. E.; Knust, K. N.; Scida, K.; Crooks, R. M. Bipolar electrochemistry. *Angew. Chem. Int. Ed.* **2013**, *52*, 10438-10456.
- (22) Qi, W.; Lai, J.; Gao, W.; Li, S.; Hanif, S.; Xu, G. Wireless electrochemiluminescence with disposable minidevice. *Anal. Chem.* **2014**, *86*, 8927-8931.
- (23) Sentic, M.; Loget, G.; Manojlovic, D.; Kuhn, A.; Sojic, N. Light-emitting electrochemical "swimmers". *Angew. Chem. Int. Ed.* **2012**, *51*, 11284-11288.
- (24) Chow, K.-F.; Mavr e, F.; Crooks, J. A.; Chang, B.-Y.; Crooks, R. M. A large-scale, wireless electrochemical bipolar electrode microarray. *J. Am. Chem. Soc.* **2009**, *131*, 8364-8365.
- (25) Fosdick, S. E.; Crooks, J. A.; Chang, B.-Y.; Crooks, R. M. Two-dimensional bipolar electrochemistry. *J. Am. Chem. Soc.* **2010**, *132*, 9226-9227.
- (26) Mavr e, F.; Chow, K.-F.; Sheridan, E.; Chang, B.-Y.; Crooks, J. A.; Crooks, R. M. A theoretical and experimental framework for understanding electrogenerated chemiluminescence (ECL) emission at bipolar electrodes. *Anal. Chem.* **2009**, *81*, 6218-6225.
- (27) Bouffier, L.; Zigah, D.; Adam, C.; Sentic, M.; Fattah, Z.; Manojlovic, D.; Kuhn, A.; Sojic, N. Lighting up redox propulsion with luminol electrogenerated chemiluminescence. *ChemElectroChem* **2014**, *1*, 95-98.
- (28) Sentic, M.; Arbault, S.; Goudeau, B.; Manojlovic, D.; Kuhn, A.; Bouffier, L.; Sojic, N. Electrochemiluminescent swimmers for dynamic enzymatic sensing. *Chem. Commun.* **2014**, *50*, 10202-10205.
- (29) Zhan, W.; Crooks, R. M. Microelectrochemical logic circuits. *J. Am. Chem. Soc.* **2003**, *125*, 9934-9935.
- (30) Bouffier, L.; Arbault, S.; Kuhn, A.; Sojic, N. Generation of electrochemiluminescence at bipolar electrodes: concepts and applications. *Anal. Bioanal. Chem.* **2016**, *408*, 7003-7011.
- (31) Li, H.; Garrigue, P.; Bouffier, L.; Arbault, S.; Kuhn, A.; Sojic, N. Double remote electrochemical addressing and optical readout of electrochemiluminescence at the tip of an optical fiber. *Analyst* **2016**, *141*, 4299-4304.
- (32) Fang, H.; Kaur, G.; Wang, B. Progress in boronic acid-based fluorescent glucose sensors. *J. Fluoresc.* **2004**, *14*, 481-489.
- (33) Bull, S. D.; Davidson, M. G.; van den Elsen, J. M. H.; Fossey, J. S.; Jenkins, A. T. A.;

Jiang, Y.-B.; Kubo, Y.; Marken, F.; Sakurai, K.; Zhao, J.; James, T. D. Exploiting the reversible covalent bonding of boronic acids: recognition, sensing, and assembly. *Acc. Chem. Res.* **2013**, *46*, 312-326.

(34) Lorand, J. P.; Edward, J. O. Polyol complexes and structure of the benzenboronate ion. *J. Org. Chem.* **1959**, *24*, 769-774.

(35) Nishiyabu, R.; Kubo, Y.; James, T. D.; Fossey, J. S. Boronic acid building blocks: tools for self assembly. *Chem. Commun.* **2011**, *47*, 1124-1150.

(36) Larkin, J. D.; Fossey, J. S.; James, T. D.; Brooks, B. R.; Bock, C. W. A Computational Investigation of the nitrogen-boron Interaction in o-(N, N-dialkylaminomethyl) arylboronate Systems. *J. Phys. Chem. A* **2010**, *114*, 12531-12539.

(37) Nishiyabu, R.; Kubo, Y.; James, T. D.; Fossey, J. S. Boronic acid building blocks: tools for sensing and separation. *Chem. Commun.* **2011**, *47*, 1106-1123.

(38) Milutinovic, M.; Sallard, S.; Manojlovic, D.; Mano, N.; Sojic, N. Glucose sensing by electrogenerated chemiluminescence of glucose-dehydrogenase produced NADH on electrodeposited redox hydrogel. *Bioelectrochemistry* **2011**, *82*, 63-68.

(39) de Poulpiquet, A.; Diez Buitrago, B.; Dumont Milutinovic, M.; Sentic, M.; Arbault, S.; Bouffier, L.; Kuhn, A.; Sojic, N. Dual enzymatic detection by bulk electrogenerated chemiluminescence. *Anal. Chem.* **2016**.

(40) Park, S.; Boo, H.; Chung, T. D. Electrochemical non-enzymatic glucose sensors. *Anal. Chim. Acta.* **2006**, *556*, 46-57.

(41) Pandya, A.; Sutariya, P. G.; Menon, S. K. A non enzymatic glucose biosensor based on an ultrasensitive calix [4] arene functionalized boronic acid gold nanoprobe for sensing in human blood serum. *Analyst* **2013**, *138*, 2483-2490.

(42) Lacina, K.; Skládal, P.; James, T. D. Boronic acids for sensing and other applications-a mini-review of papers published in 2013. *Chem. Centr. J.* **2014**, *8*, 1.

(43) Arimori, S.; Bell, M. L.; Oh, C. S.; Frimat, K. A.; James, T. D. Modular fluorescence sensors for saccharides. *J. Chem. Soc., Perkin Trans 1* **2002**, 803-808.

(44) Leland, J. K.; Powell, M. J. Electrogenerated chemiluminescence : an oxidative-reduction type ECL reaction sequence using tripropyl amine. *J. Electrochem. Soc.* **1990**, *137*, 3127-3131.

(45) Knight, A. W.; Greenway, G. M. Relation between structural attributes and observed electrogenerated chemiluminescence (ECL) activity of tertiary amines as potential analytes for the tris(2,2-bipyridine)ruthenium ECL reaction. *Analyst* **1996**, *121*, 101R-106R.

(46) Bock, C. R.; Connor, J. A.; Gutierrez, A. R.; Meyer, T. J.; Whitten, D. G.; Sullivan, B. P.; Nagle, J. K. Estimation of excited-state redox potentials by electron-transfer quenching. Application of electron-transfer theory to excited-state redox processes. *J. Am. Chem. Soc.* **1979**, *101*, 4815-4824.

(47) Sun, X.; James, T. D. Glucose sensing in supramolecular chemistry. *Chem. Rev.* **2015**, *115*, 8001-8037.

(48) Kanoufi, F.; Zu, Y.; Bard, A. J. Homogeneous oxidation of trialkylamines by metal complexes and its impact on electrogenerated chemiluminescence in the trialkylamine/Ru(bpy)<sub>3</sub><sup>2+</sup> system. *J. Phys. Chem. B* **2001**, *105*, 210-216.

(49) Smith, J. R. L.; Masheder, D. Amine oxidation. Part IX. The electrochemical oxidation of some tertiary amines: the effect of structure on reactivity. *J. Chem. Soc., Perkin*

*Trans* **2** **1976**, 47-51.

(50) Masui, M.; Sayo, H.; Tsuda, Y. Anodic oxidation of amines. Part I. Cyclic voltammetry of aliphatic amines at a stationary glassy-carbon electrode. *J. Chem. Soc. B.* **1968**, 973-976.

(51) Zhu, L.; Shabbir, S. H.; Gray, M.; Lynch, V. M.; Sorey, S.; Anslyn, E. V. A Structural investigation of the N–B interaction in an o-(N,N-Dialkylaminomethyl)arylboronate system. *J. Am. Chem. Soc.* **2006**, *128*, 1222-1232.

(52) López-Higuera, J. M.: *Handbook of optical fibre sensing technology*; Wiley, 2002.

(53) Orellana, G.; Haigh, D. New trends in fiber-optic chemical and biological sensors. *Curr. Anal. Chem.* **2008**, *4*, 273-295.

(54) Walt, D. R. Fibre optic microarrays. *Chem. Soc. Rev.* **2010**, *39*, 38-50.

(55) Epstein, J. R.; Walt, D. R. Fluorescence-based fibre optic arrays: a universal platform for sensing. *Chem. Soc. Rev.* **2003**, *32*, 203-214.

(56) Wolfbeis, O. S. Fiber-optic chemical sensors and biosensors. *Anal. Chem.* **2006**, *78*, 3859-3874.

(57) Narayanaswamy, R.; Wolfbeis, O. S.: *Optical sensors: industrial, environmental and diagnostic applications*; Springer, 2004; Vol. 1.

(58) Albert, K. J.; Lewis, N. S.; Schauer, C. L.; Sotzing, G. A.; Stitzel, S. E.; Vaid, T. P.; Walt, D. R. Cross-reactive chemical sensor arrays. *Chem. Rev.* **2000**, *100*, 2595–2626.

(59) Pantano, P.; Walt, D. R. Analytical applications of optical imaging fibers. *Anal. Chem.* **1995**, *67*, 481A-487A.

(60) Ferguson, J. A.; Steemers, F. J.; Walt, D. R. High-density fiber-optic DNA random microsphere array. *Anal. Chem.* **2000**, *72*, 5618-5624.

(61) Walt, D. R. Imaging optical sensor arrays. *Curr. Op. Chem. Biol.* **2003**, *6*, 689-695.

(62) Guieu, V.; Lagugné-Labarhet, F.; Servant, L.; Talaga, D.; Sojic, N. Ultrasharp optical - fiber nanoprobe array for raman local - enhancement imaging. *Small* **2008**, *4*, 96-99.

(63) White, D. J.; Stoddart, P. R. Nanostructured optical fiber with surface-enhanced Raman scattering functionality. *Opt. Lett.* **2005**, *30*, 598-600.

(64) White, D. J.; Mazzolini, A. P.; Stoddart, P. R. Fabrication of a range of SERS substrates on nanostructured multicore optical fibres. *J. Raman. Spectrosc.* **2007**, *38*, 377-382.

(65) Guieu, V.; Garrigue, P.; Lagugné-Labarhet, F.; Servant, L.; Sojic, N.; Talaga, D. Remote surface enhanced Raman spectroscopy imaging via a nanostructured optical fiber bundle. *Opt. Express* **2009**, *17*, 24030.

(66) Zamuner, M.; Talaga, D.; Guieu, V.; Deiss, F.; Kuhn, A.; Ugo, P.; Sojic, N. Multiscaled nanostructured array fabricated on an etched imaging bundle for surface-enhanced raman scattering. *Adv. Funct. Mat.* **2009**, *19*, 3129–3135.

(67) Walt, D. R. Optical methods for single molecule detection and analysis. *Anal. Chem.* **2013**, *85*, 1258-1263.

(68) Rissin, D. M.; Kan, C. W.; Campbell, T. G.; Howes, S. C.; Fournier, D. R.; Song, L.; Piech, T.; Patel, P. P.; Chang, L.; Rivnak, A. J.; Ferrell, E. P.; Randall, J. D.; Provuncher, G. K.; Walt, D. R.; Duffy, D. C. Single-molecule enzyme-linked immunosorbent assay detects serum proteins at subfemtomolar concentrations. *Nat. Biotechnol.* **2010**, *28*, 595-599.

(69) Rissin, D. M.; Walt, D. R. Digital concentration readout of single enzyme molecules using femtoliter arrays and poisson statistics. *Nano. Lett.* **2006**, *6*, 520-523.

- (70) Lee, Y.; Bard, A. J. Fabrication and characterization of probes for combined scanning electrochemical/optical microscopy experiments. *Anal. Chem.* **2002**, *74*, 3626-3633.
- (71) Wang, H.; Xu, G.; Dong, S. Electrochemiluminescent microoptoprobe with mini-grid working electrode and self-contained sample container. *Electrochem. Commun.* **2002**, *4*, 214-217.
- (72) Szunerits, S.; Garrigue, P.; Bruneel, J.-L.; Servant, L.; Sojic, N. Fabrication of a sub-micrometer electrode array: electrochemical characterization and mapping of an electroactive species by confocal Raman microspectroscopy. *Electroanalysis* **2003**, *15*, 548-555.
- (73) Lee, Y.; Amemiya, S.; Bard, A. J. Scanning electrochemical microscopy 41: Theory and characterization of ring electrodes. *Anal. Chem.* **2001**, *73*, 2261-2267.
- (74) Konry, T.; Bouhifd, M.; Cosnier, S.; Whelan, M.; Valsesia, A.; Rossi, F.; Marks, R. S. Electrogenerated indium tin oxide-coated glass surface with photosensitive interfaces: Surface analysis. *Biosens. Bioelectron.* **2007**, *22*, 2230.
- (75) Khan, S. S.; Jin, E. S.; Sojic, N.; Pantano, P. A fluorescence-based imaging fiber electrode chemical sensor for hydrogen peroxide. *Anal. Chim. Acta* **2000**, *404*, 213-221.
- (76) Ongaro, M.; Roche, J.; Kuhn, A.; Ugo, P. Asymmetric modification of TiO<sub>2</sub> nanofibers with gold by electric-field-assisted photochemistry. *ChemElectroChem* **2014**, *1*, 2048-2051.
- (77) Descamps, E.; Duroure, N.; Deiss, F.; Leichle, T.; Adam, C.; Mailley, P.; Ait-Ikhlef, A.; Livache, T.; Nicu, L.; Sojic, N. Functionalization of optical nanotip arrays with an electrochemical microcantilever for multiplexed DNA detection. *Lab. Chip* **2013**, *13*, 2956-2962.
- (78) Loget, G.; Roche, J.; Gianessi, E.; Bouffier, L.; Kuhn, A. Indirect bipolar electrodeposition. *J. Am. Chem. Soc.* **2012**, *134*, 20033-20036.
- (79) Loget, G.; Kuhn, A. Electric field-induced chemical locomotion of conducting objects. *Nat. Commun.* **2011**, *2*, 535.
- (80) Loget, G.; Roche, J.; Kuhn, A. True bulk synthesis of Janus objects by bipolar electrochemistry. *Adv. Mat.* **2012**, *24*, 5111-5116.
- (81) Laws, D. R.; Hlushkou, D.; Perdue, R. K.; Tallarek, U.; Crooks, R. M. Bipolar electrode focusing: Simultaneous concentration enrichment and separation in a microfluidic channel containing a bipolar electrode. *Anal. Chem.* **2009**, *81*, 8923-8929.
- (82) Zhan, W.; Alvarez, J.; Crooks, R. M. Electrochemical sensing in microfluidic systems using electrogenerated chemiluminescence as a photonic reporter of redox reactions. *J. Am. Chem. Soc.* **2002**, *124*, 13265-13270.
- (83) Arora, A.; Eijkel, J. C. T.; Morf, W. E.; Manz, A. A Wireless electrochemiluminescence detector applied to direct and indirect detection for electrophoresis on a microfabricated glass device. *Anal. Chem.* **2001**, *73*, 3282-3288.
- (84) Chow, K.-F.; Mavr e, F.; Crooks, R. M. Wireless electrochemical DNA microarray sensor. *J. Am. Chem. Soc.* **2008**, *130*, 7544-7545.
- (85) Chang, B.-Y.; Mavr e, F.; Chow, K.-F.; Crooks, J. A.; Crooks, R. M. Snapshot voltammetry using a triangular bipolar microelectrode. *Anal. Chem.* **2010**, *82*, 5317-5322.
- (86) Wu, M.-S.; Yuan, D.-J.; Xu, J.-J.; Chen, H.-Y. Electrochemiluminescence on bipolar electrodes for visual bioanalysis. *Chem. Sci.* **2013**, *4*, 1182-1188.

(87) Wu, M. S.; Xu, B. Y.; Shi, H. W.; Xu, J. J.; Chen, H. Y. Electrochemiluminescence analysis of folate receptors on cell membrane with on-chip bipolar electrode. *Lab. Chip* **2011**, *11*, 2720-2724.

(88) Wu, S. Z.; Zhou, Z. Y.; Xu, L. R.; Su, B.; Fang, Q. Integrating bipolar electrochemistry and electrochemiluminescence imaging with microdroplets for chemical analysis. *Biosens. Bioelectron.* **2014**, *53*, 148-153.

(89) Shi, H. W.; Wu, M. S.; Du, Y.; Xu, J. J.; Chen, H. Y. Electrochemiluminescence aptasensor based on bipolar electrode for detection of adenosine in cancer cells. *Biosens. Bioelectron.* **2014**, *55*, 459-463.

(90) Bard, A.; Debad, J.; Leland, J.; Sigal, G.; Wilbur, J.; Wohlsatdter, J.; Meyers, R., Eds.; Meyers Ed., *Encyclopedia of analytical chemistry: applications, theory and instrumentation*; 2000.

(91) Pantano, P.; Walt, D. R. Toward a near-field optical array. *Rev. Sci. Instrum.* **1997**, *68*, 1357-1359.

(92) Pantano, P.; Walt, D. R. Ordered nanowell arrays. *Chem. Mater.* **1996**, *8*, 2832-2835.

## General conclusions

The studies presented in this doctoral thesis aim at the finding of new ECL luminophores, the formation of stimuli-responsive ECL hydrogel films and the development of new ECL assays. As introduced in the first chapter, ECL is a very powerful analytical technique with a spread commercialization of immunoassays and many applications in biosensing, where the analytical signal is the light intensity. The pursuing of better performance in ECL is always a challenge work. During this process, the properties of ECL luminophores play an important role since the ECL emission is given by the relaxation of its excited state. Moreover, ECL is a flexible technique that employs different materials, or is combined with other analytical methods, which allows inventing new smart ECL assays.

In the second chapter of the thesis, we presented three types of organic dyes used as ECL luminophores for ECL investigations. Firstly, the electrochemistry, spectroelectrochemical and ECL properties were demonstrated on series of spirofluorene dyes. Dye **1** built from a spirofluorene core and triphenylamine end groups connected *via* thiophene moieties shows three reversible oxidation waves, indicating that the radicals are stable even at the high oxidized states. Such intrinsic characteristic allows the generation of intensive and large ECL signal with TPrA as co-reactant, which is 4.5 times higher ECL efficiency than that of the reference compound  $\text{Ru}(\text{bpy})_3^{2+}$  under the same conditions. In addition, thanks to the molecular structure of dye **1**, FONs of dye **1** formed by the nano-precipitation in water retains fluorescence. The capability to generate strong ECL signal with FONs in water leads them to the ECL nanoemitters. Then, the electrochemical, fluorescence and ECL properties of eight cationic triangulenes were investigated. The voltammetry data show that the nature of the heteroatoms in the core structure has a strong influence on the electrochemical behaviors. ECL generation according to the reductive-oxidation pathway was studied by using BPO as co-reactant. The ECL efficiency is dramatically different from one molecule to the next due to the progressively changing nature of the heteroatoms inside the triangulenium cores and the pending chemical groups in

these compounds. This evolution was then rationalized and illustrated by using a new ECL “wall” presentation that can predict the ECL capability of triangulene dyes simply based on the redox and fluorescence data. The further ECL studies reveal the key factors that govern ECL efficiency. They are the electro-donating effects, which control the monocation stabilization and the corresponding redox potential values. Finally, cationic helicene dyes have similar configuration to cationic triangulene dyes. Their electrochemical, fluorescent and ECL properties could be tuned by the same protocols (*i.e.* changing the heteroatoms and the pending chemical groups). Depending on the oxidation and reduction processes, ECL of these helicene dyes could be produced by either annihilation pathway or co-reactant pathway with BPO or TPrA. Upon these ECL studies, we move forward to the establishing ECL “map”, which is derived from the ECL “wall” formalism. It provides a global overview of energy sufficiency required with different co-reactants. The studies on organic ECL have provided different organic materials that are capable to generate ECL. It will be of interests to prepare water-soluble organic dyes by tuning their molecular structures. Organic ECL in aqueous solution may be suitable for bio-analytical applications. Also, the ability to tune the luminescence properties makes them attractive candidates for multiple wavelength ECL labels.

In the third chapter of the thesis, we demonstrated the ECL signal amplification on thermo-responsive pNIPAM hydrogel films covalently grafting with Ru(bpy)<sub>3</sub> luminophores. The free radical polymerization of monomers in the degassed solution is then triggered by the electrochemically reduced initiator. The formation of the hydrogel films on the conductive object can be achieved by two different experimental setups (*i.e.* a conventional three-electrode system and a wireless bipolar electrochemistry system). The electrochemical and ECL properties were firstly studied on hydrogel films modified GCE at different temperatures. By raising the temperature above the VPTT, hydrogel films collapsed and more Ru(bpy)<sub>3</sub> centers are electrochemically accessible. ECL signals of the hydrogel films amplified significantly with the films collapsed, and up to 58-fold of enhancement was observed with oxalate co-reactant. These studies of the films deposited on GCE allow

deciphering the enhanced ECL emission and determining the main factor governing the ECL process. That is the decreased distance between Ru(bpy)<sub>3</sub> centers in the films at the collapsed state responsible for ECL signal amplification. Then, similar hydrogel films were deposited on a micro object carbon fiber by bipolar electrochemistry method. The variation of hydrogel films thickness below and above the VPTT was studied by *in-situ* optical microscopy imaging and 2 times of decrease in the thickness of the films was found when heated above the VPTT. The asymmetric reactivity induced by bipolar electrochemistry is also exploited to promote ECL in a wireless manner on one side of the modified object. ECL enhancement of the films on carbon fiber was also observed upon the hydrogel films collapsed. The studies of the ECL on hydrogel films have been proved that the concept of ECL amplification using responsive redox pNIPAM hydrogel is a general process. It will be useful to design new ultrasensitive assays with less efficient co-reactant. It could be extended to other types of stimulus in order to design new biosensors. For example, glucose-responsive hydrogels could be designed by incorporating simultaneously glucose sensitive moieties and luminophores in the hydrogel layer.

In the last chapter of the thesis, we developed two new different ECL assays. The first ECL assay based on boronic acid modified co-reactant was created for saccharides sensing. Boronic acids are well-known receptors for saccharides due to their abilities to bind with diol units to form cyclic boronate esters. The integrating a boronic acids receptor to the chemical structure of tertiary amine co-reactant allows modulating ECL response in the presence of D-glucose or D-fructose. Indeed, the heterogeneous oxidation of the modified co-reactants becomes a very inefficient process after binding saccharides, which drastically limits the generation of ECL. By shortening the linker length of a bis-boronic acid amine coreactant, the binding capability toward fructose is lost, while it is normal toward glucose. By using this co-reactant, we have obtained excellent D-glucose selectivity in the ECL assays. This approach allows manipulating ECL process by an additional specific input parameter, which could be extended to various luminophore and co-reactant systems for biological and chemical sensing and further incorporated in molecular logic gates. The second ECL assay is

based on a gold coated optical fiber bundle. An optical fiber bundle coated with a nanometer-thin gold film acts as a dual platform, on the one hand to locally generate ECL of Ru(bpy)<sub>3</sub><sup>2+</sup>/TPrA mode system in a wireless manner by bipolar electrochemistry, and on the other hand to guide the resulting ECL signal. The light emission is triggered and collected at one end, transmitted by the waveguide and remotely detected at the opposite end. The powerful features of this simultaneous generation, collection and transmission of ECL provides many opportunities to develop remote ECL applications, ranging from high-throughput catalyst screening to massive parallel biochemical analysis.

## Experimental section

### 1. Chapter 2

#### 1.1. Materials

All the organic dyes and organic nanoparticles used in this study were provided and characterized by our two research partners (the group of Mireille Blanchard-Desce, University of Bordeaux and the group of Professor Jérôme Lacour, University of Geneva). The other chemicals, including tri-*n*-propylamine ( $\cong 98\%$ ), benzoyl peroxide, ferrocene and *n*-tetrabutylammonium hexafluorophosphate, were purchased from Sigma-Aldrich and used without purification unless otherwise stated.

#### 1.2. Apparatus

Cyclic voltammetric experiments were performed with a PGSTAT30 Autolab potentiostat and a  $\mu$ -Autolab Type III connected to a conventional three-electrode cell, consisting in a silver-wire quasi-reference electrode, a platinum-wire counter electrode, and a platinum working electrode. Potential calibration of the silver-wire was performed using a standard Fc/Fc<sup>+</sup> redox couple after the measurements, or the potential was referred to SCE in the case of spirofluorene dyes ( $E^\circ$  of Fc/Fc<sup>+</sup> redox couple was taken as 0.342V vs. SCE)<sup>1</sup>. For the study of organic nanoparticles in aqueous solution, a glassy carbon (GC) electrode and an Ag/AgCl electrode were used as working electrode and reference electrode, respectively. But the potential was presented by referring to SCE. Prior to measurement, both Pt disk and GC electrode were polished with alumina slurry, rinsed thoroughly with Milli-Q water between each polishing step, and sonicated in water and ethanol respectively, followed by a final rinse with acetone and dried with N<sub>2</sub> stream.

Absorption and fluorescent spectra were collected in quartz cuvette cells (10 mm in length) on Cary 100scan UV-visible spectrophotometer and Cary Eclipse spectrophotometer, respectively. Spectroelectrochemical spectra were recorded on the Cary 100scan UV-visible spectrophotometer and Cary Eclipse spectrophotometer with a  $\mu$ -Autolab type III potentiostat. Herein, spectroelectrochemical cell was constructed

by loading a transparent Pt mesh working electrode into 1mm path length thin layer channel in the quartz cuvette and mounting the other two electrodes above the channel.

ECL intensity was measured using a Hamamatsu photomultiplier tube R5070 with a Hamamatsu C9525 high voltage power supply. The PMT detector was held at  $-750$  V and placed a few millimeters in front of the working electrode. The output signal was amplified by a Keithley 6485 Picoammeter before acquisition via the second input channel of the PGSTAT30 AUTOLAB potentiostat. ECL spectra were recorded using a Princeton Instruments Acton SpectraPro 2300i after the CCD camera cooled to  $-115^{\circ}\text{C}$  with liquid  $\text{N}_2$ . The electrochemical cell is built with a glass slide on the bottom in order to record the ECL signal. The optical fiber connected to the device is placed close to this glass slide in front of the working electrode.

## **2. Chapter 3**

### **2.1. Materials**

All the reagents were purchased from Sigma-Aldrich unless otherwise noted. N-isopropylacrylamide (NIPAM) was recrystallized from hexane (ICS) and dried under vacuum prior to use. The cross-linker N,N'-methylenebis(acrylamide) (BIS) and the initiator potassium persulfate were used as received. Ruthenium(II) (4-vinyl-4'-methyl-2,2'-bipyridine)bis(2,2'-bipyridine)bis(hexafluorophosphate)[Ru(bpy) monomer)] was synthesized according to the procedure described by Spiro *et al.*<sup>2</sup> The coreactants, tri-*n*-propylamine ( $\cong 98\%$ ), dibutylaminoethanol and sodium oxalate, were purchased from Sigma-Aldrich. De-ionized water, obtained with a Milli-Q system, was used for all synthesis reactions, purification and solution preparation. Glassy carbon electrode (3mm in diameter) was used as working electrode. Carbon fibers (Grade P100, Goodfellow) with a diameter of  $10\ \mu\text{m}$  were employed as bipolar electrodes for the asymmetric electrodeposition.

### **2.2. pNIPAM hydrogel films preparation**

1) On GCE

GCEs were polished with wet alumina powder on a polishing cloth, and then washed

ultrasonically with ethanol and water, respectively. In a typical process, the electrode was immersed in an aqueous solution containing 70 mM NIPAM, 1.75 mM BIS (2.5 mol % against NIPAM), 0.14 mM of Ru(bpy) monomer (0.2 mol % of Ru monomer against NIPAM), and 1.5 mM  $K_2S_2O_8$  in 0.2 M  $KNO_3$  solution. Prior to electrochemically assisted polymerization, the reaction solution was deoxygenated by bubbling nitrogen gas for 30 min at room temperature. The potential was applied by cycling between -0.35 and -0.95 V at 100 mV/s for 60 cycles. After the polymerization, the electrodes modified with pNIPAM-Ru films were thoroughly washed with double-distilled water to remove the monomers and stored in Milli-Q water.

## 2) On carbon fiber

The BPE cell consist of two compartments, containing the feeder electrodes (graphite rods), connected with a glass capillary (outer diameter: 2 mm, inner diameter: 1.12 mm; length: 25 mm), A carbon fiber (diameter = 10  $\mu$ m, length: 2mm or 10 mm) was placed in the middle of the glass capillary. The degassed  $KNO_3$  solution containing also NIPAM monomer, BIS as cross-linker, and Ru(bpy)<sub>3</sub> monomer as ECL luminophore was injected into the BPE cell. Asymmetric carbon fibers were generated by applying the requested potential difference between the two feeder electrodes. After the deposition, the sample was carefully removed from the cell and washed with Milli-Q water.

## 2.3. Characterization

*Scanning electron microscopy (SEM):* Prior to the observation, the samples were immersed in a water bath and frozen rapidly in liquid nitrogen. Then the dried sample was placed directly on a conductive double-sided sticky carbon tape, coated with gold by sputtering (Emitech K550X). SEM observation was carried out with a Hitachi TM-1000 instrument to study the surface morphology of the hydrogel films by applying 15 kV accelerating voltage.

*Temperature control:* The temperature on GCE samples was controlled using a thermostatically controlled cell compartment. The measurements were taken under equilibrium conditions after holding the sample for 15 min at each temperature. On

the carbon fiber, a heat controller TC 324C (Warner Instrument) connected with an imaging chamber (RC-21BRW, 214 Warner Instrument) was employed. The sample was placed in the imaging chamber and placed on the stage of the microscope.

*Imaging Setup and Fluorescence Recording:* An optical microscope (Leica DM6000B) was used to observe the thickness and the length of the polymer deposited on the carbon fiber. For the fluorescence mode with a filter cube I3, an excitation filter in the range 450–490 nm and an emission filter of 515 nm fluorescent microscope was used. PL imaging on GCE were recorded using horizontal epifluorescence microscope (Olympus BXFM-ILHSPU). The microscope was equipped with mercury lamp. Specific set of filters was used to select the excitation and emission wavelength of Ru(bpy)<sub>3</sub><sup>2+</sup>-fluorophore. Only the light that correspond to the excitation of luminophore passes through and is reflected by dichroic mirror toward the sample.

*Electrochemical measurements:* Differential pulse voltammetry (DPV) experiments were performed with a  $\mu$ -Autolab Type III electrochemical station. The three-electrode system consisted in a GCE as a working electrode, Ag/AgCl as a reference and a platinum wire as a counter-electrode.

*ECL measurements:* ECL experiments were performed with a  $\mu$ -Autolab Type III electrochemical station. ECL intensity was measured by using a Hamamatsu photomultiplier tube R5070A. The signal was amplified by a Keithley Picoammeter before acquisition *via* the second input channel of the  $\mu$ -Autolab. ECL spectra were recorded using a Princeton Instrument spectrograph Spectra pro 2300i under potential scanning between 0 and 1.5 V at a scan rate of 50 mV/s, in an aqueous solution containing the co-reactant and the supporting electrolyte. The ECL imaging of carbon fiber was performed using a horizontal epifluorescence microscope Olympus BXFM-ILHSPU equipped with a Hamamatsu EM-CCD camera.

### **3. Chapter 4**

#### **3.1. Materials**

The phenylboronic acid compounds were synthesized and characterized by the group of Professor Tony D. James from University of Bath. The other chemicals were

analytical reagent grade and used as received. Tris(2,2'-bipyridyl) dichlororuthenium(II) hexahydrate, sodium phosphate dibasic heptahydrate, sodium phosphate monobasic monohydrate, tri-*n*-propylamine, D-fructose and D-glucose were purchased from Sigma-Aldrich. Solutions used in the experiments were prepared with water purified by MilliQ station. Phosphate buffer solution (PBS, 100 mM or 10 mM, pH7.4) was prepared from sodiumphosphate dibasic heptahydrate and sodium phosphate monobasic monohydrate.

### 3.2. Electrochemical setup

A conventional three-electrode system was applied for this study of the boronic acid compounds with a GCE (d=3 mm) as working electrode, an Ag/AgCl as reference and a Pt wire as counter-electrode. Prior to each measurement, GCE was polished with alumina slurry, rinsed thoroughly with water after each polishing step, and sonicated in ethanol/water.

A 50 cm-long silica optical fiber bundle (FIGH-06-300s, Fujikura Ltd) comprising 6000 individually cladded optical fibers with a diameter of 3–4  $\mu\text{m}$  was used in the study of remote sensing. The outer layer of the optical fiber bundle was removed with acetone prior to gold coating (length: 4 cm). The distal face of the optical fiber bundle was mounted on a spinning holder and coated with a gold layer by using a magnetron sputtering setup (Emitech K550X) for 12 min (thickness  $\sim$  500 nm). After that, the coated part was shortened by cleaving in such a way that the final length of the gold coating along the fiber wall is  $L_{\text{elec}} = 2$  cm. Finally, a second gold coating was deposited for only 20 s (thickness  $\sim$  20 nm) in order to form a thinner gold layer on the cross-section of the fiber bundle where ECL light is collected. The gold-coated distal face of the optical fiber bundle was used as BE and placed into a homemade bipolar cell in the middle of the glass capillary between the two feeder electrodes. The appropriate electric field was applied with a DC power supply (Sodilec).

### 3.3. ECL measurements

Cyclic voltammetry was performed with a  $\mu$ -Autolab Type III potentiostat connected

to a homemade spectroelectrochemical cell. ECL intensity was measured simultaneously at the bottom of the cell by a Hamamatsu photomultiplier tube R5070. The PMT detector was held at -750 V powered by Hamamatsu C9525 high-voltage power supply. The ECL output signal was amplified by a Keithley 6485 Picoammeter before acquisition *via* the second input channel of the potentiostat. A stock solution of PBS containing 1 M D-glucose or 1 M D-fructose was prepared and used for the voltammetric and ECL experiments. After adding the D-fructose to the PBS solution which contains already the luminophore and the coreactant, we stirred it for 30 s and perform the voltammetric and ECL measurements. If we stirred for 5 or 10 min., the same values of the voltammetric and ECL signals were obtained indicating that the recognition of the saccharide by the synthesized co-reactants is very fast. Experiments were performed on glassy carbon electrode (GCE) at a scan rate of 100 mV/s. ECL spectra were recorded using a Princeton Instruments Acton SpectraPro 2300i after the CCD camera cooled to  $-115^{\circ}\text{C}$  with liquid  $\text{N}_2$ . The electrochemical cell is built with a glass slide on the bottom in order to record the ECL signal. The optical fiber connected to the device is placed close to this glass slide in front of the working electrode. Photoluminescence spectra were collected on a Cary Eclipse spectrophotometer, using a 1 cm-path length quartz cuvette.

Direct ECL images on the optical fiber were recorded using a commercial digital camera (Canon EOS 70D). ECL is generated by BPE at the distal face of the bundle and is detected at its proximal face with either a photomultiplier tube (PMT, Hamamatsu R5070) or a microscope (BX-30, Olympus) equipped with a CCD camera (Hamamatsu 9100-13, 16 bit).

(1) Pavlishchuk, V. V.; Addison, A. W. Conversion constants for redox potentials measured versus different reference electrodes in acetonitrile solutions at 25 C. *Inorg. Chim. Acta.* **2000**, *298*, 97-102.

(2) Ghosh, P.; Spiro, T. G. Photoelectrochemistry of tris (bipyridyl) ruthenium (II) covalently attached to n-type tin (IV) oxide. *J. Am. Chem. Soc.* **1980**, *102*, 5543-5549.

## List of publications

1. Electrogenenerated chemiluminescence of cationic triangulene dyes: Crucial influence of the core heteroatoms.  
*Chem. Eur. J.* **2015**, 21, 19243–19249.  
Catherine Adam, Antoine Wallabregue, Haidong Li, Jérôme Gouin, Rémi Vanel, Stéphane Grass, Johann Bosson, Laurent Bouffier, Jérôme Lacour, Neso Sojic.
2. Bright electrochemiluminescence tunable in the near-infrared of chiral cationic helicene chromophores.  
*J. Phys. Chem. C.* **2016**, 121, 785–792.  
Haidong Li, Antoine Wallabregue, Catherine Adam, Johann Bosson, Laurent Bouffier, Jérôme Lacour, Neso Sojic.
3. Bright electrogenerated chemiluminescence of a bis-donor quadrupolar spirofluorene dye and its nanoparticles.  
*Chem. Eur. J.* **2016**, 22, 12702–12714.  
Haidong Li, Jonathan Daniel, Jean-Baptiste Verlhac, Mireille Blanchard-Desceand Neso Sojic.
4. Antagonistic effects leading to turn-on electrochemiluminescence in thermoresponsive hydrogel films.  
*Phys. Chem. Chem. Phys.* **2016**, 18, 32697–32702.  
Haidong Li, Milica Sentic, Valérie Ravaine, Neso Sojic.
5. Synthesis and activation of electrochemiluminescent thermoresponsive Janus objects using bipolar electrochemistry.  
*Langmuir.* **2016**, 32, 12995–13002.  
Oranit Phuakkong, Milica Sentic, Haidong Li, Chompunuch Warakulwit, Jumras Limtrakul, Neso Sojic, Alexander Kuhn, Valerie Ravaine, Dodzi Zigah.
6. Selective electrochemiluminescent sensing of saccharides using boronic acid-modified co-reactant.  
*Chem. Commun.* **2016**, 52, 12845–12848.  
Haidong Li, Adam C. Sedgwick, Meng Li, Richard A. R. Blackburn, Steven D. Bull, Stéphane Arbault, Tony D. James, Neso Sojic.
7. Double remote electrochemical addressing and optical readout of electrochemiluminescence at the tip of an optical fiber.  
*Analyst*, **2016**, 141, 4299–4304.  
Haidong Li, Patrick Garrigue, Laurent Bouffier, Stéphane Arbault, Alexander Kuhn, Neso Sojic.
8. Physicochemical and electronic properties of cationic[6]helicenes: from chemical and electrochemical stabilities to far-red (polarized) luminescence.  
*Chem. Eur. J.* **2016**, 22, 18394–18403.  
Johann Bosson, Geraldine M. Labrador, Simon Pascal, François-Alexandre Miannay, Oleksandr Yushchenko, Haidong Li, Laurent Bouffier, Neso Sojic, Roberto C. Tovar, Gilles Muller, Denis Jacquemin, Adèle D. Laurent, Boris Le Guennic, Eric Vauthey, Jérôme Lacour.
9. Essential role of electrode materials in electrochemiluminescence applications.

- ChemElectroChem*, **2016**, 3, 1990–1997.  
Giovanni Valenti, Andrea Fiorani, Haidong Li, Neso Sojic, Francesco Paolucci.
10. Energetic wall for efficient annihilation electrochemiluminescence of cationic helicene luminophores.  
*ChemElectroChem*, **2017**, DOI: 10.1002/celec.201600906.  
Haidong Li, Silvia Voci, Antoine Wallabregue, Catherine Adam, Geraldine M. Labrador, Romain Duwald, Irene Hernández Delgado, Simon Pascal, Johann Bosson, Jérôme Lacour, Laurent Bouffier, Neso Sojic.
11. Spatially-resolved multicolor bipolar electrochemiluminescence.  
*Electrochem. Commun.*, **2017**, 77, 10–13.  
Haidong Li, Laurent Bouffier, Stéphane Arbault, Alexander Kuhn, Conor F. Hogan, Neso Sojic.